

NMR-Spectroscopic Investigations  
on Aminocatalysis:  
Experimental and Quantum Chemical  
Studies on Dienamine- and  
Enamine-Intermediates.



**Dissertation**

zur Erlangung des Doktorgrades  
der Naturwissenschaften (Dr. rer. nat.)  
der Fakultät für Chemie und Pharmazie  
der Universität Regensburg

vorgelegt von

**Michael M. Hammer**  
aus Wasserburg am Inn

2015



Die vorliegende Dissertation beruht auf Arbeiten, die zwischen Oktober 2011 und Juni 2015 im Arbeitskreis von Professor Dr. Ruth M. Gschwind am Institut für Organische Chemie der Universität Regensburg durchgeführt wurden.

Promotionsgesuch eingereicht am: 25. Juni 2015

Die Arbeit wurde angeleitet von: Prof. Dr. Ruth M. Gschwind

Prüfungsausschuss:

Vorsitzender:	PD Dr. S. Amslinger
1. Gutachter:	Prof. Dr. R. M. Gschwind
2. Gutachter:	Prof. Dr. B. König
3. Prüfer:	Prof. Dr. A. Slenczka





DANKSAGUNG



**WIDMUNG**



**NMR-Spectroscopic Investigations on  
Aminocatalysis: Experimental and Quantum  
Chemical Studies on Dienamine- and  
Enamine-Intermediates.**

Michael M. Hammer



## Unrelated publications of the author

- Evelyn Hartmann, Michael M. Hammer and Ruth M. Gschwind, "Structures and Interligand Interaction Pattern of Phosphoramidite Pd Complexes by NMR Spectroscopy: Modulations in Extended Interaction Surfaces as Stereoselection Mode of a Privileged Class of Ligands", *Chemistry - A European Journal* **2013**, 232, 10551-10562
- Tobias Simbeck, Michael M. Hammer, Stefan Thomaier, Christoph Stock, Edmund Riedl and Heiner J. Gores, "Kinetics of adsorption of poly(vinylimidazole) (PVI) onto copper surfaces investigated by quartz crystal microbalance studies", *Journal of Solid State Electrochemistry* **2012**, 16, 3467-3472

## Parts of this work have been presented at national and international conferences

1. Markus B. Schmid, Michael M. Hammer, Kirsten Zeitler and Ruth M. Gschwind, "Conformational preferences of prolinol (ether) enamines", SMASH-Small molecule NMR conference, Chamonix, France, **2011**
2. Michael M. Hammer, Michael H. Haindl, Diana Drettwann, Matthias Fleischmann, Markus B. Schmid, Kirsten Zeitler and Ruth M. Gschwind, "NMR spectroscopic investigations on reaction mechanisms - organocatalysis", FeUR, Regensburg, Germany, **2012**
3. Michael M. Hammer and Ruth M. Gschwind, "Structural diversity in enamines and iminium ions revealed by NMR", SMASH-Small molecule NMR conference, Providence/Rhode Island, USA, **2012**
4. Michael M. Hammer and Ruth M. Gschwind, "Structural and mechanistic studies on enamines and dienamines", Gordon Research Conference - Physical Organic Chemistry, Holderness/New Hampshire, USA, **2013**
5. Michael M. Hammer and Ruth M. Gschwind, "Structural and mechanistic studies on dienamine intermediates", SMASH-Small molecule NMR conference, Santiago de Compostella, Spain, **2013**
6. Michael M. Hammer, Andreas J. Seegerer and Ruth M. Gschwind, "Organocatalytic reaction mechanisms unravelled by NMR spectroscopy", Gordon Research Conference - Green Chemistry, Chinese University of Hong Kong, Hongkong, **2014**
7. Michael M. Hammer and Ruth M. Gschwind, "Unraveling organocatalytic reaction mechanisms by NMR spectroscopy", SMASH-Small molecule NMR conference, Atlanta/Georgia, USA, **2014**

# Contents

<b>1</b>	<b>Introduction and Outline</b>	<b>13</b>
<b>2</b>	<b>Structural preferences in dienamine intermediates investigated by <i>in situ</i>-NMR spectroscopy.</b>	<b>17</b>
2.1	Abstract . . . . .	18
2.2	Manuscript . . . . .	19
2.3	Supporting Information . . . . .	36
2.4	References . . . . .	43
<b>3</b>	<b>The mechanism of stereinduction in dienamine catalyzed <math>\gamma</math> alkylation revealed by a combined <i>in situ</i> NMR and quantum-chemical study.</b>	<b>47</b>
3.1	Abstract . . . . .	48
3.2	Manuscript . . . . .	49
3.3	Supporting Information . . . . .	69
3.4	References . . . . .	91
<b>4</b>	<b>Enamine and oxazolidinone intermediates investigated by quantum chemical calculations.</b>	<b>95</b>
4.1	Organocatalytic intermediates investigated by quantum chemical calculations.	96
4.2	Results of the conformational space screening . . . . .	117
4.3	References . . . . .	126
<b>5</b>	<b>The mechanism of enamine formation investigated by quantum chemical calculations.</b>	<b>141</b>
5.1	Enamine formation pathways deduced by quantum chemistry . . . . .	142
5.2	Combined calculation results . . . . .	151
5.3	References . . . . .	156
<b>6</b>	<b>Stereinduction in enamine catalysis- "late" conformational lock.</b>	<b>159</b>
6.1	"Late" conformational lock in enamine-electrophile complexes . . . . .	160
6.2	References . . . . .	172
<b>7</b>	<b>Kinetic data visualization for the easy, quick and straightforward reaction condition optimization.</b>	<b>175</b>
7.1	Manuscript . . . . .	176



7.2	References . . . . .	185
<b>8</b>	<b>NMR methodology for the fast acquisition of nD spectra.</b>	<b>189</b>
8.1	Ultrafast NMR spectroscopy . . . . .	190
8.2	Non-Uniform Sampling (NUS-Sampling) . . . . .	193
8.3	Supporting Information . . . . .	197
8.4	References . . . . .	201
<b>9</b>	<b>Summary and Outlook</b>	<b>205</b>



# 1 Introduction and Outline

Sparked by the publication of List, Lerner and Barbas III (*J. Am. Chem. Soc.* **2000**, *122*, 2395-2396), in the last 10 to 15 years, the catalysis of chemical reactions with the help of small organic molecules *i. e.* organocatalysis has emerged as one major pillar of asymmetric catalysis and experienced an astonishing rate of development. Different concepts have been developed independently, namely catalysis through hydrogen bonding or phase transfer catalysis. Especially organocatalysis by secondary amines, offering enamine, dienamine, trienamine, iminium or SOMO activation has grown to be one of the most widely applicable principles. Employing amine catalysts, typically originating from the chiral pool, chemical reactions can be catalyzed in an asymmetric fashion in a huge number of applications rather easily and therefore gained interest and became very popular. Organocatalysis shows vast advantages in comparison to biocatalysis and metal catalysis, since it proves to often be convenient, versatile, low cost, non-toxic and sustainable.

However, with respect to the number of synthetic applications of asymmetric organocatalysis, the number of studies aiming at the mechanistic understanding of organocatalytic reactions is very sparse. The intimate knowledge of reaction pathways, formation mechanisms, stability of intermediates and intermediate structures may provide a huge advantage for the further development of activation modes and the expansion of the catalyst pool.

This thesis attempts therefore to provide mechanistic and structural insight into the underlying concepts of dienamine and enamine catalysis. Modern NMR methodology was employed to investigate intermediate properties, reaction pathways and to explore chemical transformations in order to advance the understanding of organocatalyzed reactions.

For dienamine activation a steric shielding model is proposed to account for the stereoselectivity, however structural information to confirm this shielding model is lacking. In chapter 2, the structural features of dienamine intermediates are investigated by *in situ* NMR spectroscopy utilizing mostly coupling constant as well as NOE and HOE analysis. The dienamines from  $\alpha,\beta$ -unsaturated aldehydes and secondary amine catalysts **3E** and **3Z** evidence a strong conformational preference for the whole of the structure but the second dienamine double bond, which was found to be predominantly **3Z** configured. The pyrrolidine catalyst substructure

was found to be *down* puckered associated with a predominance of *sc-exo* conformation of the exocyclic biaryl substituents dependent on catalyst utilized. The diene system is found in an *s-trans-1E-s-trans* conformation with dominance of *3Z* over *3E* conformation. No difference in quality for the shielding was identified for both *3E*- and *3Z*-dienamines leading us to conclude that a simple steric shielding model can not account for the stereocontrol in dienamine activation.

To offer an alternative model for stereocontrol, in chapter 3, the stereoinduction mechanism in dienamine catalysis is investigated thoroughly. The stereochemical outcome is evidenced to be entirely independent of the distribution of *3E* and *3Z*-dienamines and a *3Z/3E*-dienamine equilibrium with subsequent exclusive consumption of *3Z*-dienamine is also ruled out. However, quantum chemical calculations together with *ee*-determination can show that both dienamine configurational isomers do feed into the major product enantiomer and product iminium stabilization is responsible for the stereocontrol in dienamine activation.

Chapter 4 deals with the accurate calculation of enamine and oxazolidinone intermediates by high level quantum chemical calculations. The reproduction of experimental values for the oxazolidinone species is straightforward, the calculation of enamine intermediates however is highly dependent on polarizable proton consideration and is best achieved by using dispersion corrected methods. In addition, the explicit consideration of a DMSO molecule as suggested in literature in the enamine structure led to the best representation of experimentally found enamine stabilization.

This allowed us to perform a preliminary high level transition state calculations in chapter 5. Here we could identify a transition state connecting the iminium species with the enamine intermediate. We could also evidence transition states also between the oxazolidinone and the iminium species. This study could help identify theoretical needs to accurately model the connecting transition states.

The fact that enamine intermediates of proline and proline-derived organocatalyst do not exhibit structural lock is addressed in chapter 6. We present the concept, that for successful stereoinduction required conformational lock of enamine intermediates is not, as has been assumed, achieved in the intermediates themselves, but rather in the "late" enamine-electrophile complex. This is experimentally approached by the spectroscopic investigation of an enamine/DBU complex providing first hints on the validity of the concept.

In chapter 7, a novel type of plot is introduced for the quick and easy visualization and optimization of reaction conditions of competitive chemical reaction. Plotting the ratio of desired

---

over undesired product as the function of the amount of desired product yields a handy and ostensive depiction of reaction condition and reaction outcome. Temporal information is only indirectly accessible, this however leads to far less occasions of a mismatch in scaling to compare different reaction conditions. This plot will accelerate the speed at which chemists can process, interpret and understand the large amounts of data produced by reaction monitoring.

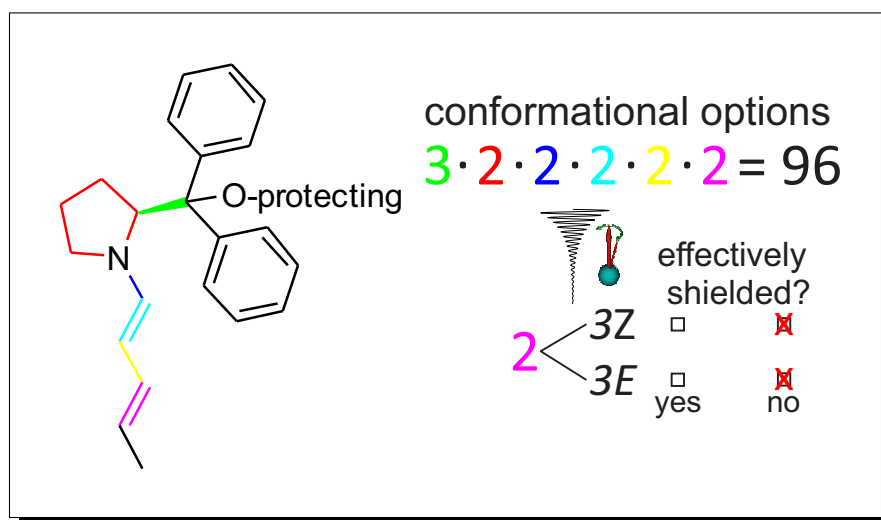
In chapter 8, modern NMR methodology is introduced providing access to n-dimensional NMR spectra in significantly reduced experiment time. The concept, implementation and preliminary application of ultrafast-NMR spectroscopy is shown, however limits in gradient stability hampered our efforts to pursue this approach to acquire 2D spectra within seconds. NUS spectroscopy is also introduced. Not recoding the whole of the  $t_1$ - $t_2$ -map and suitable mathematical reconstruction allows the acquisition of nD spectra in considerable less time than conventional multidimensional NMR spectroscopy. The application as well as representative examples are provided.



## 2 Structural preferences in dienamine intermediates.

Article

*"Structural preferences in dienamine intermediates investigated by in situ-NMR spectroscopy."*



Dienamines composed of aldehyde **4** was investigated by Andreas J. Seegerer. Quantum chemical calculations were performed by Dr. Johnny Hioe.

Michael M. Hammer, Andreas J. Seegerer, Johnny Hioe and Ruth M. Gschwind

## 2.1 Abstract

The knowledge of reactive intermediate structures in organocatalytic reactions is a vital tool to understand their mechanistic underpinnings. In the field of dienamine catalysis structural information on the involved intermediates is sparse. Although steric shielding of one side of the dienamine  $\pi$ -system is proposed, no structural evidence is provided as yet. Here, we report the investigation of structural preferences of dienamine intermediates derived of  $\alpha,\beta$ -unsaturated aldehydes with prolinol-type secondary amine organocatalysts of the Jørgensen-Hayashi type. Strong structural preference for the catalyst substructure was identified through  $^1\text{H}$ ,  $^1\text{H}$ -NOE,  $^1\text{H}$ ,  $^{19}\text{F}$ -HOE and coupling constant analysis. The pyrrolidine ring adopts *down* puckering and preference for *sc-exo* conformation of the exocyclic CC bond. This is dependent on the catalyst substitution pattern, but independent of the configuration of the dienamines second double bond. In the diene-subsystem, by means of  $^1\text{H}$ ,  $^1\text{H}$ -NOESY and coupling constant analysis, the exclusive adoption of *s-trans* conformation for both diene single bonds was shown. By proving steric proximity of the bulky catalyst residue to the diene moiety, we could evidence the orientation of the bulky catalyst residue over one side of the dienamines  $\pi$ -system. Altogether we could show that for both *3E* and *3Z*-dienamines the same structural preferences were identified in all respects but the configuration of the second double bond. This hints to the invalidity of a pure shielding model in dienamine catalysis, since no difference in the quality of shielding for the two differently configured *3E*- and *3Z*-dienamines is evidenced.



## 2.2 Manuscript

### Introduction

Intimate knowledge of the structures of intermediates is crucial for the understanding of organic reactions.<sup>[1]</sup> In the vastly expanding field of asymmetric organocatalysis,<sup>[2,3]</sup> insights into intermediate structures should further our ability to understand and develop mechanistic concepts. Catalysis by secondary amines in the form of dienamine activation<sup>[4–9]</sup> has emerged as the vinylogous option to enamine activation.<sup>[10,11]</sup> Although the number of applications of dienamine catalysis is rising in the last few years,<sup>[12]</sup> studies on the mechanistic understanding of dienamine catalysis are very rare. While computational studies of the mechanistic pathways have proven to be useful in the interpretation of reaction outcomes,<sup>[4,9]</sup> the experimental knowledge of intermediate properties is often missing.

Among a large variety of catalytic scaffolds, typically originating from the chiral pool, Jørgensen-Hayashi type prolinol ethers<sup>[13–15]</sup> have demonstrated extraordinary performance in enamine and in dienamine catalysis.<sup>[4–8]</sup> Prolinol ether derived dienamine intermediates have been detected in solution before,<sup>[9]</sup> however information on their structural features are sparse, even though this information should provide the tools to understand the mechanisms and develop novel concepts. Preliminary studies have been performed on some characteristic features of  $\alpha$ -alkylated dienamines.<sup>[9]</sup> There, the conformation of the diene  $\pi$ -system was addressed only briefly. For iminium ions a more extensive study on the structural features is available.<sup>[16]</sup> Dienamine activation is associated with a number of inherent challenges, conformational control and distance to the stereocenter are the most pronounced among them.<sup>[4]</sup> A stereoselection mode has been discussed (see Fig. 2.1),<sup>[17]</sup> albeit no evidence for the validity of shielding of one side of the dienamine intermediate were presented so far. To fill this gap, we performed

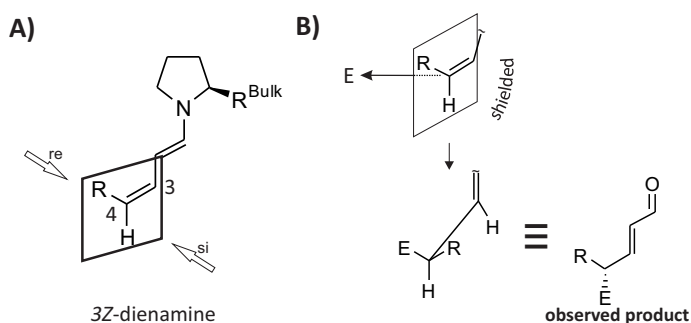


**Fig. 2.1:** **A)** Definition of *re*- and *si*-face of the second double ( $C_3=C_4$ ) bond in secondary amine derived dienamines with 3Z configuration of the second dienamine double bond. **B)** Visualization of the proposed stereoselective step. The 3Z-dienamine attacks on the *re* face, since its *si*-face is effectively shielded by the bulky catalyst residue and forms, after hydrolysis, the stereoproduct.

*in situ* NMR studies on reactive prolinol-ether dienamine intermediates. In this chapter we report the first detailed study on the structure of dienamines derived from prolinol ether-type organocatalysts and  $\alpha,\beta$ -unsaturated aldehydes.  $^1H, ^1H$ -NOESY spectra reveal the preference

for an *s-trans* arrangement of the N-C<sub>1</sub>-bond in the dienamine intermediates due to the steric demand of the bulky catalyst residue. Scalar coupling constants in the aldehyde substructure show the preference for *1E* and *s-trans* (C<sub>1</sub>-C<sub>2</sub>) conformation, albeit with a distribution of *3E*- and *3Z*-configured dienamine independent of the aldehyde used. Scalar coupling constants in the catalyst substructure reveal the adoption of the *down* conformation of the five-membered pyrrolidine ring which allows the intramolecular CH/ $\pi$  interaction between the pyrrolidine protons and the aryl group of the bulky catalyst residue. In addition, the dienamines present preference for *sc-exo* conformation regarding the rotation of the exocyclic CC bond in the catalyst substructure dependent on this catalyst. Most interestingly the quality of shielding is identical for both, the *3E*- and *3Z*-dienamines, thus a pure shielding model for the  $\gamma$ -alkylation of  $\alpha,\beta$ -unsaturated aldehydes can be excluded. Both dienamines present one open face for the attack on the electrophile and the detected ratio of 1.1-3:1 for *3Z*:*3E*-dienamine does not translate to the observed enantiomeric excess in the products.<sup>[4,7-9]</sup>

## Results and Discussion

**Model dienamines.** Prolinol-ether catalysts were selected for our dienamine study, which are synthetically used (see Fig 2.2 **A** and **B**).<sup>[4,13-15,18,19]</sup> Less pronounced is the utilization of prolinol-type organocatalysts in dienamine catalysis, since they perform considerably worse.<sup>[8]</sup> Differently substituted aliphatic  $\alpha,\beta$ -unsaturated aldehydes (see Fig. 2.2 **C**) were chosen with regard to their significantly changing steric demand and electronics in the diene-system.

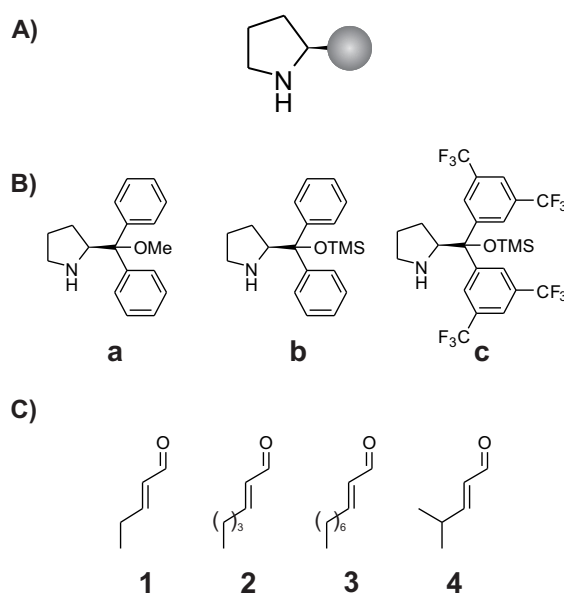


**Fig. 2.2:** **A)** General catalyst structure. **B)** Investigated catalysts developed by Jørgensen and Hayashi.<sup>[13-15]</sup> **C)** Investigated aldehydes with changing steric demand and electronic influence on the developing dienamine double bonds.

Dienamines formed from aldehyde **1** are the smallest which allow the investigation of conformational change in the second double bond of the diene-system. Since toluene is the main

experimental solvent<sup>[4,5,9,20]</sup> all studies unless otherwise indicated were performed in toluene- $d_8$ .

All experiments mentioned in this chapter if not otherwise stated were performed inside standard 5 mm NMR tubes by mixing the given amounts of aldehyde and catalyst (and additive if mentioned) to obtain an aldehyde concentration of 50 mmol L<sup>-1</sup>. NMR spectra were recorded at 300-318 K (see experimental section for detailed information).

**Dienamine detection.** The detection of the diene moiety was accomplished straightforwardly on the basis of the characteristic coupling pattern and resonance of the <sup>1</sup>H-NMR spectra, in particular the doublet for H<sub>1</sub> (see Fig. 2.3 for denomination of proton and carbon positions and <sup>1</sup>H-NMR excerpt) proved to be characteristic and recognizable due to its appearance in the non-crowded spectral region between 6.64 and 6.33 ppm. For all dien-

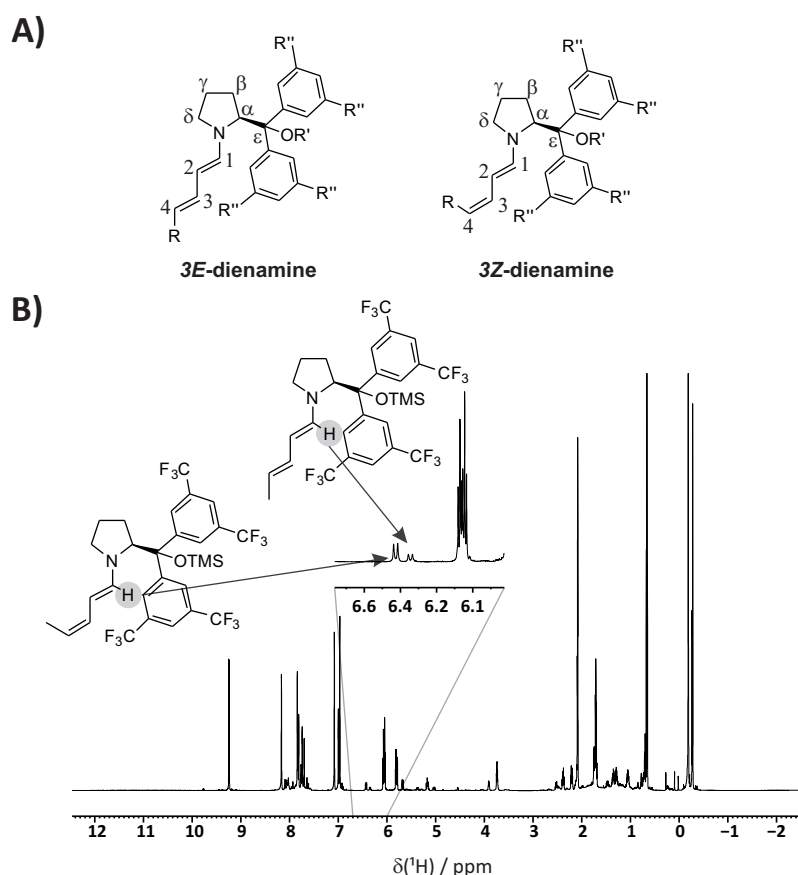


**Fig. 2.3:** **A)** Denomination of the proton and carbon positions in the dienamine structures. **B)** Typical <sup>1</sup>H-NMR spectrum of the *in situ* formed dienamine mixture of 3E-1.c and 3Z-1.c in toluene- $d_8$  at 313.15 K.

amines the configuration was found to be 1E for the first dienamine double bond by their coupling constant of <sup>3</sup>J<sub>H<sub>1</sub>H<sub>2</sub></sub>=13.27-13.53 Hz. No 1Z-configured species were detected, as was not in previous publications dealing with dienamine intermediates.<sup>[9]</sup> This is in strong agreement with theoretical calculations<sup>[4]</sup> and our experimental findings on enamine intermediates.

Merely in solutions with stabilizing DBU present, *Z*-enamines were detected.<sup>[21–26]</sup> For all dienamines investigated, two configurations of the second dienamine double bond (C<sub>3</sub>=C<sub>4</sub>) were detected (denominated as *3E*- and *3Z*-dienamine name, e.g. *3Z*-**1.a**). The coupling constants were found to be <sup>3</sup>*J*<sub>H3H4</sub>=13.3-14.9 Hz for the *3E*-dienamine and <sup>3</sup>*J*<sub>H3H4</sub>=10.4-11.0 Hz for the *3Z*-dienamine.

We identified a ratio of 1.1-3:1 for *3Z*:*3E*-dienamines independent of catalyst employed, which is in agreement with the literature<sup>[4,8,9]</sup> and our findings (see chapter 3). This separation in two configurations of the second double bond is believed to play a vital role in the stereoinduction model of dienamine catalysis.<sup>[4]</sup> To this end, we investigated the structural preferences of both the *3E* and *3Z*-dienamine simultaneously to obtain possible differences and explain the mode of stereoinduction. The reasons for the separation in two differently configured dienamines is addressed in chapter 3 and will not be a matter of investigation here.

**Dienamine Conformations.** How the stereoselectivity is controlled in the bond formation step is highly important for the understanding of asymmetric organocatalyzed reactions. It is assumed that the protected ether-substituent of the pyrrolidine ring shields one face of the dienamine  $\pi$ -system.<sup>[4]</sup> Mostly dienamines obtained from aldehyde **1** were used as model for our structural studies because it represents the smallest entity to have access to all structural features. Additionally, important resonances for our structural studies were not as crowded or overlapped compared to other dienamines detected. We employed mainly <sup>1</sup>H,<sup>1</sup>H-NOESY spectroscopy and coupling constant analysis in order to address the structural preferences of the pyrrolidine ring, the exocyclic C <sub>$\alpha$</sub> -C <sub>$\epsilon$</sub>  bond and the  $\pi$ -system of the former aldehyde substructure. In addition, <sup>1</sup>H,<sup>19</sup>F-HOE spectroscopy was used to investigate the structural features.

**Conformation in the catalyst substructure.** To provide a conclusive picture of the dienamine structural features, we divided our investigation into two sub-moieties. We investigated the catalyst substructure in regards to pyrrolidine puckering and conformation of the exocyclic C <sub>$\alpha$</sub> -C <sub>$\epsilon$</sub>  bond first. The conformation of the dienamine  $\pi$ -system will be addressed secondly further down.

**Conformation of the pyrrolidine ring: *up* or *down*** The puckering of the pyrrolidine ring proved to be a very decisive structural feature in order to describe the stereoselectivity in enamine catalysis by prolinols and prolinol-ethers by evidencing an open attack path.<sup>[24]</sup> We consider it therefore also as an important feature in the vinylogous dienamine catalysis. As basis for this study, analogous to our enamine investigations<sup>[24]</sup> proline side-chain conformations in peptides were used to gain reference values.<sup>[27]</sup> For proline residues two distinct conformations of the pyrrolidine ring are reported which are commonly designated as "*up*" and "*down*" (see Fig. 2.4 **B**). This simple model should be transferable to our investigated prolinol-ether dienamines, since planarity can be assumed for the amide group in peptides and the dien-

amine moiety in organocatalytically active intermediates (on the basis of DFT calculations<sup>[4]</sup>). Additionally the scalar coupling constant ( $J$ ) criteria can be applied to diarylprolinol-ether dienamines since no systematic shift of the  ${}^3J_{\text{H}\alpha,\text{H}\beta 1/2}$  was observed for our model dienamines, potentially stemming from electronic influences of the  $\text{C}_\epsilon$  substituent. *Down* puckering would exhibit a small  ${}^3J_{\text{H}\alpha,\text{H}\beta 2}$  coupling constant of 2-3 Hz accompanied with a  ${}^3J_{\text{H}\delta 1,\text{H}\gamma 2}$  coupling constant of approx. 8-12 Hz.<sup>[27]</sup> For the *up* puckered pyrrolidine ring the coupling constants would be the opposite ( ${}^3J_{\text{H}\delta 1,\text{H}\gamma 2}$ =2-3 Hz,  ${}^3J_{\text{H}\alpha,\text{H}\beta 2}$ =7-11 Hz). For this investigation dienamines formed from catalyst **b** is depicted exemplarily (see Fig. 2.4 C). Only aldehyde **1** was investigated since crowding in the signal region of both  $\text{H}_\alpha$  as well as  $\text{H}_\delta$  prohibited us from coupling constant determination for other aldehydes.

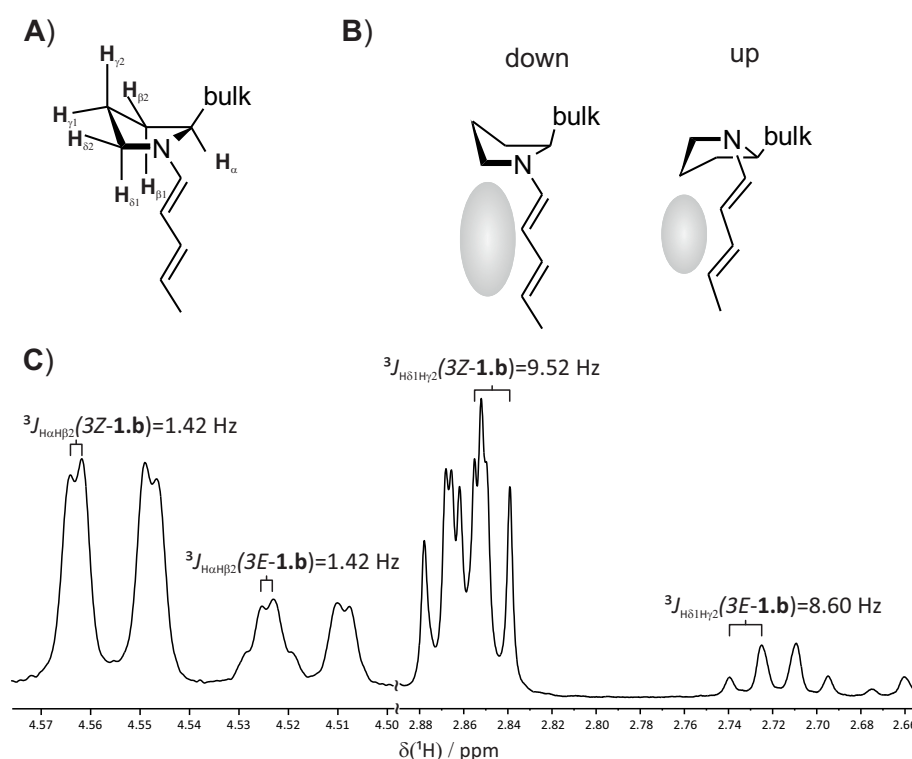


**Fig. 2.4:** **A)** Denomination of protons in the pyrrolidine substructure of the dienamine intermediates. **B)** Representation of the down and up configured pyrrolidine ring in dienamine intermediates with resulting "open" attack space for both conformations (shaded area). *Note:* The "open" attack space is much more pronounced in the intermediate with down conformation. **C)**  ${}^1\text{H}$ -NMR region ( $\text{DMSO-d}_6$ , 300 K) for  $\text{H}_\alpha(3\text{Z-1.b})$  and  $\text{H}_\alpha(3\text{E-1.b})$  as well as  $\text{H}_{\delta 1}(3\text{Z-1.b})$  and  $\text{H}_{\delta 1}(3\text{E-1.b})$  for the determination of coupling constants to deduce pyrrolidine puckering.

The results for the coupling constant analysis are shown in Tab. 2.1. For dienamines **1.a** the coupling constants were found to be  ${}^3J_{\text{H}\alpha,\text{H}\beta 2}$  = 1.55 Hz for **3Z-1.a** and  ${}^3J_{\text{H}\alpha,\text{H}\beta 2}$  = 1.45 Hz for **3E-1.a**, respectively. The  ${}^3J_{\text{H}\delta 1,\text{H}\gamma 2}$  coupling constants for **1.a** were not accessible due to severe signal overlap. For both **3Z-1.b** and **3E-1.b** a coupling constant of  ${}^3J_{\text{H}\alpha,\text{H}\beta 2}$  = 1.42 Hz was identified. The associated  ${}^3J_{\text{H}\delta 1,\text{H}\gamma 2}$  coupling constant was found at 9.52 Hz and 8.60 Hz for **3Z-1.b** and **3E-1.b**, respectively. For the  $\text{CF}_3$ -substituted dienamine **1.c** coupling constants of  ${}^3J_{\text{H}\alpha,\text{H}\beta 2}$  = 2.25 Hz and  ${}^3J_{\text{H}\alpha,\text{H}\beta 2}$  = 2.08 Hz were detected for **3Z-1.c** and **3E-1.c**. The  ${}^3J_{\text{H}\delta 1,\text{H}\gamma 2}$

**Tab. 2.1:** Coupling constants for  $^3J_{H\alpha,H\beta 2}$  and  $^3J_{H\delta 1,H\gamma 2}$  in Hz to determine the pyrrolidine puckering with reference values.<sup>[27]</sup>

entry	dienamine		$^3J_{H\alpha,H\beta 2}$ / Hz	$^3J_{H\delta 1,H\gamma 2}$ / Hz	pyrrolidine puckering
	reference <sup>a</sup>		2-3 7-11	8-12 2-3	down up
1	3Z-	<b>1.a<sup>b</sup></b>	1.55	overlapped	down
2	3E-		1.45		down
3	3Z-	<b>1.b<sup>b</sup></b>	1.42	9.52	down
4	3E-		1.42	8.60	down
5	3Z-	<b>1.c</b>	2.25	8.54	down
6	3E-		2.08	overlapped	down

<sup>a</sup> Reference values taken from Krishnamoorthi and coworkers.<sup>[27]</sup><sup>b</sup> In DMSO-d<sub>6</sub>

coupling constant for 3E-**1.c** was not accessible however for 3Z-**1.c** a coupling constant of  $^3J_{H\delta 1,H\gamma 2}$  = 8.54 Hz was found. All these coupling constants evidence the adoption of *down* puckering in the dienamine intermediates.

This coupling constant patterns are comparable to our findings for enamine intermediates.<sup>[24]</sup> Here, strong preference for the adoption of *down* conformation in the pyrrolidine ring was evidenced as well.

In conclusion we could identify the *down*-conformation of the pyrrolidine ring in both 3Z- and 3E-dienamines to be predominant. This is vital for the adoption of CH/ $\pi$  interactions between pyrrolidine protons and aryl substituents on the catalyst evidenced next.

**Conformation of the exocyclic C <sub>$\alpha$</sub> -C <sub>$\epsilon$</sub>  bond: *sc-exo*, *sc-endo* or *ap*.** The protected ether-substituent of the pyrrolidine ring is assumed to be oriented over one face of the  $\pi$ -system of the dienamine. In order to rationalize this orientation in a comprehensive and conclusive manner, the rotation of the C <sub>$\alpha$</sub> -C <sub>$\epsilon$</sub>  bond was investigated thoroughly by  $^1H$ ,  $^1H$ -NOESY spectroscopy,  $^1H$ ,  $^{19}F$ -HOESY spectroscopy as well as chemical shift analysis. Three conformations are possible for this exocyclic rotation of the C <sub>$\alpha$</sub> -C <sub>$\epsilon$</sub>  bond, namely *ap*, *sc-exo* and *sc-endo* (see Fig. 2.5 **A**). The *sc-exo* conformation leads to an orientation of one aryl ring of the catalyst substructure above the pyrrolidine ring, while the O-protecting group is in close proximity to the diene system. In the *sc-endo* conformation, the O-protecting group is oriented above the pyrrolidine ring, leading to close proximity of one aryl ring with the diene moiety. In the *ap* conformation, again one aryl ring is positioned above the pyrrolidine ring, albeit with the other oriented in close proximity with the diene system. It is generally assumed that stereoelectronic influence of 1,2-electronegativity in di-substituted ethane moieties adopt a synclinal conformation (*gauche* effect) and therefore favor the *sc-endo* and *sc-exo* conformation. However, this does not exclude the *ap* conformation to have a share in the investigated intermediates.

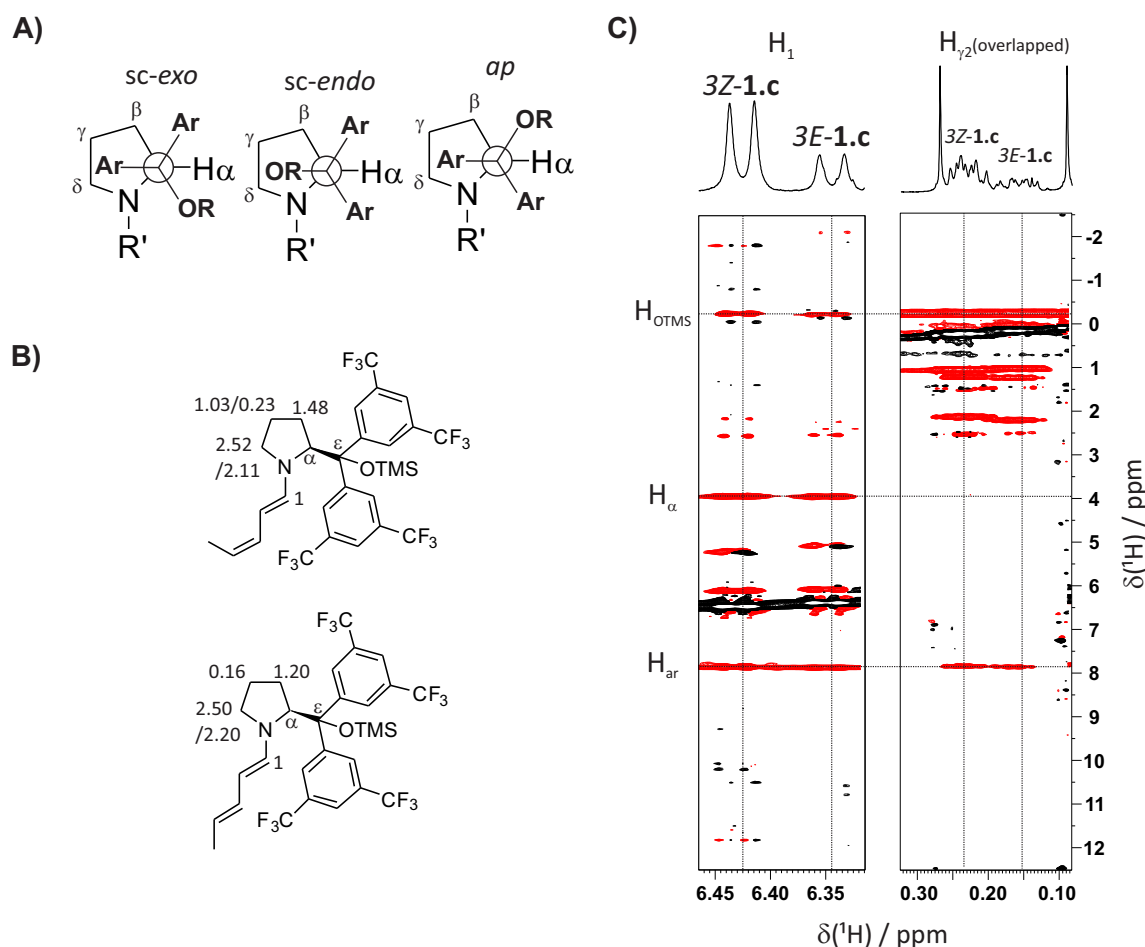


**Fig. 2.5:** **A)** Possible staggered conformation for the  $C_\alpha-C_\epsilon$  bond in the dienamines with denomination. Conformation *sc-exo* would display a strong  $^1H, ^1H$ -NOE contact of proton  $H_1$  with the O-protecting group and possible CH/ $\pi$  interaction of protons in the pyrrolidine ring with one of the aryl substituents. Conformation *sc-endo* would display a strong  $^1H, ^1H$ -NOE contact of some pyrrolidine protons with the O-protecting group and possible CH/ $\pi$  interaction of proton  $H_1$  with one of the aryl substituents. Conformation *ap* would display two possible CH/ $\pi$  interaction of the proton  $H_1$  and some of the pyrrolidine protons with the aryl substituents, additionally it would display the absence of an  $^1H, ^1H$ -NOE contact of proton  $H_1$  with the O-protecting group. **B)** Found chemical shifts (in ppm) for characteristic protons  $H_\gamma$  and  $H_\beta$  and  $H_\delta$  showing strong indications for a possible CH/ $\pi$ -interaction in dienamines **1.c**. **C)**  $^1H, ^1H$ -NOE-traces ( $t_m=450$  ms, 313.15 K, 100 mol% catalyst loading, toluene- $d_8$ ) for protons  $H_1$  and  $H_{\gamma 2}$  for both **3Z-1.c** and **3E-1.c** showing the close proximity of  $H_1$  to the OTMS group ( $H_{OTMS}$ ) and of  $H_{\gamma 2}$  to the aryl protons ( $H_{ar}$ ). Thus it can be concluded the *sc-exo* conformation is adopted by both **3Z-1.c** and **3E-1.c**. Note:  $H_\alpha$  resonance for intensity comparison. Data for catalysts **a** and **b** are shown in Tab. 2.2.

Owing to the *down*-conformation of the pyrrolidine ring (*vide supra*), proton  $H_{\gamma 2}$  is in the case of *sc-exo* and *ap* conformation in close proximity to the aryl substituents on  $C_\epsilon$ . Additionally, it is known that pyrrolidine protons have shown preferences to adopt  $CH/\pi$ -interactions.<sup>[24]</sup>  $^1H, ^1H$ -NOE spectra were used on the model dienamines as visualized in Fig. 2.5 C for dienamine **1.c** to investigate the conformation.  $H_{\gamma 2}$  was found in close proximity to aryl protons  $H_{ar}$ . Additionally, the chemical shift of proton  $H_{\gamma 2}$ (**1.c**) was found to be high-field shifted at around 0.16 ppm and 0.23 ppm providing evidence for the involvement of proton  $\gamma 2$  in  $CH/\pi$  interactions.

The results for all investigated dienamines are collected in Tab. 2.2 and show that for all dienamines independent of the configuration of the second double bond, chemical shifts for protons  $\gamma 2$  were found at low chemical shifts of around 0.1-0.38 ppm proving involvement in  $CH/\pi$ -interactions. Additionally, close proximity of  $H_1$  to the O-protecting group and no low-field shift is observed for protons  $H_1$ . Remarkable shift of protons  $H_\delta$  were identified in comparison to protons  $H_\beta$  with  $\Delta$  values of approx. 1 ppm (for full characterization of the investigated dienamines see the SI 2.3).

**Tab. 2.2:** Chemical shifts (ppm) of characteristic protons  $H_1$ ,  $H_{\gamma 2}$  and  $H_{\delta 2}$ . Relative NOE intensities  $H_1$ - $H_{O\text{-protecting}}$ / $H_1$ - $H_\alpha$  (respective O-protecting group in brackets, see Fig. 2.3). Concluded conformation of the  $C_\alpha$ - $C_\epsilon$  bond in the catalyst substructure for all investigated dienamines.

Dienamine	$H_1$	$H_{\gamma 2}$	$H_{\delta 2}$	$H_1$ - $H_{O\text{-protecting}}$ / $H_1$ - $H_\alpha$	conformation
3Z- <b>1.a</b> <sup>a</sup>	6.41	0.12	2.41	1.63 (O-CH <sub>3</sub> )	<i>sc-exo</i>
3E- <b>1.a</b>	6.33	0.12	2.18	2.44 (O-CH <sub>3</sub> )	<i>sc-exo</i>
3Z- <b>1.b</b> <sup>a</sup>	6.64	0.38	2.62	1.76 (O-Si(CH <sub>3</sub> ) <sub>3</sub> )	<i>sc-exo</i> + <i>sc-endo</i>
3E- <b>1.b</b>	6.54	0.38	2.34	1.94 (O-Si(CH <sub>3</sub> ) <sub>3</sub> )	<i>sc-exo</i> + <i>sc-endo</i>
3Z- <b>1.c</b>	6.43	0.23	2.11	4.78 (O-Si(CH <sub>3</sub> ) <sub>3</sub> )	<i>sc-exo</i>
3E- <b>1.c</b>	6.34	0.16	2.20	4.81 (O-Si(CH <sub>3</sub> ) <sub>3</sub> )	<i>sc-exo</i>
3Z- <b>2.c</b>	6.43	n.d. <sup>b</sup>	n.d.	n.d.	
3E- <b>2.c</b>	6.36	n.d.	n.d.	n.d.	
3Z- <b>3.c</b>	6.46	0.13	2.10	n.d.	<i>sc-exo</i>
3E- <b>3.c</b>	6.39	0.10	2.18	n.d.	<i>sc-exo</i>
<b>4.c</b> <sup>c</sup>	6.40	0.13	2.17	n.d.	<i>sc-exo</i>

<sup>a</sup> in DMSO- $d_6$

<sup>b</sup> not determined

<sup>c</sup> no differentiation between 3Z- and 3E-dienamine possible

Assessing the chemical shift patterns and  $^1H, ^1H$ -NOE contacts identified, preference for *sc-exo* conformation can be assigned to all investigated dienamines for the exocyclic  $C_\alpha$ - $C_\epsilon$  bond. Only this conformation allows the simultaneous shielding of proton  $\gamma 2$  with identified close proximity of those protons with an aryl moiety and close proximity of the proton  $H_1$  with the O-protecting group. Additionally, the de-shielding of the  $\delta$  protons is furthermore evidenc-



ing a CH/ $\pi$  interaction of neighboring protons. Only for **1.b** the shielding of H $_{\gamma 2}$  is not as pronounced, potentially stemming from share of *sc-endo* conformation.

Although the lack of accurate quantum chemical calculations regarding reliable distances of H $_1$  or any pyrrolidine protons to the C $_{\epsilon}$  substituents does not allow for unambiguous quantification, relative NOE intensities can be deduced. This relative NOE assignment should allow to deduce the strength of preference for the adoption of *sc-exo* conformation. Utilizing the H $_1$ -H $_{\alpha}$  (see Fig. 2.3) NOE cross peaks as internal reference, for catalyst **b** the cross peak to the O-protecting group is far less pronounced than in the case of catalyst **c** (see Tab. 2.2). Comparing catalyst **a** is impossible due to the fact that the O-CH $_3$  protecting group in **a** is inherently associated with different distances compared to O-Si(CH $_3$ ) $_3$  in **b** and **c**.

This leads us to believe that, albeit with *sc-exo* conformation for all dienamines in play, the preference in the case of catalyst **c** is much more pronounced than **b**. This is further backed up by the less pronounced shielding of H $_{\gamma 2}$  for dienamines **1.b**. Assuming shielding of one side of the dienamine  $\pi$ -system to be partially responsible for the stereochemical outcome of the  $\gamma$ -functionalization, this finding is in strong agreement with synthesis, since catalyst **c** outperforms catalysts **a** and **b** by far in regards to enantiomeric excess.<sup>[4,9]</sup>

Additionally to  $^1\text{H}$ ,  $^1\text{H}$ -NOE contacts  $^1\text{H}$ ,  $^{19}\text{F}$ -HOE contacts were utilized to gain further insight in the structural preference of the bulky catalyst residue. To this end, dienamine **1.c** was examined in detail.  $^1\text{H}$ ,  $^{19}\text{F}$ -HOE contacts should allow better understanding of steric arrangements in the dienamine structures. The  $^1\text{H}$ ,  $^{19}\text{F}$ -HOE traces for H $_1$  and H $_2$  in *3E*- and *3Z*-**1.c** dienamines are visualized in Fig. 2.6.

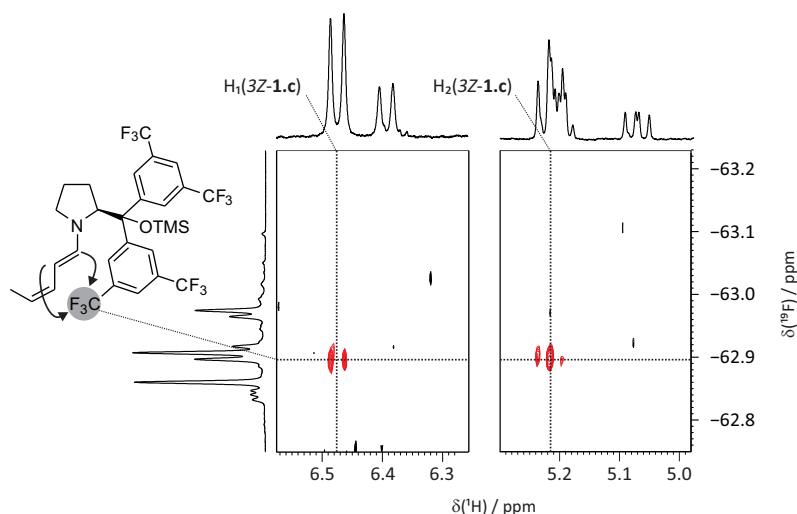


**Fig. 2.6:** Traces of the  $^1\text{H}$ ,  $^{19}\text{F}$ -HOESY ( $t_m=450$  ms, 313.15 K, 100 mol% catalyst loading, toluene- $d_8$ ) for H $_1$ (*3Z*-**1.c**) and H $_2$ (*3Z*-**1.c**) showing HOE contacts to the CF $_3$  group in the catalyst substructure (highlighted region in the structural representation). No such interaction was identified for the corresponding *3E*-**1.c** species, possibly due to the closeness to the detection limit.

For both the H $_1$ (*3Z*-**1.c**) and H $_2$ (*3Z*-**1.c**) a strongly pronounced  $^1\text{H}$ ,  $^{19}\text{F}$ -HOE contact to a CF $_3$  group is identified. This contact proves the close proximity of these protons to the diene system

in the *3Z* configured dienamines. For *3E*-**1.c** no  $^1\text{H}$ ,  $^{19}\text{F}$ -HOE contact is detected, however the detection limit in combination with the lower amount of *3E*-dienamine might alter our ability to detect the cross peak. These identified HOE contacts are in strong agreement with an adoption of *sc-exo* conformation of the exocyclic  $\text{C}_\alpha\text{-C}_\epsilon$  bond (see Fig. 2.5 **A**).

In conclusion, with a combination of  $^1\text{H}$ ,  $^1\text{H}$ -NOE and  $^1\text{H}$ ,  $^{19}\text{F}$ -HOE contacts we could evidence the preference for the adoption of the *sc-exo* conformation for the investigated prolinol-ether derived dienamine species. This preference is evidenced to be more pronounced in the case of catalyst **c** possibly explaining its better performance in synthesis. Most strikingly no different shielding quality could be deduced for both *3E*- and *3Z*-dienamines, which would be vital to validate a pure shielding model for the mode of stereoinduction in dienamine catalysis.

**Conformations in the diene moiety.** Having assessed the conformational preferences in the catalyst moiety, the aldehyde derived diene moiety was addressed next, since its orientation is influencing the stereochemical outcome in prolinol-ether facilitated dienamine catalysis strongly. For this purpose, both single bonds  $\text{N-C}_1$  and  $\text{C}_2\text{-C}_3$  were investigated using  $^1\text{H}$ ,  $^1\text{H}$ -NOE contacts and coupling constant evaluation.

The first dienamine double bond was independently of all employed variations found to adopt *1E* configuration. The second double bond is responsible for the separation in two species *3E* and *3Z*-dienamines. We could, as was in literature before, detect a ratio of 1.1-3:1 for *3Z*:*3E*-dienamines.<sup>[4,8,9]</sup> The matter of separation in *3E* and *3Z*-dienamines will not be discussed in detail in this chapter, is however addressed in chapter 3.

**Conformation of the  $\text{N-C}_1$  single bond: *s-cis* or *s-trans*** The conformation of the  $\text{N-C}_1$  bond exists in two possible conformations termed *s-trans* and *s-cis* conformation (see Fig. 2.7 **A**) with consequently opposite effect on the nature of the shielded side of the dienamine intermediate. In order to investigate this issue, the  $^1\text{H}$ ,  $^1\text{H}$ -NOE pattern of protons  $\text{H}_1$  in the diene moiety and  $\text{H}_\alpha$  and  $\text{H}_\delta$  in the pyrrolidine ring were used to differentiate between the two conformers. The expected  $^1\text{H}$ ,  $^1\text{H}$ -NOE contact pattern is significantly different for both the *s-trans* and *s-cis* conformation of the  $\text{N-C}_1$  bond. A strong  $^1\text{H}$ ,  $^1\text{H}$ -NOE contact for  $\text{H}_1\text{-H}_\alpha$  and a weak  $^1\text{H}$ ,  $^1\text{H}$ -NOE contact for  $\text{H}_1\text{-H}_\delta$  in the case of *s-trans* and the opposite situation in the case of *s-cis* conformation is expected. To illustrate this approach the  $^1\text{H}$ ,  $^1\text{H}$ -NOE trace for model dienamine **1.c** is shown in Fig. 2.7 **B** and shows a strong  $^1\text{H}$ ,  $^1\text{H}$ -NOE contact for  $\text{H}_1(3Z\text{-1.c})\text{-H}_\alpha(3Z\text{-1.c})$  as well as for  $\text{H}_1(3E\text{-1.c})\text{-H}_\alpha(3E\text{-1.c})$  and weak  $^1\text{H}$ ,  $^1\text{H}$ -NOE contacts for  $\text{H}_1(3Z\text{-1.c})\text{-H}_\delta(3Z\text{-1.c})$  as well as for  $\text{H}_1(3E\text{-1.c})\text{-H}_\delta(3E\text{-1.c})$ .

The found quantitative  $^1\text{H}$ ,  $^1\text{H}$ -NOE contact values are summarized in Tab. 2.3. The reference values for expected  $^1\text{H}$ ,  $^1\text{H}$ -NOE intensities from DFT calculations (see coordinates of corresponding structures in the SI 2.3) are 87-90 ( $\text{H}_1\text{-H}_\alpha$ ) to 13-10 ( $\text{H}_1\text{-H}_{\delta 1} + \text{H}_1\text{-H}_{\delta 2}$ ) for the *s-trans* conformation of the  $\text{N-C}_1$  bond in the dienamine intermediates. Dienamines derived from aldehyde **1** with prolinol-methyl-ether catalyst **a** (Tab. 2.3 entries 1 and 2) show a  $^1\text{H}$ ,  $^1\text{H}$ -NOE

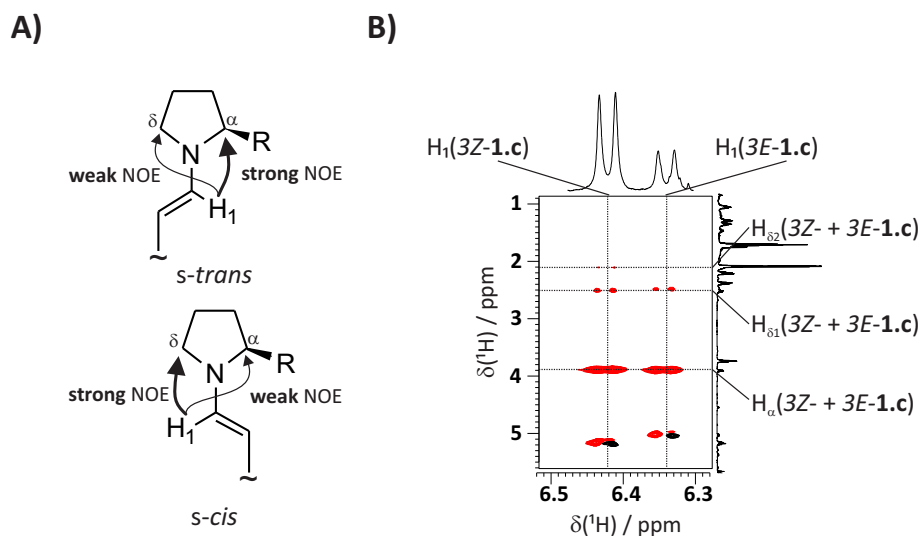


**Fig. 2.7:** **A)** Expected  $^1\text{H}, ^1\text{H}$ -NOE patterns for both the *s-trans* and *s-cis* conformation of the N-C<sub>1</sub> bond in the dienamine structures. Weak NOE contact would be expected for the H<sub>1</sub>-H<sub>δ</sub> or H<sub>1</sub>-H<sub>α</sub> for the *s-trans* and *s-cis* conformation, respectively. Accordingly a strong NOE contact is expected for H<sub>1</sub>-H<sub>δ</sub> and H<sub>1</sub>-H<sub>α</sub> for *s-cis* and *s-trans* configuration, respectively. **B)** NOE trace for H<sub>1</sub>(3E-1.c) and H<sub>1</sub>(3Z-1.c) ( $t_m$ =450 ms, 313.15 K, 100 mol% catalyst loading, toluene- $d_8$ ) showing close contact of protons H<sub>1</sub> with protons H<sub>α</sub> and reduced  $^1\text{H}, ^1\text{H}$ -NOE intensity for the H<sub>1</sub>-H<sub>δ</sub> contact. This is consistent with an adoption of *s-trans* conformation of both 3E- and 3Z-1.c. *Note:* Protons H<sub>α</sub>, H<sub>δ1</sub> and H<sub>δ2</sub> show almost indistinguishable chemical shifts for both 3Z-1.c and 3E-1.c.

intensity distribution of 95:5 and 100:0 for H<sub>1</sub>-H<sub>α</sub>:H<sub>1</sub>-H<sub>δ1</sub>+H<sub>1</sub>-H<sub>δ2</sub> in the case of 3Z-1.a and 3E-1.a, respectively. This corresponds to a >99.9 % *s-trans* conformation share for the 3Z- and 3E configured 1.a dienamine. For dienamines derived from catalyst **b** and **c** except from 2.c, which were not determined, a  $^1\text{H}, ^1\text{H}$ -NOE intensity pattern with resulting exclusive adoption of *s-trans* conformation is evidenced (see Tab 2.3).

The found exclusive *s-trans* conformation of all dienamine species can be explained by the bulkiness of the catalyst residue. Since *sc-exo* conformation of the exocyclic C<sub>α</sub>-C<sub>ε</sub> bond is in play, mostly the O-protecting group is decisive for the steric demand of the catalyst residue in close proximity to the diene moiety.

**Tab. 2.3:** Experimental quantitative relative NOE intensities of  $H_1-H_\alpha$  and  $H_1-H_{\delta 1}+H_1-H_{\delta 2}$  (the sum of NOE cross peak intensities  $H_1-H_\alpha$ ,  $H_1-H_{\delta 1}+H_1-H_{\delta 2}$  was set to 100) for all investigated dienamines at 100 mol% catalyst loading. NOE references were calculated from quantum chemical structures at a B3LYP/6-31G(d) level of theory by equation 2.1. The stationary point coordinates can be found in the SI (2.3) *Note:* NOE peaks were quantified by integrating 2D-NOE spectra and manual area selection.

Entry	dienamine	NOE intensity <sup>a</sup>		conformation / % <i>s-trans</i>
	reference	$H_1-H_\alpha$ 87-90 <sup>b</sup>	$H_1-H_{\delta 1}+H_1-H_{\delta 2}$ 13-10 <sup>b</sup>	100
1	3Z- <b>1.a</b> <sup>c</sup>	95	5	> 99.9
2	3E- <b>1.a</b> <sup>c</sup>	100	0 <sup>d</sup>	> 99.9
3	3Z- <b>1.b</b> <sup>c</sup>	100	0 <sup>d</sup>	> 99.9
4	3E- <b>1.b</b> <sup>c</sup>	100	0 <sup>d</sup>	> 99.9
5	3Z- <b>1.c</b> <sup>e</sup>	95	5	> 99.9
6	3E- <b>1.c</b> <sup>e</sup>	97	3	> 99.9
7	3Z- <b>2.c</b>		n.d. <sup>f</sup>	
8	3E- <b>2.c</b>		n.d.	
9	3Z- <b>3.c</b>	90	10	~ 99.9
10	3E- <b>3.c</b>	89	11	98.9
11	<b>4.c</b> <sup>g</sup>	95	5	> 99.9

<sup>a</sup> Sum of both crosspeaks is set to 100

<sup>b</sup> Reference calculated using equation 2.1 and distances by quantum-chemical calculations, coordinates can be found in the SI (2.3)

<sup>c</sup> In deuterated DMSO

<sup>d</sup> no cross peak identified

<sup>e</sup> T=313.15K

<sup>f</sup> Not determined

<sup>g</sup> No differentiation between 3Z- and 3E-dienamine possible

**Conformation of the C<sub>2</sub>-C<sub>3</sub> single bond: *s-cis* or *s-trans*** As above, the C<sub>2</sub>-C<sub>3</sub> single bond exists in two possible conformations, termed *s-cis* and *s-trans* (see Fig. 2.8 A for schematic representation) again with two completely opposite effects on the supposedly exposed face. In order to differentiate the two conformers, not <sup>1</sup>H, <sup>1</sup>H-NOE contacts, but rather coupling constant analysis was utilized. <sup>1</sup>H, <sup>1</sup>H-NOE contacts were not easily accessible due to signal overlap. Literature references allow the unambiguous assignment of either the *s-trans* or *s-cis* conformation of single bonds framed in a diene-system.<sup>[28]</sup> The reference values for a *s-trans* conformation are found to be <sup>3</sup>J<sub>H,H</sub>=10-11 Hz and for a *s-cis* conformation at <sup>3</sup>J<sub>H,H</sub>=6-7 Hz. Although strongly crowded, coupling values can be deduced from <sup>1</sup>H-NMR spectra for the investigated dienamine species, exemplarily shown for dienamines **3Z-1.c** and **3E-1.c** in Fig. 2.8 B.

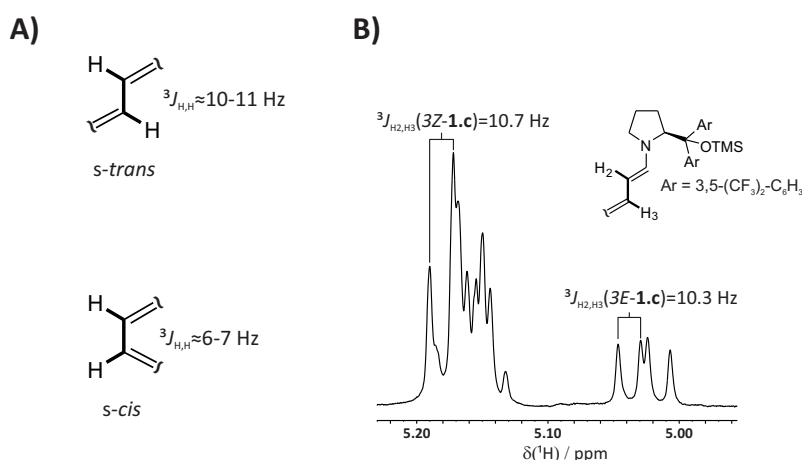


**Fig. 2.8:** **A)** Possible single bond conformations of the C<sub>2</sub>-C<sub>3</sub> dienamine single bond with associated expected coupling constants according to literature.<sup>[28]</sup> *S-trans* configuration would result in coupling constants of <sup>3</sup>J<sub>H<sub>2</sub>,H<sub>3</sub></sub>=10-11 Hz, *s-cis* configuration in a coupling constant of <sup>3</sup>J<sub>H<sub>2</sub>,H<sub>3</sub></sub>=6-7 Hz. **B)** Excerpt of the <sup>1</sup>H-NMR spectrum of dienamine **1.c** in toluene-d<sub>8</sub> at 313.15 K for the H<sub>2</sub> resonances of both **3E-** and **3Z-1.c** dienamines. Coupling constants are found at <sup>3</sup>J<sub>H<sub>2</sub>,H<sub>3</sub></sub>(**3Z-1.c**)=10.7 Hz and <sup>3</sup>J<sub>H<sub>2</sub>,H<sub>3</sub></sub>(**3E-1.c**)=10.3 Hz evidencing the adoption of a *s-trans* conformation for the C<sub>2</sub>-C<sub>3</sub> single bond for both **3E-** and **3Z-1.c** dienamine species.

For all investigated dienamines the H<sub>2</sub>-H<sub>3</sub> coupling constants are summarized in Tab. 2.4. All <sup>3</sup>J<sub>H<sub>2</sub>,H<sub>3</sub></sub> values for the dienamines are found at 10.2 Hz (entry 7 in Tab. 2.4) up to 11.4 Hz (entry 1 in Tab. 2.4). These coupling constants all correspond to a *s-trans* conformation of the investigated single bond.

The exclusive adoption of an *s-trans* conformation of the C<sub>2</sub>-C<sub>3</sub> bond is explained by a resulting steric repulsion of protons 2 and 3 in an *s-cis* conformer.<sup>[29]</sup> The barrier of rotation of such a diene centered single bond is approximately 33.5 kJ mol<sup>-1</sup> and thus a rotation or even a share of *s-cis* conformation is not to be expected. Additionally, favorable overlap of the HOMO orbitals with a minimized dipole moment are only present in the *s-trans* and not in the *s-cis* diene species.<sup>[29]</sup>

In summary, we could prove the predominant adoption of *s-trans* conformations for both the

**Tab. 2.4:** Reference<sup>[28]</sup> and experimental coupling constants  $^3J_{\text{H}_2,\text{H}_3}$  in Hz for all investigated dienamine species with resulting concluded conformation of the C<sub>2</sub>-C<sub>3</sub> single bond.

entry	dienamine		$^3J_{\text{H}_2,\text{H}_3}$ / Hz	conformation
	reference <sup>a</sup>		10-11	<i>s-trans</i>
1	3 <i>Z</i>	<b>1.a<sup>b</sup></b>	11.4	<i>s-trans</i>
2	3 <i>E</i>		10.5	<i>s-trans</i>
3	3 <i>Z</i>	<b>1.b<sup>b</sup></b>	11.3	<i>s-trans</i>
4	3 <i>E</i>		10.3	<i>s-trans</i>
5	3 <i>Z</i>	<b>1.c</b>	10.7	<i>s-trans</i>
6	3 <i>E</i>		10.3	<i>s-trans</i>
7	3 <i>Z</i>	<b>2.c</b>	10.2	<i>s-trans</i>
8	3 <i>E</i>		11.1	<i>s-trans</i>
9	3 <i>Z</i>	<b>3.c</b>	11.1	<i>s-trans</i>
10	3 <i>E</i>		10.1	<i>s-trans</i>
11		<b>4.c<sup>c</sup></b>	10.8	<i>s-trans</i>

<sup>a</sup> Reference values taken from Reich et al.<sup>[28]</sup><sup>b</sup> In DMSO-*d*<sub>6</sub><sup>c</sup> No differentiation between 3*Z*- and 3*E*-dienamine possible

first (N-C<sub>1</sub>) and second (C<sub>2</sub>-C<sub>3</sub>) diene subsystems single bonds in both 3*E*- and 3*Z*-dienamines. These findings are of utmost importance for the conclusive description of the orientation of the catalyst residue within the intermediates.

**Quantum chemical calculations on the dienamine structures.** Besides experimental data, quantum chemical calculations were performed to further our insight into the structural features of the dienamine intermediates. This was especially necessary, since previously reported quantum chemical calculations could not be compared to experimental structural preferences at all.<sup>[4,9]</sup> Additionally, the relative stabilities found in the dienamine calculations always favored 3*E*-dienamines significantly, which is in strong disagreement with the literature<sup>[4,9]</sup> and our findings (see chapter 3). Due to our structural findings we expected close proximity of the CF<sub>3</sub> group to the diene system and were aware of possible non-covalent interactions in this position. In addition, CH/π-interactions were also evidenced experimentally. To account for these possibilities we employed a quantum chemical method which is designed to account for dispersive and non-covalent interactions, namely PBE0-D3/def2-SVP.<sup>[30–37]</sup> The minimum structures (2.9 **A**), together with schematic representation of the identified C<sub>α</sub>-C<sub>ε</sub> conformation (2.9 **B**) are depicted in Fig. 2.9.

The structures identified as minima were both in the *sc-exo* conformation, which is identical to our experimental findings. The diene-substructure was evidencing *s-trans* conformation for both, the N-C<sub>1</sub> and C<sub>2</sub>-C<sub>3</sub> bonds. The pyrrolidine puckering was again, as found in the

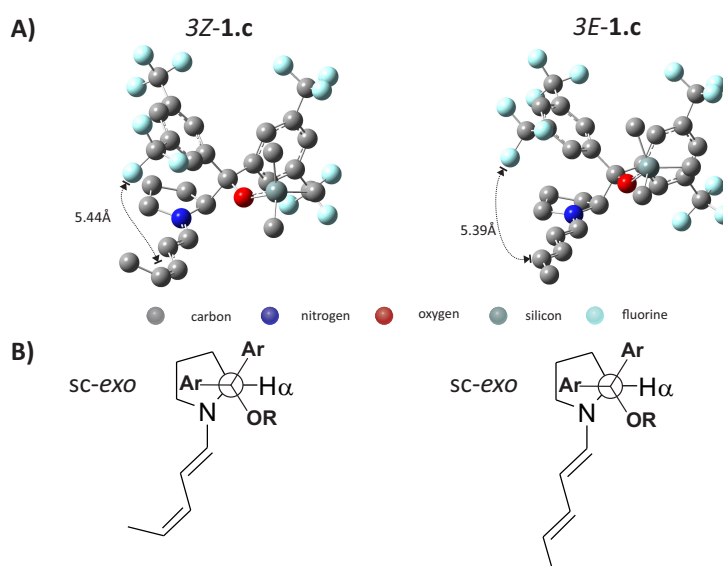


**Fig. 2.9:** **A)** Minimum structures found at a PBE0-D3/def2-SVP level of theory<sup>[30–37]</sup> for both, the 3Z-1.c and 3E-1.c dienamine structures. Found intramolecular distance of the closest catalyst group to Carbon C<sub>4</sub>, the point of further reaction. **B)** Identified *sc-exo* conformation of the exocyclic C<sub>α</sub>-C<sub>ε</sub> bond in both structures. Additionally, all minimized structures were found to be in the *down* conformation of the pyrrolidine puckering, with *s-trans* conformation of the N-C<sub>1</sub> as well as the C<sub>2</sub>-C<sub>3</sub> bond. The energy difference between both structures was found to be  $\Delta G^{298} = 14.2 \text{ kJ}\cdot\text{mol}^{-1}$  with preference for the 3Z-1.c dienamine structure. *Note:* Hydrogen atoms omitted for clarity.

NMR spectroscopic investigations, evidenced to adopt *down* conformation. Interestingly the energy difference for the both minimum structures 3Z-1.c and 3E-1.c was calculated to be  $\Delta G^{298} = 14.2 \text{ kJ}\cdot\text{mol}^{-1}$  in favor of the 3Z-dienamine structure. The distances of the closest catalyst moiety, a CF<sub>3</sub> group to the  $\gamma$ -C<sub>4</sub> are 5.44 Å and 5.39 Å in 3Z-1.c and 3E-1.c, respectively, evidencing no quality difference in shielding of this position.

Successfully calculating the experimental structures in quantum chemical calculations can be largely attributed to the use of a theoretical method to include non-covalent, dispersive interactions. This is especially evidenced by the found orientation of one aryl-group over the proton H<sub>γ</sub> in the *down* puckered pyrrolidine ring evidencing CH/π interactions, which was also found in experiments.

In conclusion, the quantum chemical calculations do evidence all of our experimental findings and besides the configuration of the second double bond, identical structural preferences and features are identified for 3Z- and 3E-dienamines. In addition, the found distance of the bulky catalyst residue to the point of stereoiduction at C<sub>4</sub> is identical for both 3Z- and 3E-dienamines and thus no difference in quality of shielding is active in the two configuration isomers.

## Conclusion

In summary, we have investigated the structural preferences of reactive dienamine intermediates derived of  $\alpha,\beta$ -unsaturated aldehydes and prolinol-ether organocatalysts of the Jørgensen-Hayashi type by *in situ* NMR spectroscopy and quantum chemical calculations. The dienamines were evidencing strong conformational preferences in both, the catalyst as well as the aldehyde substructure. The catalyst substructure, by means of coupling constant analysis,  $^1\text{H},^1\text{H}$ -NOESY spectroscopy and  $^1\text{H},^{19}\text{F}$ -HOESY spectroscopy, was found to be in the *down* conformation for the pyrrolidine puckering and preference for *sc-exo* conformation for the exocyclic  $\text{C}_\alpha\text{-C}_\epsilon$  bond was evidenced to be dependent on the catalyst substructure, with the  $\text{CF}_3$  substituted catalyst showing the highest preference. In the diene-system the single bonds are identified to adopt exclusively the *s-trans* conformation. Most strikingly, we could evidence that absolutely no difference in quality of the shielding for both *3Z*- and *3E*-dienamines is present (see Fig. 2.10). This in combination with the detected ratio of 1.1-3:1 of *3Z*:*3E*-dienamine strongly hints to the invalidity of a pure shielding model for the mode of stereoinduction in dienamine catalysis.

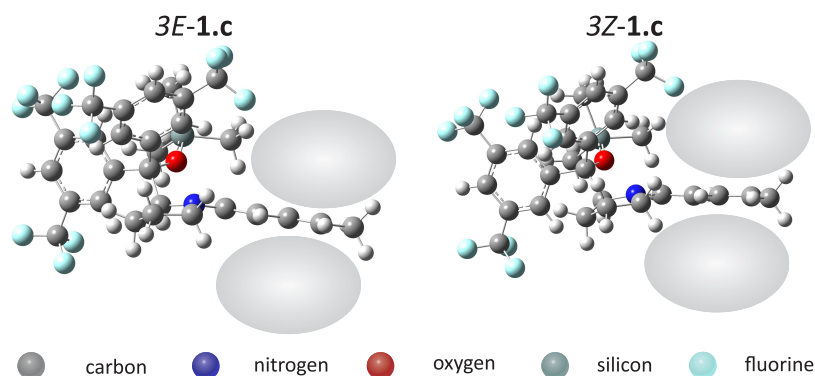


**Fig. 2.10:** Representation of the quality of shielding in both *3E*- and *3Z*-dienamines. Highlighted region represent open space for the subsequent attack on an electrophile. Absolutely no difference in the quality of shielding is present for the configurational isomers.



## Experimental Section

### NMR measurements

Dienamines were created *in situ* inside standard 5 mm NMR tubes by addition of freshly distilled aldehyde (25  $\mu$ mol) to a solution of organocatalyst (1 equiv.) and additive (as stated) in deuterated solvent (0.5 mL). All chemicals were used as purchased (if not otherwise stated). Chemicals were purchased from Sigma Aldrich and TCI Europe. NMR measurements were performed at 300–315 K on a Bruker Avance III HD 600 (600.13 MHz), a Bruker Avance DRX 600 (600.13 MHz) and a Bruker Avance III 600 (600.25 MHz) spectrometer, the latter equipped with a TCI cryoprobe with z-gradient (53.5 G cm<sup>-1</sup>). Reaction monitoring (*react*-NMR) by 1D <sup>1</sup>H-NMR spectra was employed to identify appropriate time slots for more detailed 2D NMR spectroscopic investigations. <sup>1</sup>H,<sup>1</sup>H-COSY, <sup>1</sup>H,<sup>1</sup>H-NOESY ( $t_m$ =450 ms), <sup>1</sup>H,<sup>13</sup>C-HSQC (<sup>1</sup> $J_{\text{HC}}$ =145 Hz) and <sup>1</sup>H,<sup>13</sup>C-HMBC (long range coupling 10 Hz) as well as <sup>1</sup>H,<sup>19</sup>F-HOESY ( $t_m$ =450 ms) spectra were recorded for the characterization of the observed species if information from the 1D NMR spectra proved to be insufficient. Kinetic data was processed with Bruker Dynamics Center 2. All spectra were processed and evaluated with Bruker Topspin 3.2.

### Quantum chemical calculations

The geometries were optimized at PBE0-D3/def2-SVP<sup>[30–32]</sup> level of theory. Thermochemical analysis was also performed at geometry optimization level and added to the total energy. Single points were calculated at SCS-RIMP2/aug-TZVP<sup>[34–36]</sup> level of theory using split-J for the coulomb term and semi numerical approximation (RIJCOSX)<sup>[37]</sup> for the exchange term for the reference wavefunction. The software used were Gaussian09 subversion D.01<sup>[38]</sup> for the geometry optimization and frequency analysis, as well as ORCA-3.0.3<sup>[39]</sup> for the single point calculations.

## 2.3 Supporting Information

### NMR-Assignments

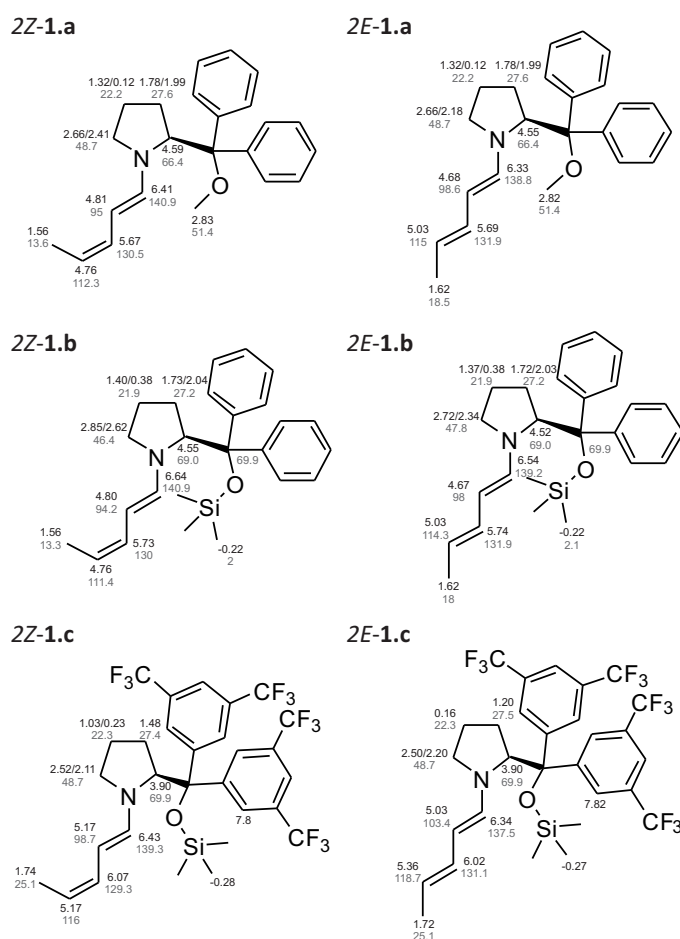


**Fig. 2.11:**  $^1\text{H}$  and  $^{13}\text{C}$ -chemical shifts of dienamines **1.a** (DMSO- $d_6$ , 300 K), **1.b** (DMSO- $d_6$ , 300 K), **1.c** (toluene- $d_8$ , 313.15 K). *Note:*  $^1\text{H}$ -chemical shifts in black,  $^{13}\text{C}$ -chemical shifts in grey.

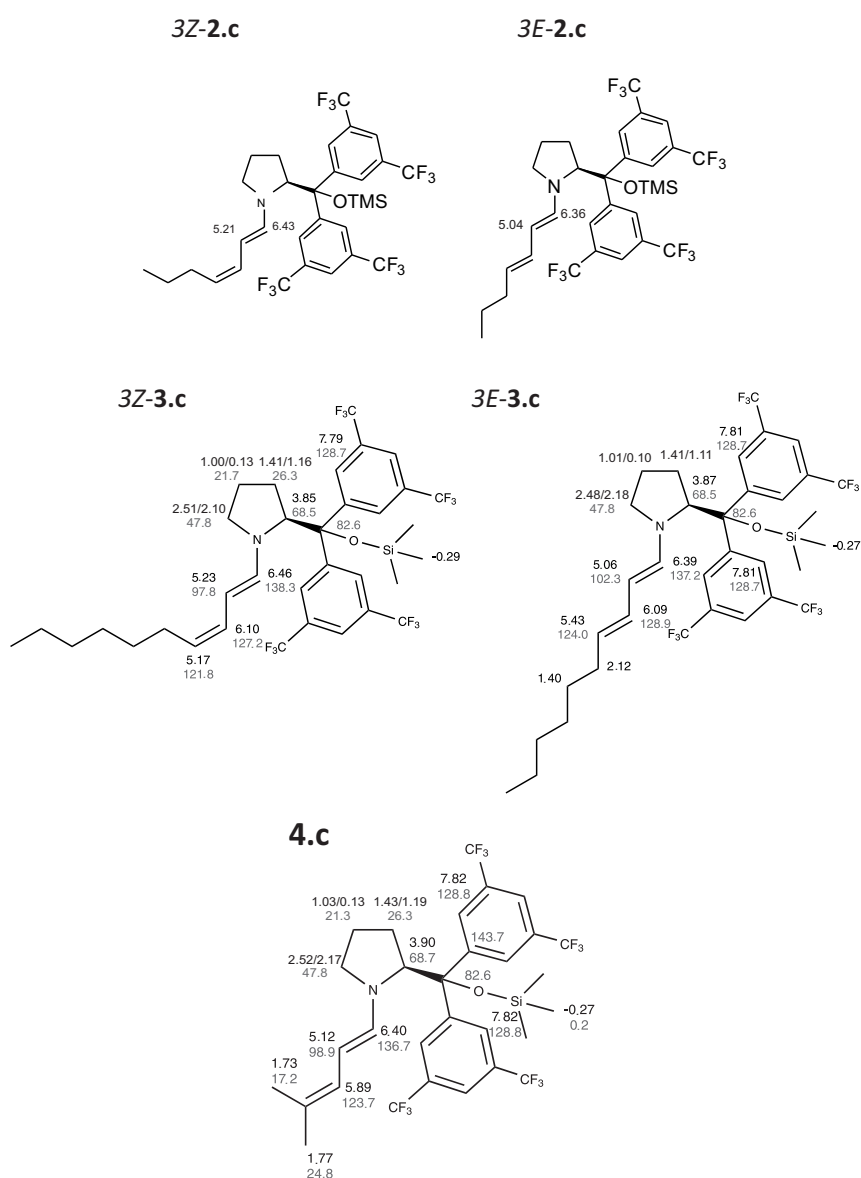


**Fig. 2.12:**  $^1\text{H}$  and  $^{13}\text{C}$ -chemical shifts of dienamines **2.c** (toluene- $\text{d}_8$ , 313.15 K), **3.c** (toluene- $\text{d}_8$ , 318 K) and **4.c** (toluene- $\text{d}_8$ , 318 K). *Note:*  $^1\text{H}$ -chemical shifts in black,  $^{13}\text{C}$ -chemical shifts in grey.

**<sup>1</sup>H,<sup>1</sup>H-NOE reference value calculation and coordinates of stationary points at B3LYP/6-31G(d)<sup>[40]</sup> level of theory**

The calculation of  $^1\text{H}, ^1\text{H}$ -NOE reference values for the *s-trans* dienamine was achieved via:

$$\begin{aligned}
I_{a-b}^{NOE} &\propto r_{ab}^{-6} \\
I_{\delta_1-H1} + I_{\delta_2-H1} + I_{\alpha-H1} &\stackrel{!}{=} 100 \\
\frac{I_{\delta_1-H1} + I_{\delta_2-H1}}{I_{\alpha-H1}} &= \frac{(r_{\delta_1-H1})^{-6} + (r_{\delta_2-H1})^{-6}}{(r_{\alpha-H1})^{-6}} \quad (2.1)
\end{aligned}$$

using distances from DFT calculations. The stationary points for the reference dienamines are given for three different conformations of the exocyclic conformation of the  $C_{\alpha}$ - $C_{\epsilon}$ -bond in the following.

**ap-3E-1.c**,  $r_{H1-H\alpha}=2.42511\text{\AA}$ ,  $r_{H1-H\delta1}=3.63863\text{\AA}$ ,  $r_{H1-H\delta2}=3.88176\text{\AA}$

```
1\1\GINC-LX64A476\F0pt\RB3LYP\6-31G(d)\C29H29F12N10Si1\DI56F0V\27-Apr
-2014\0\#\P b3lyp/6-31G(D) scf=tight opt\Title\0,1\C,-0.3890781687,-
0.2433725702,-0.2358428036\C,-0.4398243895,-0.4263789837,1.2969873964\
C,0.7246855328,0.4166642386,1.8477113784\C,1.7685433245,0.3922601829,0
.7221706438\H,-0.6314243564,-1.1923120448,-0.726609549\H,-1.4104385183
,-0.1525944595,1.7138180282\H,-0.2752112557,-1.4862035388,1.5214071708
\H,0.4017225906,1.4413516871,2.0503058388\H,1.1260672559,0.0101046782,
2.7805979035\H,2.3113206793,1.3421934939,0.6382209934\H,2.5164084911,-
0.4030524006,0.8667309858\N,0.9987129756,0.1189533454,-0.4957703628\C,
1.6476711109,-0.2149340558,-1.6686524264\H,1.0003079336,-0.6374161434,
-2.4326850145\C,2.9685917583,-0.0611258068,-1.9316966044\H,3.628644275
2,0.3780044467,-1.1867562903\C,3.5623566362,-0.45666924,-3.1940080332\
H,2.8834749898,-0.8925471701,-3.9309408628\C,4.8618034833,-0.330924671
6,-3.5193574083\H,5.5454621125,0.1028985088,-2.7874801029\C,-1.4716730
793,0.7945872743,-0.7899360354\C,-1.2056380178,2.1714054312,-0.1701152
068\C,-2.0633756667,2.6865077905,0.80517842\C,-0.048622444,2.901333762
8,-0.4826545281\C,-1.7877325328,3.897821371,1.4422226268\H,-4.32984718
51,1.7943916278,-2.8412445645\C,0.2352576506,4.1021740759,0.172104856\
H,0.6457243091,2.5322657064,-1.2279447946\C,-0.6321720292,4.6142533915
,1.1355260761\H,-0.4146097107,5.5529812251,1.6300334037\C,-1.479792282
5,0.8003704027,-2.3358177066\C,-1.6859464337,-0.4166136605,-3.00226596
08\C,-1.3821354528,1.9570835699,-3.1159000559\C,-1.7725371405,-0.47669
08858,-4.3925242744\H,-6.3381604752,0.4125060499,0.7424618801\C,-1.470
1066671,1.8965390065,-4.5097967996\H,-1.2445636245,2.9246630616,-2.650
5558756\C,-1.6619821027,0.6811696708,-5.1611854931\H,-1.7226701415,0.6
357460335,-6.2415928641\0,-2.7079117958,0.2626967969,-0.3322121669\Si,
-4.3489116444,0.3762733384,-0.7530340369\C,-4.8758257451,-1.2230633559
,-1.600499915\H,-4.435933814,-1.3562201849,-2.5941725634\H,-4.60224573
73,-2.0939099653,-0.9924630772\H,-5.9667339694,-1.2397084172,-1.720583
8721\C,-4.7407004992,1.8745758738,-1.8301266702\H,-4.3680603081,2.8053
177255,-1.387510029\H,-5.8301431715,1.9712653721,-1.9234005781\H,-2.94
52209953,2.1277852964,1.0847004902\C,-5.2564722098,0.5170066902,0.8941
229639\H,-4.9438013952,-0.2725350977,1.5873349926\H,-5.090312988,1.481
7000466,1.3876506572\H,-1.7969018036,-1.3335095684,-2.4347957407\C,-1.
4330420574,3.1795839753,-5.3009648072\F,-1.085102844,2.9684082344,-6.5
871248357\F,-2.6451815943,3.7815674061,-5.3081509681\F,-0.5582620989,4
.0635201961,-4.7770014203\C,-2.0478435766,-1.8079897817,-5.0411145939\
F,-1.2937294296,-2.7882313767,-4.4973428429\F,-3.3430715108,-2.1746994
994,-4.8733280443\F,-1.8072946053,-1.7907020978,-6.3664361373\C,1.5289
646476,4.8034363468,-0.1502713727\F,1.713055894,4.9199288062,-1.482187
```

4309\F,1.5869339688,6.0405143714,0.3829299058\F,2.5905465122,4.1089690  
 655,0.3313478532\C,-2.7214832314,4.3864894021,2.5185235633\F,-2.436343  
 6122,3.8245890648,3.7154648664\F,-2.6497593739,5.7238626477,2.67990625  
 2\F,-4.0093298253,4.0764746237,2.2386726067\C,5.4637130764,-0.74396500  
 19,-4.8300299384\H,5.9311924498,0.1064707935,-5.3468860876\H,6.2543565  
 151,-1.4958077767,-4.6936905036\H,4.7093953379,-1.1698473515,-5.501250  
 5028\\Version=AM64L-G09RevD.01\State=1-A\HF=-2740.1874618\RMSD=4.060e-  
 09\RMSF=2.488e-06\Dipole=-0.6735284,-0.7141373,0.6470911\Quadrupole=3.  
 3512947,-3.063506,-0.2877887,0.9060116,3.317213,-4.468379\PG=C01 [X(C2  
 9H29F12N101Si1)]\@

**sc-exo-3E-1.c**,  $r_{H1-H\alpha}=2.39017\text{\AA}$ ,  $r_{H1-H\delta1}=3.64082\text{\AA}$ ,  $r_{H1-H\delta2}=3.86651\text{\AA}$

1\1\GINC-LX64A483\F0pt\RB3LYP\6-31G(d)\C29H29F12N101Si1\DI56FOV\26-Apr  
 -2014\0\#P b3lyp/6-31G(D) scf=tight opt\\Title\\0,1\C,0.1719429284,-0  
 .4406652657,-0.6232888495\C,0.6938818717,-1.1686986047,0.6381772531\C,  
 1.4830845107,-0.1100327472,1.4316030062\C,2.011406711,0.8394627278,0.3  
 497867084\H,0.2724886108,-1.0763577501,-1.5105078041\H,-0.1019482732,-  
 1.630865068,1.228141766\H,1.3639515433,-1.9755309956,0.3210765835\H,0.  
 8319097731,0.4203986724,2.1313848383\H,2.2949675671,-0.5542279314,2.01  
 47998178\H,2.0633716983,1.8801435048,0.6932804299\H,3.0227209819,0.555  
 8024037,0.015882086\N,1.0694604474,0.7052871972,-0.761809648\C,1.37877  
 37871,1.2405622985,-1.9972564432\H,0.718447016,0.9101149608,-2.7924103  
 335\C,2.3753050763,2.1190989437,-2.2690363936\H,3.0186083407,2.4744869  
 426,-1.4694203479\C,2.6022038324,2.6193918961,-3.6119529587\H,1.914455  
 1735,2.2366328464,-4.3682073105\C,3.5479626808,3.4862096785,-4.0264214  
 707\H,3.5609542695,3.7457613075,-5.0845411415\C,-1.3578978523,-0.02264  
 63876,-0.6105552552\C,-2.2892267305,-1.240455671,-0.4282067575\C,-1.92  
 10838135,-2.5233575643,-0.8593566643\C,-3.5918696915,-1.0680082159,0.0  
 53681219\C,-2.8206040041,-3.5880043016,-0.8023269464\H,-4.0164177027,-  
 1.4463287852,-2.9976259076\C,-4.4974558568,-2.1304331171,0.0966845099\  
 H,-3.9172778513,-0.091860708,0.3929319327\C,-4.1190800863,-3.400868401  
 5,-0.3267563905\H,-4.8185039845,-4.2272417066,-0.2888123232\C,-1.58500  
 42156,1.0611148257,0.4532062821\C,-1.806663467,0.748705422,1.799620297  
 1\C,-1.4918860448,2.4095270571,0.0974394158\C,-1.9360507571,1.75640982  
 ,2.7582278765\H,-4.8886078073,1.1012634464,-1.4309166939\C,-1.66099342  
 43,3.4153790882,1.0506987631\H,-1.2879245376,2.6731190065,-0.932469304  
 1\C,-1.8774519345,3.099493661,2.3901140055\H,-2.0002478096,3.880515314  
 6,3.1299408736\O,-1.571629881,0.5230421168,-1.9097609837\Si,-2.8828382  
 208,0.8090186272,-2.9467458564\C,-2.1122777912,1.8933467071,-4.2772926  
 776\H,-1.7363309464,2.8359822608,-3.8637232424\H,-2.8468040747,2.13969  
 06845,-5.0538122261\H,-1.2714763402,1.3867756122,-4.7649511308\C,-3.50  
 51266482,-0.797554802,-3.7161933728\H,-2.6827394062,-1.3704277383,-4.1  
 602510069\H,-4.2181142019,-0.5706842046,-4.5193479784\H,-0.9287631669,  
 -2.7134355595,-1.2478213206\C,-4.3106651257,1.7281480112,-2.1179723853  
 \H,-3.9743565506,2.6175596403,-1.5731718076\H,-5.0039268145,2.06843635  
 85,-2.8986177263\H,-1.8861823795,-0.2853390886,2.1180176833\C,-1.64781

44243,4.8473197747,0.5837774405\F,-1.6920032511,5.7218040841,1.6096260  
587\F,-0.5452890663,5.1235385953,-0.1437400711\F,-2.7148301855,5.10343  
09341,-0.2123535745\C,-2.0737436784,1.3596055758,4.2036884663\F,-0.890  
525242,0.9181129888,4.6974064747\F,-2.4745073692,2.384508843,4.9814141  
504\F,-2.9599524573,0.3517366653,4.3619109455\C,-5.8829114596,-1.86996  
89807,0.6296514473\F,-6.4202235773,-0.7627720018,0.0632096934\F,-6.721  
6674832,-2.8972977033,0.3915737731\F,-5.8682435881,-1.656976666,1.9631  
517858\C,-2.410442646,-4.9369338478,-1.3368682668\F,-1.0849123208,-5.1  
522021447,-1.1883708345\F,-3.0617497351,-5.9404889302,-0.7127006518\F,  
-2.6833082332,-5.0455510991,-2.656504877\C,4.6048118349,4.1501802851,-  
3.1903661038\H,5.611957636,3.9057734234,-3.5571110779\H,4.5159857652,5  
.2449960378,-3.2346600601\H,4.5581010538,3.8583387411,-2.1370594072\\V  
ersion=AM64L-G09RevD.01\State=1-A\HF=-2740.1836135\RMSD=5.447e-09\RMSF  
=7.493e-06\Dipole=0.1082418,-0.6171017,-0.1042754\Quadrupole=2.7408835  
, -4.7046923,1.9638088,-4.062726,9.2241794,-0.0914881\PG=C01 [X(C29H29F  
12N101Si1)]\\@

**sc-endo-3E-1.c**,  $r_{H1-H\alpha}=2.30016\text{\AA}$ ,  $r_{H1-H\delta1}=3.59389\text{\AA}$ ,  $r_{H1-H\delta2}=3.92863\text{\AA}$

1\1\GINC-LX64A390\F0pt\RB3LYP\6-31G(d)\C29H29F12N101Si1\DI56F0V\25-Apr  
-2014\0\0\#P b3lyp/6-31G(D) scf=tight opt\\Title\\0,1\C,0.0098370386,-0  
.0621213961,-0.2841534004\C,-0.4075074062,-0.3571783627,1.1761450279\C  
,0.8964733542,-0.2376137142,1.9821353259\C,1.9736577189,-0.7231302553,  
1.0021592481\H,-0.5780514756,-0.6644541836,-0.9853188849\H,-1.19264806  
15,0.3062277421,1.5429525858\H,-0.7892317175,-1.3836898671,1.224161434  
7\H,1.0700161459,0.8033218294,2.2617259509\H,0.8805387887,-0.839713692  
,2.8956204733\H,2.9233409601,-0.1849261343,1.1182163539\H,2.1886437974  
, -1.7951442629,1.1295797676\N,1.3978053467,-0.5070360103,-0.3292278022  
\C,1.8980671125,-1.2017140884,-1.4169103918\H,1.2430131111,-1.19691937  
66,-2.2856785076\C,3.0914201391,-1.837899185,-1.4911889298\H,3.7718855  
559,-1.8252987489,-0.6423577803\C,3.5314493609,-2.5385025516,-2.682297  
4255\H,2.8451070441,-2.5250722935,-3.5321463059\C,4.7007472123,-3.1900  
667326,-2.8150579878\H,5.3900530301,-3.2061732238,-1.9689332558\C,-0.2  
469968061,1.4610606903,-0.6961321316\C,0.3602494376,1.7922330701,-2.07  
93963572\C,1.7579170667,1.7734256109,-2.2138438699\C,-0.3939865259,2.1  
673261046,-3.1963329965\C,2.3712196037,2.0946110494,-3.4235729294\H,-0  
.8351619663,4.9752768056,-0.9468535942\C,0.2232668977,2.4938147782,-4.  
4080242687\H,-1.4729026986,2.2277481832,-3.1425259108\C,1.6085124681,2  
.4554076059,-4.534432101\H,2.0853758569,2.7088670874,-5.4738065737\C,-  
1.7782969085,1.642964927,-0.6602380944\C,-2.3713680344,2.5296506512,0.  
2408476508\C,-2.6266797948,0.8763111499,-1.4743983747\C,-3.757919719,2  
.6779645403,0.3059740845\H,0.5894464291,3.6877914467,2.929988832\C,-4.  
0135847453,1.0225934912,-1.4083438523\H,-2.2173027299,0.1691522006,-2.  
1876643287\C,-4.5918637535,1.9303991457,-0.5218060788\H,-5.6675115991,  
2.0559772009,-0.4844306308\O,0.3730126173,2.2597839946,0.2982496686\Si  
,0.9272440868,3.8575472875,0.4550080873\C,2.812075269,3.8622782247,0.4  
66756162\H,3.2547029764,3.6055725629,-0.5001226791\H,3.1774376861,4.85

97654013,0.7427729162\H,3.2010379011,3.1562802391,1.2105234004\C,0.257  
 4999655,5.0169425654,-0.8743585814\H,0.5275478883,6.0485184166,-0.6138  
 844778\H,0.6702753038,4.8088728082,-1.8663038382\H,2.3692112848,1.5080  
 197164,-1.3634470793\C,0.3283888973,4.4188888814,2.1558004005\H,0.8078  
 938625,5.3680304087,2.4268515601\H,-0.7547189599,4.5808663204,2.200378  
 0147\H,-1.7472842183,3.101026468,0.9117288498\C,-4.8945301438,0.150624  
 0798,-2.2669934338\F,-6.0694627473,0.751184602,-2.5482231842\F,-4.2999  
 801024,-0.1593844971,-3.439534423\F,-5.1825344913,-1.0175846323,-1.649  
 2688054\C,-4.3513779243,3.6156212939,1.3258658917\F,-3.5303606641,4.66  
 10886946,1.5808882894\F,-5.5351486973,4.1170828806,0.9171350048\F,-4.5  
 690095364,2.9910404689,2.5048875897\C,-0.6228361842,2.9685860649,-5.56  
 12204987\F,-0.8507620308,4.3003405238,-5.4910846493\F,-0.0299810736,2.  
 7299422344,-6.7500943186\F,-1.8310104089,2.3639692925,-5.5767104683\C,  
 3.8700737256,1.9920295489,-3.5451626899\F,4.2594240247,0.7424035869,-3  
 .8691997079\F,4.3509704167,2.820202492,-4.4983789926\F,4.4874667649,2.  
 3110888067,-2.3826881082\C,5.1500686427,-3.908143964,-4.0532085516\H,6  
 .0900097966,-3.4919983068,-4.443282693\H,5.34041321,-4.9732517226,-3.8  
 574202051\H,4.3999083283,-3.842952974,-4.8493384199\\Version=AM64L-G09  
 RevD.01\State=1-A\HF=-2740.1835649\RMSD=5.256e-09\RMSF=6.146e-06\Dipol  
 e=0.256619,0.1293843,1.0854495\Quadrupole=-6.842782,3.7001185,3.142663  
 5,3.1075186,4.6269535,-0.8855529\PG=C01 [X(C29H29F12N101Si1)]\\@

### Coordinates of high level structural conformation calculations at a pbe0-D3/def2svp level of theory.

#### 3E-1.c

1\1\GINC-WORKER\FOpt\RPBE1PBE\def2SVP\C29H29F12N101Si1\JHIOE\07-Apr-20  
 15\0\#p pbe1pbe/def2svp empiricaldispersion=gd3bj opt freq scf=tight\  
 \title\0,1\C,-0.3727977855,-1.156573205,-1.7707496052\C,-0.0656452777  
 ,-0.2954001632,-2.999676444\C,-1.346644698,0.5034400492,-3.2610523026\  
 C,-2.4692752332,-0.3722119201,-2.7070440433\H,0.0837809285,-2.15790080  
 92,-1.8422555862\H,0.8151923038,0.3481867963,-2.8605577001\H,0.1537674  
 246,-0.9588543645,-3.8500451416\H,-1.3170449762,1.468401318,-2.7372946  
 787\H,-1.4845759641,0.7240655554,-4.3285125853\H,-3.2351407147,0.22454  
 86295,-2.1814756483\H,-2.9949472883,-0.9424924987,-3.4968552375\N,-1.8  
 065141718,-1.2908481829,-1.8064035966\C,-2.4845020764,-2.2762643815,-1  
 .1456968122\H,-1.8402825188,-3.0079439332,-0.6522278905\C,-3.832056969  
 ,-2.3920733438,-1.0465132197\H,-4.4846089743,-1.6381919688,-1.49735019  
 86\C,-4.4609386456,-3.4807566794,-0.3321780696\H,-3.7834899769,-4.2232  
 423736,0.1126164107\C,-5.7855641284,-3.649668714,-0.1658484953\H,-6.46  
 27877711,-2.9086643391,-0.6103464256\C,0.1308635533,-0.5870869736,-0.3  
 96261133\C,1.6550115843,-0.4917551354,-0.3267018242\C,2.2495521038,0.2  
 746813465,0.678419529\C,2.4905793464,-1.2382061713,-1.1614159705\C,3.6  
 31837203,0.2978376435,0.8449933221\H,2.3184632382,-1.6298254958,2.6781  
 913358\C,3.8741202024,-1.209220108,-0.9995709054\H,2.0779242837,-1.852

```

0536134,-1.9610499161\C,4.457595618,-0.4408120902,0.0043487668\H,5.541
2505638,-0.409967662,0.1241336823\C,-0.5559126344,0.7507320632,-0.1703
058325\C,0.0144622382,1.9713485565,-0.5351401611\C,-1.8697905823,0.739
4586067,0.3000137108\C,-0.7155830214,3.1539556516,-0.4277883292\H,-0.4
147970495,-0.4725520257,4.2727655969\C,-2.5945367941,1.9232983933,0.40
74964\H,-2.3317252417,-0.2114531918,0.5709222508\C,-2.0249603584,3.140
7963904,0.0466569245\H,-2.5920985192,4.067656965,0.1363458169\O,-0.303
2826419,-1.5309530277,0.5414393784\Si,-0.1501456445,-1.7917841661,2.20
95588126\C,-1.4366198164,-3.1098022175,2.5172347015\H,-2.4334422425,-2
.7657661293,2.2000777807\H,-1.2002832534,-4.0268223159,1.9552949535\H,
-1.4862042686,-3.3709656592,3.5860029969\C,1.5648091814,-2.4276822936,
2.6174829844\H,1.5433406264,-2.9388924043,3.5936437819\H,1.8970525824,
-3.1575590777,1.8627961315\H,1.6275661203,0.873366183,1.3458503241\C,-
0.5410937765,-0.2482094517,3.2008403616\H,-1.5783164279,0.0839459,3.04
55446364\H,0.1229990432,0.5965154846,2.9643078349\H,1.0359470715,2.013
7624018,-0.9167849949\C,-4.0166733788,1.8444965639,0.8900978199\F,-4.5
438249188,3.0506887125,1.1007290762\F,-4.7929878952,1.2166601366,-0.00
20601825\F,-4.1031054353,1.1569192831,2.033850206\C,-0.1055116054,4.43
80806767,-0.9169591128\F,-0.2774345445,4.5723155574,-2.2390156471\F,-0
.6562793625,5.5044461819,-0.33646605\F,1.2092508785,4.4790591222,-0.68
81473608\C,4.7471968974,-2.0565189743,-1.8867978894\F,4.1677628071,-2.
2920460059,-3.0668829421\F,5.9233322137,-1.471259468,-2.1187292917\F,4
.9989612041,-3.2431454017,-1.3256568776\C,4.2115807143,1.0837463533,1.
9894707427\F,3.5800083371,2.2480684574,2.1524230299\F,4.0884132169,0.4
079154271,3.1406947698\F,5.5072121508,1.3389032437,1.8148691965\C,-6.4
189627692,-4.7726049837,0.5833982136\H,-7.0314280532,-4.4059447109,1.4
25742014\H,-7.0990483806,-5.3587914333,-0.0591956278\H,-5.6646188502,-
5.4623875856,0.9916392361\Version=ES64L-G09RevD.01\State=1-A\HF=-2735
.7452013\RMSD=9.194e-09\RMSF=4.486e-06\Dipole=0.2983014,-0.3151621,-0.
1751112\Quadrupole=-7.8023655,-1.9418188,9.7441844,-2.960358,1.1549393
,-3.998617\PG=C01 [X(C29H29F12N101Si1)]\@

```

### 3Z-1.c

```

1\1\GINC-WORKER\F0pt\RPBE1PBE\def2SVP\C29H29F12N101Si1\JHIOE\06-Apr-20
15\0\#p pbe1pbe/def2svp empiricaldispersion=gd3bj opt freq scf=tight\
\title\0,1\C,-0.3496193553,-1.5572241328,-1.6535853706\C,0.0033718043
,-0.9012910813,-2.9902246409\C,-1.2644780085,-0.1621923706,-3.44065357
54\C,-2.4178248583,-0.8290594392,-2.6826872722\H,0.1001707658,-2.55892
57707,-1.5549524525\H,0.8797413168,-0.2408629008,-2.9187848631\H,0.263
2462712,-1.6921967163,-3.7091490915\H,-1.2087633124,0.9065770081,-3.19
69550314\H,-1.4026703429,-0.2284391135,-4.5286323051\H,-3.0692583423,-
0.0801503421,-2.1960938062\H,-3.0710062093,-1.4349753326,-3.3369913914
\N,-1.780715218,-1.6952876035,-1.7154484758\C,-2.4911327177,-2.5087061
488,-0.879189533\H,-1.8784048675,-3.2308031953,-0.3329530243\C,-3.8309
585875,-2.4689620492,-0.6725503689\H,-4.4309527669,-1.7049155359,-1.17

```



30310759\C,-4.4935595674,-3.3902491691,0.2253414111\H,-3.8628043491,-4  
.1903878558,0.6321629183\C,-5.7839496655,-3.3600669201,0.6150851982\H,  
-6.1223310693,-4.1484421841,1.2964568599\C,0.1095252908,-0.7908851752,  
-0.3603196535\C,1.6237817202,-0.6065571163,-0.2890376126\C,2.484655194  
3,-1.5846042114,-0.7941538429\C,2.1831168101,0.4411309852,0.4457837084  
\C,3.8571414727,-1.5156350429,-0.5694861472\H,2.5921251816,-1.57914200  
24,2.4056047744\C,3.5562836069,0.5083393609,0.6710165163\H,1.542125338  
2,1.2172957357,0.8664275066\C,4.4068060162,-0.4689637394,0.1656465875\  
H,5.4810669358,-0.4182449252,0.3437089461\C,-0.6660905748,0.5162276788  
, -0.2949896079\C,-0.2329441912,1.6823130974,-0.9265517727\C,-1.9216772  
574,0.514777811,0.3144757526\C,-1.0347771704,2.8233318344,-0.938164457  
8\H,0.561459046,0.6385184043,2.8967742457\C,-2.7220052436,1.6525919456  
,0.2950111577\H,-2.2845039999,-0.3994799615,0.7852827409\C,-2.28442961  
24,2.8199669232,-0.3261475373\H,-2.9067381651,3.715291984,-0.331318914  
4\O,-0.2738788511,-1.6389639925,0.6861403846\Si,0.0925223867,-1.761761  
1943,2.3387313043\C,-1.1491103097,-3.0335794908,2.9090279534\H,-2.1773  
568708,-2.7048201469,2.6910836715\H,-1.0666331139,-3.2106487591,3.9927  
586141\H,-0.9856883421,-3.9935594747,2.3949765594\C,1.8483453135,-2.36  
9496752,2.5858787007\H,2.0805596587,-3.2163729835,1.9217876268\H,1.974  
4806822,-2.7120089156,3.6258684339\H,2.0904727899,-2.4296350893,-1.359  
2468005\C,-0.1564003702,-0.1282454116,3.2236494177\H,-1.1745066152,0.2  
639563233,3.0820339016\H,-0.0002462719,-0.2780901476,4.3045816455\H,0.  
7391534545,1.7152373291,-1.4220923864\C,-4.0997972681,1.5743492202,0.8  
932926821\F,-4.5895788245,2.7816565626,1.1790787317\F,-4.9568934706,0.  
990078063,0.0433674958\F,-4.1063498911,0.8532775992,2.0160830708\C,-0.  
5556009924,4.032966424,-1.6912450547\F,-0.7173623595,3.8647968573,-3.0  
118658054\F,-1.2203172671,5.1349727788,-1.3468700826\F,0.7449165257,4.  
2555277256,-1.4855603767\C,4.083703663,1.6193131578,1.5375424118\F,3.7  
340265043,1.4267831056,2.8166023343\F,5.4122146743,1.7027817657,1.4927  
822615\F,3.5844036393,2.8015832964,1.1710452323\C,4.7261442859,-2.6356  
656599,-1.0749968754\F,4.4274619389,-2.9519564727,-2.3382783467\F,6.02  
09808941,-2.3255867058,-1.0260895428\F,4.5484729588,-3.7414485175,-0.3  
431926017\C,-6.8088787561,-2.351411038,0.2102036746\H,-7.5159093784,-2  
.761174734,-0.5333974836\H,-7.41570519,-2.0393575573,1.0756668355\H,-6  
.3600505455,-1.4439738983,-0.2179630867\\Version=ES64L-G09RevD.01\Stat  
e=1-A\HF=-2735.7446593\RMSD=9.578e-09\RMSF=3.341e-06\Dipole=0.5412158,  
-0.2964955,-0.212334\Quadrupole=-7.9460885,-3.0493006,10.9953892,-4.11  
80115,1.6665986,-1.7940684\PG=C01 [X(C29H29F12N101Si1)]\\@



## 2.4 References

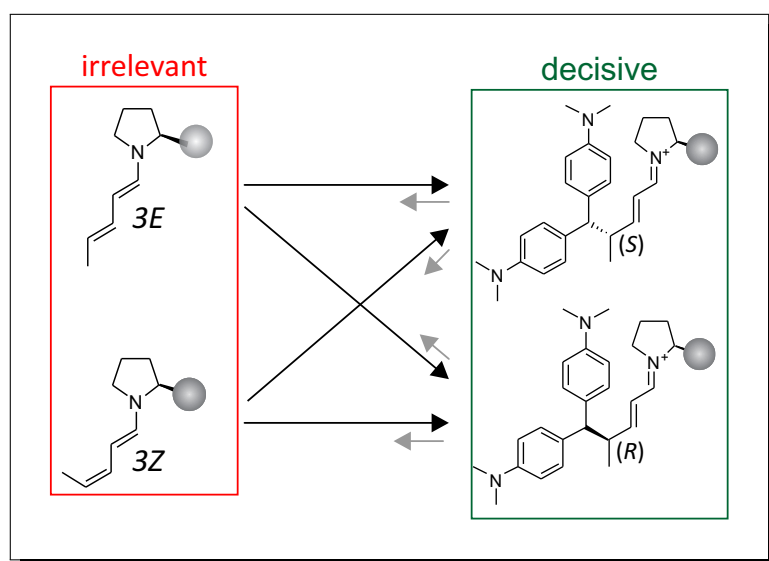
- [1] M. C. Holland, R. Gilmour, *Angew. Chem. Int. Ed.* **2015**, *54*, 3862–3871.
- [2] B. List, *Chem. Commun.* **2006**, 819–824.
- [3] G. Lelais, D. W. C. MacMillan, *Enantioselective Organocatalysis: Reactions and Experimental Procedures*, Wiley Online Library, **2007**.
- [4] S. Bertelsen, M. Marigo, S. Brandes, P. Dinér, K. A. Jørgensen, *J. Am. Chem. Soc.* **2006**, *128*, 12973–12980.
- [5] R. M. de Figueiredo, R. Fröhlich, M. Christmann, *Angew. Chem.* **2008**, *120*, 1472–1475.
- [6] A. Mielgo, C. Palomo, *Chem. Asian J.* **2008**, *3*, 922–948.
- [7] E. Marqués-López, R. P. Herrera, T. Marks, W. C. Jacobs, D. Könnig, R. M. De Figueiredo, M. Christmann, *Org. Lett.* **2009**, *11*, 4116–4119.
- [8] J. Stiller, E. Marqués-López, R. P. Herrera, R. Fröhlich, C. Strohmann, M. Christmann, *Org. Lett.* **2010**, *13*, 70–73.
- [9] M. Silvi, C. Cassani, A. Moran, P. Melchiorre, *Helv. Chim. Acta* **2012**, *95*, 1985–2006.
- [10] S. Mukherjee, J. W. Yang, S. Hoffmann, B. List, *Chem. Rev.* **2007**, *107*, 5471–5569.
- [11] P. Pihko, I. Majander, A. Erkkilä, *Asymmetric Organocatalysis* **2009**, *291*, 29–74.
- [12] D. B. Ramachary, Y. V. Reddy, *Eur. J. Org. Chem.* **2012**, 865–887.
- [13] Y. Chi, S. H. Gellman, *Org. Lett.* **2005**, *7*, 4253–4256.
- [14] Y. Hayashi, H. Gotoh, T. Hayashi, M. Shoji, *Angew. Chem. Int. Ed.* **2005**, *44*, 4212–4215.
- [15] M. Marigo, T. C. Wabnitz, D. Fielenbach, K. A. Jørgensen, *Angew. Chem. Int. Ed.* **2005**, *44*, 794–797.
- [16] Y. Hayashi, D. Okamura, T. Yamazaki, Y. Ameda, H. Gotoh, S. Tsuzuki, T. Uchamaru, D. Seebach, *Chem. - A Eur. J.* **2014**, *20*, 17077–17088.
- [17] B. Matos Paz, H. Jiang, K. A. Jørgensen, *Chem. - A Eur. J.* **2014**, *21*, 1846–1853.
- [18] Ł. Albrecht, G. Dickmeiss, C. F. Weise, C. Rodríguez-Esrich, K. A. Jørgensen, *Angew. Chem. Int. Ed.* **2012**, *51*, 13109–13113.
- [19] T. K. Johansen, C. V. Gómez, J. R. Bak, R. L. Davis, K. A. Jørgensen, *Chem. - A Eur. J.* **2013**, *19*, 16518–16522.
- [20] G. Talavera, E. Reyes, J. L. Vicario, L. Carrillo, *Angew. Chem. Int. Ed.* **2012**, *51*, 4104–4107.

- [21] M. B. Schmid, K. Zeitler, R. M. Gschwind, *Angew. Chem. Int. Ed.* **2010**, *49*, 4997–5003.
- [22] M. B. Schmid, K. Zeitler, R. M. Gschwind, *J. Am. Chem. Soc.* **2011**, *133*, 7065–7074.
- [23] M. B. Schmid, K. Zeitler, R. M. Gschwind, *J. Org. Chem.* **2011**, *76*, 3005–3015.
- [24] M. B. Schmid, K. Zeitler, R. M. Gschwind, *Chem. Sci.* **2011**, *2*, 1793–1803.
- [25] M. H. Haindl, M. B. Schmid, K. Zeitler, R. M. Gschwind, *RSC Advances* **2012**, *2*, 5941–5943.
- [26] M. B. Schmid, K. Zeitler, R. M. Gschwind, *Chem. - A Eur. J.* **2012**, *18*, 3362–3370.
- [27] M. Cai, Y. Huang, J. Liu, R. Krishnamoorthi, *J. Biomol. NMR* **1995**, *6*, 123–128.
- [28] H. Reich, *Proton-Proton Coupling Constants*, **2011**, <http://www.chem.wisc.edu/areas/reich/handouts/nmr-h/h-coupling.htm>.
- [29] K. P. C. Vollhardt, N. E. Schore, *Organic chemistry: structure and function*, WH Freeman New York, **2011**.
- [30] C. Adamo, V. Barone, *J. Chem. Phys.* **1999**, *110*, 6158–6170.
- [31] F. Weigend, R. Ahlrichs, *Phys. Chem. Chem. Phys.* **2005**, *7*, 3297–3305.
- [32] F. Weigend, *Phys. Chem. Chem. Phys.* **2006**, *8*, 1057–1065.
- [33] A. V. Marenich, C. J. Cramer, D. G. Truhlar, *J. Phys. Chem. B* **2009**, *113*, 6378–6396.
- [34] S. Grimme, *J. Chem. Phys.* **2003**, *118*, 9095–9102.
- [35] R. A. Kendall, T. H. Dunning Jr, R. J. Harrison, *J. Chem. Phys.* **1992**, *96*, 6796–6806.
- [36] D. E. Woon, T. H. Dunning Jr, *J. Chem. Phys.* **1993**, *98*, 1358–1371.
- [37] S. Kossmann, F. Neese, *J. Chem. Theory Comput.* **2010**, *6*, 2325–2338.
- [38] M. J. Frisch, G. W. Trucks, H. B. Schlegel, G. E. Scuseria, M. A. Robb, J. R. Cheeseman, G. Scalmani, V. Barone, B. Mennucci, G. A. Petersson, H. Nakatsuji, M. Caricato, X. Li, H. P. Hratchian, A. F. Izmaylov, J. Bloino, G. Zheng, J. L. Sonnenberg, M. Hada, M. Ehara, K. Toyota, R. Fukuda, J. Hasegawa, M. Ishida, T. Nakajima, Y. Honda, O. Kitao, H. Nakai, T. Vreven, J. A. Montgomery, Jr., J. E. Peralta, F. Ogliaro, M. Bearpark, J. J. Heyd, E. Brothers, K. N. Kudin, V. N. Staroverov, R. Kobayashi, J. Normand, K. Raghavachari, A. Rendell, J. C. Burant, S. S. Iyengar, J. Tomasi, M. Cossi, N. Rega, J. M. Millam, M. Klene, J. E. Knox, J. B. Cross, V. Bakken, C. Adamo, J. Jaramillo, R. Gomperts, R. E. Stratmann, O. Yazyev, A. J. Austin, R. Cammi, C. Pomelli, J. W. Ochterski, R. L. Martin, K. Morokuma, V. G. Zakrzewski, G. A. Voth, P. Salvador, J. J. Dannenberg, S. Dapprich, A. D. Daniels, . Farkas, J. B. Foresman, J. V. Ortiz, J. Cioslowski, D. J. Fox, *Gaussian 09 Revision D.01*, Gaussian Inc. Wallingford CT 2009.
- [39] F. Neese, *Wiley Interdisciplinary Reviews: Computational Molecular Science* **2012**, *2*, 73–78.
- [40] A. D. Becke, *J. Chem. Phys.* **1993**, *98*, 1372–1377.

### 3 Stereoinduction in dienamine catalysis.

Article

***"The mechanism of stereoinduction in dienamine catalyzed  $\gamma$  alkylation revealed by a combined in situ NMR and quantum-chemical study."***



Quantum theoretical calculations were performed by Dr. Johnny Hioe. Synthesis for the enantiomeric excess determination was performed by Dr. Fabio Morana. Synthesis for compound **5** was performed by Andreas Seegerer. Andreas Seegerer provided the NMR spectroscopic investigations for aldehydes **4** and **5** and the kinetics for dienamine formation of **3**. The product dienamine was characterised by Andreas Seegerer. We would like to thank Patrick Fuchs for the help with the enantiomeric excess determination.

Michael M. Hammer, Andreas J. Seegerer, Johnny Hioe, Fabio Morana and Ruth M. Gschwind

## 3.1 Abstract

Dienamine activation allows the stereoselective functionalization of  $\alpha,\beta$ -unsaturated carbonyl compounds and expands the field of organocatalysis. The mode of stereoselection for dienamine activation is proposed to be governed by steric shielding, however the remote control over 5 bonds remained unclear. Therefore in this study we used kinetic NMR studies, quantum chemical calculations and *ee* determination on varying experimental conditions to elucidate the step of stereocontrol in dienamine catalysis. All experimental data confirm that the *3E/3Z*-dienamine ratio of dienamine and product dienamine are irrelevant for the stereochemistry. Fast equilibration between *3Z*- and *3E*-dienamine and subsequent reaction exclusively from *3Z*-dienamine was also experimentally excluded. Theoretical calculations show the product iminium species to be decisive. The energy gap between major enantiomer product iminium and minor enantiomer product iminium governs the stereocontrol. That leads to the conclusion that in reactions without sufficient steric hindrance of the catalyst, the interactions in down-stream product species can be successfully used for stereocontrol in catalysis.

## 3.2 Manuscript

### Introduction

Intimate knowledge of the mode of stereoselection and determining the role of intermediates<sup>[1]</sup> in a catalytic process is very useful in order to understand and further develop the process. In the field of organocatalysis, that has emerged as one of the pillars of modern organic chemistry, the number of synthetic applications by far outnumbers the studies dealing with the underlying mechanisms. The knowledge of these underlying mechanisms should however help increase our ability to develop even more and more successful catalytic activation protocols.

In the field of organocatalysis, besides enamine<sup>[2,3]</sup> and iminium ion activation,<sup>[4]</sup> in the last few years, dienamine catalysis<sup>[5–11]</sup> has emerged as a powerful strategy to access previously inaccessible  $\gamma$ -functionalized  $\alpha,\beta$ -unsaturated aldehydes (see Fig. 3.1 **A**). In dienamine catalysis as well as in trienamine catalysis<sup>[12]</sup> a shielding model is proposed to be responsible for the stereoselection observed for the  $\gamma$ -alkylation of linear aldehydes (see Fig. 3.1 **B**).<sup>[7–10]</sup> In this

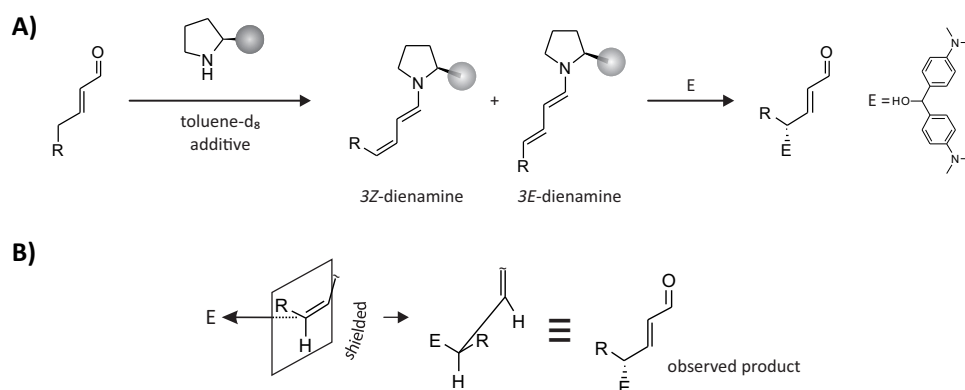


**Fig. 3.1:** **A)** Investigated chemical transformation. **B)** Associated shielding model allowing attack on the electrophile for the *3Z*-dienamine leading to the major stereoproduct.

model the *si*-face of the dienamine  $\pi$ -system is supposedly effectively shielded by the bulky catalyst residue and therefore the attack on the electrophile solitarily occurs on the *re*-face of the *3Z*-dienamine forming the major enantiomer. However, in previous studies a distribution in *3E* and *3Z*-dienamine was reported<sup>[7,10]</sup> and we could show that both intermediates experience the same quality of shielding from the catalyst residue (see chapter 2). Both dienamines should therefore, in the simple shielding model, give rise to opposite enantiomers since both provide open space for attack. The ratio of *3Z*- to *3E*-dienamine is only slightly dependent on the catalyst, aldehyde or solvent and varies between 1.1/1 and 3/1, yet this distribution does not at all translate into observed enantiomeric excess in synthesis which are commonly above 80 % *ee* that would translate into *3Z/3E*-dienamine ratio of 9/1 and higher.<sup>[7–10]</sup> This excludes a simple shielding model to be active for the  $\gamma$ -functionalization via dienamine activation by secondary amines. To fill this gap, we performed *in situ* NMR spectroscopic investigations on

formation kinetics and distributions of the dienamine intermediates. In addition, experimental investigations on the reactivity of both dienamines together with quantum chemical calculations can offer an alternate model for the mode of stereinduction in dienamine catalysis. This investigation demonstrates that the energetic distribution of downstream intermediates is decisive for the successful stereinduction in dienamine catalysis.

## Results and Discussion

**Model system.** Three secondary amine catalysts were selected for our study, which proved to be most successfully applied in synthesis (see Fig 3.2 **A**).<sup>[13–15]</sup> In addition, several  $\alpha,\beta$ -unsaturated aldehydes were chosen representing different electronic and steric influence on the developing diene double bonds (Fig. 3.2 **B**). Michler's hydrol (Fig. 3.2 **C**) was used as model electrophile since its performance in synthesis was shown to be excellent.<sup>[10]</sup> Additionally DEAD (Diethyl diazenedicarboxylate) was utilized (Fig. 3.2 **C**). The dienamine intermediates will be termed designated as "**3E- or 3Z-aldehyde number.catalyst character**", e.g. **3E-1.a** (see Fig. 3.2), since the second double bond is the only differentiating factor in the dienamines, while the remainder of the structure was shown to be identical for both dienamines (see chapter 2). Since toluene is the main experimental solvent<sup>[7–11]</sup> all studies unless otherwise indicated were performed in toluene- $d_8$ . All experiments mentioned in this paper if not

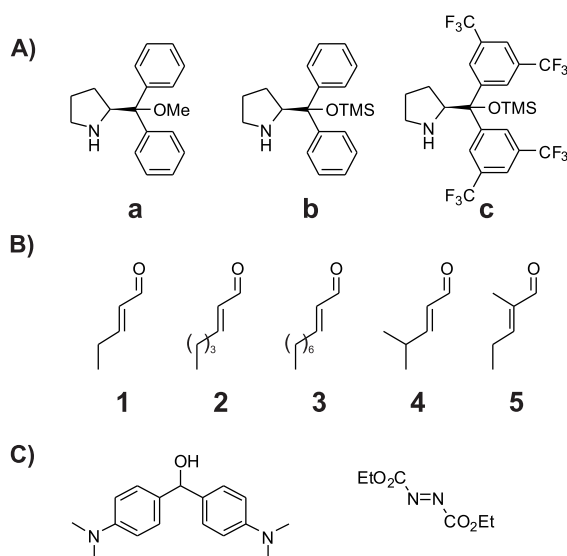
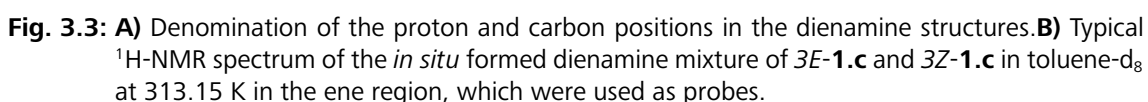


**Fig. 3.2:** **A)** Investigated model catalysts developed by Jørgensen and Hayashi.<sup>[13–15]</sup> **B)** Model aldehydes. **C)** Michler's hydrol and DEAD as model electrophiles.<sup>[10]</sup>

otherwise stated were performed inside NMR tubes by mixing the given amounts of aldehyde and catalyst (and additive if mentioned) to obtain an aldehyde concentration of  $50 \text{ mmol L}^{-1}$ . NMR spectra were recorded at 300–318 K (see experimental section for detailed information).





---

51

tected (denominated as *3E*- and *3Z*-dienamine name, e.g. *3Z*-**1.a**). The coupling constants were found to be  $^3J_{\text{H3H4}} = 13.3\text{--}14.9$  Hz for the *3E*-dienamine, and  $^3J_{\text{H3H4}} = 10.4\text{--}11.0$  Hz for the *3Z*-dienamine.

For  $\gamma$  methyl-substituted aldehyde **4** the dienamine structure was detected with a coupling constant of  $^3J_{\text{H1H2}} = 13.34$  Hz. No dienamine was detected for aldehyde **5**.<sup>a</sup> This is in strong accordance with our findings on enamine species, where similarly virtually no enamines could be detected for  $\alpha$ -substituted aldehydes.<sup>[16–21]</sup>

**Dienamine formation as rate determining step.** For the related enamine activation it was shown that dependent on the nature and ultimately the reactivity of the electrophile the enamine formation rate is either slow compared to the consumption of the enamine by reaction with the electrophile and constitutes the rate determining step<sup>[22]</sup> or the subsequent CC bond formation step is rate determining.<sup>[23]</sup> For DEAD as electrophile, which is also applied in dienamine catalysis, the enamine formation was evidenced to be the rate limiting step.<sup>[24]</sup> This was so far not investigated for the vinylogous dienamine activation. For this purpose, dienamine reaction profiles were collected for the  $\gamma$ -alkylation of **1** catalyzed by **b** with delayed electrophile addition (see Fig. 3.4 **A**).<sup>b</sup> The electrophile was added after an initial waiting period so dienamine could be accumulated in the solution and possible different consumption rates for both dienamines would be distinguishable on the NMR sensitivity scale (see Fig. 3.4 **B**). The electrophile DEAD was added after approximately 35 min in an under-stoichiometric amount (0.2 equiv.), in order to observe any changes in the reaction behavior after the consumption of electrophile.

The kinetic profile in Fig. 3.4 **B** shows, that before the addition of electrophile, dienamine *3Z*-**1.b** is formed predominantly up to 15 mM. The *3E*-**1.b** dienamine is formed to a lesser extent and reaches a level of approximately 7 mM. The progression of *trans*-2-pentenal consumption reaches 30 mM after approximately 35 minutes. After the addition of electrophile DEAD the consumption rate of *trans*-2-pentenal is increasing. Both *3E*- and *3Z*-**1.b** drop below the detection limit and only reach detectable values after the whole of the electrophile is consumed after approximately 1.5 hours. After the electrophile is consumed the progression of all depicted species is comparable to the progression before the electrophile addition.

This experiment demonstrates that both the *3E*- and *3Z*-dienamines are consumed with the same or at least comparable velocity on the NMR timescale when electrophile is added to the solution. Additionally the fast consumption of the dienamines compared to their formation leads us to conclude that the dienamine formation is the rate determining step.

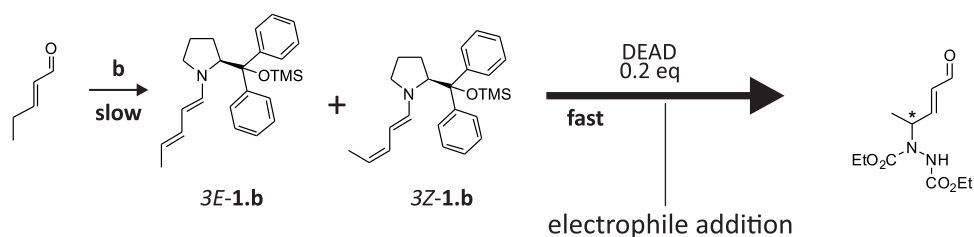
Both dienamine configurational isomers do react and if *3Z*-dienamine is to be considered

---

<sup>a</sup>This is most probably due to the steric hindrance of the  $\alpha$ -substituted aldehyde which prevents the formation of precursor species, like iminium ions.

<sup>b</sup>We utilized catalyst **b** since it provides relatively large amounts of up to 15–30 mM (**c** approx. up to 5 mM) of dienamine intermediates for our experimental conditions.

A)



B)

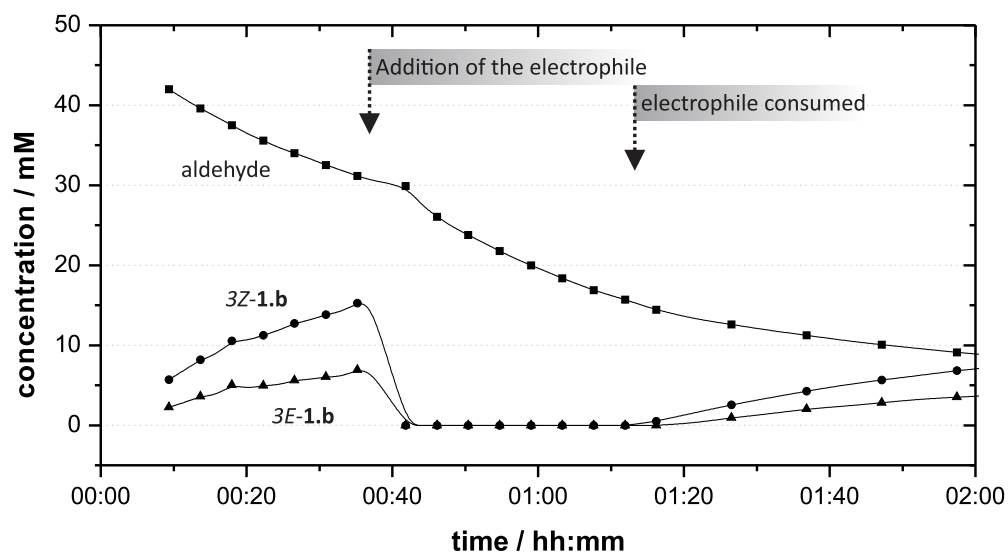


**Fig. 3.4: Dienamine formation as rate limiting step.** Kinetic profiles (B) for the delayed addition of the electrophile (DEAD) to a preformed dienamine solution (A) shows that both 3E and 3Z-dienamines react fast compared to the dienamine formation. After the addition of electrophile no dienamines are detectable until the electrophile is consumed. The reaction was carried out at 313.15 K at 100 mol% catalyst loading. A dead time of approx. 7 min was needed to prepare the reaction vessel for the first spectrum as well as for the addition of electrophile after approx. 35 min. *Note:* Additional peaks in the dienamine area are visible after the consumption of electrophile, however an assignment to any structure was not performed.

the productive intermediate, several theories could explain the stereoselectivity in dienamine activation. First, the *3Z/3E*-dienamine ratio could directly correlate to the enantiomeric excess with *3Z*-dienamine feeding into the major product and *3E*-dienamine into the minor product enantiomer. Second, *3E*- and *3Z*-dienamine could exist in a rapid equilibrium and only *3Z*-dienamine reacts further to the product. Third, possible initial formation differences for the *3Z*-dienamine and *3E*-dienamine could explain stereocontrol.

***3E/3Z*-dienamine ratio irrelevant for stereoselectivity.** First we were interested whether the *3Z/3E*-dienamine ratio of 1.1-3:1 can be directly correlated to the enantiomeric excess achieved in synthesis of 20-30 % *ee* for **a**, 45-52 % *ee* for **b** and approx. 80 % *ee* for catalyst **c**. We did determine the enantiomeric excess as a function of employed catalyst ourselves (*vide infra*) and did not rely on literature values. We did this due to the fact that no reliable source could be identified that presents a solution of known *3Z/3E*-dienamine ratio with achieved enantiomeric excess. To this end, we determined the dienamine ratio as a function of catalyst with aldehyde **1** at 100 mol% catalyst **a-c** loading at rt in toluene- $d_8$  (Fig. 3.5 **A**). The expected *ee*-values were deduced and compared to the experimental values (see Fig. 3.5 **B** for **c**).

For all catalysts the expected (from *3Z/3E*-dienamine ratio) and experimentally determined *ee*-values differ significantly. For **a** the expected *ee* of 41-42 % *ee* (*3Z/3E*=2.4/1-2.5/1) is higher than the achieved 20-30 % *ee*. For **b** the expected 27-33 % *ee* (*3Z/3E*=1.8/1-2/1) is lower than the experimentally determined 45-52 % *ee*. Most pronouncedly the expected 42-50 % *ee* (*3Z/3E*=2.5/1-3/1) for catalyst **c** is far worse than the experimentally achieved of approx. 80 % *ee*.

In summary, we could confirm that the enantiomeric excess in synthesis can not be directly correlated to the *3Z/3E*-dienamine ratio that is observable by NMR (Fig. 3.5 **B**).

**No fast equilibration of *3Z*- and *3E*-dienamine with subsequent exclusive consumption of *3Z*-dienamine.** Secondly, we were investigating whether a rapid equilibration of *3E*- and *3Z*-dienamine with productive consumption of *3Z* species could explain the stereoselectivity in synthesis (see Fig. 3.6 **B**). Therefore we followed the dienamine formation of aldehyde **1** at 20 mol% of catalyst **c** at 313.15 K in toluene- $d_8$  which represents synthetically used conditions.<sup>[7,8,10]</sup> Rapid equilibration of *3Z*- and *3E*-dienamine without consumption of the dienamines would lead to a constant ratio of *3Z/3E*-dienamine with time. The concentration profiles as well as the *3Z/3E*-dienamine ratio as a function of time are depicted in Fig. 3.6 **A**.

The amount of *3Z*-**1.c** reaches approximately 1.5-3 mM after 1-2 hours, while *3E*-**1.c** reaches around 1 mM after the same time period. Both vanish slowly with time most probably due to polymerization, albeit with *3E*-**1.c** experiencing the steeper slope leading to the *3Z/3E*-dienamine ratio to rise with time, starting from approximately 2 at the beginning of the reaction to almost 10 after 10 hours of reaction time.

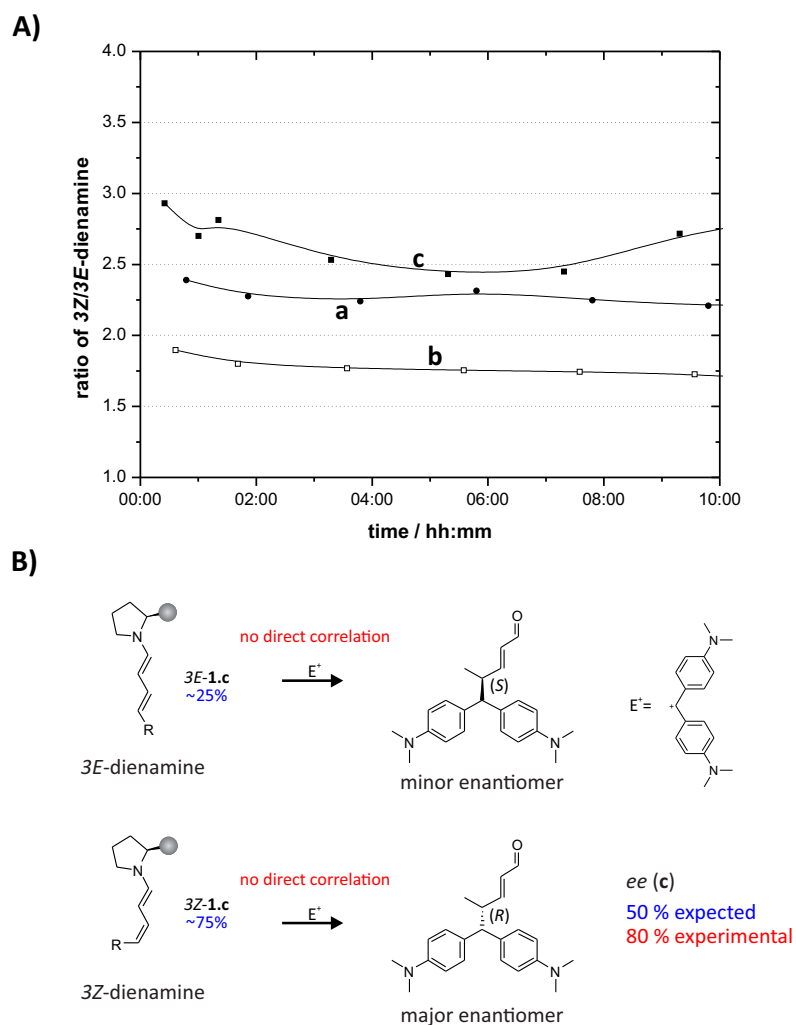


**Fig. 3.5: 3Z/3E-ratios deviate from experimental stereoselectivity.** Constant 3Z/3E-ratios (**A**) for the different catalysts translate into different *ee*-values than determined experimentally as shown for catalyst **c** (**B**). The 3Z/3E-ratios were determined at 100 mol% catalyst loading at 300 K in toluene- $d_8$ . The depicted experimental *ee*-value was determined for the reaction of **1** with Michler's hydrol catalyzed by **c**.

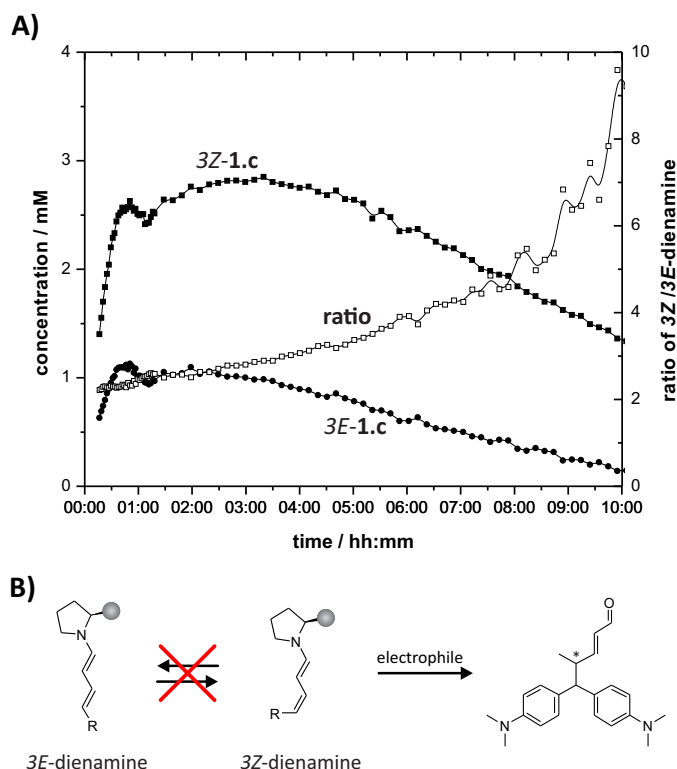


**Fig. 3.6: No fast equilibration of 3Z- and 3E-dienamine with subsequent exclusive consumption of 3Z-dienamine.** Fast up-stream equilibration and predominant reaction of 3Z-dienamine as source of stereoselection can be excluded. The kinetic profiles as well as the 3Z/3E-ratio (A) for **1.c**-dienamine at 20 mol% catalyst loading at 313.15 K in toluene- $d_8$  show that no fast equilibration between both 3Z- and 3E-dienamine is present, thus no sorting in potentially exclusively productive 3Z-dienamine is possible (B). *Note:* The first observed point is approximately 5-10 min after start of the reaction, since transfer into the spectrometer and preparation for spectroscopic investigation is necessary. Dienamines are consumed with time, presumably due to slow polymerization. The kinetic progress is not shown over the full observed range. A reasonable S/N-ratio allows the interpretation of the tendency for the ratio progression.

The *3E/3Z*-ratio does not stay constant. This does exclude that the two configurational isomers exist in rapid equilibrium with the exclusive consumption of *3Z*-dienamine to be responsible for stereinduction (Fig. 3.6 **B**).

In summary, we could show that no fast equilibration is present between the *3E*- and *3Z*-dienamine intermediates.

**Artificial access to initial *3Z/3E*-dienamine ratios.** The *3Z/3E*-dienamine ratio detected by NMR without electrophile addition may deviated from the initially formed *3Z/3E*-dienamine ratio not accessible by NMR methods. In the absence of equilibration between *3E*-dienamine and *3Z* this is highly unlikely but nevertheless we wanted to be sure that this aspect can be excluded. Therefore, we used a delayed addition of electrophile and subsequently determined the *ee* values.

We selected different delays for the electrophile addition that correspond to significantly differing *3E*-dienamine contents (see Fig. 3.7 **A**). We performed the experiment for all three catalysts since the inherently achieved enantiomeric excess, the *3Z/3E*-dienamine ratios and the overall amount of formed *3E*-dienamine do differ significantly (see Fig. 3.7 **B**). If the formation rate of *3Z*-dienamine is different at the start of the reaction and thus the *3Z/3E*-ratio, the enantiomeric excess without delayed addition of electrophile would exhibit significantly different values than those with delayed electrophile addition.

Independent of the *3E*-dienamine content which reaches 17 % for **a**, 15 % for **b** and 4 % for **c** after 2 hours and the *3E/3Z*-dienamine ratios (Fig. 3.7 **A**) the enantiomeric excess does not change for any organocatalyst (Fig. 3.7 **B**). While **c** yields enantiomeric excess of approx. 80 %, **b** stays at 50 % and **a** at approximately 25 % with increase to closely over 30 %.

First, *3Z*-dienamine formation can not be favoured highly at the beginning of the reaction since the enantiomeric excess achieved without and with delayed electrophile addition does not differ. Second, these findings prove that *3E*-dienamine must be productive towards the major product enantiomer (Fig. 3.7 **C**).

**Low reaction barrier for the *3Z*-dienamine formation.** Since there is no preferred *3Z*-dienamine formation corresponding to the *ee* value neither in the initial nor in the later part of the reaction we wanted to corroborate this with quantum chemical calculations. Quantum chemistry was applied to the investigated formation before, however the ratio of *3Z* to *3E* dienamine could not be reproduced.<sup>[7]</sup> Additionally, the formation pathway from the upstream iminium ions was not addressed in detail. Since our structural studies (see chapter 2) show that CH/ $\pi$ -interactions are in effect, we utilized a theoretical method accounting for non-covalent, dispersive interactions developed by Grimme and co-workers.<sup>[25]</sup> Catalyst **c** was investigated to possibly clarify the role of CF<sub>3</sub> groups in stabilizing either the intermediates or transition states. The intermediates for dienamines **1.c** were modeled using our structural data and for

3 The mechanism of stereoselection in dienamine catalyzed  $\gamma$  alkylation revealed by a combined *in situ* NMR and quantum-chemical study.

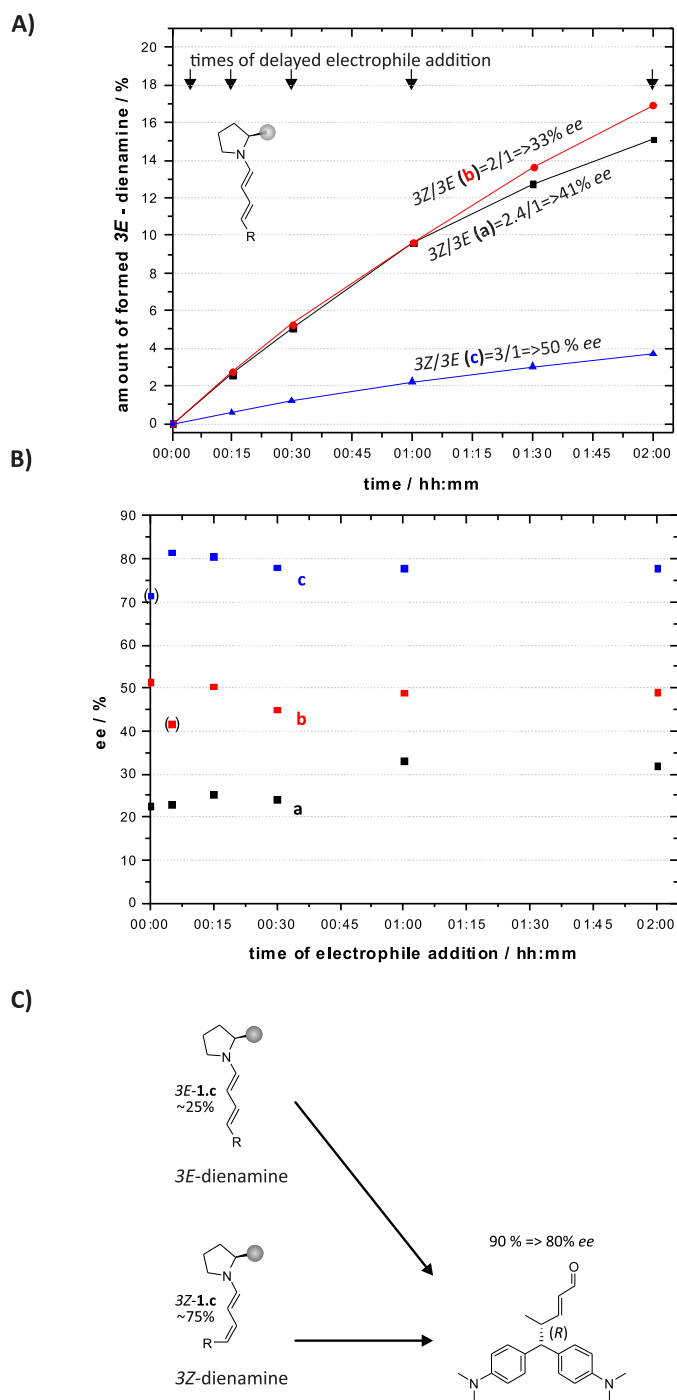


**Fig. 3.7: Stereoselectivity independent of  $3E$ -dienamine amount.** A delayed electrophile addition (amount of  $3E$ -dienamine with corresponding  $3Z/3E$ -ratios and expected  $ee$ -values in **A**) does not alter the  $ee$ -values (**B**). That excludes an initial  $3Z$ -dienamine dominance and proves that both  $3E$  and  $3Z$ -dienamines form the major enantiomer (**C**) with the stereoselective step in a down-stream intermediate. Experimental stereoselectivity in (**B**): each data point represents an independent experiment with delayed electrophile addition at the time of the data point. The  $3E$ -amounts and  $3Z/3E$ -ratios were determined at 100 mol% catalyst loading at 300 K in toluene- $d_8$ . The procedure for the  $\gamma$ -alkylation of **1** can be found in the SI 3.3. The amounts in **A** were referenced to the sum of all aldehyde derived species in the first spectrum set to 100 %. *Note:* Data points in brackets are considered outliers.



the transition states, OH<sup>-</sup> as counter ion (which is expelled from the carbinolamine species to form the iminium-precursor species) and deprotonation agent was replaced by NMe<sub>3</sub> to overcome large problems with the collapsing of the separated iminium·OH<sup>-</sup> to the carbinolamine in the quantum chemical calculations. The combined reaction path of dienamine formation from precursor species, which were defined as iminium species, is depicted in Fig. 3.8 on the example of dienamines **1.c** at a PBE0-D3/def2-SVP//SCS-MP2/AUG-TZVP + SMD solv ( $\epsilon=2.4$ , toluene) level of theory.<sup>[25–32]</sup>

The found minimum structures present experimentally detected structural features (chapter 2) with an *sc-exo* conformation of the exocyclic C <sub>$\alpha$</sub> -C <sub>$\epsilon$</sub>  bond in the catalyst residue for all species pre-3*E*-, pre-3*Z*-, 3*E*- and 3*Z*-dienamines (only 3*E*- and 3*Z*-dienamines were accessible to NMR spectroscopic investigations). The first double bond was selected to be 1*E* configured and the C<sub>2</sub>-C<sub>3</sub> bond was set as *s-trans* configured as found experimentally. Evaluating the precursor species, the pre-3*E*-dienamine species is found to be 1.52 kJ mol<sup>-1</sup> less stable than the pre-3*Z*-dienamine. The transition state for the reaction from pre-3*E*-dienamine to 3*E*-dienamine was found with a reaction barrier of E<sub>A</sub>=52.14 kJ mol<sup>-1</sup>. The reaction barrier for pre-3*Z*-dienamine to 3*Z*-dienamine is found at E<sub>A</sub>=46.86 kJ mol<sup>-1</sup>. The dienamine species show an energy difference of 14.20 kJ mol<sup>-1</sup> with the 3*Z*-**1.c** dienamine being the more stable one. The associated reaction energies are  $\Delta G^{298}=+2.47$  kJ mol<sup>-1</sup> and  $\Delta G^{298}=-10.20$  kJ mol<sup>-1</sup> for the 3*E*-**1.c** and 3*Z*-**1.c** formation, respectively.

Assuming the validity of the Eyring-Polanyi or transition state theory for this reaction,<sup>[33]</sup> as the trajectory of the transition state is found to be separated from all other movements, the reaction barrier translates to an almost 4 times higher reaction rate for the formation of 3*Z*-**1.c** in comparison to 3*E*-**1.c** from pre-3*Z*- and pre-3*E*-iminium structures respectively. Reaction rates can be calculated at 3.79·10<sup>4</sup> s<sup>-1</sup> for TS<sub>3*Z*</sub> and 0.96·10<sup>4</sup> s<sup>-1</sup> for TS<sub>3*E*</sub>.<sup>[34]</sup> The lower activation barrier for 3*Z* explains the predominant formation of 3*Z*-dienamine independent of catalyst structure. This also contradicts the notion that possibly the initial formation rates for both dienamines differ that significantly and direct consumption could explain the mode of stereocontrol.

In summary, we could rationalize the faster buildup of 3*Z*-dienamine by clarifying the mode of formation to be determined by a lower associated reaction barrier. Additionally, we could not establish any reason why the formation rate of 3*Z*-dienamine should change with reaction time, thus excluding a favouring of 3*Z*-formation with subsequent exclusive consumption to be responsible for stereocontrol.

**Influence of down-stream intermediates.** Having shown that the formation rates and the ratio of 3*Z*- to 3*E*- dienamines does not impact the stereochemical outcome of the reaction, we next focused on down-stream intermediates that might potentially be responsible for the stereoselective step.

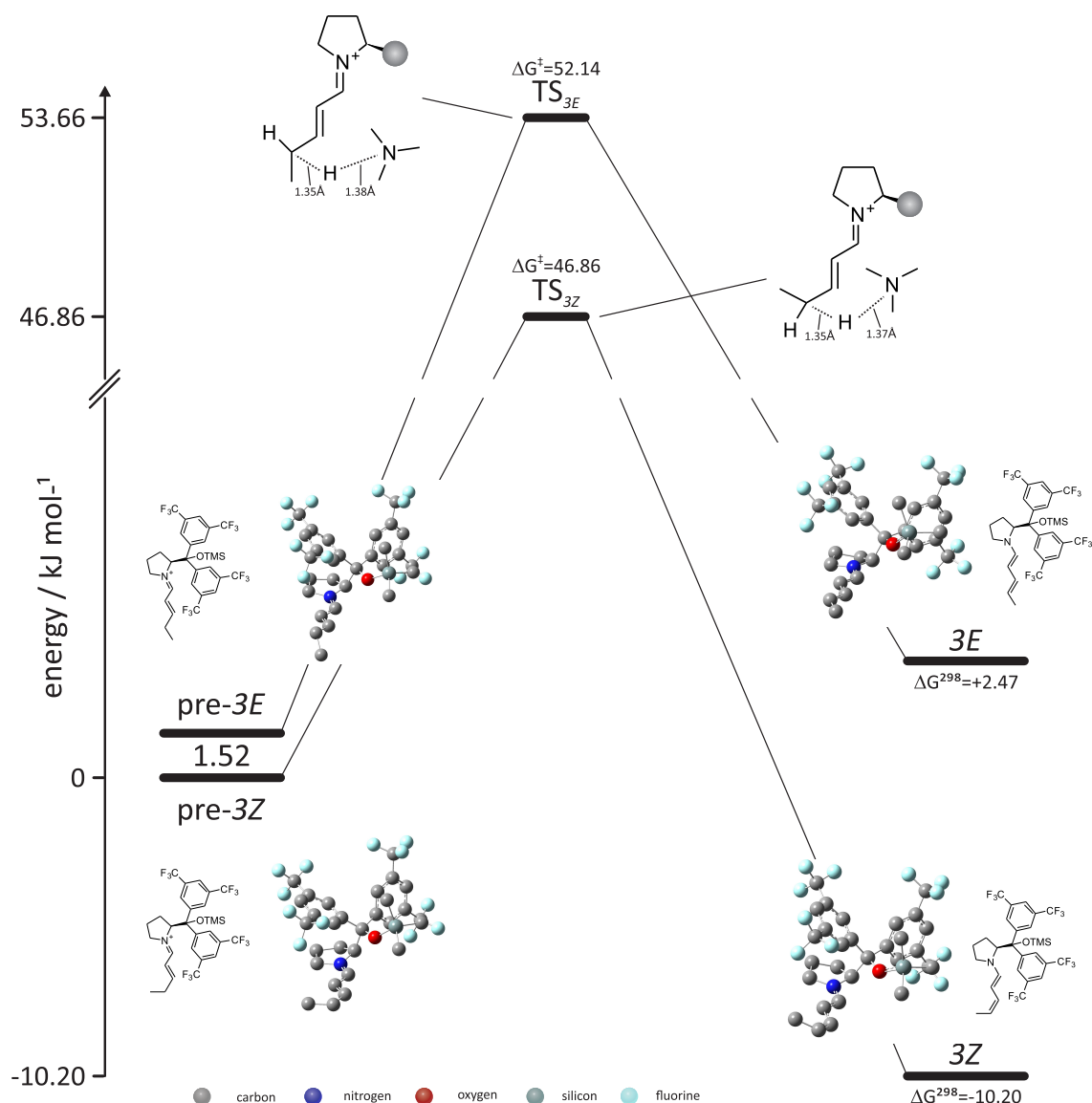


**Fig. 3.8: Low reaction barrier for 3Z-dienamine formation.** The formation of 3Z-dienamine is 4 times faster than the reaction to 3E-dienamine which however not translates into experimental *ee*-values. Relative energies in  $\text{kJ mol}^{-1}$  for the pre-3E-**1.c** and pre-3Z-**1.c** equilibrium as well as for the 3E-**1.c** and 3Z-**1.c** equilibrium calculated at a PBE0-D3/def2-SVP//SCS-MP2/AUG-TZVP + SMD solv ( $\epsilon=2.4$ , toluene) level of theory.<sup>[25–32]</sup> Transition states between the pre-dienamine species and the dienamine species TS<sub>3E</sub> and TS<sub>3Z</sub>. Reaction energies  $\Delta G^{298}$  and Gibbs free energy of activation  $\Delta G^\ddagger$  in  $\text{kJ mol}^{-1}$ . Structures of found minima and schematic representation of the transition states with distances in the deprotonation/protonation region. All found species show the *sc-exo*-conformation of the exocyclic  $C_\alpha$ - $C_\epsilon$  bond in the catalyst residue. No significant structural change is observed comparing the pre-3E- and 3E as well as the pre-3Z and 3Z species, respectively. *Note:* Hydrogens omitted for clarity. Coordinates of the stationary points can be found in the SI (3.3).

**Configuration of product dienamines.** First we speculated about the formation of product dienamine species, which were already mentioned in literature<sup>[10]</sup> that after possible stereoselective hydrolysis could be responsible for stereoselection. However, experimental data on formed product dienamine species with DEAD as electrophile and the  $\gamma$ -disubstituted aldehyde **4** showed that the formation of such dienamine species is extremely slow compared to the formation of non-crowded dienamines ( $k_{3E/3Z}=0.014-0.021\text{ min}^{-1}$  for **1.c-3.c** and  $k=0.007\text{ min}^{-1}$  for **4.c**,<sup>c</sup> see in the SI 3.3) and were moreover not detected in reactive solutions. Additionally, we identified a ratio of 70/30 for 3Z/3E-product dienamines which again, do not translate into the experimental enantiomeric excess in the products (see the SI 3.3 for further information). Therefore the contribution of 3Z- and 3Z-product dienamines to stereocontrol could be excluded.

**The energetic distribution of down-stream product iminium species.** Secondly, we were interested in the way iminium ions, which are formed after the electrophile attack by the dienamines, play a role in the mode of stereoinduction. Since we cannot access those intermediates via NMR spectroscopy, we again employed high level quantum chemical calculations to obtain the energetics of the formed species. As shown above, the used quantum chemical method accounting for non-covalent interactions was able to accurately reproduce experimental findings. Thus we feel confident that the same method can account for the interactions in the product-iminium species and reliable energies were calculated.

Quantum chemical calculations on the reaction of dienamine intermediates with Michler's hydrol as electrophile are missing in literature, however the transition states for the attack on DEAD as electrophile have already been evaluated by Jørgensen and co-workers.<sup>[7]</sup> In their study the  $\gamma$ -selectivity was attributed to the broken resonance of the resulting double bonds in the product and the stereoselectivity was attributed to a Diels-Alder type transition state. A comparable transition state is not feasible for the substituted benzhydrol electrophiles we investigated since Michler's hydrol does not possess the ability to partake in Diels-Alder type reactions. In their study, 3Z-**1.c** was calculated to be  $5.86\text{ kJ}\cdot\text{mol}^{-1}$  less stable than 3E-**1.c** at B3LYP/6-31G(d) (CPCM)//B3LYP/6-31G(d) level of theory which is in strong disagreement with our calculation results in respect to 3Z-dienamine stabilization. We feel confident that this discrepancy to our findings can largely be attributed to the lack of dispersive interactions accounted for in their used method. However, we think considering dispersive interactions is necessary to obtain correct results, not least because Jørgensen and co-workers speculated about an interaction of the  $\text{CF}_3$  groups with the diene system, which can be taken into consideration with our approach.

In addition, they calculated down-stream iminium ions of the DEAD reaction with dienamines **1.c** already. They found the iminium ion associated with the major enantiomer to be  $14.98\text{ kJ}\cdot\text{mol}^{-1}$  more stable than the product iminium ion associated with the minor one.<sup>[7]</sup>

<sup>c</sup>no differentiation in *E*- or *Z*-dienamine possible.

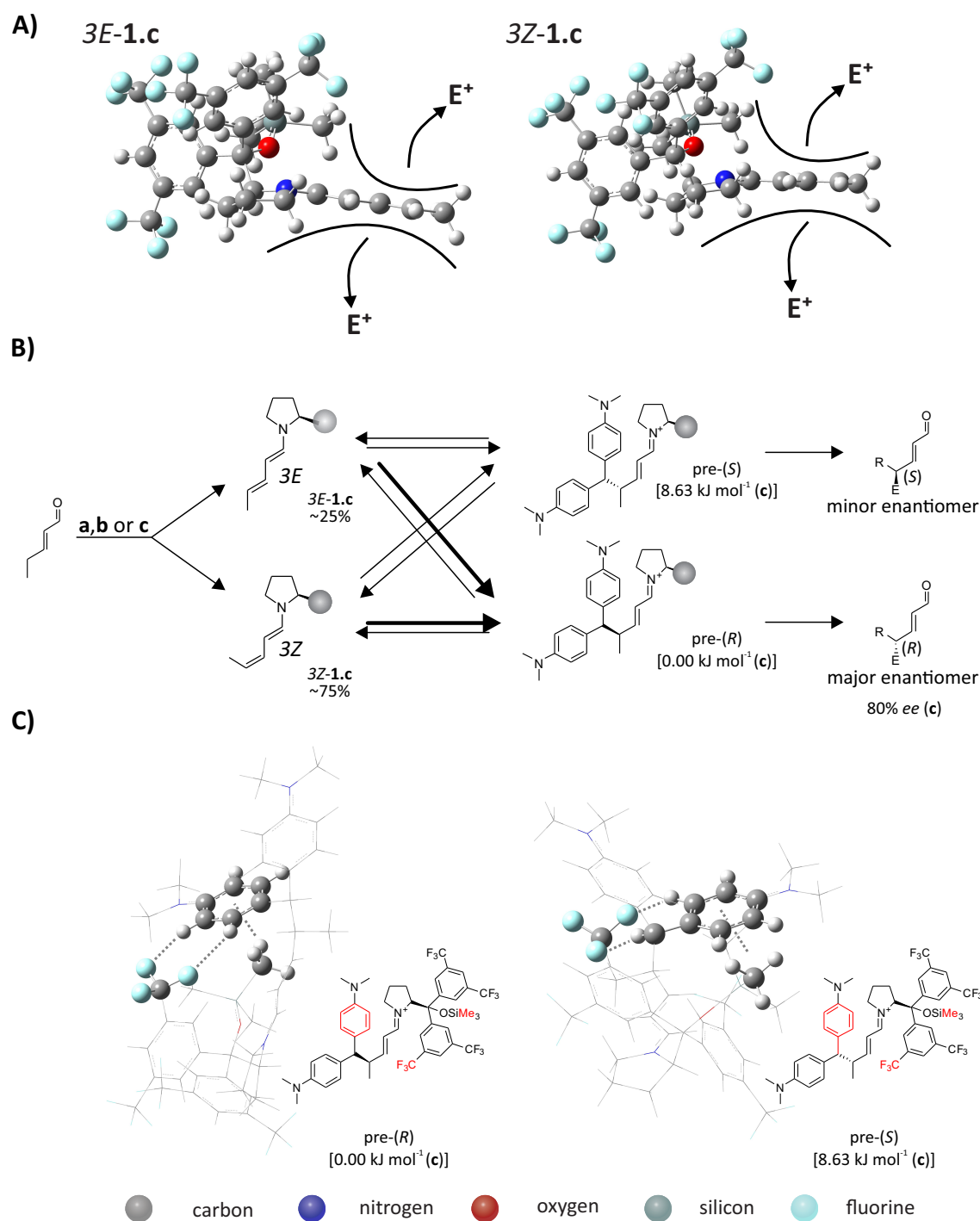


**Fig. 3.9: Product iminium stabilisation as key to stereoselection.** Identical qualitative shielding of both 3E and 3Z-dienamines allow the reaction with electrophile from both sides (**A** and chapter 2). Theoretical calculations show a preference of the pre-(R) iminium intermediate (**B**) corresponding to the experimental *ee*-values due to more favorable interactions (red in the schematic representation) of a CF<sub>3</sub> group and a CH<sub>3</sub> group with one aromatic ring in the electrophile-submoiety (**C**). For pre-(S) the interactions are weaker due to longer distances and unfavorable orientation (shifted CH/ $\pi$ ). Structures in **A** and energies in **B** determined at PBE0-D3/def2-SVP//SCS-MP2/AUG-TZVP + SMD solv ( $\epsilon=2.4$ , toluene) level of theory.<sup>[25–32]</sup> Coordinates for the stationary points can be found in the SI 3.3. Parts of the structures in **C** omitted for clarity.

We expanded on these investigations and were interested in the down-stream iminium ion energetics as a function of employed catalyst with the substituted benzhydrol electrophiles. The identical structures (*vide supra* and chapter 2) show that no difference in the quality of shielding in the dienamines is present and so attack on the electrophile can occur on both the "open" and "shielded" face of both 3*E* and 3*Z*-dienamines (see Fig. 3.9 **A**). We modeled iminium ions as result for the front- ("shielded") and back-side ("open") attack of both the 3*E*- and 3*Z*-dienamines on Michler's hydrol and investigated the formed species (see Fig. 3.9 **B**).

The pre-(*R*) product iminium constitutes for all catalysts employed the more stable intermediate species and is associated with the major product enantiomer (*R*).<sup>[10]</sup> For **a**, the pre-(*S*) product iminium is 6.53 kJ·mol<sup>-1</sup> less stable than the pre-(*R*) species. Virtually the same situation is found for **b**, with a energy difference of 5.69 kJ·mol<sup>-1</sup> in favor of the pre-(*R*) product iminium species. For the best performing catalyst **c** the energy gap is much more pronounced with the major enantiomer precursor being 8.63 kJ·mol<sup>-1</sup> more stable compared to the minor enantiomer precursor. This energy gap is explained by favorable interactions that are more pronounced in the pre-*R*-iminium species for **1.c**. CF<sub>3</sub>/CH as well as CH/π interactions could be identified for both precursor species, however their orientation leads to more favorable interactions in pre-*R*. The most obvious interactions in both dienamines are presented in Fig. 3.9 **C**. For pre-(*R*)-iminium a single catalyst CF<sub>3</sub> group exhibits two hydrogen bonds with a aromatic CH bond in the electrophile submoiety. In addition, a centered CH<sub>3</sub>/π interaction is also connecting the catalyst substructure with the electrophile moiety. For pre-(*S*)-iminium also one single CF<sub>3</sub> group is involved in hydrogen bonding. In this case, only one hydrogen bond is directed towards an aromatic CH group, the other to a aliphatic CH group. Just as for pre-(*R*) a CH<sub>3</sub>/π interaction is identified, however the orientation allows only a shifted one, which is to be considered not as favorable as in pre-(*R*).

We did not investigate the transition states connecting the dienamines with the iminium species, since the size and the degrees of freedom of the dienamine-electrophile system would lead to very high computational costs. We did not investigate the transition since we presume that, since for both 3*E* and 3*Z*-dienamine the quality on both the "open" and "shielded" side are effectively equal, also the activation barriers for electrophile attack are qualitatively equal. The thermodynamic energetic trend for **a** and **b** are practically indistinguishable, however the much more pronounced energy gap for catalyst **c** very well explains its better performance in synthesis. Both dienamines 3*E* and 3*Z* do feed into both product precursor iminium species since no face of either dienamine is effectively shielded. The rate constants for this is presumably similar for both "open" and "shielded" face attacks, and therefore we suggest that the attack of the electrophile on the dienamine intermediate is a reversible reaction and the subsequent hydrolysis is slow compared to the electrophile attack.<sup>d</sup> This would lead to a

<sup>d</sup>Non-reversible reactions for the formation of both product iminium species might also be viable, however one could expect comparable reaction rate constants for both "open" and "shielded" side attacks, which would render non-reversible reactions impossible to concur with the stereoselection results. Experiments towards a possible electrophile-exchange reaction proving the existence of an equilibration between the dienamine species and the product iminium species will be performed in due course. Additionally, the 3*Z*/3*E*-ratio will be

sorting into the more stable pre-(*R*) iminium species that, after hydrolysis, affords the major enantiomer. Thus, the stereochemical performance is dependent on the energy gap of the product iminium species due to steric interactions in the down-stream intermediates and not on the distribution, shielding or reactivity of the dienamine species. This might explain why solely considerably large electrophiles are found in literature allowing successful stereocontrol in dienamine activation.

In summary, successful stereinduction in the  $\gamma$ -alkylation of linear  $\alpha,\beta$ -unsaturated aldehydes by dienamine activation is independent of the eponymous species distribution (3*Z*/3*E*-dienamine ratio) or reactivity but rather dependent on the energetic distribution of the down-stream iminium intermediates.

---

altered by changing the preform temperature and the resulting *ee*-values will be determined to obtain further information on the nature of the reaction to the product species. Experiments to prove the hydrolysis being the rate determining step will be performed. If the hydrolysis is the rate determining step in this process, heavy water would significantly slow down the reaction.

---

## Conclusion

In summary, using *in situ* NMR reaction profiles and theoretical methods we could show that neither the *3Z/3E*-distribution or initial formation rate, nor the fast equilibration of *3Z*- and *3E*-dienamine with subsequent exclusive consumption of *3Z*-dienamine are directly correlated with stereoselectivity. This together with within the experimental error identical shielding of *3E*- and *3Z*-dienamines show that both have to feed into the major product. Product dienamines as stereogenic intermediates were excluded as well. In stead product iminium species were found to be decisive. The energy trend as a function of employed catalyst could show that the stabilization of major enantiomer product iminium compared to minor enantiomer product iminium concurs with the observed product distribution. The (de)-stabilization is governed by steric interactions and can explain why solely large electrophiles were successfully applied in dienamine activation so far, since merely the steric interactions in the product iminium species is decisive for stereoselection success. These findings show that if remote stereocontrol is impossible due to insufficient steric hindrance, the interactions in down-stream intermediates can be successfully applied for stereocontrol in catalysis. In addition, these findings demonstrate that the term dienamine activation needs to be refined, since the HOMO activation is achieved in the eponymous intermediates however stereocontrol is achieved in down-stream iminium species.

## Experimental Section

### NMR measurements

Dienamines species were created *in situ* inside standard 5 mm NMR tubes by addition of freshly distilled aldehyde (25  $\mu$ mol) to a solution of organocatalyst (1 equiv.) and additive (as stated) in deuterated solvent (0.5 mL). All chemicals were used as purchased (if not otherwise stated). Chemicals were purchased from Sigma Aldrich and TCI Europe. NMR measurements were performed at 300-315 K on a Bruker Avance III HD 600 (600.13 MHz), a Bruker Avance DRX 600 (600.13 MHz) and a Bruker Avance III 600 (600.25 MHz) spectrometer, the latter equipped with a TCI cryoprobe with z-gradient (53.5 G cm<sup>-1</sup>). Reaction monitoring (*react*-NMR) by 1D <sup>1</sup>H-NMR spectra was employed to identify appropriate time slots for more detailed 2D NMR spectroscopic investigations. <sup>1</sup>H,<sup>1</sup>H-COSY, <sup>1</sup>H,<sup>1</sup>H-NOESY ( $t_m$ =450 ms), <sup>1</sup>H,<sup>13</sup>C-HSQC (<sup>1</sup> $J_{HC}$ =145 Hz) and <sup>1</sup>H,<sup>13</sup>C-HMBC (long range coupling 10 Hz) as well as <sup>1</sup>H,<sup>19</sup>F-HOESY ( $t_m$ =450 ms) spectra were recorded for the characterization of the observed species if information from the 1D NMR spectra proved to be insufficient. Kinetic data was processed with Bruker Dynamics Center 2. All spectra were processed and evaluated with Bruker Topspin 3.2.

### Quantumchemical calculations

The geometries were optimized at PBE0-D3/def2-SVP<sup>[26–28]</sup> level of theory. Thermochemical analysis and solvent correction (SMD in toluene)<sup>[29]</sup> were also performed at geometry optimization level and added to the total energy. Single points were calculated at SCS-RIMP2/aug-TZVP<sup>[25,30,31]</sup> level of theory using split-J for the coulomb term and semi numerical approximation (RIJCOSX)<sup>[32]</sup> for the exchange term for the reference wavefunction. The software used were Gaussian09 subversion D.01<sup>[35]</sup> for the geometry optimization, frequency analysis and solvent correction, as well as ORCA-3.0.3<sup>[36]</sup> for the single point calculations.

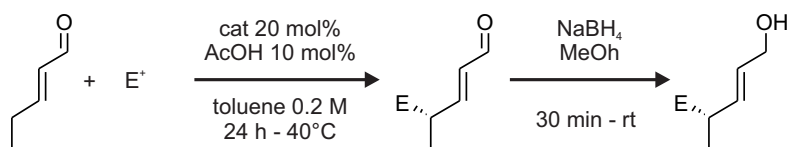
### Synthesis of not already reported aldehyde substrates

#### E-2-methylpent-2-enal (5)

To a solution of 4-methyl-benzoic acid (0.1 equiv.) and pyrrolidine (0.05 equiv.) in DCM was added propanol (2 equiv.). After refluxing for 1.5 h the solution was allowed to cool to room temperature and sodiumbicarbonate solution was added (7 % in water) and the organic phase separated. The water phase was extracted with DCM and the organic phases combined. The organic phase was dried over sodiumsulfate and after removal of the solvent the product was collected (58 %) <sup>1</sup>H-NMR (400 MHz, CDCl<sub>3</sub>)  $\delta$  / ppm, 9.40 (s, 1H), 6.52-6.43 (m, 1H), 2.37 (m, 2H), 1.74 (d,  $J$ = 1.1 Hz, 3H), 1.12 (t,  $J$ =7.6 Hz, 3H). <sup>13</sup>C-NMR (100 MHz, CDCl<sub>3</sub>)  $\delta$  / ppm, 195.4, 156.3, 138.8, 22.3, 12.8, 8.9.



### Procedure for the gamma-alkylation of *trans*-pentenal



To a solution of the catalyst ((*S*)-2-(bis(3,5-bis(trifluoromethyl)phenyl)((trimethylsilyl)oxy)methyl)pyrrolidine, 20 mol%, 0.04 mmol) in toluene (1 mL, 0.2 M), *trans*-2-pentenal (2.0 equiv, 0.4 mmol) was added and the solution was stirred for the stated time at 40 °C in order to favor the formation of the dienamine. The electrophile (bis(4-(dimethylamino)phenyl)methanol, 1.0 equiv, 0.2 mmol) and acetic acid (10 mol%, 0.02 mmol) were added and the reaction was stirred at 40 °C for 24 h. Then the reaction mixture was filtrated through a plastic syringe with a layer of silica inside using  $\text{Et}_2\text{O}$  as eluent. The solvent was evaporated and the crude product was purified by flash chromatography ( $\text{SiO}_2$ , pentane/EtOAc 8/2,  $R_f$  0.35) to give a pale yellow oil. The purified aldehyde was dissolved in MeOH (1 mL) and  $\text{NaBH}_4$  (1.2 eq on theoretic 100 % yield, 0.24 mmol) was added and the reaction was stirred at rt for 30 minutes. Then, EtOAc (3 mL) and water (1 mL) were added, and the biphasic mixture was strongly stirred for 5 min. The organic phase was collected and the aqueous phase was extracted once with EtOAc (2 mL). The crude alcohol solution was dried over  $\text{Na}_2\text{SO}_4$ , evaporated and purified by preparative TLC ( $\text{SiO}_2$ , pentane/EtOAc 1/1,  $R_f$  0.30) to afford a colorless oil. The synthesis of the racemic references was carried out using a racemic mixture of catalyst (10 mol% for each enantiomer). Enantiomeric excess was determined by chiral HPLC (Lux 5u Cellulose-1 by Phenomenex).



## 3.3 Supporting Information

### Solvent dependency of the dienamine formation.

Besides the catalyst and catalyst loading screening, we investigated the dienamine distribution in different solvents, which are employed in synthesis.<sup>[7–11]</sup> For this purpose catalyst **b** was used, since it proved to be soluble in all investigated solvents. Although in hydrogen bonding

**Tab. 3.1:** Solvent dependency of dienamine intermediate ratio and proton chemical shift of H<sub>1</sub> in intermediate **1.b** at 100 mol% catalyst loading at 300 K. The solvent parameters are given as:  $\alpha$ : hydrogen bond donor capabilities,  $\beta$ : hydrogen bond acceptor capabilities and  $\pi^*$ : polarizability.<sup>[37,38]</sup>

Solvent	rel. amount <sup>a</sup> / %		solvent parameter		
	3Z- <b>1.b</b>	3E- <b>1.b</b>	$\alpha$	$\beta$	$\pi^*$
methanol-d <sub>4</sub>	n.d. <sup>b</sup>		0.98	0.66	0.60
chloroform-d <sub>1</sub>	n.d.		0.20	0.10	0.58
toluene-d <sub>8</sub>	41.5	18.6	0.00	0.11	0.54
THF-d <sub>8</sub> <sup>c</sup>	24.5	10.5	0.00	0.55	0.58
DMSO-d <sub>6</sub> <sup>d</sup>	40.2	19.8	0.00	0.76	1.00

<sup>a</sup> The amount of all aldehyde derived species was set to 100 %

<sup>b</sup> not detected

<sup>c</sup> THF: tetrahydrofuran

<sup>d</sup> DMSO: dimethylsulfoxide

solvents like methanol or chloroform dienamines could not be detected, for the remainder of the screened solvents the relative ratio of dienamines detected remains at 2:1 for 3Z:3E. This finding contradicts the validity of a simple steric shielding model determined by preferential 3Z-dienamine formation, since the found ratio should lead to comparable reaction outcomes in the different solvents, however this is not the case.

### Catalyst-loading dependency of the dienamine formation.

We additionally performed kinetic investigations into the formation of dienamine species of **1** as a function of catalyst **c** loading varying from 20-100 mol%. The kinetic profiles can be found in Fig. 3.10.

While for 50 and 100 mol% the progression appears constant at around 2-3/1 for 3Z/3E-**1.c** with only a slight increase with time, the progression for 20 mol% differs significantly (*vide supra*).

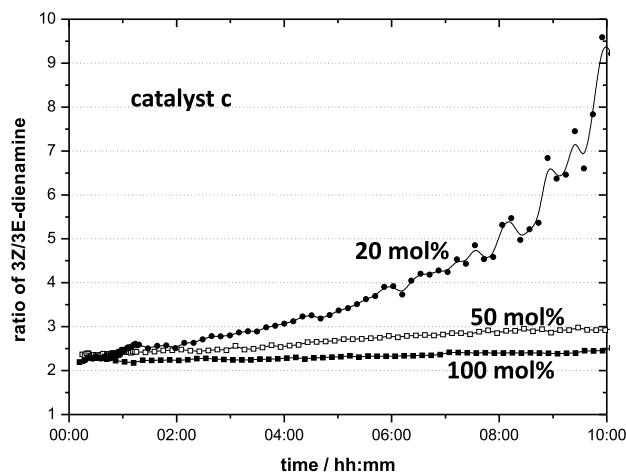


**Fig. 3.10:** Progression of the 3Z/3E-ratio with time for catalysts **c** dependent on catalyst loading in toluene- $d_8$  at 313.15 K.

### Lack of chemical exchange shown by lack of EXSY cross-peaks.

To further provide experimental evidence for the absence of rapid chemical exchange between both dienamine species we utilized  $^1\text{H}$ ,  $^1\text{H}$ -EXSY spectroscopy with mixing times up to 2 s. Here we did not identify any exchange peak connecting both dienamine structures in dienamines **1.c** (see Fig. 3.11).

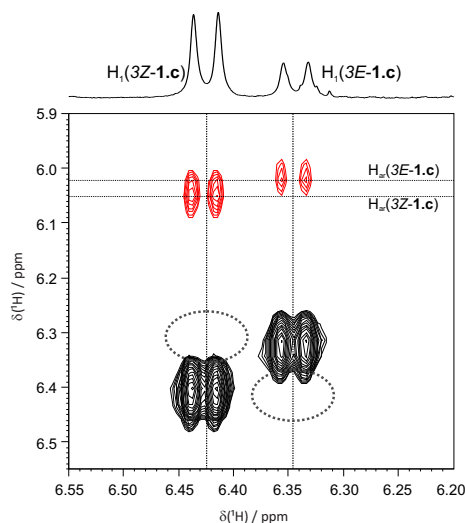


**Fig. 3.11:**  $^1\text{H}$ ,  $^1\text{H}$ -EXSY traces of protons  $\text{H}_1$  (highlighted) for both 3E and 3Z-**1.c** at 313.15 K in toluene- $d_8$ . The mixing time was set to  $t_m=2$  s. No chemical exchange peak (dotted ellipses) is visible corroborating exchange between both species.

Here besides the diagonal peaks for both  $\text{H}_1$  of 3E- and 3Z-**1.c** only NOE cross peaks to the corresponding aromatic protons  $\text{H}_{\text{ar}}$  are evidenced, but no EXSY crosspeaks are visible (encircled area).

### The formation of product-dienamine species.

We addressed the possibility of the formation of an product-dienamine species, which was speculated before in literature (schematically presented in Fig. 3.12).<sup>[10]</sup>

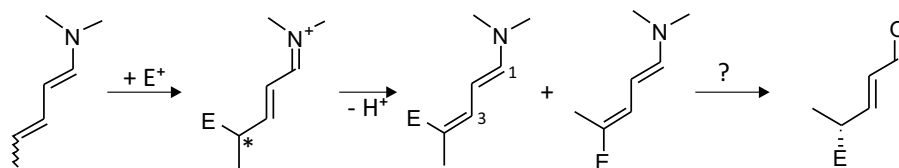


**Fig. 3.12:** Possible formation of product dienamine species after the attack of the dienamines on the electrophile.

In these product dienamines the formation of the two double bonds in 1 and 3 position would potentially destroy the stereochemical information and again *3E* to *3Z*-share would determine the stereochemical outcome in the subsequent hydrolysis reaction to the form the products. This theory can largely be excluded, since we did not detect product-dienamine species when we mixed either, aldehyde, catalyst, acidic additive (to activate the electrophile) and electrophile or we let dienamines allow to preform and then acidic additive and electrophile was added.

**Tab. 3.2:** Rate constants through fitting for the formation of dienamines from catalyst **c** and the abreaction of aldehydes **1-4** in toluene-*d*<sub>8</sub> at 313.15 K and 100 mol% catalyst loading.  $\gamma$ -crowding largely hampers the formation of dienamines or renders it very slow.

System	1.c	2.c	3.c	4.c
$k_{3Z} / \text{min}^{-1}$	0.021	0.019	0.019	0.007 <sup>a</sup>
$k_{3E} / \text{min}^{-1}$	0.017	0.014	0.016	
$k_{\text{ald}} / 10^{-6} \text{ s}^{-1\text{b}}$	-5.33	-11.2	-10.3	-8.38

<sup>a</sup> No differentiation between *3Z*- and *3E*-dienamine possible

<sup>b</sup> Side reactions to unidentified species alter the aldehyde consumption rate and renders them incomparable.

In addition, the formation of dienamines from  $\gamma$ -alkylated aldehydes can be shown to progress very slowly (see Tab. 3.2), compared to the formation of the non-alkylated dienamines, since  $\gamma$ -crowding largely hampers the deprotonation step. This is shown by the slow formation of **4.c**, although for **4** only a single CH<sub>3</sub> group is crowding the  $\gamma$ -position. In possible product dienamine species however, large substituents crowd the  $\gamma$ -position, making it even less likely to deprotonate in this position. To experimentally exclude the *3E*- to *3Z*-product dienamine share to be decisive for stereoinduction, we mixed product, which we isolated from the dienamine catalyzed  $\gamma$ -alkylation with catalyst in toluene-*d*<sub>8</sub>, and investigated the ratio of *3E*- to *3Z*-product-dienamine species. As was shown for all other dienamines, a ratio of around

2:1 was achieved non reflecting the enantiomeric excess achieved in the reaction. Thus we can exclude the formation of product-dienamines from being responsible for the success in stereinduction.

### Influence of water content on the dienamine formation.

In the condensation reaction forming the precursor iminium species water is expelled into the solution. Since water is additionally also known to stabilize certain hydrogen bond acceptor and hydrogen bond donor moieties, we investigated the impact of water content on the dienamine formation and ratio. The summed up experimental results can be found in Fig. 3.13.

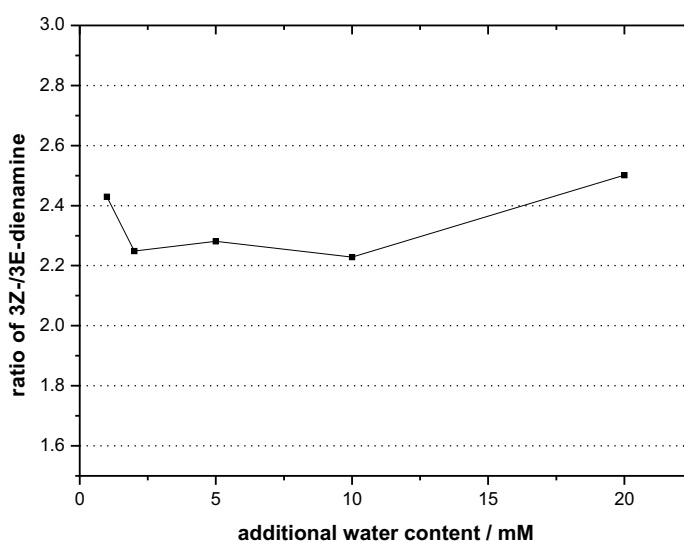


**Fig. 3.13:** Influence of water on the ratio of 3Z-/3E-**1.c** in toluene- $d_8$  at 100 mol% catalyst loading at 300 K. *Note:* Since water is expelled also in the reaction, additional water content is displayed.

It is clearly visible that water contents, ranging from 1 mM to 20 mM added, do not alter the overall dienamine ratio. In addition, no change in formation slope or consumption velocity were identified (Data not shown).

In conclusion we could show that additional water content does not alter the dienamine formation or the dienamine distribution.

## NMR-Assignments

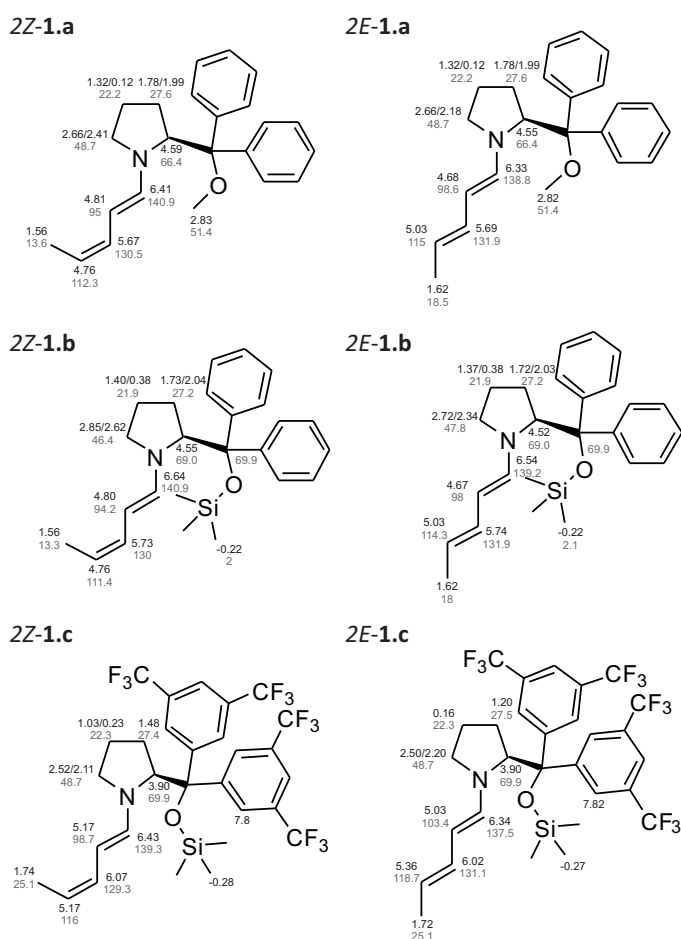


**Fig. 3.14:**  $^1\text{H}$  and  $^{13}\text{C}$ -chemical shifts of dienamines **1.a** (DMSO- $d_6$ , 300 K), **1.b** (DMSO- $d_6$ , 300 K), **1.c** (toluene- $d_8$ , 313.15 K). *Note:*  $^1\text{H}$ -chemical shifts in black,  $^{13}\text{C}$ -chemical shifts in grey.

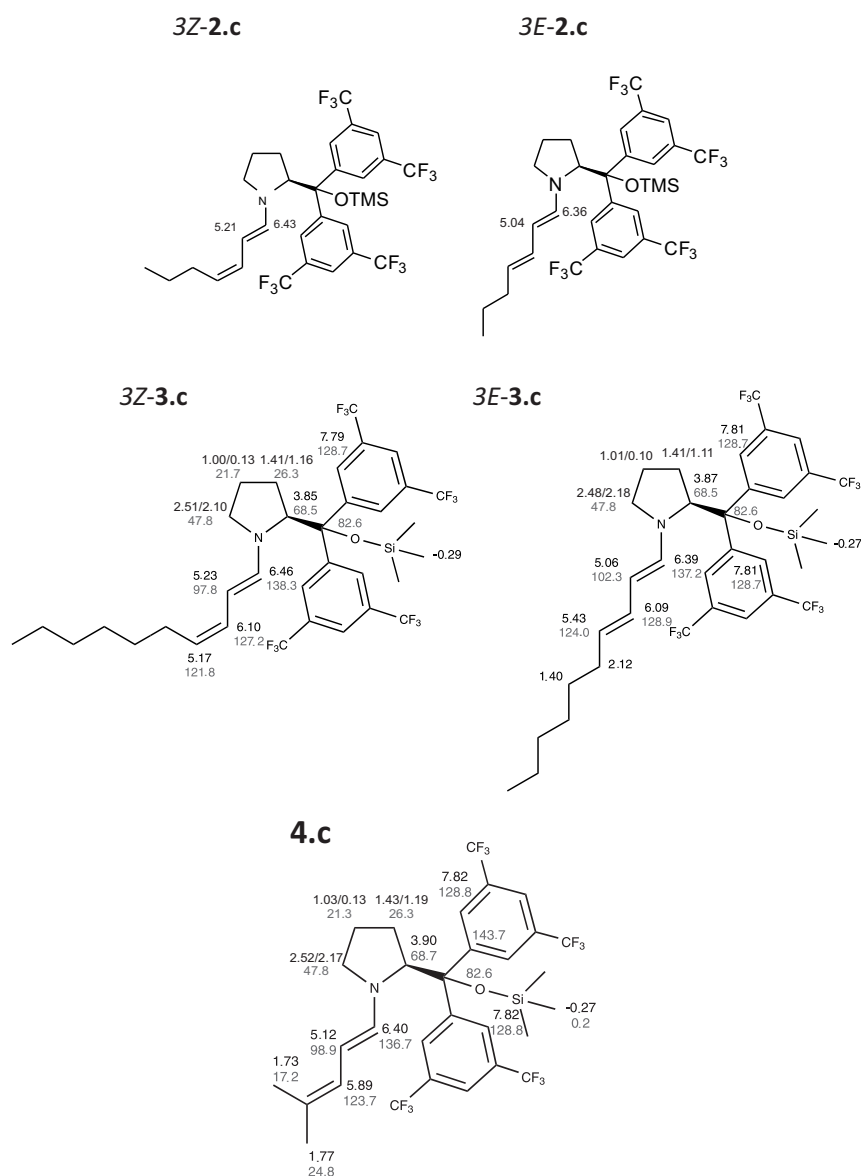


**Fig. 3.15:** <sup>1</sup>H and <sup>13</sup>C-chemical shifts of dienamines **2.c** (toluene-d<sub>8</sub>, 313.15 K), **3.c** (toluene-d<sub>8</sub>, 318 K) and **4.c** (toluene-d<sub>8</sub>, 318 K). *Note:* <sup>1</sup>H-chemical shifts in black, <sup>13</sup>C-chemical shifts in grey.

## Coordinates of stationary points at a pbe0-D3/def2svp//scs-mp2/aug-tzvp + SMD level of theory

### pre-3E

```
1\1\GINC-WORKER\FOpt\RPBE1PBE\def2SVP\C29H30F12N101Si1(1+)\JHIOE\06-Apr-2015\0\#p opt freq pbe1pbe/def2svp empiricaldispersion=gd3bj scf=tight\\title\\1,1\C,0.0436877711,-0.9915226507,1.9745375283\C,-0.4235252291,-0.0810899486,3.1073023054\C,0.7875159843,0.7657054651,3.5289143539\C,2.0182236792,0.0742424741,2.9403545501\H,-0.3450687501,-2.0138425857,2.0697547777\H,-1.282290428,0.5310419275,2.8019710402\H,-0.7696479779,-0.7042942415,3.9438922633\H,0.7160738454,1.7935864762,3.153864562\
```



H,0.8600806719,0.834003589,4.6219734946\H,2.5995060221,0.7375225638,2.2808153854\H,2.6963635322,-0.327090145,3.7074121572\N,1.5013359185,-1.0477546974,2.1448288333\C,2.2489462712,-1.9232087561,1.5409096878\H,1.7143293377,-2.7016994569,0.9905115952\C,3.6705836358,-1.8812448445,1.4884629935\H,4.2168860555,-1.0928850969,2.0114024512\C,4.3352491375,-2.7590736021,0.6967847767\H,3.7509931017,-3.5291851628,0.1731296961\C,5.79061936,-2.7459179303,0.4371682308\H,6.2873085103,-2.0101579432,1.0882338416\C,-0.2858517397,-0.5559327532,0.4996549906\C,-1.7890243811,-0.3764962231,0.3083352533\C,-2.2764410431,0.5192278402,-0.6438472434\C,-2.6954750069,-1.2289534334,0.9436639884\C,-3.6328442181,0.5544960764,-0.9608181248\H,-2.0540187686,-3.5195132911,-2.819752702\C,-4.0505037044,-1.187786687,0.6298437354\H,-2.3614008358,-1.9581784316,1.6832031\C,-4.5315610111,-0.2958798449,-0.3259668989\H,-5.5934353631,-0.2665302609,-0.5733635074\C,0.5269224161,0.6944426465,0.1750254559\C,0.1494841558,1.968444494,0.6050338892\C,1.7520958734,0.5485931031,-0.4728486153\C,0.9950901772,3.0592053447,0.4106908861\H,-0.1713660158,-1.2500414685,-4.1235496557\C,2.5965926204,1.6386935099,-0.6637441352\H,2.0519832535,-0.4373851859,-0.8262118353\C,2.2269229767,2.9057611337,-0.2228471022\H,2.883046039,3.763679384,-0.3747982765\O,0.1614635013,-1.6302137731,-0.2744927503\Si,-0.2314472242,-2.1794984918,-1.8614327856\C,1.1145510213,-3.4523440188,-2.1107177444\H,2.1125544179,-2.9858111384,-2.0895692318\H,1.0729257433,-4.2385492735,-1.3401835576\H,1.0042232224,-3.9452346395,-3.0892519379\C,-1.9314743601,-2.9467425267,-1.88612458\H,-2.0893282874,-3.6389782886,-1.0453274776\H,-2.7275442974,-2.1880514048,-1.8596235112\H,-1.5962638583,1.1957849673,-1.1631617805\C,-0.094688146,-0.8028565805,-3.11856263\H,0.8660897186,-0.2691957291,-3.0684581256\H,-0.9108881385,-0.0707827022,-3.0356639852\H,-0.8144349207,2.12710791,1.0928809445\C,3.9288902072,1.3845425126,-1.3172122692\F,4.5930112707,2.5028484879,-1.565595753\F,4.6980317089,0.6185496255,-0.5193443149\F,3.7829674481,0.7144368768,-2.4623101474\C,0.573951759,4.3983167043,0.9626322664\F,0.701083589,4.4020743276,2.2985551223\F,1.3138132147,5.3890693553,0.4826024837\F,-0.7037590372,4.6510233596,0.6887988343\C,-4.9708211946,-2.1866665993,1.2855450759\F,-4.7922441751,-3.3996616143,0.7534006204\F,-4.7124746534,-2.2876994181,2.5919980425\F,-6.2476365427,-1.8574019417,1.1365689666\C,-4.0826918704,1.4982509865,-2.0478838781\F,-5.4050184768,1.5712054981,-2.1286579898\F,-3.6048178814,2.7254522977,-1.8393950385\F,-3.6176068071,1.0895692556,-3.2349574522\C,6.439480246,-4.1238272856,0.5472454473\H,7.5055178212,-4.0620251175,0.2895206077\H,6.361513816,-4.5219244426,1.5694130625\H,5.9709428562,-4.8465658913,-0.13796953\H,5.9134614357,-2.3694526741,-0.5979307296\\Version=ES64L-G09RevD.01\State=1-A\HF=-2736.1425081\RMSD=4.582e-09\RMSF=3.177e-06\Dipole=3.7049344,-2.8770682,1.9594924\Quadrupole=14.6914873,-8.0583201,-6.6331673,-17.6561546,9.7977762,1.5023986\PG=C01 [X(C29H30F12N10Si1)]\ \@

**pre-3Z**

```
1\1\GINC-WORKER\FOpt\RPBE1PBE\def2SVP\C29H30F12N10Si1(1+)\JHIOE\06-Ap
r-2015\0\#p opt freq pbe1pbe/def2svp empiricaldispersion=gd3bj scf=ti
ght\title\1,1\C,0.0320692041,-0.9096820598,2.0072661385\C,-0.4110169
287,0.0520734723,3.1062278231\C,0.8158149297,0.9023674978,3.46549225\C
,2.0313519824,0.119719849,2.9675264685\H,-0.3879435831,-1.916210793,2.
1331465553\H,-1.2695496139,0.6594877411,2.7911308999\H,-0.7444261238,-
0.5325611193,3.9756549531\H,0.7767402369,1.8886771016,2.9886389121\H,0
.8757232708,1.0775907783,4.547380291\H,2.6876237095,0.7202621217,2.319
3686224\H,2.6421003559,-0.2924579591,3.7844553312\N,1.4854529335,-1.00
44631476,2.1928145357\C,2.2069543789,-1.9412586227,1.6522994816\H,1.65
20310642,-2.7336216391,1.1441222683\C,3.6297145304,-1.9594274743,1.627
2366842\H,4.1930153019,-1.1374628405,2.072563336\C,4.2702762728,-2.961
2301138,0.9728665835\H,3.6580013946,-3.7579418065,0.5297780091\C,5.730
4987976,-3.077656774,0.7753754023\H,5.8928001694,-3.2146774888,-0.3113
069648\C,-0.273391733,-0.512915258,0.5172151797\C,-1.7750806407,-0.362
498996,0.2884978693\C,-2.2385767492,0.4433215765,-0.7521200195\C,-2.70
03710987,-1.1446198354,0.984511035\C,-3.5884784428,0.4586619572,-1.096
5652035\H,-1.9390846981,-3.6435573867,-2.6915421481\C,-4.049785646,-1.
1204553528,0.6453420245\H,-2.3912070002,-1.7969738518,1.8019784598\C,-
4.5059035846,-0.3196226053,-0.3996413515\H,-5.5639839135,-0.3006170737
,-0.6643209594\C,0.5173847341,0.7485098325,0.1821486175\C,0.0681090578
,2.0271398153,0.5189812549\C,1.7877339603,0.6157851777,-0.3762139901\C
,0.885960016,3.1385465203,0.3236200755\H,0.0268513938,-1.4286613136,-4
.0865856887\C,2.6094859347,1.725555968,-0.5529017581\H,2.142436416,-0.
3731830766,-0.6661636192\C,2.1662785818,2.9988244764,-0.2074758451\H,2
.804831771,3.8712475383,-0.352488798\O,0.2146845696,-1.5937750804,-0.2
212899313\Si,-0.1422985687,-2.2346009961,-1.7791484071\C,1.2194213551,
-3.5067623172,-1.93043209\H,2.2126031646,-3.030809694,-1.9013040332\H,
1.1603192067,-4.2577355457,-1.1264288579\H,1.1405135128,-4.0453404545,
-2.8876851342\C,-1.832186894,-3.0246699096,-1.7858995354\H,-1.98442847
92,-3.6788060529,-0.9139193831\H,-2.6404121921,-2.2787883514,-1.800460
4835\H,-1.5433265241,1.0661500721,-1.3168386579\C,0.0125626663,-0.9269
833132,-3.1049397697\H,0.9428333197,-0.3452801502,-3.0184799167\H,-0.8
396396459,-0.2326124903,-3.1168201881\H,-0.9302977575,2.1729543716,0.9
364511151\C,4.013938002,1.4892769871,-1.0380561578\F,4.6209559731,2.60
63340426,-1.4060365871\F,4.7469941686,0.9329886794,-0.0501317983\F,4.0
39934074,0.633420406,-2.0604369037\C,0.3857533102,4.486663272,0.778992
8529\F,0.4548546191,4.5704743194,2.1157959766\F,1.1049280606,5.4799380
373,0.2725579971\F,-0.8879644611,4.6680754098,0.4379993598\C,-5.001745
5268,-2.0329463474,1.3780191727\F,-4.9641666773,-3.2627492737,0.859046
6873\F,-4.6667431788,-2.1365639198,2.6670494799\F,-6.2536331357,-1.596
9446987,1.3065882556\C,-4.0117037935,1.3053711719,-2.2706722864\F,-5.3
314265938,1.3625934782,-2.3934578034\F,-3.5451306322,2.5486739296,-2.1
525771226\F,-3.5121378764,0.802079184,-3.4067135916\C,6.5882031397,-1.
```

9510985624,1.3176501871\H,7.648108305,-2.1403895791,1.101077299\H,6.32  
14557234,-0.9880244251,0.8572230475\H,6.4896821697,-1.8540272953,2.409  
6082981\H,6.0332121453,-4.0563678097,1.197332084\\Version=ES64L-G09Rev  
D.01\State=1-A\HF=-2736.1451651\RMSD=7.586e-09\RMSF=3.393e-06\Dipole=3  
.7147068,-3.0203507,2.0742515\Quadrupole=13.7125347,-6.6274979,-7.0850  
368,-18.0823894,11.3470434,0.3748067\PG=C01 [X(C29H30F12N101Si1)]\@

### 3E

1\1\GINC-WORKER\FOpt\RPBE1PBE\def2SVP\C29H29F12N101Si1\JHIOE\07-Apr-20  
15\0\#p pbe1pbe/def2svp empiricaldispersion=gd3bj opt freq scf=tight\  
\title\0,1\C,-0.3727977855,-1.156573205,-1.7707496052\C,-0.0656452777  
, -0.2954001632, -2.999676444\C, -1.346644698, 0.5034400492, -3.2610523026\  
C, -2.4692752332, -0.3722119201, -2.7070440433\H, 0.0837809285, -2.15790080  
92, -1.8422555862\H, 0.8151923038, 0.3481867963, -2.8605577001\H, 0.1537674  
246, -0.9588543645, -3.8500451416\H, -1.3170449762, 1.468401318, -2.7372946  
787\H, -1.4845759641, 0.7240655554, -4.3285125853\H, -3.2351407147, 0.22454  
86295, -2.1814756483\H, -2.9949472883, -0.9424924987, -3.4968552375\N, -1.8  
065141718, -1.2908481829, -1.8064035966\C, -2.4845020764, -2.2762643815, -1  
.1456968122\H, -1.8402825188, -3.0079439332, -0.6522278905\C, -3.832056969  
, -2.3920733438, -1.0465132197\H, -4.4846089743, -1.6381919688, -1.49735019  
86\C, -4.4609386456, -3.4807566794, -0.3321780696\H, -3.7834899769, -4.2232  
423736, 0.1126164107\C, -5.7855641284, -3.649668714, -0.1658484953\H, -6.46  
27877711, -2.9086643391, -0.6103464256\C, 0.1308635533, -0.5870869736, -0.3  
96261133\C, 1.6550115843, -0.4917551354, -0.3267018242\C, 2.2495521038, 0.2  
746813465, 0.678419529\C, 2.4905793464, -1.2382061713, -1.1614159705\C, 3.6  
31837203, 0.2978376435, 0.8449933221\H, 2.3184632382, -1.6298254958, 2.6781  
913358\C, 3.8741202024, -1.209220108, -0.9995709054\H, 2.0779242837, -1.852  
0536134, -1.9610499161\C, 4.457595618, -0.4408120902, 0.0043487668\H, 5.541  
2505638, -0.409967662, 0.1241336823\C, -0.5559126344, 0.7507320632, -0.1703  
058325\C, 0.0144622382, 1.9713485565, -0.5351401611\C, -1.8697905823, 0.739  
4586067, 0.3000137108\C, -0.7155830214, 3.1539556516, -0.4277883292\H, -0.4  
147970495, -0.4725520257, 4.2727655969\C, -2.5945367941, 1.9232983933, 0.40  
74964\H, -2.3317252417, -0.2114531918, 0.5709222508\C, -2.0249603584, 3.140  
7963904, 0.0466569245\H, -2.5920985192, 4.067656965, 0.1363458169\O, -0.303  
2826419, -1.5309530277, 0.5414393784\Si, -0.1501456445, -1.7917841661, 2.20  
95588126\C, -1.4366198164, -3.1098022175, 2.5172347015\H, -2.4334422425, -2  
.7657661293, 2.2000777807\H, -1.2002832534, -4.0268223159, 1.9552949535\H,  
-1.4862042686, -3.3709656592, 3.5860029969\C, 1.5648091814, -2.4276822936,  
2.6174829844\H, 1.5433406264, -2.9388924043, 3.5936437819\H, 1.8970525824,  
-3.1575590777, 1.8627961315\H, 1.6275661203, 0.873366183, 1.3458503241\C, -  
0.5410937765, -0.2482094517, 3.2008403616\H, -1.5783164279, 0.0839459, 3.04  
55446364\H, 0.1229990432, 0.5965154846, 2.9643078349\H, 1.0359470715, 2.013  
7624018, -0.9167849949\C, -4.0166733788, 1.8444965639, 0.8900978199\F, -4.5  
438249188, 3.0506887125, 1.1007290762\F, -4.7929878952, 1.2166601366, -0.00  
20601825\F, -4.1031054353, 1.1569192831, 2.033850206\C, -0.1055116054, 4.43

80806767,-0.9169591128\F,-0.2774345445,4.5723155574,-2.2390156471\F,-0.6562793625,5.5044461819,-0.33646605\F,1.2092508785,4.4790591222,-0.6881473608\C,4.7471968974,-2.0565189743,-1.8867978894\F,4.1677628071,-2.2920460059,-3.0668829421\F,5.9233322137,-1.471259468,-2.1187292917\F,4.9989612041,-3.2431454017,-1.3256568776\C,4.2115807143,1.0837463533,1.9894707427\F,3.5800083371,2.2480684574,2.1524230299\F,4.0884132169,0.4079154271,3.1406947698\F,5.5072121508,1.3389032437,1.8148691965\C,-6.4189627692,-4.7726049837,0.5833982136\H,-7.0314280532,-4.4059447109,1.425742014\H,-7.0990483806,-5.3587914333,-0.0591956278\H,-5.6646188502,-5.4623875856,0.9916392361\\Version=ES64L-G09RevD.01\\State=1-A\\HF=-2735.7452013\\RMSD=9.194e-09\\RMSF=4.486e-06\\Dipole=0.2983014,-0.3151621,-0.1751112\\Quadrupole=-7.8023655,-1.9418188,9.7441844,-2.960358,1.1549393,-3.998617\\PG=C01 [X(C29H29F12N101Si1)]\\@

### 3Z

1\\1\\GINC-WORKER\FOpt\RPBE1PBE\def2SVP\C29H29F12N101Si1\JHIOE\06-Apr-2015\\0\\#p pbe1pbe/def2svp empiricaldispersion=gd3bj opt freq scf=tight\\title\\0,1\C,-0.3496193553,-1.5572241328,-1.6535853706\C,0.0033718043,-0.9012910813,-2.9902246409\C,-1.2644780085,-0.1621923706,-3.4406535754\C,-2.4178248583,-0.8290594392,-2.6826872722\H,0.1001707658,-2.5589257707,-1.5549524525\H,0.8797413168,-0.2408629008,-2.9187848631\H,0.2632462712,-1.6921967163,-3.7091490915\H,-1.2087633124,0.9065770081,-3.1969550314\H,-1.4026703429,-0.2284391135,-4.5286323051\H,-3.0692583423,-0.0801503421,-2.1960938062\H,-3.0710062093,-1.4349753326,-3.3369913914\N,-1.780715218,-1.6952876035,-1.7154484758\C,-2.4911327177,-2.5087061488,-0.879189533\H,-1.8784048675,-3.2308031953,-0.3329530243\C,-3.8309585875,-2.4689620492,-0.6725503689\H,-4.4309527669,-1.7049155359,-1.1730310759\C,-4.4935595674,-3.3902491691,0.2253414111\H,-3.8628043491,-4.1903878558,0.6321629183\C,-5.7839496655,-3.3600669201,0.6150851982\H,-6.1223310693,-4.1484421841,1.2964568599\C,0.1095252908,-0.7908851752,-0.3603196535\C,1.6237817202,-0.6065571163,-0.2890376126\C,2.4846551943,-1.5846042114,-0.7941538429\C,2.1831168101,0.4411309852,0.4457837084\C,3.8571414727,-1.5156350429,-0.5694861472\H,2.5921251816,-1.5791420024,2.4056047744\C,3.5562836069,0.5083393609,0.6710165163\H,1.5421253382,1.2172957357,0.8664275066\C,4.4068060162,-0.4689637394,0.1656465875\H,5.4810669358,-0.4182449252,0.3437089461\C,-0.6660905748,0.5162276788,-0.2949896079\C,-0.2329441912,1.6823130974,-0.9265517727\C,-1.9216772574,0.514777811,0.3144757526\C,-1.0347771704,2.8233318344,-0.9381644578\H,0.561459046,0.6385184043,2.8967742457\C,-2.7220052436,1.6525919456,0.2950111577\H,-2.2845039999,-0.3994799615,0.7852827409\C,-2.2844296124,2.8199669232,-0.3261475373\H,-2.9067381651,3.715291984,-0.3313189144\O,-0.2738788511,-1.6389639925,0.6861403846\Si,0.0925223867,-1.7617611943,2.3387313043\C,-1.1491103097,-3.0335794908,2.9090279534\H,-2.1773568708,-2.7048201469,2.6910836715\H,-1.0666331139,-3.2106487591,3.9927586141\H,-0.9856883421,-3.9935594747,2.3949765594\C,1.8483453135,-2.36

9496752,2.5858787007\H,2.0805596587,-3.2163729835,1.9217876268\H,1.974  
 4806822,-2.7120089156,3.6258684339\H,2.0904727899,-2.4296350893,-1.359  
 2468005\C,-0.1564003702,-0.1282454116,3.2236494177\H,-1.1745066152,0.2  
 639563233,3.0820339016\H,-0.0002462719,-0.2780901476,4.3045816455\H,0.  
 7391534545,1.7152373291,-1.4220923864\C,-4.0997972681,1.5743492202,0.8  
 932926821\F,-4.5895788245,2.7816565626,1.1790787317\F,-4.9568934706,0.  
 990078063,0.0433674958\F,-4.1063498911,0.8532775992,2.0160830708\C,-0.  
 5556009924,4.032966424,-1.6912450547\F,-0.7173623595,3.8647968573,-3.0  
 118658054\F,-1.2203172671,5.1349727788,-1.3468700826\F,0.7449165257,4.  
 2555277256,-1.4855603767\C,4.083703663,1.6193131578,1.5375424118\F,3.7  
 340265043,1.4267831056,2.8166023343\F,5.4122146743,1.7027817657,1.4927  
 822615\F,3.5844036393,2.8015832964,1.1710452323\C,4.7261442859,-2.6356  
 656599,-1.0749968754\F,4.4274619389,-2.9519564727,-2.3382783467\F,6.02  
 09808941,-2.3255867058,-1.0260895428\F,4.5484729588,-3.7414485175,-0.3  
 431926017\C,-6.8088787561,-2.351411038,0.2102036746\H,-7.5159093784,-2  
 .761174734,-0.5333974836\H,-7.41570519,-2.0393575573,1.0756668355\H,-6  
 .3600505455,-1.4439738983,-0.2179630867\\Version=ES64L-G09RevD.01\Stat  
 e=1-A\HF=-2735.7446593\RMSD=9.578e-09\RMSF=3.341e-06\Dipole=0.5412158,  
 -0.2964955,-0.212334\Quadrupole=-7.9460885,-3.0493006,10.9953892,-4.11  
 80115,1.6665986,-1.7940684\PG=C01 [X(C29H29F12N10Si1)]\\@

### TS<sub>3E</sub>

1\1\GINC-LOGIN\FTS\RPBE1PBE\def2SVP\C32H39F12N20Si1(1+)\JHIOE\06-Apr-  
 2015\0\#p opt=(ts,calcf,oeigen) freq pbe1pbe/def2svp empiricaldispe  
 rsion=gd3bj scf=tight\\title\\1,1\C,-0.3436115995,-0.7811253222,2.0241  
 659618\C,-0.9485766492,0.0787560213,3.1327200141\C,0.1230841374,1.1144  
 636477,3.4948803965\C,1.4533652456,0.476803972,3.0937306544\H,-0.61390  
 92623,-1.8408900739,2.1296016356\H,-1.8994444099,0.5375050317,2.829261  
 3286\H,-1.1703494688,-0.5643757704,3.9969060875\H,-0.0331896472,2.0534  
 626313,2.9502685577\H,0.102342509,1.3619807468,4.564261082\H,2.1060563  
 175,1.1716053977,2.5412224693\H,2.0231027466,0.1010196095,3.9597321612  
 \N,1.0939089383,-0.6583297315,2.2472053247\C,1.9818152646,-1.503727447  
 ,1.7482962064\H,1.5540181842,-2.3485020851,1.2031501716\C,3.3638744597  
 ,-1.397054404,1.8570480546\H,3.8175956741,-0.5397637078,2.3607748078\C  
 ,4.1813394403,-2.413168705,1.3585233295\H,3.6656746526,-3.2643569765,0  
 .8888497439\C,5.5871745727,-2.4411392588,1.3418293007\H,6.0613875654,-  
 1.7069047111,2.012560979\C,-0.7131527223,-0.4057409044,0.5489573311\C,  
 -2.2118296849,-0.5440687778,0.2898864015\C,-2.8134011902,0.1805344264,  
 -0.7397911482\C,-2.9735062685,-1.5169172915,0.9437435129\C,-4.13439398  
 91,-0.0619453814,-1.1107465088\H,-1.7129343457,-3.5509299981,-2.919173  
 7108\C,-4.293392502,-1.7563443989,0.5737416473\H,-2.5505519492,-2.1181  
 550082,1.7487840882\C,-4.8870072243,-1.0304842047,-0.4567121339\H,-5.9  
 221363718,-1.2179410514,-0.7449587835\C,-0.1809301246,0.9937876969,0.2  
 62033544\C,-0.8989645359,2.1529349054,0.5664381026\C,1.1238543301,1.12  
 61897114,-0.2078683261\C,-0.3185331112,3.4094636843,0.4081435939\H,-0.  
 0644459459,-0.99955948,-4.0756482318\C,1.7053137062,2.3829606821,-0.35

```
3054983\H,1.691264137,0.2273790647,-0.4485017112\C,0.9902450247,3.5376
349889,-0.0515264993\H,1.4420782298,4.5232188018,-0.1709989402\O,-0.02
22605755,-1.3512263586,-0.2212094711\Si,-0.2096084008,-1.9507387199,-1
.8129841701\C,1.3172398216,-3.0250409802,-1.9485369225\H,2.2298293163,
-2.4353523152,-1.7718429771\H,1.2863699255,-3.8455590285,-1.2143575791
\H,1.3920552347,-3.4762905599,-2.9501289538\C,-1.7633688384,-2.9712258
291,-1.9831046727\H,-1.8800070079,-3.6843949135,-1.152927477\H,-2.6681
947726,-2.3482043591,-2.0310050778\H,-2.2489656325,0.9438907889,-1.277
2169613\C,-0.1655706098,-0.5636502149,-3.0681928824\H,0.6855957435,0.1
15698724,-2.9103138834\H,-1.0916997126,0.0295362511,-3.0713415127\H,-1
.9245275978,2.0898638587,0.9353017435\C,3.1484327178,2.4480944746,-0.7
589835253\F,3.5382418226,3.6667202312,-1.0963096026\F,3.9367080391,2.0
36246319,0.2578962314\F,3.4117799596,1.6266167823,-1.7863446091\C,-1.0
937237556,4.6272689603,0.8426195384\F,-0.9952316333,4.7823518367,2.169
5852042\F,-0.634547412,5.7355452689,0.2713462707\F,-2.3877352045,4.508
2437278,0.5521973155\C,-5.0511024956,-2.8726678993,1.2471470413\F,-6.3
648770853,-2.6884363985,1.1754004074\F,-4.7706159706,-4.0436810309,0.6
677389192\F,-4.7133170315,-2.9774427026,2.5348910047\C,-4.6970368108,0
.7157920012,-2.2724834194\F,-5.9956622381,0.4974211481,-2.4385557297\F
,-4.5095308518,2.0257447686,-2.106519276\F,-4.0725735193,0.3695291299,
-3.4062587803\C,6.3065477983,-3.7720654588,1.24591782\H,7.35679493,-3.
6479518962,0.9455787904\H,6.3115349113,-4.2988431689,2.2137371154\H,5.
8255553159,-4.4394912186,0.5130467337\H,5.8592677555,-1.8503299983,0.1
595701887\N,6.2449959837,-1.2565515334,-1.0207839126\C,5.0420217895,-1
.3137932571,-1.8423993738\H,4.2265366362,-0.7816649685,-1.3365935119\H
,5.2056707595,-0.8477622147,-2.8289931811\H,4.7485523169,-2.3626895146
,-1.9905022598\C,7.3486382085,-2.0149057784,-1.6044355686\H,7.65680568
64,-1.5835042159,-2.5725526495\H,8.2094240559,-1.9994286465,-0.9227526
917\H,7.040439425,-3.0569455364,-1.7633371988\C,6.6310996997,0.1115074
19,-0.6853427368\H,7.4865996676,0.0917139111,0.0037016859\H,6.91739549
6,0.6760600973,-1.5892561769\H,5.7923302262,0.6268586877,-0.2011513968
\\Version=ES64L-G09RevD.01\State=1-A\HF=-2910.2958594\RMSD=6.801e-09\R
MSF=1.682e-06\Dipole=5.9395879,-2.1716595,0.4618236\Quadrupole=42.1564
01,-24.5821121,-17.5742889,-16.434205,-7.9177058,5.4486261\PG=C01 [X(C
32H39F12N2O1Si1)]\@
```

### TS<sub>32</sub>

```
1\1\GINC-LOGIN\FTS\RPBE1PBE\def2SVP\C32H39F12N2O1Si1(1+)\JHIOE\06-Apr-
2015\0\#p opt=(ts,calcf,nc,eigen) freq pbe1pbe/def2svp empiricaldispe
rsion=gd3bj scf=tight\title\1,1\C,-0.4521685147,-0.5250568611,2.3181
37229\C,-1.0407947437,0.4219519447,3.3615208401\C,0.0480145623,1.46478
83598,3.6507913255\C,1.3683333871,0.8009506192,3.2521955086\H,-0.73774
20516,-1.5704249555,2.4996331751\H,-1.9848954731,0.8729182702,3.026940
2037\H,-1.2723147144,-0.1543987384,4.2690348023\H,-0.1130859117,2.3805
220373,3.0691763776\H,0.0514203585,1.7596522159,4.7082834007\H,1.98928
62427,1.4483049827,2.6119045104\H,1.978994336,0.508453343,4.1219564641
```

\N,0.9863060975,-0.4076133447,2.5266015271\C,1.8558169737,-1.302577444  
2,2.0874770955\H,1.4098219498,-2.1950468984,1.6419785979\C,3.240705268  
9,-1.1857993171,2.1355594971\H,3.7020617566,-0.2739543159,2.5192893512  
\C,4.0427067204,-2.2436068592,1.704665657\H,3.5163781041,-3.1468381915  
,1.3669838138\C,5.4458260735,-2.2568008507,1.6041886157\H,5.6276933748  
, -2.0756322145,0.2755051345\C,-0.8123804611,-0.251816512,0.8183645905\  
C,-2.311432957,-0.3893451113,0.5628539564\C,-2.8959802565,0.2620426072  
, -0.5242042977\C,-3.091086375,-1.2966010272,1.2857976078\C,-4.21642385  
69,0.006242748,-0.8875807885\H,-1.8121348284,-3.669949097,-2.392478452  
\C,-4.412047309,-1.5458237005,0.9257508576\H,-2.68245239,-1.8378341015  
,2.1394315908\C,-4.9870503958,-0.8974636951,-0.1650954989\H,-6.0224058  
168,-1.0937681546,-0.4466426436\C,-0.2611410212,1.1148461133,0.4282569  
184\C,-0.9569667338,2.3030130573,0.6652189735\C,1.0314618693,1.1944284  
654,-0.0844821259\C,-0.3641056977,3.5362864024,0.4051057952\H,-0.18217  
24256,-1.2190996102,-3.7512537076\C,1.6213921952,2.4291566327,-0.34458  
4044\H,1.5827543228,0.2728068809,-0.2709942456\C,0.9306478466,3.612254  
4517,-0.1038529548\H,1.3896664719,4.5799107497,-0.3098209092\O,-0.1318  
041652,-1.2596885267,0.1218466461\Si,-0.3145578623,-1.9773441963,-1.41  
90196403\C,1.2267273992,-3.0417940219,-1.4739749657\H,2.1272639981,-2.  
4205649324,-1.346153723\H,1.2127685659,-3.8026050287,-0.6777038048\H,1  
.3084048456,-3.5668240309,-2.4383271904\C,-1.8612701641,-3.0178339144,  
-1.5053687896\H,-1.9729016018,-3.6621826607,-0.6200868195\H,-2.7687063  
8,-2.4034903578,-1.5993149895\H,-2.3171990935,0.975086531,-1.113051422  
9\C,-0.2763649262,-0.6983527553,-2.7840401511\H,0.5765947256,-0.009333  
0836,-2.6913188078\H,-1.2019601262,-0.1065803354,-2.8333277039\H,-1.97  
54803894,2.2807900338,1.0578197658\C,3.0363294588,2.4398001793,-0.8475  
065353\F,3.4600712006,3.6522922066,-1.1684657802\F,3.8746896204,1.9484  
893038,0.0870366618\F,3.1756697557,1.6522570855,-1.9252195559\C,-1.112  
8675168,4.791051036,0.7756382369\F,-1.0045997316,5.0150298094,2.092364  
6853\F,-0.6363345254,5.8580428385,0.1437508162\F,-2.4107603556,4.68153  
20115,0.4982755249\C,-5.1915866492,-2.5919922491,1.6818333769\F,-4.864  
0408797,-2.5958518576,2.9764751136\F,-6.5017044695,-2.3942242918,1.584  
901643\F,-4.9258177311,-3.8106715236,1.2023452805\C,-4.7588123426,0.68  
82823084,-2.1171630731\F,-4.1497471907,0.2150934896,-3.2130941096\F,-6  
.064115482,0.4951631948,-2.2607724532\F,-4.5301869384,2.0014418794,-2.  
0783370986\C,6.2745602827,-1.176632258,2.2628759332\H,7.3433253232,-1.  
3046561614,2.0406591196\H,5.9867166332,-0.1693156188,1.9207740951\H,6.  
1682645895,-1.1908545335,3.3604736856\H,5.8757578461,-3.269439152,1.63  
93026114\N,5.931917897,-1.8799174634,-1.0457024413\C,5.0924066719,-0.7  
652664126,-1.4700608985\H,4.0382351343,-1.0100030286,-1.2820922051\H,5  
.3457674961,0.1336671448,-0.894810732\H,5.2181144343,-0.5497271239,-2.  
5446937763\C,5.5691088507,-3.1311067871,-1.7021075566\H,5.7206587758,-  
3.0704951763,-2.7932528858\H,6.1851343345,-3.9496854335,-1.3048043969\  
H,4.5107691197,-3.3562580696,-1.5062923905\C,7.3575432124,-1.584566221  
8,-1.1553864367\H,7.9392630043,-2.4048499606,-0.7123368091\H,7.6606154  
153,-1.4640015342,-2.209541968\H,7.583712703,-0.656414042,-0.614150374

### 3 The mechanism of stereoinduction in dienamine catalyzed $\gamma$ alkylation revealed by a combined *in situ* NMR and quantum-chemical study.

---

```
6\\Version=ES64L-G09RevD.01\\State=1-A\\HF=-2910.2967442\\RMSD=5.840e-09\\
RMSF=3.001e-06\\Dipole=5.7741878,-2.5962806,0.421413\\Quadrupole=38.3290
283,-21.0169317,-17.3120965,-22.155715,-9.3226792,8.6509539\\PG=C01 [X(
C32H39F12N2O1Si1)]\\@
```

#### **N(Me)<sub>3</sub>**

```
1\\1\\GINC-WORKER\\F0pt\\RPBE1PBE\\def2SVP\\C3H9N1\\JHIOE\\07-Apr-2015\\0\\#p p
be1pbe/def2svp opt freq empiricaldispersion=gd3bj\\Title Card Required
\\0,1\\N,0.,0.0000000003,-0.384029648\\C,0.,1.381267572,0.0173161819\\H,0
.8893035823,1.8932784508,-0.3822432224\\H,-0.8893035823,1.8932784508,-0
.3822432224\\H,0.,1.5209610111,1.1242339356\\C,-1.1962128065,-0.69063378
56,0.0173161819\\H,-2.0842790257,-0.176479731,-0.3822432224\\H,-1.194975
4434,-1.7167987189,-0.3822432224\\H,-1.3171908735,-0.7604805051,1.12423
39356\\C,1.1962128065,-0.6906337856,0.0173161819\\H,1.1949754434,-1.7167
987189,-0.3822432224\\H,2.0842790257,-0.176479731,-0.3822432224\\H,1.317
1908735,-0.7604805051,1.1242339356\\Version=ES64L-G09RevD.01\\State=1-A
1\\HF=-174.1370084\\RMSD=2.027e-09\\RMSF=2.714e-05\\Dipole=0.,0.,0.1724854
\\Quadrupole=0.8267936,0.8267936,-1.6535871,0.,0.,0.\\PG=C03V [C3(N1),3S
GV(C1H1),X(H6)]\\@
```

#### **N(Me)<sub>3</sub>·H<sup>+</sup>**

```
1\\1\\GINC-WORKER\\F0pt\\RPBE1PBE\\def2SVP\\C3H10N1(1+)\\JHIOE\\07-Apr-2015\\0\\
\\#p opt freq def2svp empiricaldispersion=gd3bj pbe1pbe\\Title Card Req
uired\\1,1\\N,0.,0.0000000003,-0.4158528305\\C,0.,1.4240292769,0.0181880
42\\H,0.8987728361,1.9191379397,-0.3690830199\\H,-0.8987728361,1.9191379
397,-0.3690830199\\H,0.,1.4560457412,1.1151812157\\C,-1.2332455293,-0.71
2014638,0.018188042\\H,-2.1114086269,-0.1812088611,-0.3690830199\\H,-1.2
126357908,-1.7379290777,-0.3690830199\\H,-1.2609726007,-0.7280228701,1.
1151812157\\C,1.2332455293,-0.712014638,0.018188042\\H,1.2126357908,-1.7
379290777,-0.3690830199\\H,2.1114086269,-0.1812088611,-0.3690830199\\H,1
.2609726007,-0.7280228701,1.1151812157\\H,0.,0.0000000003,-1.4431837151
\\Version=ES64L-G09RevD.01\\State=1-A1\\HF=-174.511941\\RMSD=8.508e-09\\RM
SF=2.277e-05\\Dipole=0.,0.,-0.3619333\\Quadrupole=0.5399958,0.5399958,-1
.0799916,0.,0.,0.\\PG=C03V [C3(N1H1),3SGV(C1H1),X(H6)]\\@
```

#### **pre-(R) for catalyst a**

```
1\\1\\GINC-WORKER\\F0pt\\RPBE1PBE\\def2SVP\\C40H48N3O1(1+)\\JHIOE\\27-May-2015
\\0\\#p freq def2svp pbe1pbe opt empiricaldispersion=gd3 int=ultrafine\\
\\title\\1,1\\C,1.9115808572,-0.1682449353,-2.3288452582\\C,2.8096690656,
0.8413307733,-3.0401778302\\C,1.9929924448,2.1360342253,-3.1161612857\\C
,0.5340945238,1.6878317673,-3.1364546948\\H,2.0098581743,-1.1833340282,
-2.7358644443\\H,3.766428515,0.9736024415,-2.5184227372\\H,3.0400368412,
0.4671803159,-4.0492190969\\H,2.1774617296,2.7642327009,-2.2358297765\\H
,2.2439484429,2.7309574537,-4.004336911\\H,-0.1046529586,2.2997126628,-
```



2.4826979117\H,0.0977280157,1.6894906441,-4.1480844244\N,0.5575353872,  
0.3013428829,-2.6548627349\C,-0.4976861538,-0.4518343081,-2.5251478086  
\H,-0.3045641421,-1.4874371734,-2.2357481627\C,-1.8422222802,-0.021747  
5956,-2.6597627971\H,-2.0723220017,1.0298620993,-2.8490661403\C,-2.840  
6112783,-0.9143425652,-2.4261238214\H,-2.5600795672,-1.9619058758,-2.2  
489794434\C,2.0976959909,-0.308541037,-0.779992449\C,3.4556720517,-0.9  
356437268,-0.4502699437\C,4.1929307986,-1.6810819199,-1.3785396365\C,3  
.9431949217,-0.8563821548,0.8629149044\C,5.3821083996,-2.3110463751,-1  
.013522588\C,5.1257517871,-1.4914403491,1.2328733467\H,3.3924424295,-0  
.2815407,1.6102661573\C,5.8535044775,-2.2195511382,0.2933879663\H,6.78  
49100011,-2.7135521979,0.5790601135\C,1.8891424308,1.0557901676,-0.120  
6527779\C,2.9510854956,1.9447391639,0.0927398082\C,0.5895057757,1.4815  
366465,0.1812660481\C,2.7181907825,3.231962809,0.5736941327\C,0.356268  
7585,2.771473986,0.657187418\H,-0.2491043075,0.7928799574,0.0539172613  
\C,1.4181382324,3.6537636829,0.8506724443\H,1.235251515,4.6636228011,1  
.2249800748\O,1.050692596,-1.2029040787,-0.4445713291\H,3.8601714234,-  
1.7853158441,-2.4123385983\H,3.9749887697,1.6318532047,-0.1220245824\C  
, -5.0007327051,-1.1355441695,-3.6220361124\H,-4.8402039776,-2.21675312  
16,-3.7591115658\H,-6.0830264601,-0.9643424393,-3.5224559998\H,-4.6447  
585762,-0.6165896003,-4.5235848691\C,-4.2939024446,-0.6260916401,-2.36  
3799568\H,-4.4472727717,0.4643919575,-2.2949852419\C,-4.8502138015,-1.  
3026950776,-1.0753381913\H,-4.8175512126,-2.3876022281,-1.2769367921\C  
, -6.3003281739,-0.9527497569,-0.8302802163\C,-7.3143644623,-1.87117164  
49,-1.1257243632\C,-6.7009326571,0.2935717263,-0.3334431817\C,-8.65813  
72205,-1.5755762642,-0.9398419628\H,-7.0470164891,-2.8608836177,-1.509  
1979158\C,-8.0371746472,0.6134893629,-0.1427263765\H,-5.9509628742,1.0  
426381905,-0.0681315907\C,-9.0630157877,-0.3151745371,-0.4424673525\H,  
-9.3975411852,-2.3387202477,-1.1801835808\H,-8.284650336,1.5975164829,  
0.2540908508\C,-3.9330620338,-1.0622078115,0.1089137979\C,-3.415357257  
3,0.1976161286,0.4379628209\C,-3.564886369,-2.1255049138,0.9417895881\  
C,-2.5755320598,0.3903852114,1.5281641432\H,-3.6668455561,1.0695250094  
, -0.1721673632\C,-2.7175194584,-1.9602355713,2.0293942018\H,-3.9616544  
977,-3.1244851544,0.7369166271\C,-2.1844535549,-0.6905795405,2.3515779  
587\H,-2.2232442157,1.3983717266,1.7441348646\N,-10.384790101,-0.00852  
66352,-0.2545752309\C,-11.3998700847,-0.9857052515,-0.5553246718\H,-12  
.3889409821,-0.5606476624,-0.3468621418\H,-11.3837115624,-1.2872698554  
, -1.6180623481\H,-11.2928549606,-1.9002101627,0.0558778866\C,-10.75864  
53749,1.2795339936,0.2709103196\H,-11.8509300886,1.3395467702,0.346603  
6226\H,-10.3432685761,1.4556649582,1.2798326438\H,-10.4239457095,2.107  
0051893,-0.3802956764\H,-2.4786471284,-2.8311971834,2.638992538\N,-1.3  
231789328,-0.5180826493,3.4076918448\C,-1.0444210662,-1.6252698816,4.2  
883518419\H,-0.322500197,-1.3107550042,5.0516652104\H,-1.9478476521,-1  
.9965676732,4.8071682252\H,-0.5978904785,-2.4748565072,3.743616519\C,-  
0.9253207015,0.8124455988,3.7975154057\H,-0.2457163287,0.7516956559,4.  
6560797194\H,-0.3846666549,1.3295825713,2.986894328\H,-1.7851142362,1.  
4433974943,4.0909808248\C,0.925646477,-1.6580623351,0.8825782864\H,1.7

389570493,-2.3510440295,1.1528120757\H,0.8991585451,-0.8272256964,1.60  
74962496\H,-0.0368993196,-2.1843829227,0.9365243882\H,5.941973767,-2.8  
785284072,-1.7603863629\H,5.4814761434,-1.4131622661,2.2628201723\H,3.  
5601657353,3.9096805866,0.7324995707\H,-0.6653055712,3.0885620024,0.88  
23606588\\Version=ES64L-G09RevD.01\State=1-A\HF=-1789.0984265\RMSD=6.4  
55e-09\RMSF=3.482e-06\Dipole=1.4679704,0.5831079,-1.2803608\Quadrupole  
=45.4855661,-27.9767696,-17.5087965,0.4966398,-1.1625523,-0.3116315\PG  
=C01 [X(C40H48N3O1)]\@

### pre-(S) for catalyst a

1\1\GINC-WORKER\F0pt\RPBE1PBE\def2SVP\C40H48N3O1(1+)\JHIOE\27-May-2015  
\0\#p freq def2svp pbe1pbe opt empiricaldispersion=gd3 int=ultrafine\  
\title\1,1\C,-3.2152727473,-2.1612173439,-0.6748287763\C,-3.962646752  
1,-3.3249652179,-0.0260410281\C,-2.9679247427,-3.9603213127,0.95047143  
22\C,-1.5924941343,-3.6816190684,0.3522054722\H,-3.4615483236,-2.04301  
6031,-1.7383430503\H,-4.8862522802,-2.9923462121,0.4651287408\H,-4.252  
8496188,-4.0438383003,-0.8072717696\H,-3.0447700431,-3.4944292741,1.94  
07169211\H,-3.1424425892,-5.0370319235,1.0769543906\H,-0.8550586532,-3  
.3732237276,1.108113767\H,-1.1840558702,-4.542535122,-0.2011135608\N,-  
1.8086818743,-2.5867255868,-0.6010973215\C,-0.866409228,-2.0395082785,  
-1.3151335818\H,-1.1966127753,-1.2638733115,-2.0101801496\C,0.51979787  
9,-2.3177159329,-1.2113679447\H,0.8836030022,-3.0695332522,-0.50715250  
74\C,1.3838060855,-1.5327935133,-1.9118490353\H,0.9412158798,-0.793206  
9152,-2.5882409349\C,-3.41765126,-0.7489103704,-0.032022886\C,-4.86163  
01194,-0.2708823463,-0.2158792463\C,-5.7012761662,-0.7730759319,-1.218  
0136812\C,-5.3381013202,0.7901381391,0.5683212739\C,-6.977605805,-0.24  
85356543,-1.4171154573\C,-6.6091493639,1.3219425447,0.3665807381\H,-4.  
7069863377,1.2062949248,1.3561690032\C,-7.4373666475,0.8009126194,-0.6  
25696511\H,-8.4373673917,1.211736462,-0.7819274095\C,-2.9755525376,-0.  
7849603896,1.4315765863\C,-3.8632877869,-1.1172082286,2.4638525506\C,-  
1.6279086519,-0.5756778985,1.7500603806\C,-3.4125260239,-1.2548596589,  
3.775337645\C,-1.1775047753,-0.7111898877,3.0627697564\H,-0.9207111685  
, -0.2864650223,0.9698118826\C,-2.0657707726,-1.0570277287,4.0796119186  
\H,-1.713335642,-1.1619530026,5.1083200888\O,-2.5397654975,0.050641879  
9,-0.8083140819\H,-5.3809404078,-1.5900192858,-1.8664411312\H,-4.92172  
23441,-1.2718503488,2.2437773408\C,3.4907460537,-2.9147022371,-1.87637  
00701\H,3.1345956546,-3.5866199077,-1.0795850519\H,3.2618136606,-3.379  
8690908,-2.8460758435\H,4.5829429933,-2.8355990324,-1.7788782355\C,2.8  
660481179,-1.5278091424,-1.7637851728\H,3.2878111025,-0.8894592947,-2.  
5560797338\C,3.2040892444,-0.8507558123,-0.3869302115\H,2.9092398969,-  
1.5931256648,0.3750677328\C,2.3584221662,0.3822222747,-0.134609518\C,1  
.8781686673,0.6425938094,1.1535641187\C,2.0219406589,1.3104258026,-1.1  
27159188\C,1.0707045762,1.7346891503,1.4382014047\H,2.1483319802,-0.03  
73773653,1.9677132124\C,1.2145940726,2.4136907544,-0.8672131324\H,2.39  
65610243,1.1841498007,-2.1472734894\C,0.6917024254,2.645823493,0.42462  
24584\H,0.7280425753,1.8779060891,2.4624016336\H,0.9943194184,3.100332

9592,-1.6842909058\C,4.6859535483,-0.6161292893,-0.2284267453\C,5.3379  
 622014,0.4582081973,-0.846896016\C,5.4771141846,-1.4908038471,0.525312  
 9451\C,6.7055199466,0.6518694326,-0.7283403348\H,4.7607429178,1.181229  
 5997,-1.4293831455\C,6.8471085742,-1.3144120341,0.6632334753\H,5.00669  
 71034,-2.3396433059,1.0316482998\C,7.5075269592,-0.2335532789,0.033000  
 7925\H,7.1545743668,1.5100221846,-1.2271578026\N,-0.15208471,3.6974230  
 419,0.684404046\C,-0.6249884856,3.9216533936,2.0273769039\H,-1.3274998  
 125,4.7638968498,2.0304477867\H,-1.1622523387,3.0404528466,2.420262099  
 \H,0.1915839794,4.1602421886,2.7341210315\C,-0.3977559752,4.6864494815  
 ,-0.3344314186\H,-1.0792310892,5.4517801648,0.0559354635\H,0.527901786  
 6,5.1938583178,-0.6628928392\H,-0.8733352232,4.2472996519,-1.229585920  
 9\H,7.4058272524,-2.0241061556,1.2723298721\N,8.8582080968,-0.04796404  
 11,0.1570404659\C,9.6410124219,-0.9627762692,0.9485081489\H,10.6934310  
 545,-0.6558493978,0.9269420075\H,9.318980912,-0.9797342916,2.005434449  
 6\H,9.5867091626,-1.9966982949,0.5628907284\C,9.4959476598,1.070059758  
 4,-0.4910996022\H,10.571905163,1.0478940666,-0.2811154967\H,9.36949966  
 25,1.0414694736,-1.5882177681\H,9.1048509559,2.0388854884,-0.131461711  
 1\H,-4.1209649786,-1.5150110243,4.5652360577\H,-0.1226285175,-0.536884  
 5858,3.2879219727\H,-6.9543243858,2.1481215046,0.99247829\H,-7.6152208  
 42,-0.6657841279,-2.1998358417\C,-2.5072603276,1.4419811465,-0.5932155  
 869\H,-3.4236852378,1.932094227,-0.9603569622\H,-2.3622002903,1.695574  
 4603,0.4700430342\H,-1.6400392989,1.8176227799,-1.1520484005\\Version=  
 ES64L-G09RevD.01\State=1-A\HF=-1789.0967368\RMSD=8.189e-09\RMSF=4.008e  
 -06\Dipole=-1.1358621,-1.1266699,-0.4733874\Quadrupole=44.5351213,-13.  
 286646,-31.2484754,3.3205969,-1.2622583,0.7671496\PG=C01 [X(C40H48N3O1  
 )]\@

#### pre-(R) for catalyst b

1\1\GINC-LOGIN\F0pt\RPBE1PBE\def2SVP\C42H54N3O1Si1(1+)\JHI0E\26-May-20  
 15\0\#\p freq def2svp pbe1pbe opt empiricaldispersion=gd3 int=ultrafin  
 e\\title\\1,1\C,1.9610846804,-0.0867216794,-2.3737521785\C,2.787405532  
 5,0.9456159886,-3.1365135472\C,1.9345251908,2.2189772489,-3.1730057933  
 \C,0.4879690968,1.7403039377,-3.0626094703\H,2.0653323178,-1.097412863  
 2,-2.7899127458\H,3.768989621,1.1043709595,-2.6714102886\H,2.971444218  
 4,0.5729515781,-4.1555682631\H,2.1752176308,2.8737849344,-2.3268995586  
 \H,2.0975030106,2.7961551713,-4.0928253635\H,-0.0946223106,2.323304894  
 3,-2.3337747511\H,-0.0448703462,1.7570641178,-4.0264089755\N,0.5786691  
 65,0.3450669537,-2.6157008862\C,-0.4479165533,-0.4345175793,-2.4306068  
 601\H,-0.2153029697,-1.4651157003,-2.1549887215\C,-1.8083599343,-0.038  
 7854102,-2.5113142867\H,-2.0689100638,1.0017740032,-2.7215284149\C,-2.  
 7827869436,-0.9441505495,-2.2319412743\H,-2.4818057523,-1.9789556236,-  
 2.017645396\C,2.2207805617,-0.2383980746,-0.830147516\C,3.6293650282,-  
 0.7827433515,-0.5699644096\C,4.3342427421,-1.5366531637,-1.5151049803\  
 C,4.1892740655,-0.6358981086,0.7069786778\C,5.558335596,-2.1237979491,  
 -1.1966116933\H,3.444821077,-3.3549512,0.7496616844\C,5.4078227209,-1.  
 2264225029,1.0306448406\H,3.6636547139,-0.0485209367,1.462029207\C,6.0

98707697,-1.9744785875,0.0781590702\H,7.0560992776,-2.4370760639,0.328  
1512269\C,1.9732746626,1.1058473296,-0.1415801572\C,2.977716338,2.0790  
092835,-0.0467509994\C,0.6948453813,1.4147275268,0.3366197426\C,2.7077  
188838,3.3344073432,0.4937094034\H,2.0755740282,-1.1966764608,2.701089  
7921\C,0.4225599623,2.6761164014,0.8676106499\H,-0.0911400283,0.657227  
9842,0.3017056632\C,1.424604339,3.6414490307,0.9457739369\H,1.21042717  
35,4.6262633428,1.3672450427\O,1.2538438359,-1.170593997,-0.4313082004  
\Si,1.1188898197,-2.4144497959,0.7314035404\C,-0.5688354873,-3.1045098  
767,0.3146494163\H,-1.3446748126,-2.3251315396,0.3764120691\H,-0.84949  
30334,-3.8982082107,1.0247210459\H,-0.5805265915,-3.5497424403,-0.6938  
516463\C,2.439267062,-3.7142962183,0.4866775576\H,2.4635192614,-4.0613  
521605,-0.5579064233\H,2.2121424316,-4.5850033023,1.1234954261\H,3.941  
505057,-1.6893600718,-2.5216667216\C,1.1344411108,-1.7125770455,2.4632  
089411\H,0.2986230535,-1.0129029415,2.615095345\H,1.016898263,-2.53512  
46707,3.1877512898\H,3.9889577469,1.8534553831,-0.3923587738\C,-4.8996  
863787,-1.2252911364,-3.4635596905\H,-4.730550114,-2.3092811274,-3.562  
8238865\H,-5.985331648,-1.0554528258,-3.4097181212\H,-4.5111817701,-0.  
7310786839,-4.3655304685\C,-4.2407140047,-0.6753010166,-2.1941142354\H  
, -4.4094553974,0.4148034188,-2.1654685571\C,-4.8473031691,-1.317577769  
8,-0.9146240901\H,-4.791986811,-2.4091231421,-1.0736187595\C,-6.310331  
092,-0.9674136911,-0.7569593004\C,-7.3146179151,-1.8845436602,-1.08470  
15566\C,-6.7220409798,0.2916543954,-0.3034925891\C,-8.6634093023,-1.57  
27927426,-0.9733989035\H,-7.0368114205,-2.883896151,-1.4342785568\C,-8  
.0627727716,0.6277325397,-0.189100179\H,-5.9736269174,1.0335242212,-0.  
011071694\C,-9.0804264411,-0.2983715404,-0.5239295687\H,-9.3975186659,  
-2.3340097923,-1.2351723289\H,-8.3212619024,1.6209043839,0.1767516863\  
C,-4.0315609001,-1.016755027,0.327547953\C,-3.3815895989,0.2027459547,  
0.5496751136\C,-3.9456550046,-1.9683504457,1.3523145004\C,-2.663112831  
3,0.4561148168,1.7134714659\H,-3.4316217412,0.9970256778,-0.1994844054  
\C,-3.2327808414,-1.7397595367,2.5197394432\H,-4.4591777344,-2.9268377  
479,1.2321204574\C,-2.5541396951,-0.5163826639,2.7319686183\H,-2.19321  
07889,1.4308704189,1.8342367619\N,-10.4073871396,0.0238734441,-0.41147  
38766\C,-11.4150873531,-0.9505764262,-0.7435649033\H,-12.4093960975,-0  
.512316608,-0.5962029973\H,-11.3468167273,-1.275701332,-1.7972923945\H  
, -11.349247144,-1.8524608279,-0.1081731299\C,-10.7951991739,1.32626213  
19,0.0662377671\H,-11.8892941256,1.3982540156,0.0816134567\H,-10.43280  
4873,1.5203130885,1.0921960527\H,-10.4172234883,2.1364193748,-0.583067  
4806\H,-3.2048069777,-2.5245979463,3.2748020774\N,-1.821784417,-0.2866  
146288,3.8704766192\C,-1.7957937821,-1.2762040146,4.9180959379\H,-1.14  
14750819,-0.9319523939,5.7279079864\H,-2.7967339415,-1.4659571782,5.34  
74688239\H,-1.3943524822,-2.2387847306,4.5567709028\C,-1.2411716717,1.  
0122685849,4.0997204186\H,-0.7018848356,1.0068011735,5.0544323926\H,-0  
.5141563655,1.2815560339,3.313197273\H,-2.0029533185,1.8127197276,4.14  
67932015\H,6.0899337907,-2.7059024684,-1.9527843574\H,5.8205399446,-1.  
099121082,2.0340987245\H,3.5067458532,4.0761093668,0.5640065479\H,-0.5  
827742029,2.9067056918,1.228405726\\Version=ES64L-G09RevD.01\State=1-A

\HF=-2158.1533366\RMSD=4.431e-09\RMSF=2.850e-06\Dipole=1.1363424,0.667  
9573,-1.4304585\Quadrupole=43.6805813,-27.684187,-15.9963943,-0.126851  
7,-2.5153586,-1.8038448\PG=C01 [X(C42H54N3O1Si1)]\ \@

### pre-(S) for catalyst b

1\1\GINC-WORKER\FOpt\RPBE1PBE\def2SVP\C42H54N3O1Si1(1+)\JHIOE\26-May-2  
015\0\ \#p freq def2svp pbe1pbe opt empiricaldispersion=gd3 int=ultrafi  
ne\ \title\1,1\C,2.0762562347,-0.8065290241,2.0729931168\C,2.836437348  
3,-2.1304573046,2.1298392741\C,1.885407791,-3.187506875,1.5604361743\C  
,0.4826349295,-2.6484622553,1.8264348211\H,2.2691983091,-0.1792416236,  
2.9532129205\H,3.7877442027,-2.0754993497,1.5849738074\H,3.0814607872,  
-2.3553201736,3.1789503525\H,2.0382382862,-3.3093048486,0.4814140345\H  
,2.0341631381,-4.1699336188,2.0278401517\H,-0.1825984953,-2.7479730065  
,0.9555194289\H,-0.0025092455,-3.1286116169,2.6911245975\N,0.667470098  
5,-1.2252364919,2.1359721961\C,-0.3093921132,-0.4115588198,2.418566215  
2\H,-0.0158910598,0.6168134913,2.6423750237\C,-1.6867543531,-0.7530354  
751,2.4108743502\H,-1.995147962,-1.7769429517,2.1874198591\C,-2.615526  
2418,0.222031194,2.6028954684\H,-2.2469652244,1.2358956246,2.798469556  
3\C,2.3224633668,0.1278598399,0.834388886\C,3.7866807448,0.5782248612,  
0.7826688299\C,4.5719252638,0.6877687813,1.9367054258\C,4.3290437744,1  
.0297496704,-0.4283930856\C,5.8577887375,1.2229609064,1.8827297026\H,3  
.9440972906,3.4617356896,0.9218029226\C,5.6110662846,1.571215539,-0.48  
49489378\H,3.7404929632,0.95839242,-1.3446788508\C,6.3824690299,1.6691  
714844,0.6718801261\H,7.3891680898,2.0909537392,0.6298796236\C,1.87592  
33637,-0.5929020091,-0.4393519824\C,2.7253779032,-1.4822780698,-1.1128  
320602\C,0.567625495,-0.4341669666,-0.9101319528\C,2.2763679318,-2.202  
9140615,-2.2172338229\H,2.1993505667,2.6793864339,-1.6855289615\C,0.11  
59838918,-1.1610204521,-2.0120341437\H,-0.1061330192,0.2711102744,-0.4  
197602407\C,0.9653730401,-2.0495011189,-2.6679043721\H,0.6119692256,-2  
.6135453269,-3.5342019594\O,1.4882250758,1.2272888761,1.092922524\Si,1  
.5086302808,2.8917665293,0.7100762771\C,-0.0421025505,3.4704703083,1.5  
834022899\H,-0.9285364418,2.9416059154,1.1998071588\H,-0.2022785906,4.  
5482594974,1.4204355052\H,0.0329121492,3.3115721476,2.6714282243\C,3.0  
085471669,3.7462360729,1.4246242838\H,3.1159355583,3.5239658858,2.4974  
579218\H,2.8840902496,4.8366045378,1.3193921191\H,4.1927423544,0.36451  
58012,2.9076243578\C,1.3670908822,3.1436641008,-1.1371965892\H,0.42136  
09355,2.7330851949,-1.5226570552\H,1.3834738621,4.2223336709,-1.363466  
8134\H,3.7571070453,-1.6093919812,-0.7776216868\C,-4.5924714329,-1.097  
5450102,3.4134839839\H,-4.1675141913,-2.0734616115,3.1304892952\H,-4.3  
354243969,-0.9031094222,4.464878863\H,-5.6859231456,-1.1759246511,3.33  
15274912\C,-4.0902081968,0.0200258859,2.5022013126\H,-4.5875608205,0.9  
56167981,2.8002211129\C,-4.4510373115,-0.2482421082,1.0016885395\H,-4.  
0225601734,-1.2392801122,0.770961623\C,-3.7843325074,0.7434073452,0.06  
95324001\C,-3.3284675643,0.3218182669,-1.1846606074\C,-3.6241063018,2.  
1007540812,0.3705845645\C,-2.714663989,1.1870023331,-2.0793271392\H,-3  
.4647939761,-0.7245931021,-1.4750305128\C,-3.0168804709,2.9887171521,-

0.512142635\H,-3.9861562949,2.5002517597,1.3223511561\C,-2.5201009311,  
2.5514088335,-1.7595162633\H,-2.3891012213,0.7991949765,-3.0441107767\  
H,-2.9289127651,4.0341413241,-0.2188508209\C,-5.9429371516,-0.35349276  
66,0.7951231775\C,-6.7659652231,0.7784559177,0.7433370562\C,-6.5684967  
898,-1.5998536108,0.6782621849\C,-8.1402799644,0.6788538372,0.58974219  
99\H,-6.3220197604,1.7754516579,0.8082994599\C,-7.9418742853,-1.724732  
9116,0.5180686221\H,-5.9615100057,-2.5103726707,0.706582559\C,-8.77478  
65299,-0.5821490976,0.4730275377\H,-8.7271313254,1.5958757305,0.549756  
33\N,-1.8737513037,3.4047204145,-2.6190131414\C,-1.4350077158,2.931013  
0011,-3.9076220008\H,-0.9080194054,3.7374259397,-4.4315382553\H,-0.731  
3274226,2.0853505381,-3.8121061259\H,-2.2747354732,2.6037060637,-4.548  
2514294\C,-1.7827518875,4.8064237905,-2.3006793503\H,-1.2236816073,5.3  
241903104,-3.0892585037\H,-2.7750920784,5.2867612469,-2.2178178114\H,-  
1.2463064928,4.974790793,-1.3501252064\H,-8.367535352,-2.7229847563,0.  
4223397495\N,-10.1311580691,-0.6890875995,0.3181130769\C,-10.741128948  
1,-1.988175547,0.191826857\H,-11.8259053092,-1.8729361779,0.0809307966  
\H,-10.3709599728,-2.5382249567,-0.6922841468\H,-10.5616621389,-2.6193  
810458,1.0807125148\C,-10.9473150362,0.4972755619,0.2651749845\H,-11.9  
986910748,0.2113003472,0.142056427\H,-10.8706004564,1.0960022343,1.190  
4986632\H,-10.6771726756,1.1516640156,-0.5832413587\H,2.957877497,-2.8  
850533979,-2.7309124825\H,-0.909662962,-1.0194991566,-2.3576229313\H,6  
.0090693583,1.9177594444,-1.4414776536\H,6.4508912912,1.2951567814,2.7  
97205562\\Version=ES64L-G09RevD.01\State=1-A\HF=-2158.150724\RMSE=4.37  
1e-09\RMSF=2.456e-06\Dipole=0.8962271,-0.8486637,1.0277448\Quadrupole=  
43.6332409,-17.3726323,-26.2606087,3.4243909,3.0471782,-9.3117115\PG=C  
01 [X(C42H54N3O1Si1)]\@

#### pre-(R) for catalyst c

1\1\GINC-WORKER\FOpt\RPBE1PBE\def2SVP\C46H50F12N3O1Si1(1+)\JHIOE\23-Ma  
y-2015\0\#p freq def2svp pbe1pbe opt empiricaldispersion=gd3 int=ultr  
afine\\title\\1,1\C,1.9940800754,-0.1382545186,-2.4658011266\C,2.82525  
99478,0.7904557937,-3.3476678987\C,2.0047382121,2.0793311318,-3.497592  
9084\C,0.5508060695,1.6727941915,-3.2487555118\H,2.0588195075,-1.18799  
01605,-2.7833149488\H,3.8249165746,0.9700365166,-2.9299172706\H,2.9733  
64923,0.3103977261,-4.3263698503\H,2.3210180168,2.8374806032,-2.770932  
4423\H,2.1298344061,2.5237788997,-4.4936777635\H,0.0400444224,2.336135  
0898,-2.5342154789\H,-0.049188373,1.6391011006,-4.1713645998\N,0.61921  
25936,0.3131561501,-2.6992291432\C,-0.4232617509,-0.4215694412,-2.4162  
635911\H,-0.2081776398,-1.4438143359,-2.0977757955\C,-1.771004163,0.00  
90041756,-2.4506140804\H,-2.0136394192,1.0539016658,-2.661817693\C,-2.  
7599473577,-0.8769276632,-2.1440119689\H,-2.4753015126,-1.9174908013,-  
1.9359872749\C,2.2885379784,-0.1513374891,-0.9203352632\C,3.6820049001  
, -0.7034810127,-0.6186013812\C,4.3553114402,-1.5681268045,-1.482856691  
7\C,4.235620661,-0.4634607481,0.6419541123\C,5.5438021189,-2.181787169  
4,-1.0916665181\H,3.4634916711,-3.1271761669,1.0648167209\C,5.41854709  
89,-1.0837527065,1.0330236958\H,3.7340129608,0.2080681671,1.3414955352

\C,6.0851271778,-1.9475299073,0.1690375914\H,7.0147252912,-2.430328615  
9,0.4737077366\C,2.1005491663,1.2629962797,-0.3712262896\C,3.128705554  
5,2.208826175,-0.4190600199\C,0.8448152262,1.661193857,0.0888987109\C,  
2.8945846139,3.5309050345,-0.0513063404\H,2.3104550148,-1.097559099,2.  
879119036\C,0.6156437282,2.9890290675,0.4510278258\H,0.0370567375,0.92  
86765002,0.148701465\C,1.634223724,3.9349202857,0.3813533187\H,1.45034  
08382,4.9741997901,0.6574203617\O,1.3167310041,-1.0071497328,-0.405774  
8288\Si,1.1710769013,-2.1198493028,0.8963378908\C,-0.5347201717,-2.796  
7990978,0.567776869\H,-1.2910320895,-1.9969525134,0.539452032\H,-0.836  
1417782,-3.4952447698,1.3633472854\H,-0.5606971403,-3.3534467866,-0.38  
33178504\C,2.4590487674,-3.4697714351,0.777472477\H,2.5161287401,-3.89  
67090203,-0.2357799843\H,2.1802226545,-4.284682454,1.4657644208\H,3.97  
16080792,-1.7911789234,-2.4790079498\C,1.2750263775,-1.1977043448,2.52  
09509355\H,0.8327417891,-0.194015394,2.432113381\H,0.7007623828,-1.736  
0204317,3.2915581472\H,4.128947616,1.9234273519,-0.7514613154\C,-0.759  
4004833,3.3847520504,0.917447463\F,-0.9430628964,4.698293353,0.8851263  
823\F,-1.7009347871,2.8192197696,0.1426992477\F,-0.9870205967,2.973349  
1914,2.1710310502\C,4.0006550733,4.5393526993,-0.2334702905\F,4.076656  
9856,4.9038945658,-1.5212175949\F,3.7959434965,5.6365771746,0.48669638  
64\F,5.1830980993,4.0270582436,0.1033976021\C,5.9146374907,-0.84739930  
42,2.4370555215\F,5.1008386073,-1.446266107,3.3189219491\F,7.138564010  
1,-1.3268683603,2.622084986\F,5.922370733,0.4530609785,2.7313903408\C,  
6.1922048737,-3.168818487,-2.0302947985\F,6.092574633,-2.7598556696,-3  
.2985383945\F,7.4783148807,-3.3465888833,-1.7495798257\F,5.585868094,-  
4.3567544875,-1.9493170092\C,-4.8449817719,-0.9778927476,-3.4468800876  
\H,-4.6885734983,-2.0466630171,-3.6622274676\H,-5.9292254921,-0.797264  
2604,-3.3956667841\H,-4.4290736866,-0.3922647757,-4.2791476357\C,-4.21  
17975069,-0.5822042188,-2.1066272731\H,-4.3582096569,0.5032880745,-1.9  
703195959\C,-4.8686818417,-1.3419724196,-0.9241877963\H,-4.8376821106,  
-2.4110185333,-1.200920821\C,-6.3247183599,-0.967383219,-0.7616314714\  
C,-7.3472547001,-1.8154444685,-1.2007478205\C,-6.7097740705,0.25107052  
29,-0.1883267338\C,-8.6885142334,-1.4757437446,-1.082598351\H,-7.09047  
81495,-2.7819991449,-1.6457039919\C,-8.0422625306,0.6144289376,-0.0652  
372003\H,-5.9465390581,0.9355918244,0.1924635241\C,-9.0785169565,-0.24  
15107699,-0.5120581368\H,-9.4383892971,-2.1833762565,-1.4344562277\H,-  
8.2801947521,1.5725086541,0.3956871379\C,-4.0834015478,-1.1993016845,0  
.3643290354\C,-3.3960504066,-0.0344210787,0.7270529969\C,-4.0880047965  
, -2.2436391,1.299342012\C,-2.7331677074,0.0817687213,1.9451990137\H,-3  
.3775785617,0.8308922611,0.0601987064\C,-3.430984621,-2.1513870634,2.5  
165674645\H,-4.6371253515,-3.1613575463,1.0688416287\C,-2.7166781231,-  
0.9824570649,2.8733116823\H,-2.2431346006,1.0236435228,2.1798835237\N,  
-10.39739672,0.1076495749,-0.3912944916\C,-11.4255279846,-0.7972498458  
, -0.8385233988\H,-12.4097165182,-0.3461588047,-0.6646593797\H,-11.3448  
149451,-1.0156367243,-1.9184931491\H,-11.3981847015,-1.7602972836,-0.2  
971357516\C,-10.7583747606,1.365509909,0.2112857808\H,-11.8499929352,1  
.4690957312,0.213013939\H,-10.4133031298,1.4415077695,1.2584450959\H,-

10.3429565751,2.2257935228,-0.3436089894\H,-3.4795122527,-2.9994284372  
,3.1989198945\N,-2.0399083513,-0.8844914684,4.0658805724\C,-2.15639422  
91,-1.9410008148,5.0405434235\H,-1.5091836026,-1.7175211487,5.89759136  
91\H,-3.1891556799,-2.0686116361,5.4168314506\H,-1.8279498754,-2.90818  
62719,4.625346166\C,-1.5331928124,0.3980380113,4.4882191979\H,-1.00347  
30234,0.2842038701,5.4418574956\H,-0.8150685355,0.8110962392,3.7619152  
253\H,-2.3342787592,1.1485359692,4.6262884337\\Version=ES64L-G09RevD.0  
1\State=1-A\HF=-3504.0622698\RMSD=4.087e-09\RMSF=2.088e-06\Dipole=-2.5  
597013,-0.4329357,-2.0165725\Quadrupole=38.9561875,-30.0167267,-8.9394  
607,1.3862639,-0.2510385,-6.2784987\PG=C01 [X(C46H50F12N3O1Si1)]\@

#### pre-(S) for catalyst c

1\1\GINC-WORKER\FOpt\RPBE1PBE\def2SVP\C46H50F12N3O1Si1(1+)\JHIOE\22-Ma  
y-2015\0\#p freq def2svp rpbe1pbe opt empiricaldispersion=gd3 int=ult  
rafine\\title\\1,1\C,2.2230613403,-0.6283771895,2.3865536453\C,3.06684  
29527,-1.7961047552,2.8943941184\C,2.1534680483,-3.0304987375,2.886726  
6361\C,0.7219793409,-2.4901644845,2.8881890769\H,2.4242748381,0.302113  
7114,2.9347583693\H,3.9748710076,-1.93648528,2.2929494095\H,3.40147730  
22,-1.5701690261,3.917430691\H,2.3260562218,-3.6522311137,1.9999232053  
\H,2.3378468202,-3.6695462241,3.7601891908\H,0.1071216939,-2.915925668  
7,2.079670245\H,0.1978501496,-2.6632868105,3.8403456692\N,0.8480519066  
, -1.0408892142,2.6886487132\C,-0.163349105,-0.2144272871,2.6776852979\  
H,0.0893414216,0.841132419,2.5506238732\C,-1.5258533442,-0.5962423973,  
2.7382246447\H,-1.7963779645,-1.6499475136,2.8269685044\C,-2.487018272  
6,0.3536925597,2.5609344896\H,-2.1628101799,1.3957359793,2.4546737841\  
C,2.3314654485,-0.2410078966,0.8644618339\C,3.7599471285,0.1510332089,  
0.48812744\C,4.626600745,0.7425814559,1.4096510626\C,4.1603704905,0.08  
44763467,-0.8482895493\C,5.8556464315,1.2558200115,1.0031493547\H,3.78  
78619971,2.8604659188,-0.7232129842\C,5.3868934456,0.6050610735,-1.253  
1509406\H,3.5058056576,-0.3653579416,-1.5971472134\C,6.2471262815,1.19  
31258014,-0.3315075352\H,7.2083224513,1.5996892015,-0.6489737136\C,1.8  
021706486,-1.4044581233,0.0256668884\C,2.5974775824,-2.5127133564,-0.2  
78671119\C,0.4628705124,-1.4184567716,-0.3634041085\C,2.0557876671,-3.  
6185061294,-0.9291158831\H,1.9077377091,1.2725151954,-2.4910833163\C,-  
0.075327859,-2.5296854642,-1.0115858032\H,-0.1664164026,-0.5530868341,  
-0.1499375094\C,0.7131102438,-3.6394724286,-1.2992809651\H,0.291686575  
6,-4.5072313656,-1.8084315745\O,1.490973095,0.8666308338,0.7458318592\  
Si,1.3965601499,2.2656196051,-0.2515690759\C,-0.0398847569,3.152504127  
5,0.5366276774\H,-0.9529438845,2.5370103282,0.5258410659\H,-0.27748180  
56,4.0740540562,-0.0176384839\H,0.1932812077,3.4375420212,1.5751107422  
\C,2.9556310358,3.2918424438,-0.1486219953\H,3.2913186017,3.4394538309  
,0.8892181043\H,2.7442126627,4.2870140059,-0.5735236996\H,4.3606995158  
,0.8283599009,2.4640905867\C,1.0409740729,1.7562838193,-2.0155381321\H  
,0.1745300674,1.0811948788,-2.0840326623\H,0.8079065558,2.6556158681,-  
2.608944014\H,3.6565179409,-2.5235818152,-0.011675597\C,-1.5437495773,  
-2.517767059,-1.3387765258\F,-1.9126864592,-3.5579906076,-2.0718854441



\F,-2.2728104452,-2.5422518531,-0.2038730455\F,-1.8882146479,-1.402938  
3447,-1.9901676371\C,2.93453811,-4.8245546068,-1.1458028834\F,3.099195  
2287,-5.4822771505,0.0122055655\F,2.4099749982,-5.6728271984,-2.022255  
9038\F,4.1451570318,-4.4696106959,-1.5723300117\C,5.7142905278,0.58542  
67717,-2.7247607902\F,4.9233486861,1.4456048355,-3.3807110018\F,6.9751  
6017,0.9279698512,-2.9607848768\F,5.5008306961,-0.6222810124,-3.248498  
9675\C,6.7159536559,1.9589625474,2.0230297733\F,6.6968536517,1.3130741  
786,3.1924686537\F,7.9782415585,2.0596427292,1.622693249\F,6.255547251  
9,3.1940666506,2.2469896796\C,-4.4101148274,-1.2471621856,2.8930373862  
\H,-3.988247419,-2.0858174225,2.3165940807\H,-4.1409599163,-1.37630911  
53,3.9521343543\H,-5.5021315719,-1.316679009,2.8024437978\C,-3.9282054  
271,0.0927787648,2.3601046227\H,-4.4882910291,0.9066288956,2.853064707  
4\C,-4.2005082047,0.2350158232,0.8091837899\H,-3.590070067,-0.55277111  
99,0.3423038518\C,-3.7402749961,1.5569199894,0.2280480305\C,-3.1971020  
978,1.5865404738,-1.0622267922\C,-3.8945402002,2.7894824478,0.87347680  
17\C,-2.8062393021,2.7701857258,-1.6738303746\H,-3.0867550334,0.650015  
3399,-1.6143902796\C,-3.5094190898,3.986799255,0.2807268399\H,-4.33289  
35446,2.8378710723,1.8748530229\C,-2.9326052922,4.0107321951,-1.008465  
0137\H,-2.3934906969,2.722225507,-2.6810664515\H,-3.655140913,4.911835  
1935,0.8373415027\C,-5.6383589258,-0.0844497485,0.4820294886\C,-6.6872  
023254,0.790793309,0.7883675769\C,-5.9750606271,-1.2982596948,-0.12683  
81921\C,-8.0072679684,0.4765277829,0.5053232288\H,-6.4714358076,1.7586  
141215,1.249339758\C,-7.2889844365,-1.631981913,-0.4256812789\H,-5.180  
7089085,-2.0061391997,-0.3834137783\C,-8.3510922492,-0.7508896111,-0.1  
141102443\H,-8.7809950105,1.2000560919,0.7597719648\N,-2.488852959,5.1  
809773218,-1.5773757488\C,-2.0198584227,5.1777176938,-2.9400744034\H,-  
1.6896067937,6.1868593646,-3.2146503363\H,-1.1563135061,4.5024106363,-  
3.0702991288\H,-2.7993319861,4.8670307164,-3.6608523839\C,-2.757335877  
8,6.4385661136,-0.9250894767\H,-2.3158765243,7.2543363365,-1.510333745  
7\H,-3.8395517392,6.6424497622,-0.8207084346\H,-2.3088361063,6.4768180  
496,0.082248567\H,-7.4873721522,-2.5870239944,-0.9108271888\N,-9.65214  
19398,-1.066549901,-0.4006772872\C,-9.964982303,-2.3201790237,-1.03827  
71388\H,-11.0488631085,-2.3938757039,-1.1866192059\H,-9.4844223937,-2.  
4141563552,-2.028806324\H,-9.6514188188,-3.1862601668,-0.4280444189\C,  
-10.7085344347,-0.1418323411,-0.0754148765\H,-11.6723303825,-0.5685864  
814,-0.3774440042\H,-10.7603043057,0.0655442337,1.0085036965\H,-10.591  
9171865,0.8242659606,-0.5986626982\\Version=ES64L-G09RevD.01\\State=1-A  
\HF=-3504.0616638\RMSD=5.679e-09\RMSF=3.062e-06\Dipole=-2.1823782,0.40  
95055,2.4510973\\Quadrupole=32.1308284,-8.4325351,-23.6982933,-0.828875  
6,4.9344196,-12.1374923\\PG=C01 [X(C46H50F12N301Si1)]\\@



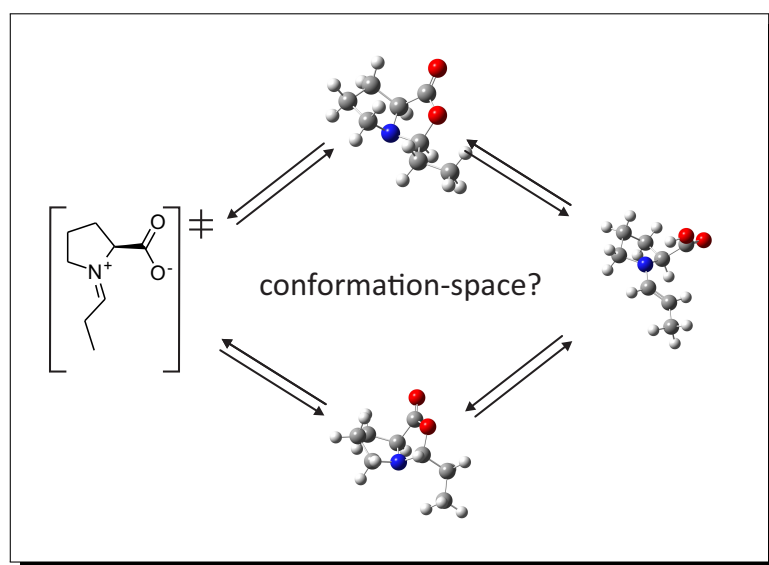
## 3.4 References

- [1] M. C. Holland, R. Gilmour, *Angew. Chem. Int. Ed.* **2015**, *54*, 3862–3871.
- [2] P. Pihko, I. Majander, A. Erkkilä, *Asymmetric Organocatalysis* **2009**, *291*, 29–74.
- [3] S. Mukherjee, J. W. Yang, S. Hoffmann, B. List, *Chem. Rev.* **2007**, *107*, 5471–5569.
- [4] A. Erkkilä, I. Majander, P. M. Pihko, *Chem. Rev.* **2007**, *107*, 5416–5470.
- [5] D. B. Ramachary, Y. V. Reddy, *Eur. J. Org. Chem.* **2012**, 865–887.
- [6] I. D. Jurberg, I. Chatterjee, R. Tannert, P. Melchiorre, *Chem. Commun.* **2013**, *49*, 4869–83.
- [7] S. Bertelsen, M. Marigo, S. Brandes, P. Dinér, K. A. Jørgensen, *J. Am. Chem. Soc.* **2006**, *128*, 12973–12980.
- [8] M. Silvi, C. Cassani, A. Moran, P. Melchiorre, *Helv. Chim. Acta* **2012**, *95*, 1985–2006.
- [9] E. Marqués-López, R. P. Herrera, T. Marks, W. C. Jacobs, D. Könning, R. M. De Figueiredo, M. Christmann, *Org. Lett.* **2009**, *11*, 4116–4119.
- [10] J. Stiller, E. Marqués-López, R. P. Herrera, R. Fröhlich, C. Strohmman, M. Christmann, *Org. Lett.* **2010**, *13*, 70–73.
- [11] G. Talavera, E. Reyes, J. L. Vicario, L. Carrillo, *Angew. Chem. Int. Ed.* **2012**, *51*, 4104–4107.
- [12] Z.-J. Jia, H. Jiang, J.-L. Li, B. Gschwend, Q.-Z. Li, X. Yin, J. Grouleff, Y.-C. Chen, K. A. Jørgensen, *J. Am. Chem. Soc.* **2011**, *133*, 5053–5061.
- [13] Y. Chi, S. H. Gellman, *Org. Lett.* **2005**, *7*, 4253–4256.
- [14] M. Marigo, T. C. Wabnitz, D. Fielenbach, K. A. Jørgensen, *Angew. Chem. Int. Ed.* **2005**, *44*, 794–797.
- [15] Y. Hayashi, H. Gotoh, T. Hayashi, M. Shoji, *Angew. Chem. Int. Ed.* **2005**, *44*, 4212–4215.
- [16] M. B. Schmid, K. Zeitler, R. M. Gschwind, *Angew. Chem. Int. Ed.* **2010**, *49*, 4997–5003.
- [17] M. B. Schmid, K. Zeitler, R. M. Gschwind, *J. Am. Chem. Soc.* **2011**, *133*, 7065–7074.
- [18] M. B. Schmid, K. Zeitler, R. M. Gschwind, *J. Org. Chem.* **2011**, *76*, 3005–3015.
- [19] M. B. Schmid, K. Zeitler, R. M. Gschwind, *Chem. Sci.* **2011**, *2*, 1793–1803.
- [20] M. H. Haindl, M. B. Schmid, K. Zeitler, R. M. Gschwind, *RSC Advances* **2012**, *2*, 5941–5943.
- [21] M. B. Schmid, K. Zeitler, R. M. Gschwind, *Chem. - A Eur. J.* **2012**, *18*, 3362–3370.
- [22] M. H. Haindl, J. Hioe, R. M. Gschwind, *J. Am. Chem. Soc.* **2015**, *submitted*,.

- [23] M. Wiesner, G. Upert, G. Angelici, H. Wennemers, *Journal of the American Chemical Society* **2010**, *132*, 6–7.
- [24] H. Zhu, F. R. Clemente, K. Houk, M. P. Meyer, *Journal of the American Chemical Society* **2009**, *131*, 1632–1633.
- [25] S. Grimme, *J. Chem. Phys* **2003**, *118*, 9095–9102.
- [26] C. Adamo, V. Barone, *J. Chem. Phys* **1999**, *110*, 6158–6170.
- [27] F. Weigend, R. Ahlrichs, *Phys. Chem. Chem. Phys.* **2005**, *7*, 3297–3305.
- [28] F. Weigend, *Phys. Chem. Chem. Phys.* **2006**, *8*, 1057–1065.
- [29] A. V. Marenich, C. J. Cramer, D. G. Truhlar, *J. Phys. Chem. B* **2009**, *113*, 6378–6396.
- [30] R. A. Kendall, T. H. Dunning Jr, R. J. Harrison, *J. Chem. Phys* **1992**, *96*, 6796–6806.
- [31] D. E. Woon, T. H. Dunning Jr, *J. Chem. Phys* **1993**, *98*, 1358–1371.
- [32] S. Kossmann, F. Neese, *J. Chem. Theory Comput.* **2010**, *6*, 2325–2338.
- [33] M. G. Evans, M. Polanyi, *Trans. Faraday Soc.* **1935**, *31*, 875–894.
- [34] J. M. Goodman, P. D. Kirby, L. O. Haustedt, *Tetrahedron Lett.* **2000**, *41*, 9879 – 9882.
- [35] M. J. Frisch, G. W. Trucks, H. B. Schlegel, G. E. Scuseria, M. A. Robb, J. R. Cheeseman, G. Scalmani, V. Barone, B. Mennucci, G. A. Petersson, H. Nakatsuji, M. Caricato, X. Li, H. P. Hratchian, A. F. Izmaylov, J. Bloino, G. Zheng, J. L. Sonnenberg, M. Hada, M. Ehara, K. Toyota, R. Fukuda, J. Hasegawa, M. Ishida, T. Nakajima, Y. Honda, O. Kitao, H. Nakai, T. Vreven, J. A. Montgomery, Jr., J. E. Peralta, F. Ogliaro, M. Bearpark, J. J. Heyd, E. Brothers, K. N. Kudin, V. N. Staroverov, R. Kobayashi, J. Normand, K. Raghavachari, A. Rendell, J. C. Burant, S. S. Iyengar, J. Tomasi, M. Cossi, N. Rega, J. M. Millam, M. Klene, J. E. Knox, J. B. Cross, V. Bakken, C. Adamo, J. Jaramillo, R. Gomperts, R. E. Stratmann, O. Yazyev, A. J. Austin, R. Cammi, C. Pomelli, J. W. Ochterski, R. L. Martin, K. Morokuma, V. G. Zakrzewski, G. A. Voth, P. Salvador, J. J. Dannenberg, S. Dapprich, A. D. Daniels, . Farkas, J. B. Foresman, J. V. Ortiz, J. Cioslowski, D. J. Fox, *Gaussian 09 Revision D.01*, Gaussian Inc. Wallingford CT 2009.
- [36] F. Neese, *Wiley Interdisciplinary Reviews: Computational Molecular Science* **2012**, *2*, 73–78.
- [37] C. Reichardt, T. Welton in *Classification of Solvents*, Wiley-VCH Verlag GmbH & Co. KGaA, **2010**, pp. 65–106.
- [38] Y. Marcus, *Chem. Soc. Rev.* **1993**, *22*, 409–416.

## 4 Enamine and oxazolidinone intermediates investigated by quantum chemical calculations.

*"Enamine and oxazolidinone intermediates investigated by quantum chemical calculations."*



Quantum chemical calculations for species **1** and **6** were performed by Michael H. Haindl.

Michael M. Hammer,\* Michael H. Haindl,\* Johnny Hioe, Hendrik Zipse and Ruth M. Gschwind

*We would like to thank the Leibnitz-Rechenzentrum in Munich for providing computational capacity.*

\* These authors contributed equally.

## 4.1 Organocatalytic intermediates investigated by quantum chemical calculations.

### Introduction

The successful calculation of reactive intermediate structures allows for the informed interpretation of reaction mechanisms and can help synthetically working chemists with the development of catalytic systems and protocols.<sup>[1]</sup> In the field of organocatalysis, especially in enamine catalysis, the number of synthetic applications is by far outnumbering the number of theoretical or experimental studies on the underlying mechanisms.

In the course of studying enamine intermediates<sup>[2–7]</sup> we did identify hints that a possible nucleophile assisted process for the formation of enamines from oxazolidinones is active. To investigate this further we employed quantum chemical calculations on the system to rationalize these findings (see Fig. 4.1). In this part we investigated the structural features and the methodic impact on the found intermediate energies to identify a starting point for the calculation of transition states connecting the intermediates (chapter 5). Although quantum chemical

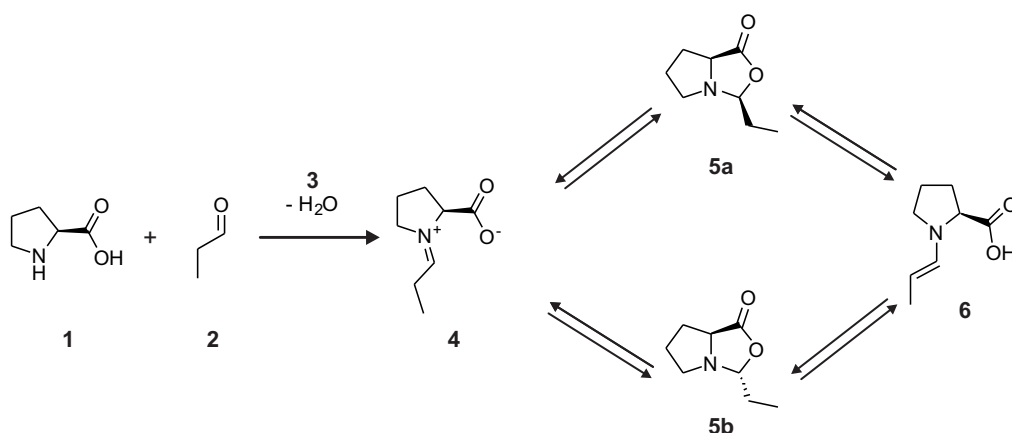


**Fig. 4.1:** Investigated system with denomination of involved species. For species **4** there were two isomers investigated denominated **4E** and **4Z** with respect to the conformation of the NC double bond.

studies on this particular reaction have been performed before,<sup>[8–12]</sup> no explicit attention has been paid to the used methodic impact on found energies and structural features. Merely in the case of prolinol-ether intermediates a lot of attention was focused on the calculation of structural features,<sup>[13,14]</sup> since for those intermediates, a steric approach for the explanation of stereoselection was proposed. Mainly the subsequent transition state of electrophilic attack was addressed in extensive detail.<sup>[8,10,12,15,16]</sup> Also prolinols and prolinol-ether<sup>[17,18]</sup> as well as proline-tetrazole derived enamine intermediates<sup>[19,20]</sup> and their involvement in transition states yielding enantiopure products were investigated. We however feel that the explicit attention to the impact of the used method on energetic distribution and identified structural features in proline enamines intermediates is an important information for the successful ap-

plication of quantum chemical calculations on mechanistic pathways. Especially the stability of enamines and iminium ions was identified to be the major problem, to overcome this issue explicit consideration of solvent molecules was necessary and successful as has already been reported by Houk and Blackmond.<sup>[8]</sup>

In a refined study in our group the intermediate geometries and transition levels connecting these intermediates were calculated with a different approach accounting for all necessities, especially solute-solvent interactions.<sup>[21]</sup> Thus this chapter is to be considered as preliminary study to identify vital calculation aspects that need to be accounted for to achieve calculation success.

## Results and Discussion

An overview of the investigated system is given in Fig. 4.1 and presents the starting material consistent of propanol **2** and the organocatalyst L-proline **1** as well as water **3** (which will be neither experimentally nor quantum chemically addressed in detail). Additionally the down-stream intermediate species are presented, consisting of an iminium species **4** (two conformations regarding the double bond conformation considered, termed **4E** and **4Z**), two oxazolidinone species, namely the *endo*-oxazolidinone **5a** and the *exo*-oxazolidinone **5b** as well as the enamine intermediate **6**. All the investigated intermediate species are intimately involved in the mechanistic underpinnings of enamine catalysis by proline and have been investigated by our group intensively.<sup>[2–7]</sup>

**Experimental pre-requisites.** In order to investigate the energetic distribution of the species a stable experimental ratio is necessary to obtain reliable reference values. The intermediate ratio (**5a:5b:6**) was determined experimentally in DMSO-*d*<sub>6</sub> and did not change within a time frame of 18 h nor did it afterwards (data not shown). From this ratio the experimental  $\Delta G^{298}$  values were deduced and are summarized in Tab 4.1 (all data relative to species **5a**). Taking the detection limit of the employed NMR equipment into account the threshold of iminium **4** detection is calculated to be below 28 kJ·mol<sup>-1</sup>. Oxazolidinone **5b** is 3.33 kJ·mol<sup>-1</sup> more stable and enamine **6** is 1.63 kJ·mol<sup>-1</sup> less stable than reference oxazolidinone **5a**.

**Tab. 4.1:** Normalized ratio (the sum of species **5a**, **5b** and **6** was set to 100 %) and determined experimental  $\Delta G^{298}$  values in kJ·mol<sup>-1</sup> (with  $\Delta G = -RT \cdot \ln(K)$ ) for the investigated species **5b** and **6** relative to species **5a** in DMSO-*d*<sub>6</sub> at 300 K.

Species	5a	5b	6
normalized ratio / %	19	72	9
$\Delta G^{298}$ / kJ·mol <sup>-1</sup>	0	-3.33	+1.63

**Computational results.** To obtain a comprehensive picture of the methodic influence on the quantum chemically identified energetic distribution overall 12 methodic approaches were selected. Besides density functional theory with B98,<sup>[22]</sup> B3LYP,<sup>[23]</sup> mPW1K<sup>[24]</sup> and MO62X,<sup>[25]</sup> Møller-Plesset theory MP2(FC)<sup>[26–30]</sup> was utilized. Additionally quadratic configuration interaction (QCISD(T))<sup>[31–33]</sup> and the advanced G3 method<sup>[34,35]</sup> for energy calculations was used. Solvent modeling was achieved with the mPW1K and the MO62X method using SMD calculations.<sup>[36]</sup> To this end, DMSO was chosen as model solvent, since our experimental data rely heavily on the use of DMSO as stabilizing solvent.<sup>[2]</sup> Accounting for dispersion interactions the B97D functional was tested as well.<sup>[37]</sup> In addition the impact of DMSO as an explicit single solvent molecule was investigated to rationalize experimentally obtained solvent dependent behavior of enamine stabilization. The chosen basis sets were used to balance the cost of the employed theoretical model and to investigate the impact of further consideration of polarizability.

The combined results for a large part of the used methods is summarized in Tab. 4.2 and represented in Fig. 4.2.

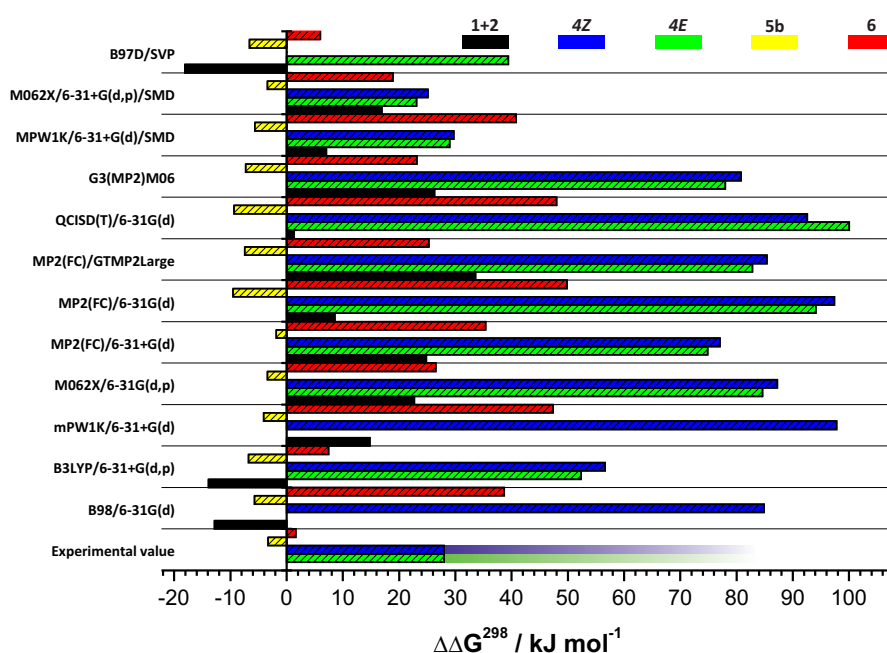


**Fig. 4.2:**  $\Delta\Delta G^{\ddagger 298}$  in  $\text{kJ}\cdot\text{mol}^{-1}$  for the investigated species relative to **5a** for the differently employed methods. The shaded region for experimental data of iminium species **4E** and **4Z** represent the fact, that only a threshold for their energy is known. *Note:* Experimental values taken from intermediate ratios (see Tab. 4.1), for B98/6-31G(d) and mPW1K/6-31+G(d) no minimum was identified for **4E**. For SMD calculations a dielectric constant  $\epsilon=46.7$  was used. For B97D/SVP only one minimum iminium structure was found.

In the case of B98/6-31G(d) the starting material (**1+2**) is identified as  $12.48 \text{ kJ}\cdot\text{mol}^{-1}$  less in energy than **5a**, while **5b** is only  $5.75 \text{ kJ}\cdot\text{mol}^{-1}$  lower and enamine **6**,  $33.86 \text{ kJ}\cdot\text{mol}^{-1}$  higher in



**Tab. 4.2:** Experimental as well as calculated Gibbs free energies  $\Delta G^{298}$  in  $\text{kJ}\cdot\text{mol}^{-1}$  for all involved species at different levels of theory. The sum of **5a** was set as reference frame. For denomination see Fig. 4.1. At B98 and mPW1K levels of theory no minimum (no min) was identified for the species **4E**. *Note:* Water **3** energy was added to all intermediate species, to obtain absolute energy values.

Species	1+2		4	5a	5b	6
Experimental value <sup>a</sup>			>28 <sup>b</sup>	0.00	-3.33	1.63
B98/6-31G(d)	-12.84	E Z	no min <sup>c</sup> 84.90	0.00	-5.75	38.68
B3LYP/6-31+G(d,p)	-10.93	E Z	52.36 56.66	0.00	-6.77	7.48
mPW1K/6-31+G(d)	14.79	E Z	no min 97.82	0.00	-4.09	47.60
M062X/6-31+G(d,p)	22.73	E Z	84.61 87.25	0.00	-3.45	26.51
MP2(FC)/6-31+G(d)	24.85	E Z	74.86 77.03	0.00	-1.84	35.38
MP2(FC)/6-31G(d)	15.61	E Z	94.10 97.39	0.00	-3.90	49.87
MP2(FC)/GTMP2Large	39.75	E Z	82.84 85.38	0.00	-2.60	25.26
QCISD(T)/6-31G(d)	8.49	E Z	100.05 92.56	0.00	-3.47	47.98
G3(MP2)M06	32.70	E Z	78.00 80.78	0.00	-2.90	23.14
MPW1K/6-31+G(d)/SMD <sup>d</sup>	7.04	E Z	29.00 29.71	0.00	-5.67	40.84
M062X/6-31+G(d,p)/SMD <sup>d</sup>	16.92	E Z	23.12 25.14	0.00	-3.43	18.87
B97D/SVP	-18.13	E/Z <sup>e</sup>	39.40	0.00	-6.62	5.98

<sup>a</sup> Values calculated from intermediate ratios (see Tab. 4.1) by  $\Delta G^{298} = -RT \cdot \ln(K)$

<sup>b</sup> Estimated by experimental signal-to-noise ratio in the NMR spectra used for intermediate ratio investigation (Tab. 4.1)

<sup>c</sup> no min: no minimum identified in geometry optimization

<sup>d</sup>  $\epsilon=46.7$

<sup>e</sup> Minimum structure chosen

energy. No minimum was identified for the **4E** species, however **4Z** is found at +84.9 kJ·mol<sup>-1</sup> higher in energy than **5a**. For B3LYP/6-31+G(d,p) again the starting material (**1+2**) is found to be lower in energy, this time by 10.93 kJ·mol<sup>-1</sup>. **5b** is calculated to be even lower in energy than in the previous case with 6.77 kJ·mol<sup>-1</sup> below **5a** and enamine **6** is found at 7.48 kJ·mol<sup>-1</sup> above the reference of **5a**. Both **4E** and **4Z**-iminium species could be calculated and give energies of +52.36 kJ·mol<sup>-1</sup> and +56.66 kJ·mol<sup>-1</sup> relative to **5a**, respectively. MPW1K/6-31+G(d) calculated the starting material (**1+2**) to be at +14.79 kJ·mol<sup>-1</sup>, **5b** to be at -4.09 kJ·mol<sup>-1</sup> and enamine **6** to be at +47.6 kJ·mol<sup>-1</sup> relative to **5a**. As in the case of B98 no minimum structure is found for **4E**. **4Z**-iminium however is calculated to be 97.82 kJ·mol<sup>-1</sup> less stable than *endo*-oxazolidinone **5a**. MO62X/6-31+G(d,p) shows a similar, however not as pronounced picture. Starting material (**1+2**) is found at +22.73 kJ·mol<sup>-1</sup> above **5a**, *exo*-oxazolidinone **5b** at -3.45 kJ·mol<sup>-1</sup> lower than **5a** and enamine **6** at +26.51 kJ·mol<sup>-1</sup> less stable than the reference *endo*-oxazolidinone. Both iminium species are identified at similar energies of +84.61 kJ·mol<sup>-1</sup> and +87.25 kJ·mol<sup>-1</sup> for **4E** and **4Z**, respectively.

Three Møller-Plesset approaches (MP2(FC)) were chosen. Using 6-31+G(d) basis set, the starting material (**1+2**) is 22.73 kJ·mol<sup>-1</sup> less stable, **5b** is 1.94 kJ·mol<sup>-1</sup> more stable and enamine **6** again +26.51 kJ·mol<sup>-1</sup> less stable than **5a**. Iminium species **4E** and **4Z** are +74.86 kJ·mol<sup>-1</sup> and 77.03 kJ·mol<sup>-1</sup> less stable, respectively. Simplifying the basis set to 6-31G(d) calculates the starting material (**1+2**) at +15.61 kJ·mol<sup>-1</sup> above **5a**, iminium ion **4E** at +94.10 kJ·mol<sup>-1</sup>, iminium ion **4Z** at 97.39 kJ·mol<sup>-1</sup>, *exo*-oxazolidinone **5b** at -3.90 kJ·mol<sup>-1</sup> and enamine **6** at 49.87 kJ·mol<sup>-1</sup>. Increasing the basis set to GTMP2Large however yields the starting material (**1+2**) at +39.75 kJ·mol<sup>-1</sup>, iminium ion **4E** at 82.84 kJ·mol<sup>-1</sup>, **4Z**-iminium at +85.38 kJ·mol<sup>-1</sup>, oxazolidinone **5b** at -2.6 kJ·mol<sup>-1</sup> and enamine **6** at +25.26 kJ·mol<sup>-1</sup> relative to **5a**.

Increasing methodic expenditure to QCISD(T)/6-31G(d) gives an energetic distribution relative to *endo*-oxazolidinone **5a** of +8.49 kJ·mol<sup>-1</sup> for the starting material (**1+2**), +100.05 kJ·mol<sup>-1</sup> for **4E**, +92.56 kJ·mol<sup>-1</sup> for **4Z**, -3.47 kJ·mol<sup>-1</sup> for *exo*-oxazolidinone **5b** and +47.95 kJ·mol<sup>-1</sup> for enamine **6**.

Utilizing very accurate methods tailored for thermochemistry like G3(MP2)MO6 (see details in the experimental section 4.1) the energies relative to **5a** are found at +32.70 kJ·mol<sup>-1</sup> for starting material (**1+2**), +78.00 kJ·mol<sup>-1</sup> for the *E*-configured iminium ion **4E**, +80.78 kJ·mol<sup>-1</sup> for the **4Z**-iminium species, -2.90 kJ·mol<sup>-1</sup> for the *exo*-oxazolidinone and +23.14 kJ·mol<sup>-1</sup> for enamine species **6**.

With solvent continuum, MPW1K/6-31+G(d)/SMD ( $\epsilon=46.7$ ) calculates starting material (**1+2**) to be at +7.04 kJ·mol<sup>-1</sup>, iminium ions **4E** and **4Z** to be at +29.00 kJ·mol<sup>-1</sup> and +29.71 kJ·mol<sup>-1</sup>, respectively. *Exo*-oxazolidinone **5b** is 5.76 kJ·mol<sup>-1</sup> more stable than **5a** while enamine **6** is 40.84 kJ·mol<sup>-1</sup> less stable. For MO62X/6-31+G(d,p)/SMD ( $\epsilon=46.7$ ) the energy for the starting material (**1+2**) is calculated to be 16.92 kJ·mol<sup>-1</sup> less stable than **5a**, iminium ions **4E** and **4Z** 23.12 kJ·mol<sup>-1</sup> and 25.14 kJ·mol<sup>-1</sup> less stable, **5b** 3.43 kJ·mol<sup>-1</sup> more and enamine **6** 18.87 kJ·mol<sup>-1</sup> less stable than the *endo*-oxazolidinone **5a**.

To overcome the issue of enamine **6** being overestimated in energy by a very large extent, we utilized a dispersion correction functional developed by Grimme and co-workers.<sup>[37]</sup> The functional B97D is designed to evaluate besides standard energy contributing factors, also the energy gain/loss by dispersion. We used explicitly the B97D with a split valence basis set.<sup>[38,39]</sup> The used dispersion correction with B97D did yield far superior results for the energy estimation of enamine **6** with a relative energy of 5.98 kJ·mol<sup>-1</sup> higher in energy than reference species **5a**. Interestingly the energy found for the starting material (**1** + **2**) is very low with -18.13 kJ·mol<sup>-1</sup> relative to **5a** compared to the other highly demanding methods shown. The energy gain by dispersion correction for enamine **6** can compensate for the gross overestimation by the gas phase as well as the SMD models, however it does not allow the correct and sufficiently accurate calculation of experimental values and was therefore omitted for our further studies.

In conclusion we could show that the use of dispersion correction to describe enamine intermediates can have a beneficial effect on the energy calculation, does however not allow for the sufficiently accurate description of energy differences.

Assessing the computational results several findings become apparent. The performance of all methods in terms of the iminium **4** energy description can not be discussed in detail, since no experimental data are accessible. However the lower energies identified with the SMD modeling, shows the continuums model ability to stabilize charge separated systems to a large extent. The estimation of oxazolidinone energies (**5a** and **5b**) is sufficiently accurate to perform further calculations in the most cases. The underestimation of enamine **6** stability is striking for all employed methods. The poor performance of DFT method, can most likely be attributed to non-consistent or non-systematic errors, which are often present in these types of DFT methods. The inability of some of the correlation methods (MP2) to give a good trend for enamine stabilization is explained by the small basis set sizes 6-31G(d) and 6-31+G(d) compared to GTMP2Large (which also accounts for p-polarization functions on hydrogen), that do not allow the accurate description of electron allocation in the system. The inability of QCISD(T) to give good results is also attributed to the same lack of sufficiently large basis set size. This however is compensated in the G3 method (see Experimental section 4.1) due to the large MP2(FC)/GTMP2Large basis set and thus provides comparable good results. It also is clearly deducible that the use of basis functions accounting for p-functions on hydrogen are necessary to gain access to at least a trend in stabilization of the enamine **6** energy.

In conclusion we could show that all but the enamine species **6** could be calculated to a sufficient extent and represent the experimentally found ratios.

**Consideration of explicit solvent molecules.** In our experimental studies on enamine intermediates derived of proline we did notice a very strongly pronounced solvent dependency.<sup>[2,5]</sup> We concluded that the combination of low H-bond donor ( $\alpha$ ) and high H-bond acceptor ( $\beta$ )<sup>[40]</sup> capabilities are vital for the successful stabilization of enamine intermediates.

Especially DMSO with its fitting solvent parameters ( $\alpha=0.00$ ,  $\beta=0.76$ ) was used and very productive in the stabilization of a number of proline derived enamine intermediates. DMF was also successful in the stabilization, however we did not assess the corresponding solute-DMF adducts.

In order to reflect and investigate the impact of DMSO we explicitly considered the existence of a single solvent molecule in our enamine structures and did calculate the energy of these adducts. This approach has been reported by Blackmond and Houk before<sup>[8]</sup> and was successful in the stabilization of enamine intermediates computationally. We here envisioned to reproduce the results and tried to identify the corresponding stabilizing interactions.

The results are schematically presented in Fig. 4.3. Here we performed geometry optimizations as well as energy calculations with either H<sub>2</sub>O or DMSO in the iminium and enamine species, respectively. Thus providing information on the impact of solute-solvent interactions on the energetics and geometries.

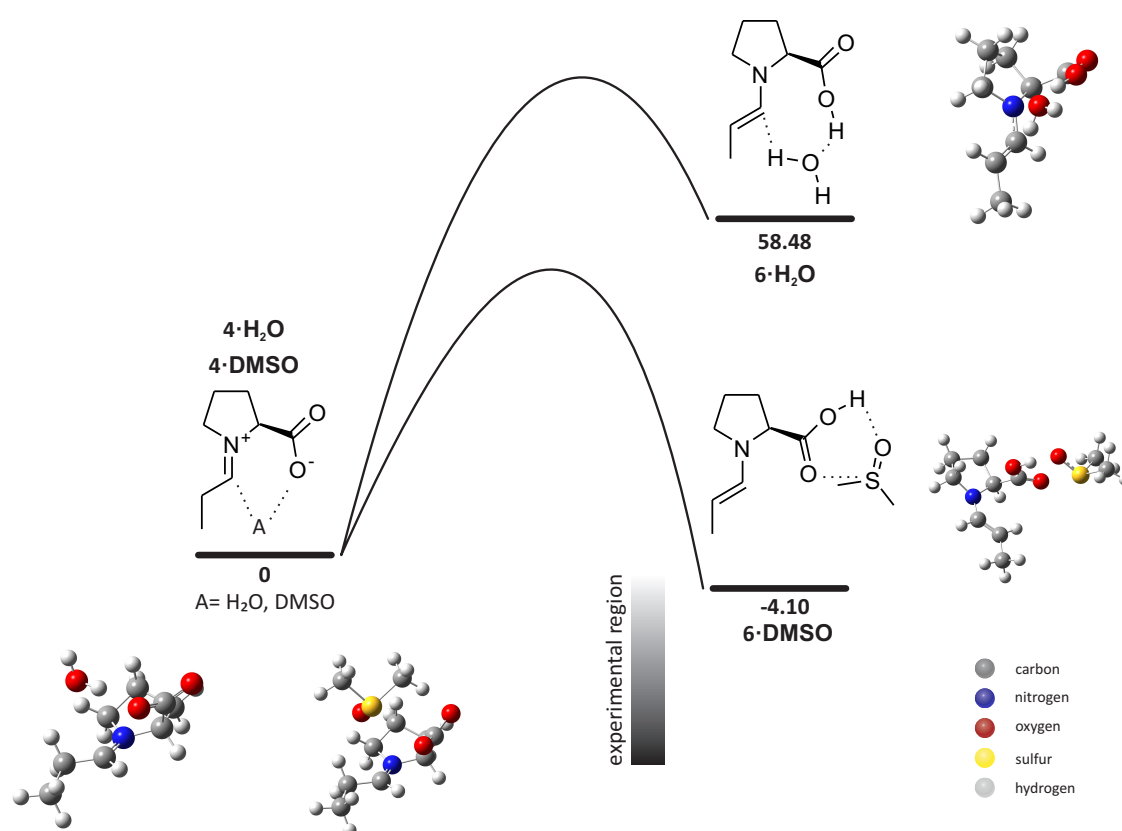


**Fig. 4.3:** Energy effect ( $\Delta G^{298}$  in kJ mol<sup>-1</sup> in kJ mol<sup>-1</sup>) of explicit consideration of solvent molecules on the relative energy of iminium **4** as well as enamine **6** species on a MO62X/6-31+G(d,p) level of theory.<sup>[25]</sup> Considering H<sub>2</sub>O as solvent molecule the relative energy of iminium **4**·H<sub>2</sub>O to enamine **6**·H<sub>2</sub>O is +58.48 kJ mol<sup>-1</sup>, while the consideration of DMSO as solvent molecule the relative energy of the enamine **6**·DMSO to iminium **4**·DMSO is -4.10 kJ mol<sup>-1</sup>. This found relative energy is close to the expected experimental region (highlighted region). Similar considerations were published by Blackmond and co-workers in 2011.<sup>[8]</sup> *Note:* Not to an absolute scale. Structures for **4**·H<sub>2</sub>O, **6**·H<sub>2</sub>O, **4**·DMSO and **6**·DMSO can be found below in section 4.2.

Starting from the iminium species **4**·H<sub>2</sub>O as reference the enamine·H<sub>2</sub>O adduct (**6**·H<sub>2</sub>O) is 55.48 kJ·mol<sup>-1</sup> more in energy. For the DMSO adduct however the solute-solvent adduct **6**·H<sub>2</sub>O is 4.10 kJ·mol<sup>-1</sup> more stable than the corresponding iminium-DMSO adduct **4**·H<sub>2</sub>O. This finding on the stabilizing effect of DMSO brings the energy identified in the experimentally obtained region (shaded area in Fig. 4.3). Addressing the identified structures one can see that, on the iminium side, both DMSO and H<sub>2</sub>O are oriented over the iminium double bond, which additionally represents the highest dipole in the molecule and stabilize this structure through H-bonding accordingly. Interestingly on the enamine side, both H<sub>2</sub>O and DMSO show significantly deviating behavior. While H<sub>2</sub>O is situated in between the carboxylic acid group and the enamine double bond, DMSO is on the outside of the enamine, situated next to the carboxylic acid group. One can conclude, that while H<sub>2</sub>O is stabilizing the acidic enamine protons as well as the carboxylic acid group, DMSO is only stabilizing the carboxylic acid group with no interaction to the enamine protons. Strikingly the enamine conformations differ significantly for **6**·H<sub>2</sub>O and **6**·DMSO, with the pyrrolidine in the H<sub>2</sub>O adduct in the *down* and in the DMSO adduct in the *up* conformation.

The capability of DMSO to stabilize enamine **6** is strongly attributed to the H-bond acceptor abilities of DMSO, which saturates the carboxylic acid residue on the proline substructure. This property is unique to DMSO in comparison to water H<sub>2</sub>O, since water is ambivalent and also needs to donate electronic density in the form of an H-bond. This hydrogen bond saturation of the carboxylic acid residue due to the DMSO molecule might very well reduce the nucleophilicity of the carboxylic acid O-atom prohibiting reaction to the iminium or oxazolidinone species. In addition, **5a** and **5b** do not possess the open carboxylic acid, and thus an impact of an explicit solvent molecule on their stability can be excluded.

In conclusion we could demonstrate the mode in which DMSO stabilizes enamine intermediates through its extraordinary ability to function as an H-bond acceptor towards the carboxylic acid residue of the proline substructure. This finding can easily explain the inability to accurately calculate the relative energy of enamine intermediate **6** in comparison to the oxazolidinones **5a** and **5b**, since in the gas-phase, SMD and even in the dispersion corrected calculations the unique solvent abilities of DMSO can not be reproduced.

**Structure - Energy relations.** In order to understand the identified energy differences between the investigated structures we investigated the energetic impact of structural features of the isolated molecules. To this end, we chose a number of distinguishable structures for species **1**, **5a**, **5b** and enamine **6** and identified the corresponding minimum structures. In the following we will only discuss the identified structures on a G3(MP2)MO6 level of theory, however the energy scattering is shown for all used methods.

**Structural features and their energetic contributions of L-proline 1** L-proline can adopt a number of structural conformers, of those we chose 8 and identified the correspond-

ing minimum structures. The computational results are schematically presented in Fig. 4.4 (exact energies can be found below in section 4.2) The energy dispersion identified for L-proline

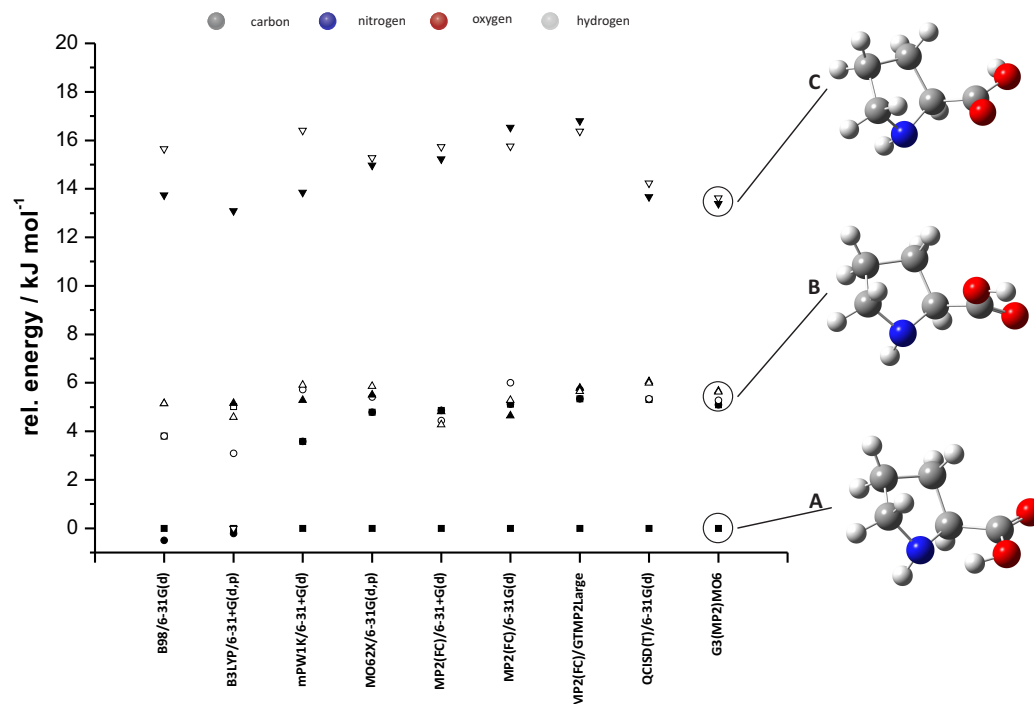


**Fig. 4.4:** Computational results for species **1** (symbols represent different conformations) for the different methods employed relative to the same conformation. There are noticeably formed three groupings. For **A** the OH group on the carboxylic residue is arranged as such as to form a stabilizing hydrogen bond to the lone-pair of the nitrogen. Group **B** represents species with the OH-group oriented away from the nitrogen atom, so no stabilizing hydrogen bond can be formed. **C** conformations show that the carboxylic group is rotated as such as the OH group is the furthest from the nitrogen atom.

**1** is at or around  $14 \text{ kJ}\cdot\text{mol}^{-1}$ . This large scattering is the first hint for major stabilizing interactions that can be identified in the structures. Three distinct groupings (**A–C** in Fig. 4.4) were identified and show significantly deviating structural features. For the highest energy group (Fig. 4.4 **C**) at approximately  $14 \text{ kJ}\cdot\text{mol}^{-1}$  the pyrrolidine is in the *up* puckered state, while the carboxylic acid proton is oriented away from the nitrogen atom in the pyrrolidine ring. The carboxylic acid carbonyl carbon is oriented above the pyrrolidine nitrogen. For grouping **B** at approximately  $5 \text{ kJ}\cdot\text{mol}^{-1}$ , again, the pyrrolidine ring is in the *up* puckered state, however contrary to grouping **C**, the carboxylic acid is oriented with the acidic proton above the pyrrolidine nitrogen, however still pointing away from it. In the case of the low energy grouping ( $0 \text{ kJ}\cdot\text{mol}^{-1}$ , Fig. 4.4 **C**) only a single structure was identified. The structure evidences the *up*-puckering in the pyrrolidine ring with the carboxylic acid proton oriented above and pointing towards the nitrogen atom, clearly demonstrating the formation of a hydrogen bond.

Interestingly no *down* puckered pyrrolidine in the proline structure could be identified amongst the minimum structures. This exclusive adoption of one of the two possible puckered states

of the pyrrolidine ring is in strong disagreement with previous studies on the same topic.<sup>[41]</sup> The major energy contributing factor identified is the rotation of the carboxylic acid group being responsible for the large energetic scattering. The main stabilizing factor was evidenced to be a formation of an intramolecular hydrogen bond, which is a large stabilizing factor in gas-phase calculations, between the carboxylic acid proton and the nitrogen atom in the pyrrolidine ring.

In conclusion, we could calculate gas-phase proline structures and determine structural features with the highest impact in our gas-phase calculations.

### Structural features and their energetic contributions of the *endo*-oxazolidinone **5a**

Minimum structures for the *endo*-oxazolidinone can be found in Fig. 4.5 (exact energies can be found below in section 4.2). Overall 5 different conformers were used to identify the energetic contributions of distinct structural features. A energy dispersion of approximately 7 kJ·mol<sup>-1</sup>

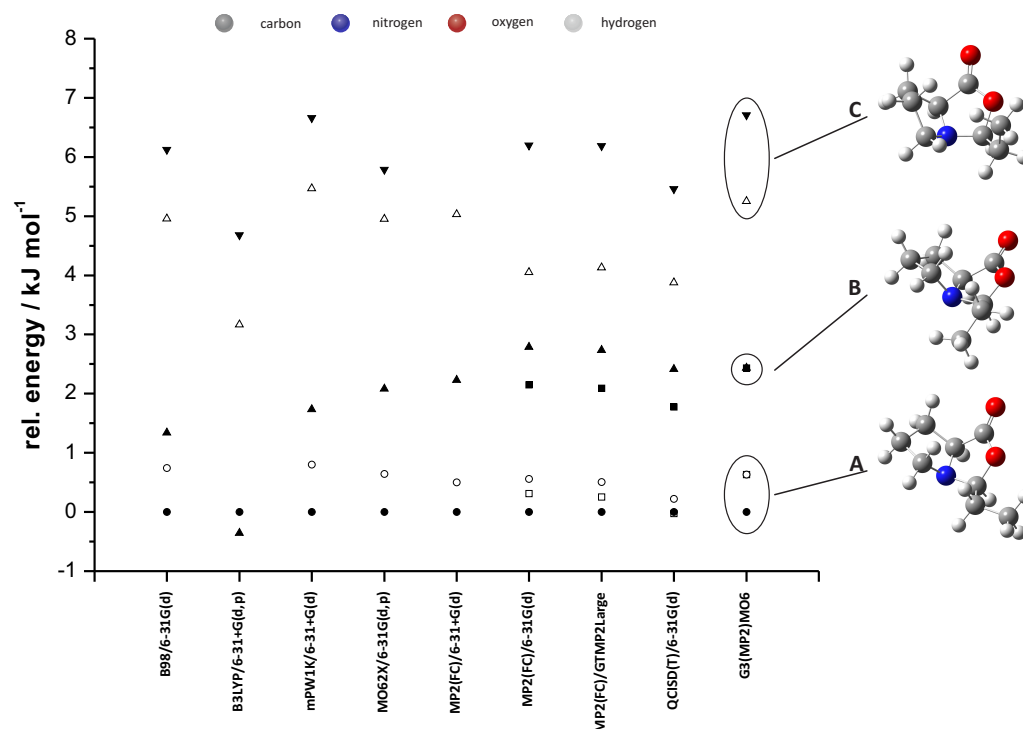


**Fig. 4.5:** Computational results for species **5a** (symbols represent different conformations) for the different methods employed relative to the same conformation. There are noticeably formed three groupings. Comparing the representative structures **A-C** the exocyclic aldehyde residues rotation is responsible for the relatively subtle change in energy.

was identified at the G3 level of theory, with the identification of three different groupings (Fig. 4.5 **A-C**). The high energy group at around 7 kJ·mol<sup>-1</sup> evidences the pyrrolidine ring to be in the *down* puckered state and the exocyclic CH<sub>3</sub> group to be oriented towards the formed cavity of the pyrrolidine and oxazolidinone ring. For group **B** at approximately 2 kJ·mol<sup>-1</sup> again a *down* puckered pyrrolidine ring is identified, however in this case the exocyclic CH<sub>3</sub> group

is facing away from the pyrrolidine-oxazolidinone cavity. The minimum grouping Fig. 4.5 **A** at around 0 kJ·mol<sup>-1</sup> evidences *up* puckering for the pyrrolidine ring and an orientation of the exocyclic CH<sub>3</sub> group at a opposite side of the pyrrolidine nitrogen atom.

In the case of *endo*-oxazolidinone a large energetic contribution can be attributed to the rotation of the exocyclic CH<sub>3</sub> group. While in grouping **C** a steric interaction of this CH<sub>3</sub> group with protons in the pyrrolidine-oxazolidinone cavity is de-stabilizing the structure, in group **B** and **A** no such steric repulsion is in play. In addition, the puckering of the pyrrolidine ring seems to impact the energy of the system as well, however since also rotation of the exocyclic CH<sub>3</sub> group is actively altering the energy from **B** to **A** no quantitative energetic contribution can be attributed to the pyrrolidine puckering. Overall the minimum structure is identified as *up*-puckered with an exocyclic conformation, so as to minimize steric repulsion in the system.

### Structural features and their energetic contributions of the *exo*-oxazolidinone **5b**

As is in the case of *endo*-oxazolidinone **5a**, overall 5 conformers were used to identify the minimum structure for species **5b**. The results are schematically summarized in Fig. 4.6 (exact energies can be found below in section 4.2). For *exo*-oxazolidinone **5b** a energy dispersion

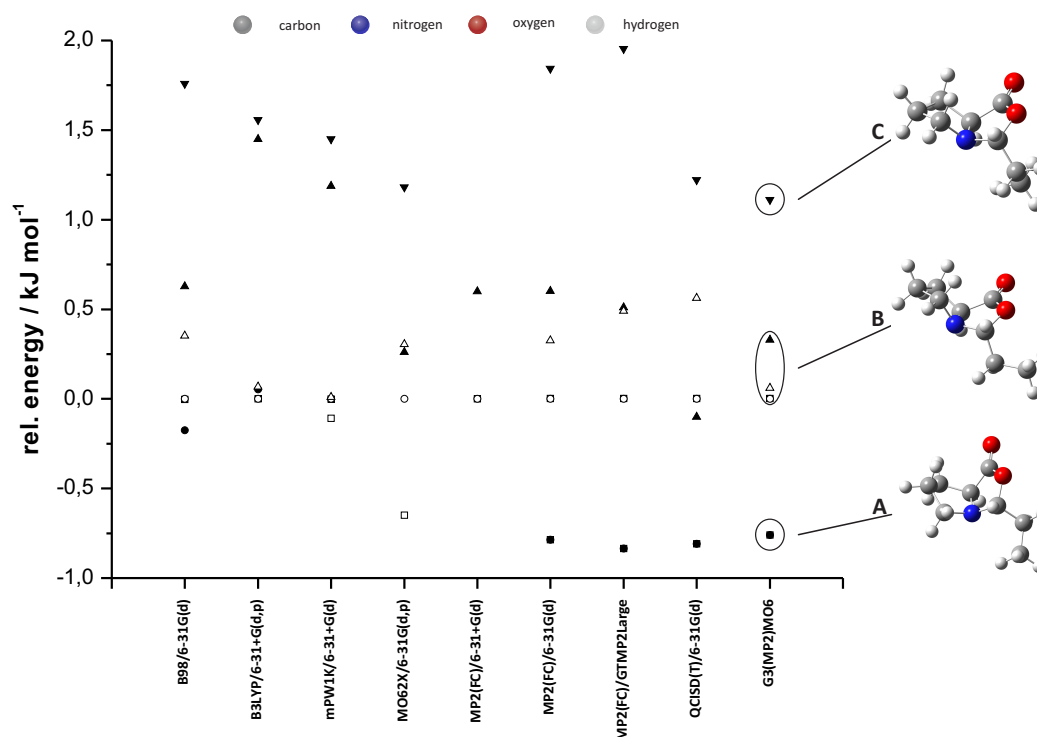


**Fig. 4.6:** Computational results for species **5b** (symbols represent different conformations) for the different methods employed relative to the same conformation. Grouping is not visible in this case, however representative structures were chosen. Comparing the representative structures **A-C** the exocyclic aldehyde residues rotation is responsible for the relatively subtle change in energy as in the energy distribution of species **5a**.

as little as approx. 3 kJ·mol<sup>-1</sup> can be identified. Nevertheless again in this case three distinct



groupings were identified (Fig. 4.6 **A-C**) with significantly deviating energies and structural features. Group Fig. 4.6 **C** at approx.  $1 \text{ kJ}\cdot\text{mol}^{-1}$  evidences structures with the exocyclic  $\text{CH}_3$  group oriented below the oxazolidinone and the pyrrolidine puckered in the *up* conformation. Group **B** is found at approximately  $0\text{-}0.25 \text{ kJ}\cdot\text{mol}^{-1}$  and shows structures again in the *up* puckering however now with the exocyclic  $\text{CH}_3$  group facing away from the two-membered ring system. At approximately  $-0.75 \text{ kJ}\cdot\text{mol}^{-1}$  the group **A** is identified showing *down*-puckering of the pyrrolidine ring with the  $\text{CH}_3$  group oriented below the nitrogen atom or more generally below the two membered ring system.

The comparable low energetic dispersion in the case of the *exo*-oxazolidinone **5a** compared to *endo*-oxazolidinone **5a** can be explained by the missing steric repulsion interaction of the exocyclic  $\text{CH}_3$  group. A similar steric repulsion as found in the case of the *endo*-oxazolidinone **5a** (Fig. 4.5 **C**) is not found in the case of *exo*-oxazolidinone **5b** and may also very well explain the overall energy difference of the two structures found to be experimentally at  $3.33 \text{ kJ}\cdot\text{mol}^{-1}$  in DMSO favoring **5b**. The distinct energetic contributions for **5b** can be attributed to first, the rotation of the exocyclic  $\text{CH}_3$  group and second, the puckering of the pyrrolidine ring. Again however no concrete differentiation between the two contributing factors can be made, since they seem to be interconnected. In contrast to the *endo*-oxazolidinone **5a** *exo*-oxazolidinone **5b** is found with a minimum structure evidencing *down* puckering of the pyrrolidine ring and the  $\text{CH}_3$  group towards the two-membered ring system.

In conclusion we could identify two almost opposite minimum structures for both oxazolidinones **5a** and **5b**. While the experimentally disfavored *endo*-oxazolidinone suffers from steric repulsion leading to higher energy content, the *exo*-oxazolidinone **5b** does not. In addition, we could identify that for both diastereomers the pyrrolidine puckering in the minimum structures is the polar opposite, with the *endo*-oxazolidinone in the *up* and the *exo*-oxazolidinone in the *down* puckered state, respectively. These findings are in strong agreement with our recent experiments towards prolinol-enamines.<sup>[3]</sup>

## Conclusion

In summary, we have investigated the energetic distribution of species involved in the enamine catalysis facilitated by L-proline with a large number of different quantum chemical methods. Oxazolidinone intermediates with their limited conformational space are easily calculated on all DFT, MP2 and more advanced theoretical methods with yielding at least trends on the energetic dispersion of the two in comparison. No theoretical method, neither gas-phase nor solution phase or with the consideration of dispersive interactions allowed the calculation of relative energetics for the enamine species. This finding is attributed to the need of an explicit solvent molecule with H-bond accepting but the lack of H-bond donating abilities, e.g. DMSO in the theoretical calculations as already reported by Blackmond and Houk. This is not surprising, since experimental studies have shown the strong solvent dependency of enamine intermediates. All together, we have shown the necessity of experimental data for the representative calculation of intermediate distributions in the case of enamine catalysis. This finding did allow us to address the connecting transition states between the investigated intermediates. This study also allowed a refined study within our group that tries to account for all drawbacks identified, especially addressing the solute-solvent interactions that are vital to accurately calculate the intermediate geometries.

## Experimental details

### NMR measurements

Enamines and oxazolidinones, respectively, were created *in situ* inside standard 5 mm NMR tubes by addition of freshly distilled aldehyde (25  $\mu$ mol) to a solution of organocatalyst (1 equiv.) and additive (as stated) in deuterated solvent (0.5 mL). All chemicals were used as purchased (if not otherwise stated). Chemicals were purchased from Sigma Aldrich and TCI Europe. NMR measurements were performed at 300–315 K on a Bruker Avance DRX 600 (600.13 MHz) and a Bruker Avance III 600 (600.25 MHz) spectrometer, the latter equipped with a TCI cryoprobe with z-gradient (53.5 G cm<sup>-1</sup>). Reaction monitoring (*react*-NMR) by 1D <sup>1</sup>H-NMR spectra was employed to identify appropriate time slots for more detailed 2D NMR spectroscopic investigations. <sup>1</sup>H,<sup>1</sup>H-COSY, <sup>1</sup>H,<sup>1</sup>H-NOESY ( $t_m$ =450 ms), <sup>1</sup>H,<sup>13</sup>C-HSQC (<sup>1</sup> $J_{\text{HC}}$ =145 Hz) and <sup>1</sup>H,<sup>13</sup>C-HMBC (long range coupling 10 Hz) spectra were recorded for the characterization of the observed species if information from the 1D NMR spectra proved to be insufficient. All spectra were processed and evaluated with Bruker Topspin 2.1, 3.0, 3.1 and 3.2.

### Quantum chemical methods

All calculations were performed within Gaussian09 subversion D.01<sup>[42]</sup>. Plausible start geometries were chosen and minimized. Frequency calculations provided evidence for the identification of minimum structures. Minimum structures at MO62X and B97D level of theory are provided below in section 4.2.

**Used theoretical methods.** Three groups of theoretical methods were utilized in the preparation of this chapter. DFT represented by B98,<sup>[22]</sup> B3LYP,<sup>[23]</sup> MPW1K<sup>[24]</sup> and MO62X,<sup>[25]</sup> Møller-Plesset theory represented by MP2(FC)<sup>[26–30]</sup> and quadratic configuration interaction (QCISD(T))<sup>[31–33]</sup> were used. While DFT methods formally scale with a factor of  $n^4$ , with regards to relative costs dependent on the calculated system size, MP2 scales with a factor of  $n^5$  and QCISD(T) even with a factor of  $n^7$  (see schematic representation in Fig. 4.7). Having reasonable large systems in the case of our study, basically only DFT calculations were found to be feasible for our purpose to obtain a good cost to gain ratio. Additionally to the employed method the used basis set is of high importance for, of course, quality of the gained results but also for the amount of calculation time to yield the results. On the example of methanol the relative calculation times as a function of basis set size is depicted in Fig. 4.8 for B3LYP, MP2 and QCISD(T). QCISD(T) always needs more time to finish the calculations independent of basis set size compared to DFT and MP2 methods, below a basis set size of 100 functions MP2 outperforms B3LYP in regards to calculation times, however increasing the basis set size leads to a almost vanishing gap in between the two methods.

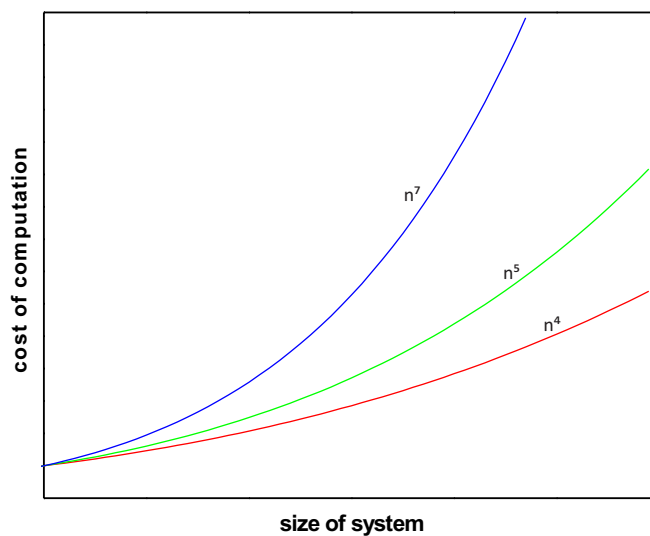


**Fig. 4.7:** Relative cost increase with increasing size of the investigated system.<sup>[43,44]</sup> While DFT methods scale with  $n^4$ , MP2 perturbation theory scales with  $n^5$ , configuration interaction methods (QCISD(T)) scale with a factor of  $n^7$ . Larger system are therefore only manageable with DFT methods in a timely fashion.

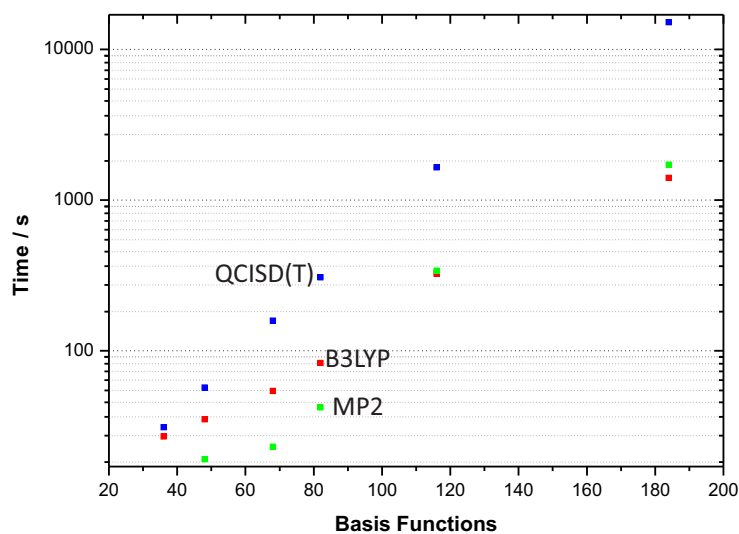


**Fig. 4.8:** Visualization of relative computation times<sup>[44]</sup> (here on the example of  $\text{CH}_3\text{OH}$ ) for three different employed theoretical methods (B3LYP, MP2, QCISD(T)) dependent on the number of basis functions. *Note:* Logarithmic ordinate.

In conclusion to obtain the best cost-to-gain ratio, only DFT methods are feasible with the simple exception of MP2 methods at low basis set levels.

**The G3 method to calculate accurate energies.** Having only access to DFT methods to accurately describe structures in a timely fashion diminishes the ability to gain high quality energy information of the found structures. This is overcome largely by the development of so called Gaussian methods for energy calculations. In particular we used the Gaussian-G3 method developed by Curtiss et al.<sup>[34,35]</sup> to obtain high level energy information on our system.

The G3 method is based on a simple scheme presented in Fig. 4.9. Calculation of energies at a

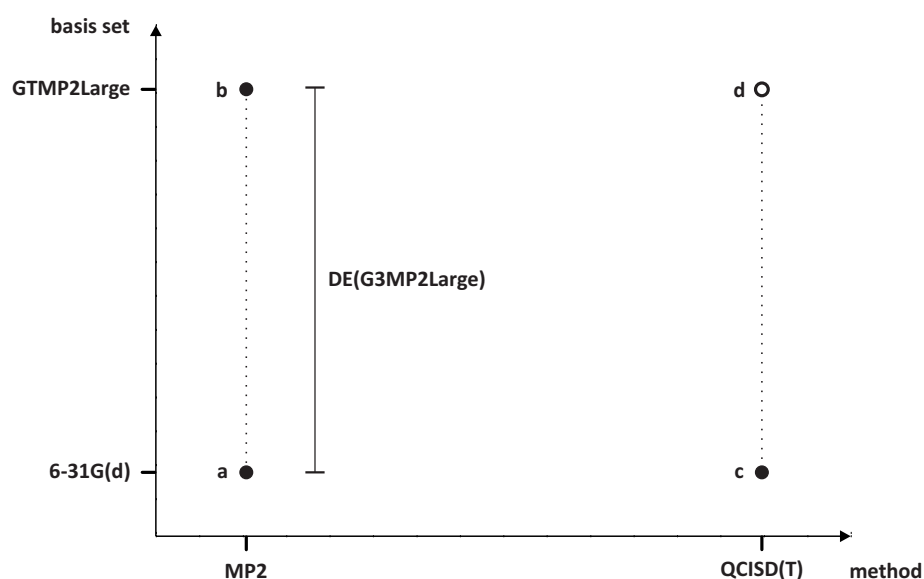


**Fig. 4.9:** Visualization of the Gaussian-3 (G3) method.<sup>[34,35]</sup> Based on geometry optimized structures at MO62X/6-31+G(d,p) single point energy calculations are performed with the MP2 method at both basis set levels, 6-31G(d) (**a**) and GTMP2Large (**b**) and with QCISD(T) method at the 6-31G (**c**) basis set level. The difference between the two level MP2 calculations is added to the low basis set QCISD(T) yielding high level energy estimation for the investigated system (**d**).

low-functional/low basis set point (Fig. 4.9 **a**), a low-functional/high basis set point (Fig. 4.9 **b**) in a combination with a high-functional/low basis set point (Fig. 4.9 **c**) allows with linear combination the approximation of a high-functional/high basis set single point energy. This is done by adding the difference of the low-functional/low basis set to low-functional/high basis set  $DE(G3MP2Large)$  to the calculated single point energy of the high-functional/low basis set point. Additionally a higher level correction HLC is applied to the calculations, supposed to compensate remaining deficiencies of the method. The utilized G3MP2Large basis set is similar to the G3 basis set, except that core polarization functions are not included.

Formally in our case the G3(MP2)MO6 energy was calculated as follows:

$$\begin{aligned}E_0(\text{G3MP2MO6}) &= E[\text{QCISD(T)}/6\text{-}31\text{G}/\text{MO62X}/6\text{-}31\text{+G(d,p)}] \\&+ \text{DE}(\text{G3MP2Large}) \\&+ \text{DE}(\text{HLC})\end{aligned}$$

$$\begin{aligned}\text{DE}(\text{G3MP2Large}) &= E[\text{MP2(FC)}/\text{G3MP2large}/\text{MO62X}/6\text{-}31\text{G(d,p)}] \\&- E[\text{MP2(FC)}/6\text{-}31\text{G(d)}/\text{MO62X}/6\text{-}31\text{+G(d,p)}] \\ \text{DE}(\text{HLC}) &= -A \cdot n(\beta) - B \cdot [n(\alpha) - n(\beta)]\end{aligned}$$

with

for molecules:  $A=10.041$  mHartree  $B=4.995$  mHartree

for atoms:  $A=10.188$  mHartree  $B=2.323$  mHartree

$n(\alpha)$                       No. of  $\alpha$  valence electrons

$n(\beta)$                       No. of  $\beta$  valence electrons

Since only single point energy calculations are performed to gain the Gaussian-G3 energy values, minimized structures from MO62X/6-31+G(d,p) calculations were utilized.

### The impact of solvent modeling.

In the course of this study it became apparent that accurate solvent modeling was necessary to obtain reliable results for the structures as well as the energies that were calculated. To this end we investigated impact of the methodic approach of SMD modelling<sup>[36]</sup> on the found energies.

**Theoretical considerations.** In principal there are two distinct methods of applying SMD modeling on ones system of investigation. Schematic representation of these approaches are depicted in Fig. 4.10.

The first approach uses the gas-phase structure (Fig. 4.10 **a**) and performs a single point energy calculation on is using SMD modeling (Fig. 4.10 **b**). Within the second approach the geometry optimization is performed with the SMD modeling active (Fig. 4.10 **c**). The energy difference of the gas-phase structure with single point SMD calculation to the SMD structure optimization is believed to be only minor and can avoid possible errors made by the geometry optimization process with active SMD modeling. However, if a solutes structure is highly dependent on the solvent surrounding it, and the continuum model proves to be sufficient the gas-phase / SMD single point approach can produce completely different structures as the SMD optimization process.

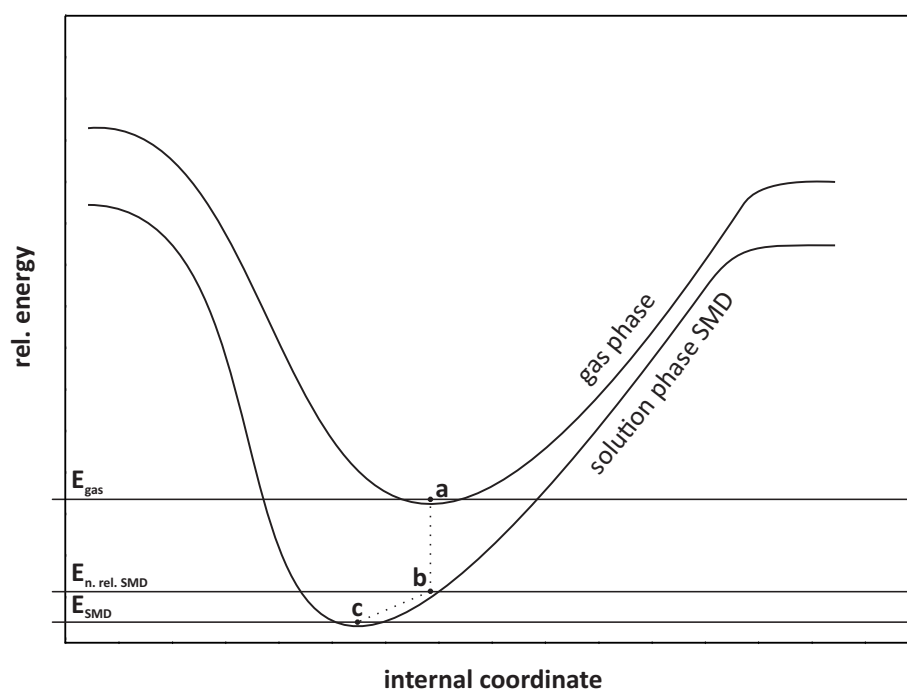


**Fig. 4.10:** Energy error representation for SMD modeling. When using gas-phase geometry (**a**) for SMD calculation (**b**), the found structure might not represent the relaxed structure in solution (**c**). The energy difference between the non relaxed ( $E_{n. \text{rel. SMD}}$ ) and the relaxed structure ( $E_{\text{SMD}}$ ) however is minimal compared to the overall energy gain by SMD calculation.

**Application of the SMD approaches.** We tested the two different approaches at MO62X/6-31G(d,p)/SMD<sup>[25,36]</sup> level of theory on our system and summarized the results in Tab. 4.3.

For all structures **1** to **6** an energy gain in both approaches could be identified. **1** gained 47.06 kJ·mol<sup>-1</sup> and 47.41 kJ·mol<sup>-1</sup> for the first (**a-b**) and second (**a-c**) approach, respectively. A large energy gain of 94.52 kJ·mol<sup>-1</sup> and an even higher energy gain of 106.59 kJ·mol<sup>-1</sup> was identified for species **4E** with the first and second approach, respectively. The same behavior is evidenced for species **4Z** with an energy gain of 102.11 kJ·mol<sup>-1</sup> for the first, and an energy gain of 113.48 kJ·mol<sup>-1</sup> for the second approach. For *endo*-oxazolidinone **5a** the energy gain in the first approach was found at 43.57 kJ·mol<sup>-1</sup> and at 48.41 kJ·mol<sup>-1</sup> with the second approach. **5b** shows again similar behavior and experiences an energy gain of 44.12 kJ·mol<sup>-1</sup> for the first, and an energy gain of 46.72 kJ·mol<sup>-1</sup> for the second approach. The case of enamine **6** needs to be looked at more carefully, since no reasonable mean value for all species could be identified. While for species **6-1** (see Fig. 4.3) an energy gain of 31.78 kJ·mol<sup>-1</sup> and 54.29 kJ·mol<sup>-1</sup> for the first and second approach could be calculated, species **6-2** experiences a very high 53.62 kJ·mol<sup>-1</sup> stabilization for the first and a 57.29 kJ·mol<sup>-1</sup> stabilization for the second approach. Species **6-3** was calculated to give an 41.38 kJ·mol<sup>-1</sup> energy gain for the first and an 42.60 kJ·mol<sup>-1</sup> energy gain for the second approach. Intriguingly the structures of species **6-1** to **6-3** differ significantly. While in **6-1** an intramolecular OH···N hydrogen bond is found, structures **6-2** and **6-3** lack this hydrogen bond. In **6-2** the carboxylic acid group is oriented away from the pyrrolidine nitrogen, however the acidic proton is pointing towards

**Tab. 4.3:** Energy gain (in  $\text{kJ}\cdot\text{mol}^{-1}$ ) by SMD calculations<sup>[36]</sup> for both approaches (**a-b** and **a-c**) compared for investigated species **1**, **4**, **5a**, **5b** and **6**. Mean values ( $\bar{N}$ ) are depicted for species **1**, **4**, **5a** and **5b**. For species **6** three different structures are shown, since the energy gain differs very much dependent on the conformations. While for non-charged species like proline **1**, oxazolidinone **5a** and oxazolidinone **5b** the energy gain is independent of relaxation in the SMD model, iminium species **4E** and **4Z** are highly effected. Species **6** shows conformational dependent behavior.  $E_{\text{gas}}-E_{\text{n. rel. SMD}}$  as energy gain by single point calculation (**b-a** in Fig. 4.10),  $E_{\text{n. rel. SMD}}-E_{\text{SMD}}$  for the error made in not optimizing the structure at SMD level (**c-b** in Fig. 4.10) and  $E_{\text{gas}}-E_{\text{SMD}}$  for overall energy gain (**a-c** in Fig. 4.10).

Species	$E_{\text{gas}}-E_{\text{n. rel. SMD}}$ ( <b>a-b</b> ) (1 <sup>st</sup> )	$E_{\text{n. rel. SMD}}-E_{\text{SMD}}$ ( <b>b-c</b> )	$E_{\text{gas}}-E_{\text{SMD}}$ ( <b>a-c</b> ) (2 <sup>nd</sup> )
<b>1</b>	-47.06	-0.35	-47.41
<b>4E</b>	-94.52	-12.07	-106.59
<b>4Z</b>	-102.11	-11.37	-113.48
<b>5a</b>	-43.57	-0.96	-48.41
<b>5b</b>	-44.12	-0.89	-46.72
<b>6</b>	-31.78 <sup>6-1</sup>	-17.11	-54.29
	-53.62 <sup>6-2</sup>	-3.22	-57.59
	-41.38 <sup>6-3</sup>	0.37	-42.60

6-1

6-2

6-3

carbon   
  nitrogen   
  oxygen   
  hydrogen

<sup>6-1</sup> The found  $\text{OH}\cdots\text{N}$  hydrogen bonded structure is highly affected by SMD calculations.

<sup>6-2</sup> With the OH group rotated the structure is less influenced by the SMD calculations.

<sup>6-3</sup> Exposing the OH group to the solvent leads to the least influence of SMD calculations on the energy gain.



the rest of the structure. This acidic proton is pointing in the complete opposite direction for species **6-3**.

In addition the error estimation for the two SMD approaches (**b-c**) is presented and shows that only for the charged iminium species **4E** and **4Z** and for two of the three enamine structures (**6-1** and **6-2**) this value deviates significantly from zero. For **4E** the error is found to be as high as 12.07 kJ·mol<sup>-1</sup>, for **4Z** to be as high as 11.37 kJ·mol<sup>-1</sup> and for **6** depending on the structure at 17.11 kJ·mol<sup>-1</sup> for **6-1** and 3.22 kJ·mol<sup>-1</sup> for **6-2**, respectively.

The overall energy gain is an intrinsic effect of the SMD modeling and will not be addressed in detail. The differently pronounced energy gain for the different species can however be explained by their structural features more or less dependent on charge separation. While L-proline **1** is not exceedingly in the need for stabilization through charge separation, the energy gain is moderate. This holds also true for both oxazolidinone species **5a** and **5b**. For the iminium species (**4E** and **4Z**) however, charge separation is of vital importance for the stabilization of the overall system, and thus a huge energetic gain was experienced through continuum SMD modeling. For the enamine **6**, the impact of SMD modeling is diverse, since, depending on the structure, more or less stabilizing can be achieved with the help of a continuum model.

Interestingly, the species experiencing the most stabilizing effect from the SMD calculation do also evidence the largest mistakes that have to be accounted for by performing single point SMD calculations on gas-phase geometries. This is largely agreed upon in the community, however these findings demonstrate the need for a accurate modeling of solute-solvent interactions for species with a known large dependency on these interactions.



## 4.2 Results of the conformational space screening

### Depiction of best structures found in the conformational space screening.

The following structures are geometry optimized structures for all species on a M062X/6-31+G(d,p)<sup>[25]</sup> level of theory.

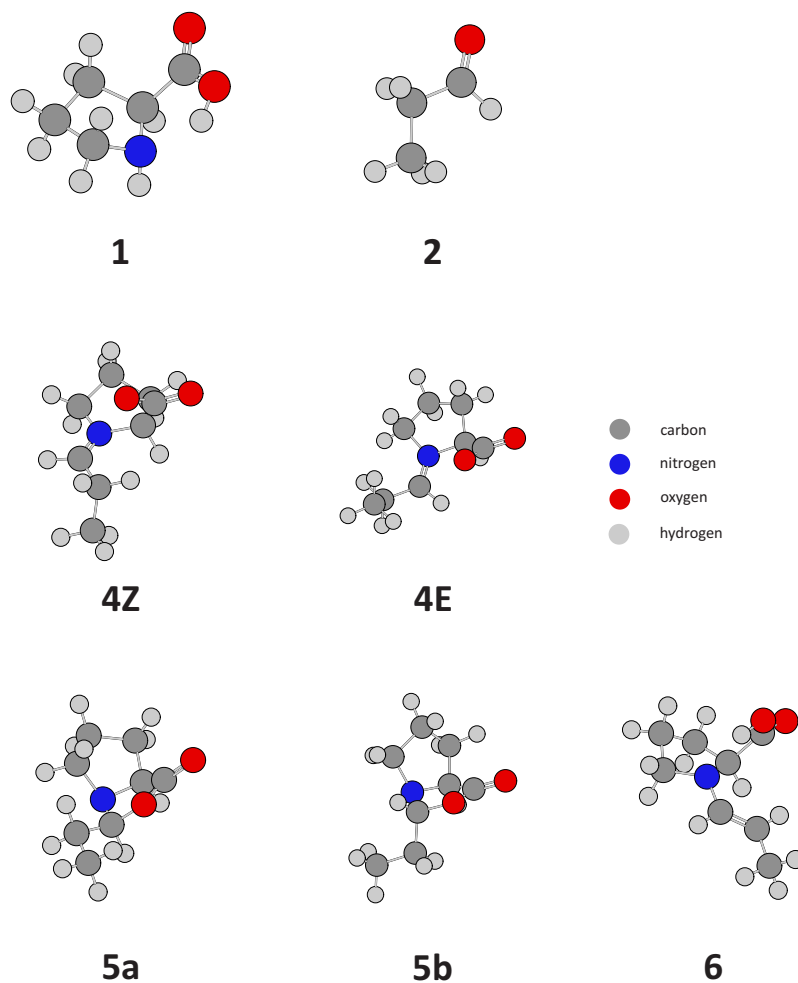


**Fig. 4.11:** Minimum structures derived on a M062X/6-31+G(d,p)<sup>[25]</sup> level of theory for all investigated structures. Water (**3**) not shown.

### Conformational space screening

In the following the energies calculated for species **1** to **6** are summarized for all employed quantum chemical methods.

**Coordinates of stationary points at M062X/6-31+G(d,p) level of theory.**

In the following the coordinates for all stationary points at a M062X/6-31+G(d,p)<sup>[25]</sup> level of theory are shown. Only the energetically best structures were chosen.

**1a**

```
1\1\GINC-PHOENIX\F0pt\RM062X\6-31+G(d,p)\C5H9N102\MHAINDL\13-Jan-2012\
0\#\P M062X/6-31+G(d,p) opt scf=tight int=finegrid\Kommentar\0,1\0,-
1.8372504734,-1.1141058923,-0.3398430493\H,-1.0724307895,-1.6930755147
,-0.1256819473\O,-2.1894097515,1.0771975926,-0.0854289199\H,1.23162940
72,-0.9760277636,-1.4732709452\H,0.2981966721,1.6363103653,-0.89431425
56\H,2.4694681711,-1.5935715299,-0.367887727\C,1.6715318566,-0.8558531
749,-0.475203975\C,-0.0926466049,0.1932242808,0.6928646236\H,2.6314124
72,1.0206348286,-1.1207349165\C,-1.4822779102,0.1116333882,0.048887754
3\C,0.7750037276,1.2987263278,0.030316265\N,0.6203671996,-1.0884083528
,0.5321977324\H,-0.2645005694,0.3996666019,1.7538679337\C,2.1082043589
,0.5954475634,-0.2605100618\H,0.8798181261,2.1716780811,0.6761559641\H
,2.7754794518,0.65388538,0.6073554231\H,1.0390796558,-1.3738501814,1.4
111231013\Version=AM64L-G09RevA.02\State=1-A\HF=-401.0136645\RMSD=8.4
68e-09\RMSF=1.437e-05\Dipole=2.1828492,-0.5382404,0.6089323\Quadrupole
=-4.9351327,0.6603837,4.274749,1.400383,-1.1794165,-0.6415341\PG=C01 [
X(C5H9N102)]\@
```

**2**

```
1\1\GINC-R1ION1\F0pt\RM062X\6-31+G(d,p)\C3H6O1\DI56F0V\22-Mar-2012\0\
#\P M062X/6-31+G(d,p) opt freq=noraman scf=tight int=finegrid\Water\0
,1\C,0.9872693193,-0.2151791247,0.\O,0.6770576322,-1.3821824986,0.\H,2
.0587604827,0.0757333814,0.\C,0.001197811,0.9245591922,0.\C,-1.4500872
905,0.4666419932,0.\H,0.2333565261,1.5503708505,0.872759605\H,0.233356
5261,1.5503708505,-0.872759605\H,-2.1263622985,1.3244158894,0.\H,-1.66
22608541,-0.145003267,-0.8799683533\H,-1.6622608541,-0.145003267,0.879
9683533\Version=EM64L-G09RevB.01\State=1-A'\HF=-193.0610862\RMSD=5.18
2e-09\RMSF=1.313e-05\Dipole=0.0568048,1.1104421,0.\Quadrupole=1.306783
1,-2.3336743,1.0268912,1.2373231,0.,0.\PG=CS [SG(C3H201),X(H4)]\@
```

**3**

```
1\1\GINC-R1I2N8\F0pt\RM062X\6-31+G(d,p)\H2O1\DI56F0V\06-Feb-2012\0\#\P
M062X/6-31+G(d,p) opt freq=noraman scf=tight int=finegrid\Water\0,1
\O,-0.476853444,0.1679509902,0.\H,-0.4489035412,1.129242132,0.\H,0.438
7569853,-0.1261931222,0.\Version=EM64L-G09RevB.01\State=1-A'\HF=-76.3
949639\RMSD=4.335e-09\RMSF=1.210e-05\Dipole=0.7121619,0.5035363,0.\Qua
drupole=0.3271979,0.8662556,-1.1934535,-0.7621728,0.,0.\PG=CS [SG(H201
)]\@
```

**4Eb**

1\1\GINC-R1ION5\F0pt\RM062X\6-31+G(d,p)\C8H13N102\DI56F0V\07-Feb-2012\0\\#P M062X/6-31+G(d,p) opt freq=noraman scf=tight int=finegrid\\Iminimum propanal\\0,1\C,1.8242483933,-0.717427875,0.7905486978\C,0.3259920172,-0.4704279529,0.7476238156\C,1.2317184682,-0.1919188419,-1.4851645213\C,2.3090779993,0.0751530883,-0.4290140525\H,2.2266488253,-0.3384598042,1.7302615496\H,2.0622215774,-1.7825385866,0.6874900953\H,-0.2822851233,-1.2307861517,1.2436288617\H,1.4344347839,-1.1035439917,-2.0571746941\H,1.0743333184,0.639782604,-2.1736967672\H,3.2982650508,-0.2209798212,-0.7827371553\H,2.3299885648,1.1407213344,-0.1816653198\C,-1.2000194056,-0.2345036371,-1.0773557671\N,0.0081451201,-0.4192907719,-0.6799743699\O,-1.024925044,1.5313820123,0.7542793815\C,-0.1011888483,0.967874836,1.3724215012\O,0.5464569881,1.259292166,2.3788227571\H,-1.9739920593,-0.3704044361,-0.3285406989\C,-1.57883803,0.2111730794,-2.4460130013\H,-2.510363936,-0.2852093359,-2.7319868069\C,-1.7882747408,1.7391456273,-2.4198800021\H,-2.1080771877,2.0836979735,-3.4056587247\H,-2.5406395074,2.0136350199,-1.6780781997\H,-0.8662922421,2.2521518958,-2.1367780686\H,-0.8146924024,-0.0655400208,-3.1773649006\\Version=EM64L-G09RevB.01\State=1-A\HF=-517.6554591\RMSE=7.879e-09\RMSF=8.642e-06\Dipole=0.1196594,-2.0902129,-3.2383796\Quadrupole=6.3727257,-0.86861,-5.5041157,1.372438,1.1128222,-6.9723788\PG=C01 [X(C8H13N102)]\\@

**4Za**

1\1\GINC-R1ION6\F0pt\RM062X\6-31+G(d,p)\C8H13N102\DI56F0V\07-Feb-2012\0\\#P M062X/6-31+G(d,p) opt freq=noraman scf=tight int=finegrid\\Iminimum propanal\\0,1\C,2.0601072304,-0.5372395026,0.6574456568\C,0.5427586458,-0.3993940657,0.8671820758\C,1.0189631281,-0.2297471872,-1.4770545532\C,2.2348980746,-0.8833544535,-0.8313928262\C,-1.2886502829,-0.4927102597,-0.7470304769\N,-0.0358723522,-0.4763691775,-0.4727855601\O,-0.8136890745,1.5981783725,0.9833339353\C,0.1212761611,1.0099705767,1.5506033569\O,0.8052693822,1.2423707981,2.548229409\H,-1.5435279878,-0.3903601515,-1.8031116104\C,-2.4012888445,-0.6703985788,0.2214123724\H,-2.8036062851,0.3365331069,0.3908426491\C,-3.4699140451,-1.6216007044,-0.3242240025\H,-4.3041055986,-1.6865752762,0.376807703\H,-3.8663720498,-1.2656314117,-1.2801984228\H,-3.0748518025,-2.6305647799,-0.4724150558\H,-2.0201583862,-0.9972232027,1.1912439494\H,1.1379555305,0.857562583,-1.550411677\H,0.7175295267,-0.6373161628,-2.4431799428\H,3.1699237712,-0.5080941658,-1.2512654404\H,2.1958551695,-1.9659134844,-0.991355198\H,2.530378273,0.4163747895,0.9100036172\H,2.4943325506,-1.2944140317,1.3113959562\H,0.1170489455,-1.1858403906,1.494691515\\Version=EM64L-G09RevB.01\State=1-A\HF=-517.6511817\RMSE=5.145e-09\RMSF=6.793e-06\Dipole=-0.3708164,-2.6776631,-2.9839049\Quadrupole=8.5660855,-5.9282961,-2.6377895,1.11493,-3.3350715,-7.6580905\PG=C01 [X(C8H13N102)]\\@

**5ac**

```
1\1\GINC-PHOBO5\SP\RM062X\6-31+G(d,p)\C8H13N1O2\MHAMMER\12-Jan-2012\0\
\#P M062X/6-31+G(d,p) scf=tight int=finegrid\\Houk Geometrien fur Oxa
zolidine aus OrgLett 5b 4-processor run, 1024MB RAM\\0,1\C,0,2.493278,
-0.126045,0.158762\C,0,1.160429,0.356331,0.75427\C,0,0.655704,-1.51096
8,-0.540744\C,0,2.168796,-1.546344,-0.347706\H,0,2.79379,0.542179,-0.6
53212\H,0,3.292419,-0.125179,0.901394\H,0,1.244502,0.701617,1.791963\H
,0,0.192195,-2.500145,-0.56478\H,0,0.411282,-0.984029,-1.479284\H,0,2.
4198,-2.288328,0.415682\H,0,2.701444,-1.801916,-1.266112\C,0,-1.069409
,-0.091033,0.538819\H,0,-1.382656,0.217698,1.545671\N,0,0.208074,-0.75
9552,0.646988\O,0,-0.820502,1.141937,-0.201568\C,0,0.482233,1.46739,-0
.057263\O,0,0.978662,2.458212,-0.517967\C,0,-2.175637,-0.867217,-0.139
22\H,0,-1.886576,-1.066978,-1.176301\C,0,-3.502955,-0.112841,-0.099577
\H,0,-3.413861,0.850165,-0.608406\H,0,-4.291129,-0.688695,-0.590127\H,
0,-3.816124,0.075352,0.932389\H,0,-2.26153,-1.83171,0.374441\\Version=
AM64L-G09RevA.02\State=1-A\HF=-517.6918219\RMSD=5.486e-09\Dipole=-0.15
41431,-1.4887893,0.3775605\Quadrupole=4.7426129,-6.3009424,1.5583295,-
1.5094045,0.2289573,4.3946974\PG=C01 [X(C8H13N1O2)]\\@
```

**5bb**

```
1\1\GINC-PHOBO5\FOpt\RM062X\6-31+G(d,p)\C8H13N1O2\MHAMMER\11-Jan-2012\
0\#P M062X/6-31+G(d,p) opt scf=tight int=finegrid\\Kommentar\\0,1\C,2
.1240863449,-0.5979319417,0.775872182\C,0.7767333613,0.1236078125,0.86
58955178\C,0.5144638139,-1.8399188931,-0.4605797541\C,1.977110039,-1.3
869599881,-0.5288208607\H,2.9508846382,0.1157926149,0.7780455759\H,2.2
390819933,-1.2758995163,1.6273967148\H,0.514847472,0.4081936258,1.8906
541282\H,0.4288032359,-2.762040698,0.1254864635\H,0.0675003158,-2.0274
609909,-1.44116052\H,2.6771192336,-2.2215938322,-0.6095416138\H,2.1351
921553,-0.7234227263,-1.3873548105\C,-1.0544438905,0.1034646682,-0.566
139014\N,-0.2191016872,-0.7631839412,0.2439049893\O,-0.2690003193,1.28
19353368,-0.8781141574\C,0.7617971212,1.3735754231,-0.0163261276\O,1.5
363068309,2.2905768022,0.0027375224\H,-1.2985215918,-0.3771854956,-1.5
193033581\C,-2.3192508619,0.5411563613,0.1552825682\H,-2.8022720526,1.
3200751856,-0.4439387972\C,-3.2623535258,-0.6335916579,0.3925050497\H,
-4.1573651768,-0.3142052183,0.9315812837\H,-3.5854021818,-1.0759884607
,-0.5562450952\H,-2.7631533142,-1.40996754,0.9782440638\H,-2.028010953
3,0.9995300699,1.1088330493\\Version=AM64L-G09RevA.02\State=1-A\HF=-51
7.6924484\RMSD=7.848e-09\RMSF=1.357e-05\Dipole=-0.4756193,-1.5206669,0
.1584833\Quadrupole=2.6335337,-5.08524,2.4517063,-5.6193976,1.0207513,
2.5803297\PG=C01 [X(C8H13N1O2)]\\@
```

**6a**

```
1\1\GINC-PHOENIX\FOpt\RM062X\6-31+G(d,p)\C8H13N1O2\MHAINDL\12-Jan-2012
\0\#P M062X/6-31+G(d,p) opt scf=tight int=finegrid\\Kommentar\\0,1\C,
```

-0.6142320982,0.1558435917,-0.6151691239\C,-1.9289213831,-0.5873906749  
 ,-0.942306908\C,-2.0315559329,-1.6457430999,0.162145365\C,-0.573362569  
 1,-2.0451516799,0.3566934555\N,0.1255894227,-0.7581754349,0.2538706093  
 \C,1.5260833109,-0.7631203881,0.2038873068\H,1.9710853773,-1.653652704  
 3,0.6461669445\C,-0.8896752104,1.499921842,0.0721627973\O,-1.365122718  
 2,2.4341594091,-0.5195185104\C,2.3092599675,0.215635589,-0.2674179168\  
 C,3.8086740919,0.1519972341,-0.2311375046\O,-0.5964498757,1.54720776,1  
 .3755940619\H,-0.0535871912,0.383730694,-1.5306208792\H,-2.7793513189,  
 0.0949357782,-0.9916143069\H,-1.829201423,-1.0753643737,-1.9162382613\  
 H,-2.4238106915,-1.2044725062,1.0848917556\H,-2.6668974543,-2.48960438  
 69,-0.1139997893\H,-0.3703982122,-2.5092990577,1.3261876704\H,-0.24948  
 20478,-2.7371995117,-0.4367052574\H,1.8644475213,1.1195435665,-0.68000  
 64228\H,-0.2078995591,0.6820956701,1.6097639601\H,4.1531688912,-0.7908  
 24738,0.2036132289\H,4.2346285335,0.2352674998,-1.2363779901\H,4.22622  
 85694,0.9710029216,0.3641347155\\Version=AM64L-G09RevA.02\State=1-A\HF  
 =-517.6779128\RMSD=3.798e-09\RMSF=9.149e-06\Dipole=0.398376,-2.1063111  
 ,0.0129175\Quadrupole=3.5348972,-4.8080379,1.2731406,5.8359553,0.18344  
 3,-1.0601389\PG=C01 [X(C8H13N102)]\@

#### 4.DMSO

1\1\GINC-R1I2N1\F0pt\RM062X\6-31+G(d,p)\C10H19N103S1\DI56F0C\13-Oct-20  
 12\0\#p opt hf/6-31+g(d,p) int=finegrid m062x scf=tight\DMSO\_Imin\0  
 ,1\C,-0.5077584448,0.6944646671,-2.0637661589\C,-1.6207035979,0.773262  
 8644,-1.0291504626\C,0.5143039766,1.3313038258,0.0099489937\C,0.722104  
 1367,0.4152608824,-1.1934446832\C,-1.5857943785,1.6630601513,1.2257486  
 974\N,-0.9592326271,1.3642335469,0.1493808305\O,-2.774971794,-0.653475  
 5897,0.5130628139\C,-2.2085868412,-0.6478149473,-0.6000576349\O,-2.038  
 4352058,-1.5543878009,-1.4262802007\H,-2.6689278518,1.5766918575,1.187  
 1092094\C,-0.8958948854,2.0532539793,2.4887964395\H,-0.1883118431,2.86  
 56451434,2.2784494109\C,-1.8811331184,2.4462692687,3.5866690173\H,-1.3  
 506245692,2.6856802003,4.5104424008\H,-2.4708515645,3.3219463167,3.300  
 3669641\H,-2.5705963756,1.6234848907,3.7952121906\H,-0.2956647393,1.17  
 9268778,2.7813081147\H,0.9497113009,0.9487520759,0.9327585686\H,0.8517  
 317032,2.3564656462,-0.1865154923\H,-2.4680479956,1.4010231548,-1.3178  
 620208\H,-0.3982329938,1.6434296503,-2.6024482114\H,-0.7211881476,-0.1  
 093960205,-2.7679894248\H,1.6709569442,0.6131522347,-1.6956867929\H,0.  
 7018320277,-0.6236076958,-0.8497409039\S,-0.9649079201,-1.882537957,2.  
 4065356555\C,-0.0078332047,-2.8204844348,3.631748191\H,0.8948307519,-3  
 .20432162,3.1506239273\H,-0.6158748268,-3.6345301297,4.033880362\H,0.2  
 637423453,-2.129430413,4.4312049247\C,-1.153600211,-3.2275555532,1.218  
 4786274\H,-0.1563437428,-3.5906488147,0.9564406232\H,-1.6701898782,-2.  
 8314231609,0.3408664848\H,-1.7499805781,-4.0165204116,1.6841555124\O,0.  
 .062753989,-0.9168948453,1.8135668466\\Version=EM64L-G09RevC.01\State=  
 1-A\HF=-1070.7699123\RMSD=6.539e-09\RMSF=8.367e-06\Dipole=1.2994834,1.  
 7524638,1.5768902\Quadrupole=-7.6793073,8.6991679,-1.0198605,-3.615758

8,-4.2736324,-8.7115845\PG=C01 [X(C10H19N103S1)]\ \@

#### 6·DMSO

1\1\GINC-R1I0N8\FOpt\RM062X\6-31+G(d,p)\C10H19N103S1\DI56F0C\19-Sep-2012\O\ \#P M062X/6-31+G(d,p) opt scf=(tight) int=finegrid\DMSO\_Enamin\0,1\C,-1.3000004333,-1.6558942991,0.8227210975\C,-0.698830326,-0.2216994211,0.8389885201\C,-2.2207991869,-0.3804934473,-0.9950501453\C,-2.5475783451,-1.5547041504,-0.0744976503\C,-1.2199567058,1.8213809617,-0.4334761618\N,-1.5272531199,0.5196084363,-0.0864200386\O,0.9344927389,-0.5424444791,-0.8583902673\C,0.7707664799,-0.2828429997,0.4220073411\O,1.6872329219,-0.1479167881,1.2182533317\H,-1.8533564453,2.2176556344,-1.2267714623\C,-0.2879350853,2.60724461,0.1307339066\C,-0.089106306,4.0424100619,-0.2662122467\H,0.9341866554,4.2256613444,-0.6129033669\H,-0.7704579555,4.3227658148,-1.0758287132\H,-0.2712893239,4.724855485,0.572043829\H,-1.5739923373,-0.6961760756,-1.8280300852\H,-3.111018666,0.1092951142,-1.4020140305\H,-2.7430352847,-2.4807205864,-0.6200242655\H,-3.429580181,-1.3108668189,0.5251049789\H,-0.5794859079,-2.3535868882,0.3863415275\H,-1.531856941,-2.0019064256,1.8315011845\H,-0.7238626571,0.2407960652,1.8323587191\H,1.9288372137,-0.6092555689,-1.0573728311\H,0.3549474406,2.2149924828,0.916072523\S,4.2684728783,0.1442204937,-0.2094022788\O,3.4744760385,-0.7127236047,-1.2067691741\C,5.9068573534,0.2120679537,-0.9655587969\H,6.2138979269,-0.8045885203,-1.2194963323\H,6.6118517239,0.6804319434,-0.2750744703\H,5.8170623255,0.8107447556,-1.8724689705\C,4.6791819379,-0.9618731772,1.1555111685\H,5.0821609217,-1.8873986156,0.7380230647\H,3.7437076046,-1.1423189133,1.6845803935\H,5.4033880466,-0.4718723778,1.810644702\Version=EM64L-G09RevC.01\State=1-A\HF=-1070.7857448\RMSD=4.941e-09\RMSF=9.700e-06\Dipole=1.3462411,-0.2713314,0.26899\Quadrupole=15.8436759,-6.9108315,-8.9328443,3.5071388,3.1770611,-3.5993995\PG=C01 [X(C10H19N103S1)]\ \@

#### 4·H<sub>2</sub>O

1\1\GINC-R1I3N11\FOpt\RM062X\6-31+G(d,p)\C8H15N103\DI56F0C\24-Apr-2012\O\ \#P M062X/6-31+G(d,p) opt scf=(tight) int=finegrid\ts\_05\_opt\_irc\_fw\_rel\0,1\C,2.0695075064,1.2971143416,-0.2879383729\C,1.0916012295,0.3143093983,-0.9181113852\C,-0.0696093535,1.6784373421,0.7405190287\C,1.4191442089,1.575677813,1.0718626032\C,-1.3233821488,0.2183146931,-0.7768971615\N,-0.2183146047,0.7523630707,-0.406878003\O,0.3178264445,-1.8840336244,-0.2853155317\C,1.3582120123,-1.204714572,-0.4836058681\O,2.5484614075,-1.5016249936,-0.4440692014\H,-1.2553568283,-0.5059447485,-1.5861691875\C,-2.6375689167,0.5127741607,-0.1392993379\H,-2.7328432781,1.5946306504,0.0151292467\C,-3.8095600002,-0.0378119177,-0.9489925611\H,-4.7526244012,0.1631434918,-0.4374329387\H,-3.8601731123,0.4178563336,-1.9420338774\H,-3.7175333695,-1.1203035539,-1.071384999\H,-2.5928695813,0.0505666395,0.858365095\H,-0.7238339393,1.3457297938,1.5474091444\H,-0.3496398689,2.6822251286,0.4000420755\H,1.0772202307,0.3319859638,-2.0110212897\H,-0.4353174647,-1.4855481468,1.2045372377\O,-0.872



3929573,-1.0177459109,1.9570246083\H,-0.7655204961,-1.5839535849,2.726  
3989627\H,2.1451140356,2.2179801065,-0.8778411466\H,3.0522181598,0.831  
5813305,-0.2114095995\H,1.7891498996,2.4797531534,1.5585665255\H,1.577  
3781862,0.7239576414,1.7409839333\\Version=EM64L-G09RevB.01\State=1-A\  
HF=-594.0787181\RMSD=3.484e-09\RMSF=1.469e-05\Dipole=-2.1606716,2.6939  
586,0.0128454\Quadrupole=-2.3277059,-3.5743637,5.9020696,7.4439646,3.0  
772953,-2.5352522\PG=C01 [X(C8H15N103)]\\@

## 6.H<sub>2</sub>O

1\1\GINC-R1I0N7\F0pt\RM062X\6-31+G(d,p)\C8H15N103\DI56F0V\05-May-2012\  
0\\#P M062X/6-31+G(d,p) opt scf=tight int=finergrid\\Im/Z/up/vorne\\0,1  
\C,-2.2681559948,0.5394170543,-0.4368372588\C,-0.8203591559,0.06545291  
77,-0.751380692\C,-1.8001479987,-1.4569023636,0.8113805593\C,-2.958882  
4014,-0.6915846132,0.1767790905\C,0.4474609513,-1.9530282653,-0.130313  
4933\N,-0.7442581816,-1.2542600299,-0.1685038853\O,0.2376873785,0.9696  
297441,1.1775714268\C,0.1764023409,1.0512236479,-0.1475486407\O,0.8056  
868971,1.8556734874,-0.8106481506\H,0.3900810314,-2.8734083631,0.44985  
26113\C,1.5918327905,-1.6263056691,-0.7529740721\C,2.8149183789,-2.497  
8559507,-0.715258409\H,3.6771614895,-1.9648830038,-0.2992549319\H,2.64  
38983144,-3.3866900109,-0.1000292288\H,3.1005857841,-2.8370416511,-1.7  
175170604\H,-1.5349080663,-1.035013376,1.7934247858\H,-2.0020565033,-2  
.5259401519,0.9289731079\H,-3.7333120322,-0.4164634404,0.8961851761\H,  
-3.4124756211,-1.304708579,-0.6074247554\H,-2.2412185504,1.3544937075,  
0.2922778874\H,-2.7698756281,0.9085106773,-1.3327360312\H,-0.606446905  
3,0.0297881708,-1.8258080254\H,0.8819512191,1.6374552562,1.5108922832\  
O,2.0066152856,3.0142826359,1.3832017878\H,1.93117983,2.9639849589,0.4  
147361592\H,1.6552560324,-0.7083017668,-1.3341641546\H,2.9407713157,3.  
0522239768,1.6087299144\\Version=EM64L-G09RevB.01\State=1-A\HF=-594.09  
09918\RMSD=7.293e-09\RMSF=7.278e-06\Dipole=-0.1363816,-0.2070669,0.350  
7044\Quadrupole=7.2447731,-3.4366658,-3.8081072,3.8171318,2.2020525,-0  
.6152042\PG=C01 [X(C8H15N103)]\\@

## Coordinates of stationary points at B97D/SVP level of theory.

In the following the coordinates for all stationary points at a B97D/SVP<sup>[37-39]</sup> level of theory are shown. Only the energetically best structures were chosen. **1**

1\1\GINC-R1I1N5\F0pt\RB97D\SVP\C5H9N102\DI56F0V\08-Oct-2012\0\\#P B97D  
/SVP opt scf=tight int=finergrid\\Prolin mit dipersions-Funktional\\0,  
1\O,-1.6549673581,-1.3356895288,-0.4209328767\H,-0.8624696128,-1.76757  
58478,0.0132053228\O,-2.1462146511,0.8569975333,-0.6305478385\H,1.2433  
75597,-1.062370291,-1.3399159127\H,0.2788685049,1.7652037255,-0.888434  
7145\H,2.5267372881,-1.5458249971,-0.1870566152\C,1.693991025,-0.83843  
95192,-0.3515804955\C,-0.1539990036,0.2332647507,0.6302140716\H,2.5778

064735,1.016144542,-1.1965951586\C,-1.4318809656,-0.0274743135,-0.2184  
359277\C,0.7472143348,1.3603387815,0.026477783\N,0.6481004183,-1.01441  
26209,0.6781280094\H,-0.5090436641,0.4869858691,1.646427268\C,2.092478  
6707,0.6498485827,-0.2730110476\H,0.870558338,2.2027661042,0.729138921  
6\H,2.8038930258,0.7960218359,0.5640075442\H,1.0809925791,-1.121754606  
7,1.5971906664\\Version=EM64L-G09RevC.01\State=1-A\HF=-400.6084758\RMS  
D=3.823e-09\RMSF=1.632e-05\Dipole=1.8909445,-0.3188187,0.91154\Quadrup  
ole=-3.9356271,0.3650365,3.5705906,0.4495259,-2.1076341,-0.1066345\PG=  
C01 [X(C5H9N102)]\\@

## 2

1\1\GINC-R1ION6\FOpt\RB97D\SVP\C3H6O1\DI56FOV\08-Oct-2012\0\\#P B97D/S  
VP opt scf=tight int=finegrid\\Propanal mit dipersions-Funktional\\0,  
1\C,-0.7846830103,-0.3531699024,-0.0000138858\C,0.4464481969,0.5512950  
142,-0.0000058141\H,0.3572083676,1.2196006468,0.8818698117\H,0.3572241  
882,1.2195895786,-0.8818918281\C,1.7768797198,-0.2114680179,0.00000835  
37\H,2.636748747,0.4834801249,0.000009081\H,1.8648104154,-0.8597231431  
,0.8939446798\H,1.8648218832,-0.8597354493,-0.8939179451\H,-0.55826823  
17,-1.4651716418,-0.0000271649\O,-1.9262552762,0.0477937898,0.00001971  
18\\Version=EM64L-G09RevC.01\State=1-A\HF=-192.8752412\RMSD=3.118e-09\  
RMSF=9.442e-06\Dipole=0.9862419,-0.0727133,-0.0000201\Quadrupole=-3.15  
03195,1.4695028,1.6808167,0.5831324,0.0000587,-0.0000075\PG=C01 [X(C3H  
6O1)]\\@

## 4

1\1\GINC-R1ION5\FOpt\RB97D\SVP\C8H13N102\DI56FOV\08-Oct-2012\0\\#P B97  
D/SVP opt scf=tight int=finegrid\\Iminium mit dipersions-Funktional\\  
0,1\C,2.1479410399,-0.8870368685,0.3185730872\C,1.0679146921,0.0479267  
381,0.8467666029\C,-0.0107957986,-1.6704774145,-0.4518270434\C,1.44940  
85249,-1.5009673702,-0.9104842746\H,3.0424364277,-0.3028789772,0.04728  
21689\H,2.4207655126,-1.665222891,1.0606865518\H,1.1574146146,0.351263  
7593,1.9035550624\H,-0.1906676149,-2.6567593067,0.0189969088\H,-0.7533  
503492,-1.5229143357,-1.2544023899\H,1.8855792355,-2.4586469059,-1.245  
1538746\H,1.4983521753,-0.7779690286,-1.7445216876\C,-1.3305293006,-0.  
1688446035,1.0199447688\N,-0.1802890409,-0.6273085894,0.5969620682\O,-  
0.1410916754,2.0490052306,0.0549268747\C,0.9924024,1.5491673641,-0.002  
5609801\O,2.0838527242,1.8628949963,-0.4757192169\H,-1.2767795083,0.63  
36279681,1.7631639989\C,-2.6530787674,-0.5864442646,0.4628403376\H,-3.  
4131116489,-0.5233189847,1.2646866902\C,-3.0615234681,0.3423906026,-0.  
7108066512\H,-4.0629251058,0.0612818039,-1.0879149493\H,-3.0751017675,  
1.3973579989,-0.3856400227\H,-2.3307113818,0.2704898551,-1.5368558809\  
H,-2.6214719195,-1.6389667764,0.1216148507\\Version=EM64L-G09RevC.01\  
State=1-A\HF=-517.1445026\RMSD=2.222e-09\RMSF=1.212e-05\Dipole=-1.46788  
95,-2.6237355,0.6212794\Quadrupole=1.6426587,-5.2134962,3.5708375,-4.2  
032146,1.1501633,2.9931187\PG=C01 [X(C8H13N102)]\\@

## 5a

1\1\GINC-R1ION6\F0pt\RB97D\SVP\C8H13N102\DI56FOV\08-Oct-2012\0\#\#P B97  
 D/SVP opt scf=tight int=finegrid\0xazolidinon 5a mit dipersions-Funk  
 tional\0,1\C,2.5066676183,-0.1275401302,0.1496570355\C,1.1682596213,0  
 .3656529701,0.7498747709\C,0.6578807676,-1.5332650089,-0.5336393641\C,  
 2.180009916,-1.5616380277,-0.342040814\H,2.8072252183,0.5381012516,-0.  
 6799850288\H,3.3198570168,-0.1176084566,0.8954811678\H,1.26314542,0.70  
 36671032,1.8029401137\H,0.1910998185,-2.534925598,-0.5345340167\H,0.40  
 75552282,-1.0337106692,-1.499462266\H,2.437151708,-2.300228679,0.43994  
 29811\H,2.7157070552,-1.8349504147,-1.2687438684\C,-1.0708678021,-0.08  
 3681357,0.5372995756\H,-1.391501861,0.2222862839,1.5559542062\N,0.2063  
 073506,-0.7472015854,0.6344786606\O,-0.8248559882,1.1882446123,-0.1883  
 767873\C,0.4897354665,1.5092452656,-0.0474430942\O,0.9922558235,2.5087  
 731985,-0.4962575957\C,-2.184370143,-0.8554644112,-0.1535781957\H,-1.8  
 876023263,-1.0387638823,-1.2033389844\C,-3.5305870206,-0.1210723952,-0  
 .0985414995\H,-3.4518091757,0.8654166646,-0.5908582412\H,-4.3201400204  
 ,-0.7049445859,-0.6070232889\H,-3.8474922287,0.045013716,0.9497155062\H,  
 -2.2514024627,-1.8415048646,0.3465910275\Version=EM64L-G09RevC.01\State=1-A\HF=-517.1641089\RMSD=7.389e-09\RMSF=1.564e-05\Dipole=-0.18015  
 92,-1.3968211,0.3513343\Quadrupole=4.008729,-5.6594906,1.6507616,-1.33  
 90576,0.1889848,3.6684171\PG=C01 [X(C8H13N102)]\@

## 5b

1\1\GINC-R1I1N5\F0pt\RB97D\SVP\C8H13N102\DI56FOV\08-Oct-2012\0\#\#P B97  
 D/SVP opt scf=tight int=finegrid\0xazolidinon 5b mit dipersions-Funk  
 tional\0,1\C,2.1333583652,-0.6189013585,0.7697051162\C,0.7825964206,0  
 .1184217273,0.8652703795\C,0.497713082,-1.8495208671,-0.4720088148\C,1  
 .9761675944,-1.4153946157,-0.5390777321\H,2.9720276469,0.099650603,0.7  
 664013227\H,2.252535812,-1.3007261893,1.6329744863\H,0.526363871,0.386  
 9320635,1.9102013676\H,0.4004372217,-2.7829886576,0.1205607864\H,0.047  
 8094023,-2.0397222852,-1.4649404843\H,2.6755782702,-2.2672271154,-0.62  
 24158102\H,2.1395345124,-0.7464400694,-1.4066486045\C,-1.0546474636,0.  
 127406792,-0.5718053386\N,-0.2174748517,-0.7517723305,0.2207118167\O,-  
 0.2648697205,1.3289750003,-0.8643189208\C,0.7735996361,1.404995644,0.0  
 094061703\O,1.55114459,2.3247280782,0.0519398419\H,-1.3015507421,-0.34  
 1268999,-1.5440123163\C,-2.3345114519,0.5569050716,0.1528491166\H,-2.8  
 282196673,1.3399602265,-0.4546192999\C,-3.274168536,-0.6294487942,0.39  
 69602585\H,-4.1816628132,-0.3138034014,0.9446557702\H,-3.5960972789,-1  
 .0851983377,-0.5607628463\H,-2.7554805555,-1.40744528,0.9877773868\H,-  
 2.0423013439,1.0261690948,1.1134753481\Version=EM64L-G09RevC.01\State  
 =1-A\HF=-517.1665685\RMSD=8.062e-09\RMSF=5.011e-05\Dipole=-0.4545674,-  
 1.3751693,0.1026716\Quadrupole=2.1546918,-4.5682692,2.4135774,-4.94913  
 43,0.7856462,2.1148276\PG=C01 [X(C8H13N102)]\@

## 6

1\1\GINC-R1ION5\F0pt\RB97D\SVP\C8H13N102\DI56FOV\08-Oct-2012\0\#\#P B97  
 D/SVP opt scf=tight int=finegrid\Enamin mit dipersions-Funktional\0

,1\C,-0.6324357237,0.1977113149,-0.6238533753\C,-1.9620884315,-0.52753  
11542,-0.9593793985\C,-2.1008716196,-1.5490970945,0.1847455992\C,-0.65  
14114842,-2.017135573,0.3696257014\N,0.1156741798,-0.7739794059,0.1889  
474481\C,1.5151814887,-0.8051884803,0.1602721915\H,1.9413033188,-1.710  
3908437,0.6188573833\C,-0.8882154564,1.5192732341,0.149419419\O,-1.367  
3071304,2.4968992912,-0.3743032459\C,2.3355693185,0.1617128575,-0.3130  
834333\C,3.8373987344,0.074803103,-0.2536823116\O,-0.5752814366,1.4571  
659395,1.4587320793\H,-0.0804003561,0.468714231,-1.545441207\H,-2.8048  
938205,0.1796752659,-1.046183308\H,-1.853618443,-1.0551321696,-1.92567  
5423\H,-2.455709726,-1.0463076374,1.1052634801\H,-2.7908459257,-2.3794  
804705,-0.0483255815\H,-0.4493245141,-2.4588246888,1.3646056569\H,-0.3  
820695992,-2.7730719063,-0.4030788036\H,1.9028823499,1.0749891409,-0.7  
469758967\H,-0.1923339854,0.5542007448,1.5782399791\H,4.1693603237,-0.  
8788833357,0.2010863836\H,4.2924510588,0.1453960811,-1.2642392475\H,4.  
2716178798,0.904999556,0.3430269105\\Version=EM64L-G09RevC.01\State=1-  
A\HF=-517.1579615\RMSD=5.297e-09\RMSF=5.102e-06\Dipole=0.2530824,-1.89  
81339,-0.0387875\Quadrupole=2.928008,-4.3438316,1.4158236,5.1749786,0.  
3292868,-1.3984746\PG=C01 [X(C8H13N1O2)]\\@

**Tab. 4.4:** Gas phase energies (in Hartree) for all systems obtained at B98/6-31G(d)<sup>[22]</sup> level of theory.

Species	Denomination	$E_{tot}$	$H_{298}$	$G_{298}$
1	c	-401.004097	-400.850111	-400.890344
	a	-401.003156	-400.848983	-400.889842
	b	-400.997557	-400.843794	-400.886040
	d	-400.997557	-400.843794	-400.886037
	f	-400.997306	-400.843290	-400.884701
	e	-400.997306	-400.843291	-400.884700
	g	-400.987754	-400.834354	-400.876092
	h	-400.986031	-400.832483	-400.874192
2		-193.064875	-192.975256	-193.007178
3		-76.381258	-76.356089	-76.378182
4	E	a	No minimum	
		b		
	Z	a	-517.648782	-517.430641
		b	-517.651114	-517.432896
5a	c	-517.687761	-517.468004	-517.514448
	d	-517.687246	-517.467438	-517.513706
	e	-517.686014	-517.466391	-517.513112
	f	-517.683149	-517.463158	-517.509493
	g	-517.682141	-517.462223	-517.508323
5b	c	-517.689567	-517.469954	-517.516639
	a	-517.689140	-517.469666	-517.516467
	d	-517.689140	-517.469666	-517.516464
	f	-517.688884	-517.469274	-517.516112
	e	-517.688333	-517.468796	-517.515836
	g	-517.687498	-517.467801	-517.514705
6	f	-517.665926	-517.447476	-517.499714
	e	-517.666303	-517.447806	-517.498886
	c	-517.667901	-517.449271	-517.498571
	b	-517.667901	-517.449273	-517.498571
	a	-517.667157	-517.448584	-517.498243
	g	-517.665713	-517.447142	-517.498162
	l	-517.664966	-517.446346	-517.497971
	d	-517.665717	-517.447137	-517.497966
	h	-517.664633	-517.446245	-517.497820
	j	-517.665092	-517.446508	-517.497143
	k	-517.665049	-517.446404	-517.497068
	m	-517.665387	-517.446642	-517.496324
	i	-517.665549	-517.446765	-517.496239
	n	-517.656285	-517.438065	-517.489615
	o	-517.656508	-517.438388	-517.489566
	q	-517.655419	-517.437112	-517.488490
	p	-517.655193	-517.437070	-517.488312

**Tab. 4.5:** Gas phase energies (in Hartree) for all systems obtained at B3LYP/6-31+G(d,p)<sup>[23]</sup> level of theory.

Species	Denomination	$E_{tot}$	$H_{298}$	$G_{298}$
1	c	-401.192152	-401.038872	-401.079173
	h	-401.191404	-401.038069	-401.078960
	a	-401.191404	-401.038069	-401.078959
	d	-401.186446	-401.033500	-401.075867
	f	-401.185797	-401.032673	-401.074380
	b	-401.185158	-401.032154	-401.073941
	e	-401.185235	-401.032078	-401.073799
	g	-401.176754	-401.024122	-401.065868
2		-193.161069	-193.071947	-193.103848
3		-76.434048	-76.408981	-76.431064
4	E	a	No minimum	
		b	-517.895071	-517.727852
	Z	a	-517.891246	-517.725302
		b	-517.893170	-517.726211
5a	d	-517.919987	-517.701332	-517.747793
	e	-517.918863	-517.700358	-517.747014
	f	-517.915707	-517.696901	-517.743490
	g	-517.914351	-517.695669	-517.741972
	c	-517.920691	-517.470891	-517.516656
5b	a	-517.921655	-517.703400	-517.750370
	d	-517.921655	-517.703400	-517.750370
	c	-517.921890	-517.703492	-517.750317
	f	-517.920287	-517.703267	-517.750302
	e	-517.920563	-517.702163	-517.748921
	g	-517.921691	-517.701765	-517.748813
6	e	-517.910655	-517.693349	-517.744943
	g	-517.910445	-517.693020	-517.744544
	c	-517.912568	-517.694953	-517.744246
	b	-517.912568	-517.694952	-517.744238
	f	-517.910221	-517.692891	-517.744081
	h	-517.909292	-517.692013	-517.744010
	a	-517.911946	-517.694372	-517.743850
	d	-517.910172	-517.692760	-517.743724
	l	-517.909591	-517.692147	-517.743466
	k	-517.909289	-517.691912	-517.743268
	m	-517.909913	-517.692370	-517.742315
	i	-517.910278	-517.692694	-517.742215
	o	-517.901235	-517.684253	-517.736031
	n	-517.901130	-517.684063	-517.735033
	p	-517.900194	-517.683182	-517.734731
	q	-517.900238	-517.683177	-517.734392
	j	-517.909502	-517.692117	-517.743521

**Tab. 4.6:** Gas phase energies (in Hartree) for all systems obtained at mPW1K/6-31+G(d)<sup>[24]</sup> level of theory.

Species	Denomination	$E_{tot}$	$H_{298}$	$G_{298}$
1	a	-401.054837	-400.896072	-400.936580
	c	-401.049601	-400.891323	-400.932994
	b	-401.049601	-400.891323	-400.932994
	e	-401.048181	-400.889702	-400.931300
	d	-401.047399	-400.889231	-400.930861
	f	-401.047416	-400.888921	-400.930670
	g	-401.039511	-400.881432	-400.922723
	h	-401.036664	-400.878531	-400.920165
2		-193.088656	-192.996536	-193.028271
3		-76.391533	-76.365725	-76.387782
4	E	a	No minimum	
		b		
	Z	a	-517.718586	-517.493977
		b	-517.720802	-517.496185
5a	c	-517.763053	-517.536763	-517.582703
	d	-517.762498	-517.536165	-517.581902
	e	-517.761084	-517.534905	-517.580972
	f	-517.758068	-517.531520	-517.577238
	g	-517.756788	-517.530417	-517.576038
5b	b	-517.764141	-517.538069	-517.584262
	a	-517.763807	-517.537839	-517.584156
	d	-517.763807	-517.537841	-517.584154
	f	-517.763847	-517.537726	-517.584145
	e	-517.763017	-517.536912	-517.582966
	g	-517.762655	-517.536409	-517.582704
6	e	-517.738045	-517.513460	-517.564575
	c	-517.740773	-517.515779	-517.564450
	b	-517.740773	-517.515783	-517.564439
	g	-517.737958	-517.513216	-517.564173
	a	-517.740233	-517.515268	-517.564136
	f	-517.737676	-517.513036	-517.563876
	d	-517.737867	-517.513130	-517.563562
	j	-517.737175	-517.512499	-517.563257
	h	-517.736643	-517.512083	-517.562884
	l	-517.736887	-517.512164	-517.562874
	k	-517.736524	-517.511851	-517.562568
	i	-517.738515	-517.513533	-517.562403
	m	-517.737885	-517.512964	-517.562216
	o	-517.728034	-517.503699	-517.554721
	n	-517.727883	-517.503494	-517.554115
	p	-517.726794	-517.502476	-517.553337
	q	-517.726711	-517.502338	-517.553015

**Tab. 4.7:** Gas phase energies (in Hartree) for all systems obtained at M062X/6-31+G(d,p)<sup>[25]</sup> level of theory.

Species	Denomination	$E_{tot}$	$H_{298}$	$G_{298}$
1	a	-401.013664	-400.858798	-400.899940
	b	-401.008508	-400.853783	-400.895155
	c	-401.008508	-400.853783	-400.895155
	d	-401.007545	-400.853088	-400.894528
	e	-401.008524	-400.853625	-400.894434
	f	-401.007881	-400.853021	-400.894084
	g	-400.997457	-400.843298	-400.884968
	h	-400.997750	-400.843223	-400.884659
2		-193.058440	-192.968452	-193.000325
3		-76.394964	-76.369549	-76.391621
4	E	a	No minimum	
		b	-517.655459	-517.435864
	Z	a	-517.651182	-517.431829
		b	-517.653780	-517.434690
5a	c	-517.691822	-517.471045	-517.517301
	d	-517.691780	-517.470891	-517.516656
	e	-517.689762	-517.468968	-517.515219
	f	-517.687722	-517.466605	-517.512349
	g	-517.686693	-517.465720	-517.511514
5b	b	-517.692448	-517.471896	-517.518616
	d	-517.692102	-517.471431	-517.517967
	e	-517.692465	-517.471813	-517.517707
	f	-517.692084	-517.471271	-517.517663
	g	-517.691885	-517.470927	-517.516785
6	a	-517.677913	-517.458009	-517.507202
	b	-517.677986	-517.458157	-517.507195
	c	-517.677986	-517.458158	-517.507194
	d	-517.676248	-517.456637	-517.507003
	e	-517.676323	-517.456739	-517.506855
	f	-517.676306	-517.456633	-517.506597
	g	-517.676463	-517.456822	-517.506510
	h	-517.674084	-517.454579	-517.506234
	i	-517.676484	-517.456780	-517.506033
	j	-517.675923	-517.456206	-517.505951
	k	-517.675103	-517.455406	-517.505887
	l	-517.673075	-517.453531	-517.505146
	m	-517.675135	-517.455394	-517.505071
	n	-517.666860	-517.447581	-517.498358
	o	-517.666786	-517.447468	-517.497831
	p	-517.664608	-517.445468	-517.497005
	q	-517.665565	-517.446188	-517.496629



**Tab. 4.8:** Gas phase energies (in Hartree) for all systems obtained at MP2(FC)/6-31+G(d)<sup>[26–30]</sup> level of theory.

Species	Denomination		$E_{tot}$	$H_{298}$	$G_{298}$
1		a	-399.952796	-399.797050	-399.837577
		f	-399.946469	-399.791066	-399.833301
		d	-399.945967	-399.790802	-399.833136
		e	-399.947045	-399.791624	-399.832767
		b	-399.946934	-399.791639	-399.832720
		c	-399.946934	-399.791639	-399.832720
		g	-399.934869	-399.780076	-399.822342
		h	-399.935265	-399.780218	-399.821847
2			-192.523231	-192.432182	-192.463930
3			-76.209777	-76.184759	-76.206859
4	E	a	No minimum		
		b	-516.247705	-516.026110	-516.075600
	Z	a	-516.243970	-516.022768	-516.072864
		b	-516.246382	-516.025144	-516.074772
5a	c	-516.280905	-516.058216	-516.104111	
	d	-516.280596	-516.057867	-516.103609	
	e	-516.278244	-516.055668	-516.101881	
	f	-516.276094	-516.053209	-516.099079	
5b	d	-516.280896	-516.058514	-516.104810	
	a	-516.280896	-516.058515	-516.104809	
	e	-516.280885	-516.058360	-516.104211	
	c	-516.281213	-516.059784	-516.058840	
6	a	-516.262379	-516.041500	-516.090634	
	c	-516.262080	-516.041284	-516.090502	
	b	-516.262080	-516.041284	-516.090500	
	i	-516.260753	-516.039890	-516.089001	
	d	-516.259105	-516.038463	-516.088950	
	h	-516.259523	-516.038734	-516.088922	
	e	-516.258118	-516.037736	-516.088850	
	f	-516.258906	-516.038358	-516.088821	
	j	-516.258287	-516.037667	-516.088048	
	g	-516.258215	-516.037583	-516.087927	
	k	-516.257771	-516.037223	-516.087855	
	m	-516.258967	-516.038176	-516.087778	
	l	-516.256779	-516.036176	-516.087287	
	n	-516.248813	-516.028556	-516.079062	
	o	-516.247738	-516.027626	-516.078915	
	p	-516.247427	-516.027102	-516.078421	
	q	-516.247669	-516.027430	-516.078152	

**Tab. 4.9:** Gas phase energies (in Hartree) for all systems obtained at MP2(FC)/6-31G(d)<sup>[26–30]</sup> level of theory.

Species	Denomination	$E_{tot}$	$H_{298}$	$G_{298}$
1	a	-399.924497	-399.769631	-399.810773
	b	-399.918780	-399.764056	-399.805428
	c	-399.918780	-399.764056	-399.805428
	f	-399.918917	-399.764056	-399.805119
	d	-399.918066	-399.763609	-399.805049
	e	-399.919083	-399.764184	-399.804993
	h	-399.907487	-399.752960	-399.794396
	g	-399.906452	-399.752293	-399.793963
2		-192.510257	-192.420269	-192.452142
3		-76.196657	-76.171242	-76.193314
4	E	a	No minimum	
		b	-516.210087	-515.990492
	Z	a	-516.208099	-515.988746
		b	-516.204664	-515.985574
5a	c	-516.250087	-516.029294	-516.075545
	d	-516.249832	-516.028943	-516.074708
	b	-516.249832	-516.028943	-516.074708
	a	-516.247413	-516.026296	-516.072040
	e	-516.247411	-516.026438	-516.072232
	f	-516.245355	-516.024578	-516.070834
	g	-516.243319	-516.022526	-516.068777
5b	c	-516.251166	-516.030495	-516.077031
	b	-516.251166	-516.030614	-516.077334
	d	-516.250633	-516.030081	-516.076801
	a	-516.250631	-516.029959	-516.076495
	f	-516.250766	-516.029953	-516.076345
	e	-516.250410	-516.029758	-516.075652
	g	-516.249644	-516.028686	-516.074544
6	e	-516.226016	-516.006432	-516.056548
	b	-516.227215	-516.007385	-516.056423
	c	-516.227214	-516.007386	-516.056422
	f	-516.226092	-516.006418	-516.056382
	a	-516.226781	-516.006877	-516.056070
	g	-516.226015	-516.006373	-516.056061
	d	-516.225229	-516.005618	-516.055984
	k	-516.225010	-516.005313	-516.055794
	h	-516.223396	-516.003891	-516.055546
	j	-516.225023	-516.005306	-516.055051
	l	-516.222701	-516.003157	-516.054772
	i	-516.225213	-516.005509	-516.054762
	m	-516.224210	-516.004470	-516.054147
	n	-516.215223	-515.995944	-516.046721
	o	-516.215166	-515.995848	-516.046211

**Tab. 4.10:** Gas phase energies (in Hartree) for all systems obtained at QCISD(T)/6-31G(d)<sup>[31–33]</sup> level of theory.

Species	Denomination	$E_{tot}$	$H_{298}$	$G_{298}$
1	a	-400.017918	-399.863051	-399.904193
	e	-400.012901	-399.858176	-399.899548
	c	-400.012422	-399.857698	-399.899070
	b	-400.012422	-399.857698	-399.899070
	f	-400.012706	-399.857845	-399.898908
	d	-400.011545	-399.856820	-399.898192
	h	-400.001523	-399.846996	-399.888432
	g	-400.000148	-399.845989	-399.887659
2		-192.565649	-192.475661	-192.507534
3		-76.207644	-76.182229	-76.204301
4	E	b	-516.347068	-516.126295
		a	No minimums	
	Z	b	-516.345052	-516.125700
		a	-516.341731	-516.122641
5a	c	-516.385204	-516.164410	-516.210661
	d	-516.384892	-516.164003	-516.209768
	b	-516.384892	-516.164003	-516.209768
	a	-516.382473	-516.161356	-516.207100
	e	-516.382471	-516.161497	-516.207291
	f	-516.380550	-516.159773	-516.206029
	g	-516.378425	-516.157631	-516.203882
5b	c	-516.386117	-516.165446	-516.211982
	b	-516.386117	-516.165565	-516.212285
	f	-516.385931	-516.165379	-516.212099
	d	-516.385634	-516.164963	-516.211499
	a	-516.385632	-516.164819	-516.211211
	e	-516.385317	-516.164666	-516.210560
	g	-516.384755	-516.163797	-516.209655
6	e	-516.361856	-516.142272	-516.192388
	b	-516.363109	-516.143279	-516.192317
	c	-516.363108	-516.143280	-516.192316
	f	-516.361940	-516.142267	-516.192231
	g	-516.362176	-516.142535	-516.192223
	a	-516.362727	-516.142823	-516.192016
	d	-516.361043	-516.141432	-516.191798
	k	-516.360885	-516.141188	-516.191669
	h	-516.359395	-516.139890	-516.191545
	l	-516.358829	-516.139285	-516.190900
	j	-516.360778	-516.141061	-516.190806
	i	-516.361142	-516.141438	-516.190691
	q	-516.350063	-516.130686	-516.181127
	p	-516.348517	-516.129377	-516.180914
	m	-516.306432	-516.086691	-516.136368
	n	-516.297480	-516.078201	-516.128978

**Tab. 4.11:** Gas phase energies (in Hartree) for all systems obtained at MP2(FC)/GTMP2Large<sup>[26–30]</sup> level of theory.

Species	Denomination	$E_{tot}$	$H_{298}$	$G_{298}$
1	a	-400.396262	-400.241395	-400.282537
	b	-400.390580	-400.235855	-400.277227
	c	-400.390580	-400.235855	-400.277227
	d	-400.390212	-400.235754	-400.277194
	f	-400.390347	-400.235487	-400.276550
	e	-400.390571	-400.235672	-400.276481
	g	-400.381360	-400.227201	-400.268871
	h	-400.381391	-400.226864	-400.268300
2		-192.745832	-192.655844	-192.687717
3		-76.314825	-76.289410	-76.311482
4	E	a	No minimum	
		b	-516.812746	-516.593151
	Z	b	-516.811040	-516.591687
		a	-516.807913	-516.588823
5a	c	-516.848456	-516.627663	-516.673914
	d	-516.848483	-516.627594	-516.673359
	b	-516.848483	-516.627594	-516.673359
	a	-516.846101	-516.624985	-516.670729
	e	-516.846101	-516.625127	-516.670921
	f	-516.843977	-516.623201	-516.669457
	g	-516.842415	-516.621621	-516.667872
5b	c	-516.849038	-516.628367	-516.674903
	b	-516.849038	-516.628486	-516.675206
	d	-516.848531	-516.627979	-516.674699
	a	-516.848528	-516.627857	-516.674393
	f	-516.848593	-516.627780	-516.674172
	e	-516.848919	-516.628267	-516.674161
	g	-516.848274	-516.627316	-516.673174
6	a	-516.835002	-516.615098	-516.664291
	b	-516.834826	-516.614997	-516.664035
	c	-516.834826	-516.614997	-516.664033
	e	-516.832993	-516.613409	-516.663525
	f	-516.833014	-516.613341	-516.663305
	d	-516.832443	-516.612832	-516.663198
	i	-516.833642	-516.613938	-516.663191
	h	-516.830604	-516.611099	-516.662754
	k	-516.831870	-516.612173	-516.662654
	j	-516.832244	-516.612526	-516.662271
	g	-516.832125	-516.612484	-516.662172
	m	-516.832123	-516.612382	-516.662059
	l	-516.828777	-516.609232	-516.660847
	n	-516.824739	-516.605460	-516.656237
	o	-516.824640	-516.605322	-516.655685
	p	-516.822203	-516.603064	-516.654601

**Tab. 4.12:** Gas phase energies (in Hartree) for all systems obtained at G3(MP2)M06<sup>[34,35]</sup> level of theory.

Species	Denomination		$E_{tot}$	$H_{298}$	$G_{298}$
1	a		-400.489682	-400.334816	-400.375958
	b		-400.484222	-400.329497	-400.370869
	c		-400.484222	-400.329497	-400.370869
	d		-400.483690	-400.329233	-400.370673
	f		-400.484136	-400.329276	-400.370339
	e		-400.484388	-400.329489	-400.370298
	g		-400.475056	-400.320897	-400.362567
	h		-400.475427	-400.320900	-400.362336
2			-192.801224	-192.711236	-192.743109
3			-76.325812	-76.300397	-76.322469
4	E	b	-516.949728	-516.730133	-516.779345
		a		No minimum	
	Z	b	-516.947994	-516.728904	-516.778284
		a	-516.944980	-516.725627	-516.775333
5a	c		-516.983573	-516.762796	-516.809052
	d		-516.983543	-516.762654	-516.808419
	b		-516.983543	-516.762654	-516.808419
	a		-516.981161	-516.760368	-516.806619
	e		-516.981160	-516.760366	-516.806617
	f		-516.979173	-516.758056	-516.803800
	g		-516.977521	-516.756548	-516.802342
5b	c		-516.983989	-516.763437	-516.810157
	b		-516.983989	-516.763437	-516.810157
	d		-516.983532	-516.762861	-516.809397
	a		-516.983530	-516.762858	-516.809394
	f		-516.983758	-516.762945	-516.809337
	e		-516.983827	-516.763175	-516.809069
	g		-516.983385	-516.762427	-516.808285
6	a		-516.970948	-516.751044	-516.800237
	b		-516.970720	-516.750891	-516.799929
	c		-516.970720	-516.750892	-516.799928
	e		-516.968833	-516.749249	-516.799365
	f		-516.968863	-516.749190	-516.799154
	i		-516.969571	-516.749867	-516.799120
	d		-516.968257	-516.748646	-516.799012
	h		-516.966603	-516.747098	-516.798753
	k		-516.967744	-516.748047	-516.798528
	g		-516.968287	-516.748645	-516.798333
	j		-516.967998	-516.748281	-516.798026
	l		-516.964904	-516.745360	-516.796975
	p		-516.958379	-516.739239	-516.790776
	q		-516.959568	-516.740191	-516.790632
	m		-516.914344	-516.694604	-516.744281
	n		-516.906996	-516.687717	-516.738494

**Tab. 4.13:** Solution phase (solvent=DMSO,  $\epsilon=46.7$ ) energies (in Hartree) for all systems obtained at mPW1K/6-31+G(d)/SMD<sup>[24,36]</sup> level of theory.

Species	Denomination		$E_{tot}$	$H_{298}$	$G_{298}$
1	a		-401.074847	-400.916840	-400.957168
	e		-401.065489	-400.907555	-400.948583
	c		-401.064435	-400.906684	-400.948488
	g		-401.063900	-400.906108	-400.948009
	f		-401.064876	-400.906859	-400.947613
	h		-401.061417	-400.903504	-400.944745
	b		-401.061417	-400.903504	-400.944745
	d		-401.060351	-400.902653	-400.943812
2			-193.097713	-193.005781	-193.037408
3			-76.400472	-76.374997	-76.397069
4	E	a	-517.758956	-517.534192	-517.583130
		b	-517.764980	-517.540028	-517.589140
	Z	a	-517.764199	-517.539135	-517.588430
		b	-517.764132	-517.539281	-517.588871
5a	c		-517.780316	-517.554555	-517.600187
	d		-517.780195	-517.554311	-517.599693
	a		-517.777976	-517.552292	-517.598215
	f		-517.775268	-517.549291	-517.594844
	g		-517.773357	-517.547581	-517.593393
5b	f		-517.781297	-517.555771	-517.602345
	a		-517.780920	-517.555631	-517.602316
	b		-517.781472	-517.555889	-517.601833
	e		-517.780255	-517.554690	-517.600490
	g		-517.780369	-517.554443	-517.599793
6	b		-517.760046	-517.535919	-517.584630
	c		-517.760046	-517.535918	-517.584626
	a		-517.759675	-517.535444	-517.584136
	e		-517.755248	-517.531592	-517.582376
	m		-517.757110	-517.532997	-517.582351
	i		-517.758233	-517.533844	-517.582283
	g		-517.754503	-517.530700	-517.581820
	h		-517.754277	-517.530344	-517.580834
	f		-517.754768	-517.530951	-517.580574
	d		-517.754333	-517.530330	-517.580236
	k		-517.754264	-517.530273	-517.580084
	l		-517.753694	-517.529692	-517.579873
	j		-517.754016	-517.530062	-517.579694
	o		-517.751286	-517.527640	-517.578285
	p		-517.750318	-517.526431	-517.576470
	n		-517.750776	-517.526940	-517.576363
	q		-517.750277	-517.526386	-517.576042

**Tab. 4.14:** Solution phase (solvent=DMSO,  $\epsilon=46.7$ ) energies (in Hartree) for all systems obtained at M062X/6-31+G(d,p)/SMD<sup>[25,36]</sup> level of theory.

Species	Denomination		$E_{tot}$	$H_{298}$	$G_{298}$
1	a		-401.033188	-400.879210	-400.919879
	f		-401.025350	-400.871094	-400.911694
	e		-401.024776	-400.870331	-400.911044
	d		-401.024116	-400.869905	-400.910925
	b		-401.023574	-400.869295	-400.910086
	h		-401.021472	-400.867161	-400.907887
	g		-401.020164	-400.866044	-400.907227
	c		-401.020164	-400.866044	-400.907227
2			-193.067155	-192.977363	-193.009135
3			-76.403657	-76.378589	-76.400676
4	E	a	-517.694997	-517.475127	-517.524183
		b	-517.696056	-517.476355	-517.525975
	Z	a	-517.695658	-517.476077	-517.525106
		b	-517.695749	-517.475956	-517.525205
5a	c		-517.708823	-517.488594	-517.534781
	d		-517.709290	-517.488803	-517.534222
	a		-517.706443	-517.486085	-517.532270
	f		-517.704657	-517.484274	-517.530310
	g		-517.703100	-517.482867	-517.529351
5b	c		-517.709551	-517.489522	-517.536087
	a		-517.709054	-517.488983	-517.535755
	f		-517.709320	-517.489086	-517.535610
	e		-517.709579	-517.489516	-517.535480
	g		-517.709481	-517.489014	-517.534452
6	a		-517.696760	-517.477853	-517.527592
	c		-517.696679	-517.477812	-517.527020
	b		-517.696679	-517.477811	-517.527011
	i		-517.695626	-517.476400	-517.524908
	m		-517.693754	-517.474638	-517.524159
	f		-517.692348	-517.473518	-517.524158
	e		-517.692670	-517.473993	-517.523905
	d		-517.691907	-517.473159	-517.523800
	g		-517.692085	-517.473239	-517.523079
	k		-517.691890	-517.472990	-517.522726
	j		-517.691550	-517.472802	-517.522604
	h		-517.691387	-517.472630	-517.522478
	l		-517.691027	-517.472223	-517.522093
	n		-517.688508	-517.469739	-517.520293
	o		-517.688901	-517.470141	-517.520079
	q		-517.688105	-517.469166	-517.518876
	p		-517.687533	-517.468803	-517.518798





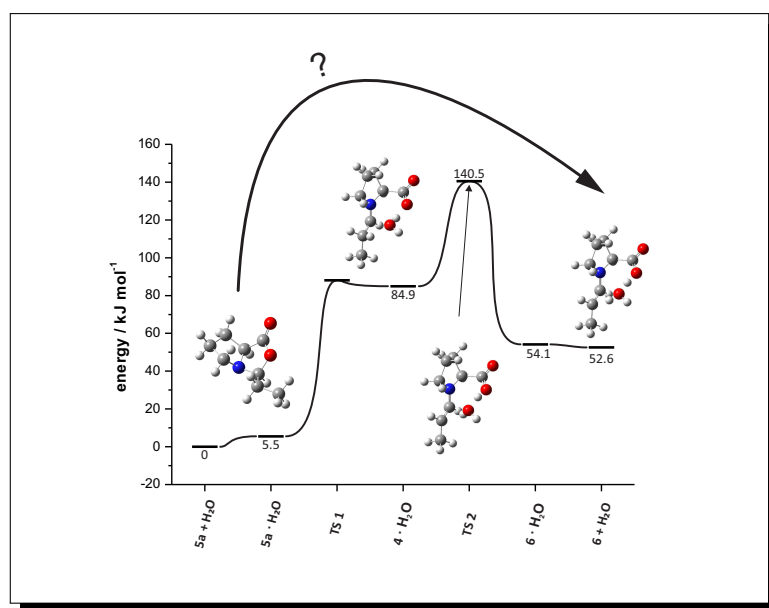
## 4.3 References

- [1] M. C. Holland, R. Gilmour, *Angew. Chem. Int. Ed.* **2015**, *54*, 3862–3871.
- [2] M. B. Schmid, K. Zeitler, R. M. Gschwind, *Angew. Chem. Int. Ed.* **2010**, *49*, 4997–5003.
- [3] M. B. Schmid, K. Zeitler, R. M. Gschwind, *J. Am. Chem. Soc.* **2011**, *133*, 7065–7074.
- [4] M. B. Schmid, K. Zeitler, R. M. Gschwind, *J. Org. Chem.* **2011**, *76*, 3005–3015.
- [5] M. B. Schmid, K. Zeitler, R. M. Gschwind, *Chem. Sci.* **2011**, *2*, 1793–1803.
- [6] M. H. Haindl, M. B. Schmid, K. Zeitler, R. M. Gschwind, *RSC Advances* **2012**, *2*, 5941–5943.
- [7] M. B. Schmid, K. Zeitler, R. M. Gschwind, *Chem. - A Eur. J.* **2012**, *18*, 3362–3370.
- [8] J. E. Hein, J. Burés, Y. Lam, M. Hughes, K. N. Houk, A. Armstrong, D. G. Blackmond, *Org. Lett.* **2011**, *13*, 5644–5647.
- [9] C. Allemann, R. Gordillo, F. R. Clemente, P. H.-Y. Cheong, K. N. Houk, *Acc. Chem. Res.* **2004**, *37*, 558–569.
- [10] A. K. Sharma, R. B. Sunoj, *Angew. Chem.* **2010**, *122*, 6517–6521.
- [11] A. K. Sharma, R. B. Sunoj, *J. Org. Chem.* **2012**, *77*, 10516–10524.
- [12] A. Armstrong, R. A. Boto, P. Dingwall, J. Contreras-Garcia, M. J. Harvey, N. J. Mason, H. S. Rzepa, *Chem. Sci.* **2014**, *5*, 2057–2071.
- [13] U. Grošelj, D. Seebach, D. M. Badine, W. B. Schweizer, A. K. Beck, I. Krossing, P. Klose, Y. Hayashi, T. Uchamaru, *Helv. Chim. Acta* **2009**, *92*, 1225–1259.
- [14] D. Seebach, U. Grošelj, D. M. Badine, W. B. Schweizer, A. K. Beck, *Helv. Chim. Acta* **2008**, *91*, 1999–2034.
- [15] P. H.-Y. Cheong, C. Y. Legault, J. M. Um, N. Çelebi-Ölçüm, K. N. Houk, *Chem. Rev.* **2011**, *111*, 5042–5137.
- [16] A. K. Sharma, R. B. Sunoj, *Chem. Commun.* **2011**, *47*, 5759–5761.
- [17] A. Capobianco, A. Russo, A. Lattanzi, A. Peluso, *Advanced Synthesis & Catalysis* **2012**, *354*, 2789–2796.
- [18] G. Sahoo, H. Rahaman, Á. Madarász, I. Pápai, M. Melarto, A. Valkonen, P. M. Pihko, *Angew. Chem. Int. Ed.* **2012**, *51*, 13144–13148.
- [19] M. Arnó, R. J. Zaragozá, L. R. Domingo, *Tetrahedron: Asymmetry* **2005**, *16*, 2764–2770.
- [20] M. Arnó, R. J. Zaragozá, L. R. Domingo, *Tetrahedron: Asymmetry* **2007**, *18*, 157–164.

- [21] M. H. Haindl, J. Hioe, R. M. Gschwind, *J. Am. Chem. Soc.* **2015**, *submitted*.
- [22] H. L. Schmider, A. D. Becke, *J. Chem. Phys.* **1998**, *108*, 9624–9631.
- [23] A. D. Becke, *J. Chem. Phys.* **1993**, *98*, 1372–1377.
- [24] C. Adamo, V. Barone, *J. Chem. Phys.* **1998**, *108*, 664–675.
- [25] Y. Zhao, D. G. Truhlar, *Theor. Chem. Acc.* **2008**, *120*, 215–241.
- [26] M. Head-Gordon, J. A. Pople, M. J. Frisch, *Chem. Phys. Lett.* **1988**, *153*, 503–506.
- [27] M. Head-Gordon, T. Head-Gordon, *Chem. Phys. Lett.* **1994**, *220*, 122–128.
- [28] M. J. Frisch, M. Head-Gordon, J. A. Pople, *Chem. Phys. Lett.* **1990**, *166*, 275–280.
- [29] M. J. Frisch, M. Head-Gordon, J. A. Pople, *Chem. Phys. Lett.* **1990**, *166*, 281–289.
- [30] S. Sæbø, J. Almlöf, *Chem. Phys. Lett.* **1989**, *154*, 83–89.
- [31] J. A. Pople, M. Head-Gordon, K. Raghavachari, *J. Chem. Phys.* **1987**, *87*, 5968–5975.
- [32] J. Gauss, D. Cremer, *Chem. Phys. Lett.* **1988**, *150*, 280–286.
- [33] E. Salter, G. W. Trucks, R. J. Bartlett, *J. Chem. Phys.* **1989**, *90*, 1752–1766.
- [34] L. A. Curtiss, K. Raghavachari, P. C. Redfern, V. Rassolov, J. A. Pople, *J. Chem. Phys.* **1998**, *109*, 7764–7776.
- [35] A. G. Baboul, L. A. Curtiss, P. C. Redfern, K. Raghavachari, *J. Chem. Phys.* **1999**, *110*, 7650.
- [36] A. V. Marenich, C. J. Cramer, D. G. Truhlar, *J. Phys. Chem. B* **2009**, *113*, 6378–6396.
- [37] S. Grimme, *J. Comput. Chem.* **2006**, *27*, 1787–1799.
- [38] A. Schäfer, H. Horn, R. Ahlrichs, *J. Chem. Phys.* **1992**, *97*, 2571–2577.
- [39] A. Schäfer, C. Huber, R. Ahlrichs, *J. Chem. Phys.* **1994**, *100*, 5829–5835.
- [40] M. H. Abraham, J. A. Platts, *J. Org. Chem.* **2001**, *66*, 3484–3491.
- [41] C. M. Venkatachalam, B. J. Price, S. Krimm, *Macromolecules* **1974**, *7*, 212–220.
- [42] M. J. Frisch, G. W. Trucks, H. B. Schlegel, G. E. Scuseria, M. A. Robb, J. R. Cheeseman, G. Scalmani, V. Barone, B. Mennucci, G. A. Petersson, H. Nakatsuji, M. Caricato, X. Li, H. P. Hratchian, A. F. Izmaylov, J. Bloino, G. Zheng, J. L. Sonnenberg, M. Hada, M. Ehara, K. Toyota, R. Fukuda, J. Hasegawa, M. Ishida, T. Nakajima, Y. Honda, O. Kitao, H. Nakai, T. Vreven, J. A. Montgomery, Jr., J. E. Peralta, F. Ogliaro, M. Bearpark, J. J. Heyd, E. Brothers, K. N. Kudin, V. N. Staroverov, R. Kobayashi, J. Normand, K. Raghavachari, A. Rendell, J. C. Burant, S. S. Iyengar, J. Tomasi, M. Cossi, N. Rega, J. M. Millam, M. Klene, J. E. Knox, J. B. Cross, V. Bakken, C. Adamo, J. Jaramillo, R. Gomperts, R. E. Stratmann, O. Yazyev, A. J. Austin, R. Cammi, C. Pomelli, J. W. Ochterski, R. L. Martin, K. Morokuma, V. G. Zakrzewski, G. A. Voth, P. Salvador, J. J. Dannenberg, S. Dapprich, A. D. Daniels, J. Farkas, J. B. Foresman, J. V. Ortiz, J. Cioslowski, D. J. Fox, *Gaussian 09 Revision D.01*, Gaussian Inc. Wallingford CT 2009.
- [43] F. Jensen, *Introduction to computational chemistry*, John Wiley & Sons, **2013**.
- [44] K. K. Irikura, D. J. Frurip, *Computational thermochemistry*, **1998**.

## 5 The mechanism of enamine formation investigated by quantum chemical calculations.

*"The mechanisms of enamine formation investigated by quantum chemical investigations."*



Species **1** and **6** as well as parts of the transition state search were calculated by Michael H. Haindl.

Michael M. Hammer,<sup>\*</sup> Michael H. Haindl,<sup>\*</sup> Johnny Hioe, Hendrik Zipse and Ruth M. Gschwind

*We would like to thank the Leibniz-Rechenzentrum in Munich for providing computational capacity.*

<sup>\*</sup> These authors contributed equally.

## 5.1 Enamine formation pathways deduced by quantum chemistry

### Introduction

The accurate calculation of reactive transition states is a highly ambitious goal of theoretical chemists and allows the interpretation and even the forecast of reaction outcomes in an informed fashion. In organocatalysis, the catalysis of organic reactions with the help of small organic molecules, the number of synthetic applications outnumbers the studies on reaction mechanisms by a large extend, however those are necessary to gain insight into the mechanistic underpinnings of the reactions and to allow the further development of catalytic systems. Enamine catalysis has proven to be one of the most applicable modes of catalysis in this context.<sup>[1]</sup> Studies have been performed on this reaction type, addressing mainly the transition states for the subsequent electrophilic functionalization of the enamine intermediate.<sup>[2–6]</sup> Sharma and Sunoj,<sup>[5]</sup> Houk and co-workers<sup>[2]</sup> as well as Seebach and co-workers did address the formation pathways of enamines and did identify different pathways. Sharma and Sunoj alongside Houk and co-workers propose a water free and water assisted pathway from the iminium species to the enamine intermediate. Also the participation of an external base was a matter of discussion. Seebach and Eschenmoser however propose the formation of the enamine intermediates from oxazolidinone species.<sup>[7]</sup> Our recent large experimental effort to investigate enamine catalysis by L-proline with the detection of the elusive enamine intermediate,<sup>[8]</sup> and our ability to obtain accurate energy and structural descriptions of reactive intermediates (see chapter 4) allows us to investigate the proline facilitated enamine catalysis reaction in regards to active transition states (see Fig. 5.1 for schematic representation of the investigated system). This is particularly interesting since experimental data did suggest the dependency of enamine formation from nucleophilic additives and we wanted to investigate the impact of nucleophiles.

We did focus on the nucleophile free transition states first to gain experience in the accurate description of transition states and to rationalize our experimental findings, that were obtained without the addition of nucleophiles in solution. Our study did not yield conclusive rational for our experimental findings and could not account for the observed direct transition from oxazolidinones to enamines.

Recently this studies have largely been refined in our group and by a combination of *in situ* NMR spectroscopic rate-constant determination and quantum-chemical calculation. Here the formation of enamines from iminium species through a List-Houk transition state was evidenced.<sup>[9]</sup>

Thus this study is to be considered a preliminary investigation to identify trends and limiting factors in the accurate description of active transition states in enamine catalysis.

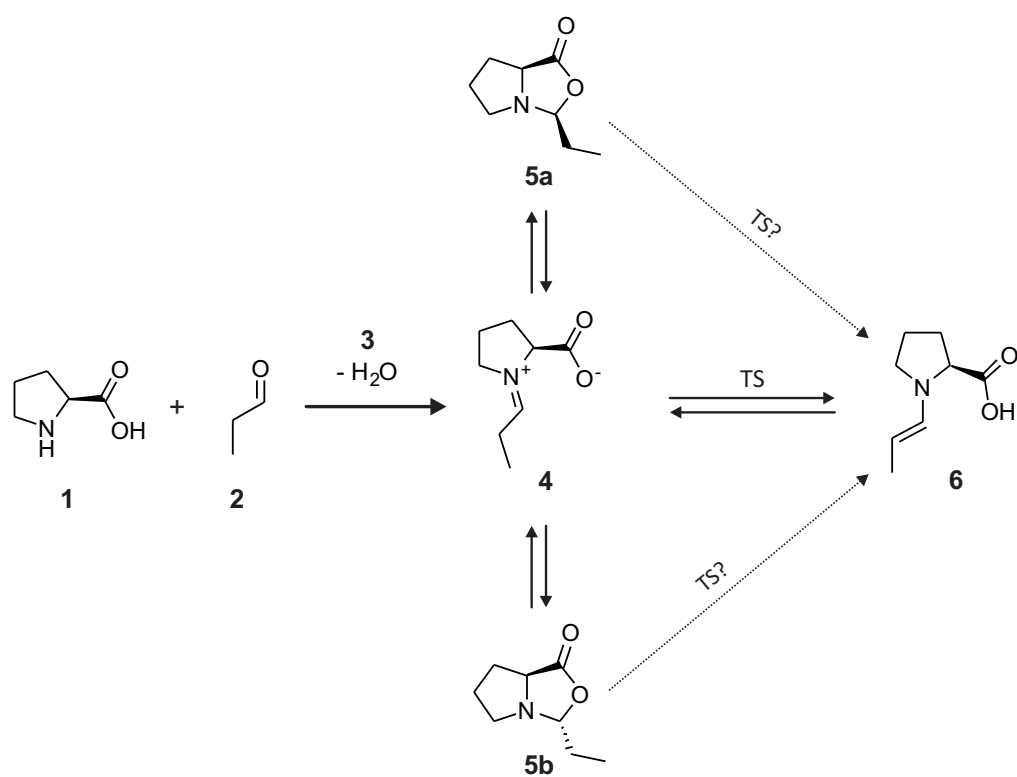


**Fig. 5.1:** Reaction and investigation scheme for the formation of enamine **6** from propanal **2** and L-proline **1**. The aldehyde and secondary amine catalyst condense to form the iminium species **4**, which is supposedly in rapid equilibrium with both oxazolidinones *endo* **5a** and *exo* **5b**. Transition states are investigated for the direct formation of enamine **6** from the iminium intermediate **4** or pathways from the respective oxazolidinone intermediates **5a** and **5b** are searched for.

## Results and Discussion

Following our search for optimized intermediate structures (see chapter 4) we performed transition state searches on a MO62X/6-31+G(d,p) level of theory in the gas phase.<sup>[10]</sup> We decided to use MO62X/6-31+G(d,p) in order to have a reasonable cost-to-gain ratio. Solvent correction did not yield superior results and was thus omitted, albeit relative energies might differ significantly for charged species (see the refined study)<sup>[9]</sup> We constructed plausible starting geometries of all investigated intermediate species **4** to **6** with the incorporation of water and minimized the structures to represent transition states. IRC calculations<sup>[11,12]</sup> lead to the starting- and the end-point of the found transition states. No transition state could be identified directly connecting the oxazolidinone species **5a** or **5b** with the enamine species **6** contrary to what was suggested experimentally.<sup>[8]</sup> The only feasible transition states were obtained for the reaction of iminium species **4** to enamine species **6**. Additionally transitions were identified yielding iminium ion **4** starting from the oxazolidinone species **5a** or **5b**. No Boltzmann averaging was performed in order to assess the structural impact on the transition state energies.

**The iminium-enamine transition state.** Having identified the transition (termed **rp**, reaction path) of iminium ion **4** to enamine **6** as being feasible for the formation of enamine intermediate, we thoroughly investigated this transition state in extensive detail. Overall seven transition state starting points were used to identify the minimum structure. Energetic representation of these transition levels is depicted in Fig. 5.2.

The minimum transition state **rp<sub>5</sub>**, connecting an *E*-configured iminium species with an *s-cis* enamine is approximately 35 kJ·mol<sup>-1</sup> lesser in energy than the high energy transition state **rp<sub>7</sub>**. The energy dispersion can be grouped in two separate parts. While **rp<sub>7</sub>** and **rp<sub>6</sub>** represent the high energy transition levels, all other can be grouped to the low energy transition levels. Addressing the main distinction regarding the structure of the two groupings, the water molecule, responsible for the proton abstraction from the iminium species is differently arranged. For **rp<sub>7</sub>**, the shuttling water molecule was arranged on the opposite side as the catalyst carboxylic acid residue with the *E*-configured iminium species **4** and leads to a significantly higher energy for the complexed structure. In **rp<sub>6</sub>** the water molecule is again oriented opposite to the exocyclic catalyst residue in combination with the *Z*-configured iminium species **4** yielding significantly higher complex and transition state energies. In the case of the low energy structures the shuttling water molecule is arranged in between the carboxylic acid residue and the developing enamine double bond (see the structural representations in Fig. 5.2). The minimum transition state **rp<sub>5</sub>** is found schematically as insert in Fig. 5.2 and shows decisive distances in Å for developing and breaking covalent bonds. The transition state bond lengths are in the region of 1.13 to 1.35 Å. No particular attention to the configuration of the iminium starting point was paid, since no experimental data is available and the subject was addressed extensively by Sunoj and Sharma already.<sup>[5]</sup>

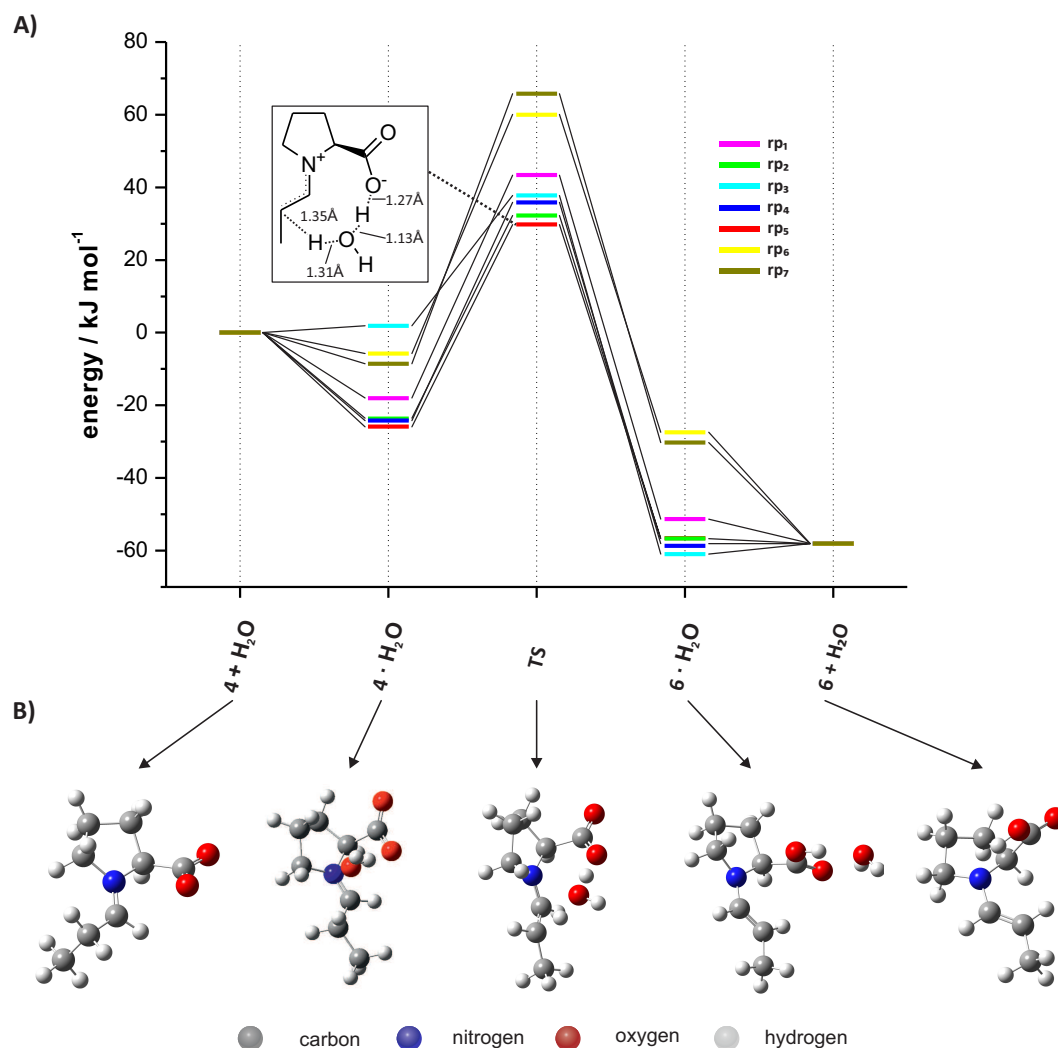


**Fig. 5.2:** **A)** Schematic representation of the identified transition states between iminium species **4** and enamine **6** using different starting geometries at the transition level. The best transition state is depicted as structural representation with distances in Å. After complexation with water to **4**·H<sub>2</sub>O the transition level is reached and subsequently **6**·H<sub>2</sub>O is formed and releases the product **6**. **B)** Best structures identified on a M062X/6-31G(d,p) level of theory for the depicted structures. *Note:* For **ts<sub>3</sub>** the transition state search yields an entirely different conformation of the complex **4**·H<sub>2</sub>O and thus shows significant higher energy in the complex structure compared to the separated species **4** and H<sub>2</sub>O. For **rp<sub>7</sub>** the shuttling water molecule was arranged on the opposite side as the catalyst carboxylic acid residue with the *E*-configured iminium species **4** and leads to a significantly higher energy for the complexed structure. In **rp<sub>6</sub>** the water molecule is again oriented opposite to the exocyclic catalyst residue in combination with the *Z*-configured iminium species **4** yielding significantly higher complex and transition state energies. Coordinates for species **4**·H<sub>2</sub>O, **6**·H<sub>2</sub>O and the best transition state **rp<sub>5</sub>** can be found in the SI 5.2.

The effect of energy gain through water complexation visible for all but the **rp<sub>3</sub>** complex **4**·H<sub>2</sub>O and can be explained by the orientation of the water molecule in the complex being oriented over the pyrrolidine ring in significant distance to the carboxylic acid residue, where

the water molecule is believed to have the highest beneficial effect on energetic stabilization, together with an orientation over the iminium double bond dipole. On the enamine **6** side the water molecule cannot effectively stabilize an enamine water complex in the case of **rp<sub>6</sub>** and **rp<sub>7</sub>** transition since the water molecule is oriented on the opposite side as the carboxylic acid residue and thus no stabilizing H-bond network can develop. Evaluating the minimum transition state, the bond lengths are all in an expected region of 1.13 Å to 1.35 Å with the highest value for the leaving proton orienting towards the shuttling water molecule.

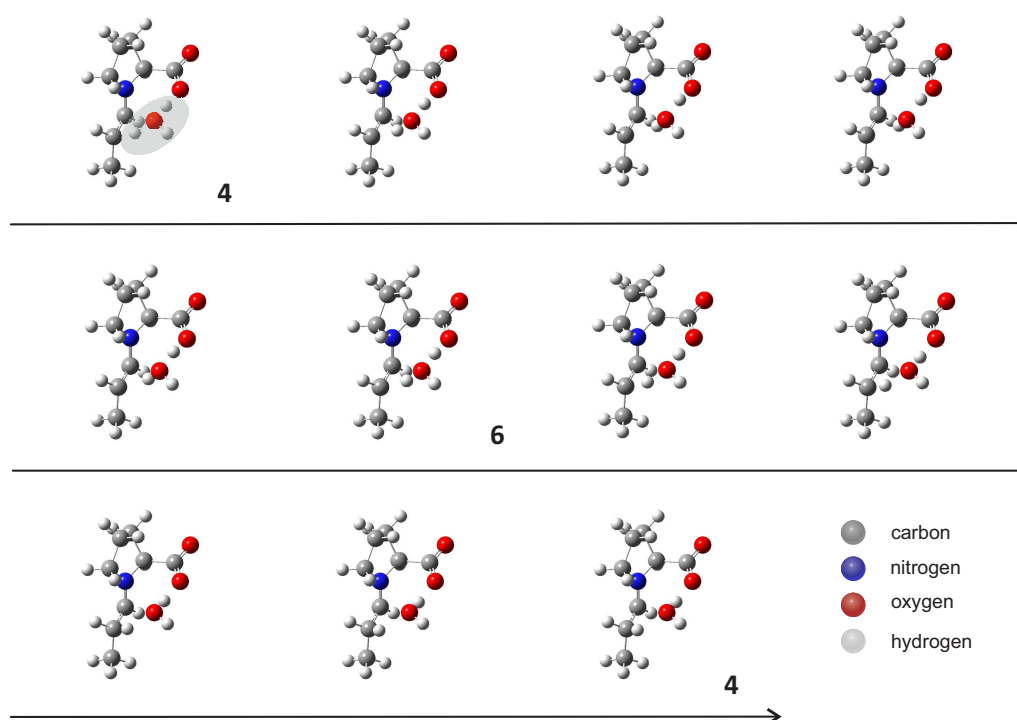


**Fig. 5.3:** Frame by frame representation of the transition between iminium species **4**·H<sub>2</sub>O and enamine **6**·H<sub>2</sub>O (back and forward) calculated at a M062X/6-31G(d,p) level of theory.<sup>[10]</sup> The proton shuttling water is intimately involved in the transition (see highlighted region in first frame).

Evaluating the transition state further, it is evidenced that the transition level only consists of the proton shuttling process between the water molecule and the developing enamine double bond. This found transition is demonstrated by a frame-by-frame representation of the proton shuttling process in Fig. 5.3.

**The oxazolidinone-iminium-enamine transition.** Having also identified a transition state between the oxazolidinone species **5a** and **5b** with the iminium species **4** we investigated the energetics of this transition in more detail. We explicitly chose *endo*-oxazolidinone **5a** as starting point, however a start from the diastereomer is believed to exhibit the same behavior, since the orientation of the exocyclic CH<sub>3</sub> group is largely lost in the iminium species (see chapter 4). Evaluating the transition state between the *endo*-oxazolidinone and the iminium species **4** and



subsequent transition to enamine **6** gave the following energy profile (see Fig. 5.4).

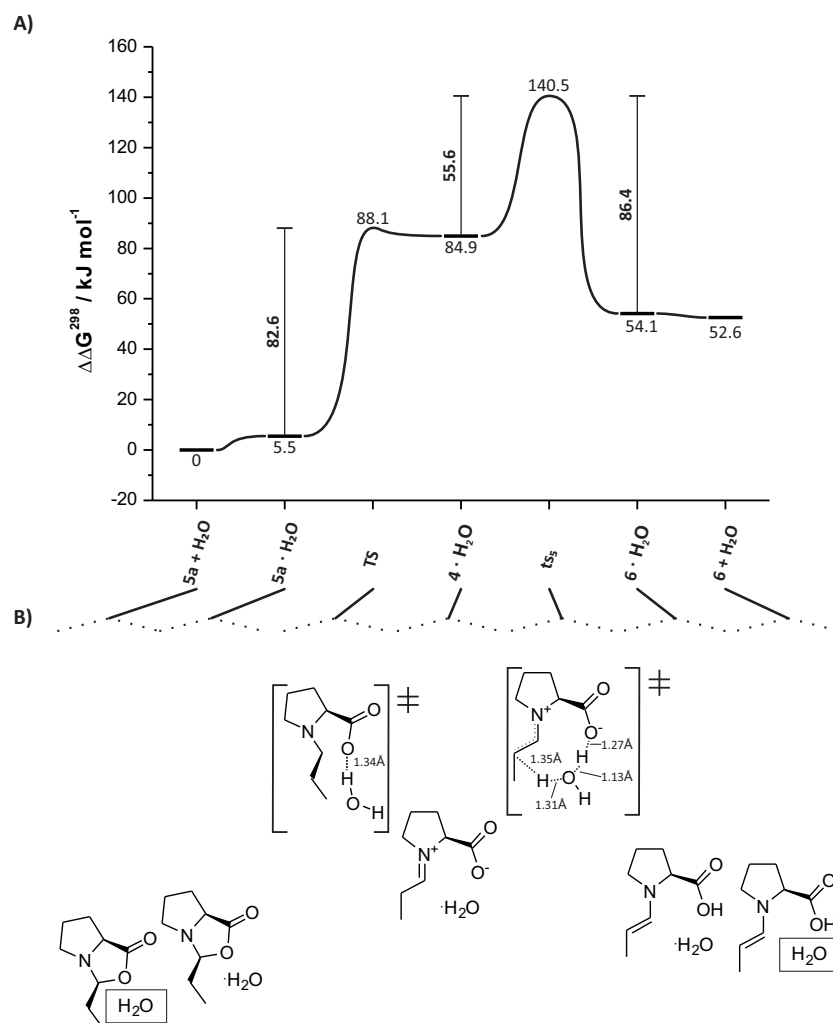


**Fig. 5.4:** Relative energies (**A**) and related schematic structures with distances in the transition states (**B**) of the combined reaction path for the formation of enamine **6** from *endo*-oxazolidinone **5a** calculated at a M062X/6-31G(d,p) level of theory.<sup>[13]</sup> After formation of a complex with water  $5a \cdot H_2O$  the transition state **TS** to form iminium species **4** was identified with a energy barrier of 82.6 kJ mol<sup>-1</sup>. The so formed complex of iminium species  $4 \cdot H_2O$  subsequently experiences the second transition state  $ts_5$  with a barrier of 55.6 kJ mol<sup>-1</sup> to form complex  $6 \cdot H_2O$  and release the product **6**. The reverse reaction is mostly prohibited by the enormous barrier of 86.4 kJ mol<sup>-1</sup> to form iminium species **4** from enamine **6**. *Note:* Structures of the presented stationary points or transition states can be found in the SI 5.2.

Complexation of oxazolidinone **5a** with H<sub>2</sub>O yielded a complex with a 5.5 kJ·mol<sup>-1</sup> higher energy content. After the formation of the transition state with a barrier of 82.6 kJ·mol<sup>-1</sup> a local minimum  $4 \cdot H_2O$  structure is found. The corresponding back-reaction has a negligible activation barrier of only 3.2 kJ·mol<sup>-1</sup>. Subsequently the minimum transition already depicted in Fig. 5.2 is passed through with a barrier of 55.6 kJ·mol<sup>-1</sup> and the complex  $6 \cdot H_2O$  is formed, which is 1.5 kJ·mol<sup>-1</sup> higher in energy as the separated species **6** + H<sub>2</sub>O. The reaction barrier

for the back-reaction of enamine **6** to iminium **4** is found to be as high as 86.4 kJ·mol<sup>-1</sup>. In the transition state structures distances for the developing or breaking bonds are depicted (for transition **4-6**, *vide supra*) and give distances of 1.34 Å for the OH bond in transition **5a-4**.

Addressing the activation barriers, one can conclude that once an iminium species **4** is formed from **5a** and not enough energy is present to facilitate further reaction to the enamine species **6** a simple back reaction is most likely to occur, since the activation barrier for that process is practically non-existent and the oxazolidinone species represents by far the most stable structure. This behavior of the transition level may very well explain the identified strong exchange between the two oxazolidinone species experimentally, assuming that rotation within the transition state species (**TS**) is fast compared to the back reaction. This is highly likely, because the water molecule is involved in hydrogen bonding to the carboxylic acid group and does not interact with the developing iminium  $\pi$ -bond and does thus not hamper rotation around the then single-bond. Both *endo*- and *exo*-oxazolidinone may be formed from within a singular pool. In addition, the failure to detect iminium species **4** in solution is also very well explained by the same rationalization. No stabilization is present for the iminium species.

Furthermore for the experimentally identified transition of oxazolidinones to the enamine species the low local minimum of iminium **4** can be the possible justification, since isolation of the iminium is thus not possible and also influence of iminium characteristics and structural preferences are to be minimal.

One must note that the application of any kind of solvent modeling in the transition state search would highly alter the picture presented, was however not performed in this study. Solvent modeling was applied in the refined study<sup>[9]</sup> and does yield a minimum for the iminium species by lowering the energy of the zwitterionic species about 32 kJ·mol<sup>-1</sup>.

## Summary

In summary, we have identified active transition states in the L-proline facilitated enamine catalysis of aldehydes (see Fig. 5.5 for a schematic representation). Transition levels between the iminium species and the enamine species were found to be energetically highly dependent on the orientation of the shuttling water molecule. With the water molecule oriented in between the carboxylic acid moiety and the developing enamine double bond minimum transition level energies were found.

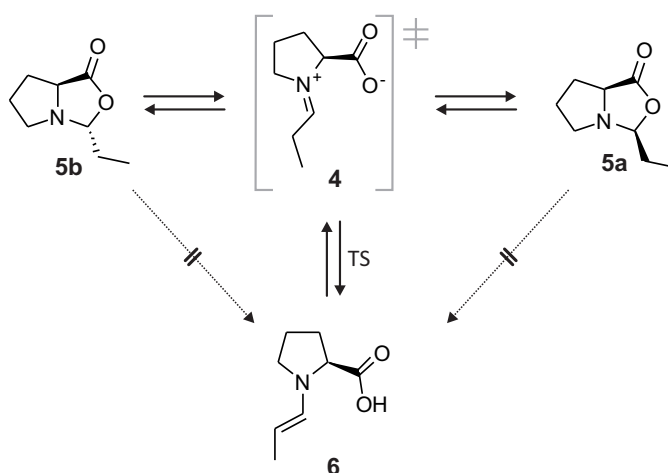


**Fig. 5.5:** Schematic representation of the identified transition states. No transition state was found offering a direct pathway from the respective oxazolidinones *endo* **5a** or *exo* **5b** to enamine **6**. The oxazolidinones collapse to the respective iminium intermediate **4** and subsequently a transition state to enamine **6** is found. This is however only achieved with the explicit involvement of a single water molecule (not shown) acting as a proton shuttle to facilitate the proton abstraction of the iminium intermediate **4**.

### **Experimental details**

All calculations were performed within Gaussian09 subversion D.01<sup>[13]</sup>. Plausible start geometries were chosen and minimized or optimized to the transition level. Frequency calculations provided evidence for the identification of minimum or transition level structures. Structures at MO62X level of theory for the minimum structures as well as the transition levels can be found in the SI 5.2.

## 5.2 Combined calculation results

### Coordinates of stationary points.

In the following the coordinates for all stationary points at a M062X/6-31+G(d,p)<sup>[13]</sup> level of theory are shown. Only the energetically best structures were chosen.

1

```
1\1\GINC-PHOENIX\F0pt\RM062X\6-31+G(d,p)\C5H9N102\MHAINDL\13-Jan-2012\
0\#\#P M062X/6-31+G(d,p) opt scf=tight int=finegrid\Komentar\0,1\0,-
1.8372504734,-1.1141058923,-0.3398430493\H,-1.0724307895,-1.6930755147
,-0.1256819473\O,-2.1894097515,1.0771975926,-0.0854289199\H,1.23162940
72,-0.9760277636,-1.4732709452\H,0.2981966721,1.6363103653,-0.89431425
56\H,2.4694681711,-1.5935715299,-0.367887727\C,1.6715318566,-0.8558531
749,-0.475203975\C,-0.0926466049,0.1932242808,0.6928646236\H,2.6314124
72,1.0206348286,-1.1207349165\C,-1.4822779102,0.1116333882,0.048887754
3\C,0.7750037276,1.2987263278,0.030316265\N,0.6203671996,-1.0884083528
,0.5321977324\H,-0.2645005694,0.3996666019,1.7538679337\C,2.1082043589
,0.5954475634,-0.2605100618\H,0.8798181261,2.1716780811,0.6761559641\H
,2.7754794518,0.65388538,0.6073554231\H,1.0390796558,-1.3738501814,1.4
11231013\Version=AM64L-G09RevA.02\State=1-A\HF=-401.0136645\RMSD=8.4
68e-09\RMSF=1.437e-05\Dipole=2.1828492,-0.5382404,0.6089323\Quadrupole
=-4.9351327,0.6603837,4.274749,1.400383,-1.1794165,-0.6415341\PG=C01 [
X(C5H9N102)]\@
```

2

```
1\1\GINC-R1ION1\F0pt\RM062X\6-31+G(d,p)\C3H6O1\DI56F0V\22-Mar-2012\0\
#P M062X/6-31+G(d,p) opt freq=noraman scf=tight int=finegrid\Water\0
,1\C,0.9872693193,-0.2151791247,0.\0,0.6770576322,-1.3821824986,0.\H,2
.0587604827,0.0757333814,0.\C,0.001197811,0.9245591922,0.\C,-1.4500872
905,0.4666419932,0.\H,0.2333565261,1.5503708505,0.872759605\H,0.233356
5261,1.5503708505,-0.872759605\H,-2.1263622985,1.3244158894,0.\H,-1.66
22608541,-0.145003267,-0.8799683533\H,-1.6622608541,-0.145003267,0.879
9683533\Version=EM64L-G09RevB.01\State=1-A'\HF=-193.0610862\RMSD=5.18
2e-09\RMSF=1.313e-05\Dipole=0.0568048,1.1104421,0.\Quadrupole=1.306783
1,-2.3336743,1.0268912,1.2373231,0.,0.\PG=CS [SG(C3H2O1),X(H4)]\@
```

3

```
1\1\GINC-R1I2N8\F0pt\RM062X\6-31+G(d,p)\H2O1\DI56F0V\06-Feb-2012\0\#P
M062X/6-31+G(d,p) opt freq=noraman scf=tight int=finegrid\Water\0,1
\0,-0.476853444,0.1679509902,0.\H,-0.4489035412,1.129242132,0.\H,0.438
7569853,-0.1261931222,0.\Version=EM64L-G09RevB.01\State=1-A'\HF=-76.3
949639\RMSD=4.335e-09\RMSF=1.210e-05\Dipole=0.7121619,0.5035363,0.\Qua
drupole=0.3271979,0.8662556,-1.1934535,-0.7621728,0.,0.\PG=CS [SG(H2O1
```

)]\@

#### 4E

```
1\1\GINC-R1ION5\FOpt\RM062X\6-31+G(d,p)\C8H13N1O2\DI56FOV\07-Feb-2012\
0\#P M062X/6-31+G(d,p) opt freq=noraman scf=tight int=finegrid\Imini
um propanal\0,1\C,1.8242483933,-0.717427875,0.7905486978\C,0.32599201
72,-0.4704279529,0.7476238156\C,1.2317184682,-0.1919188419,-1.48516452
13\C,2.3090779993,0.0751530883,-0.4290140525\H,2.2266488253,-0.3384598
042,1.7302615496\H,2.0622215774,-1.7825385866,0.6874900953\H,-0.282285
1233,-1.2307861517,1.2436288617\H,1.4344347839,-1.1035439917,-2.057174
6941\H,1.0743333184,0.639782604,-2.1736967672\H,3.2982650508,-0.220979
8212,-0.7827371553\H,2.3299885648,1.1407213344,-0.1816653198\C,-1.2000
194056,-0.2345036371,-1.0773557671\N,0.0081451201,-0.4192907719,-0.679
9743699\0,-1.024925044,1.5313820123,0.7542793815\C,-0.1011888483,0.967
874836,1.3724215012\0,0.5464569881,1.259292166,2.3788227571\H,-1.97399
20593,-0.3704044361,-0.3285406989\C,-1.57883803,0.2111730794,-2.446013
0013\H,-2.510363936,-0.2852093359,-2.7319868069\C,-1.7882747408,1.7391
456273,-2.4198800021\H,-2.1080771877,2.0836979735,-3.4056587247\H,-2.5
406395074,2.0136350199,-1.6780781997\H,-0.8662922421,2.2521518958,-2.1
367780686\H,-0.8146924024,-0.0655400208,-3.1773649006\Version=EM64L-G
09RevB.01\State=1-A\HF=-517.6554591\RMSD=7.879e-09\RMSF=8.642e-06\Dipo
le=0.1196594,-2.0902129,-3.2383796\Quadrupole=6.3727257,-0.86861,-5.50
41157,1.372438,1.1128222,-6.9723788\PG=C01 [X(C8H13N1O2)]\@
```

#### 4Z

```
1\1\GINC-R1ION6\FOpt\RM062X\6-31+G(d,p)\C8H13N1O2\DI56FOV\07-Feb-2012\
0\#P M062X/6-31+G(d,p) opt freq=noraman scf=tight int=finegrid\Imini
um propanal\0,1\C,2.0601072304,-0.5372395026,0.6574456568\C,0.5427586
458,-0.3993940657,0.8671820758\C,1.0189631281,-0.2297471872,-1.4770545
532\C,2.2348980746,-0.8833544535,-0.8313928262\C,-1.2886502829,-0.4927
102597,-0.7470304769\N,-0.0358723522,-0.4763691775,-0.4727855601\0,-0.
8136890745,1.5981783725,0.9833339353\C,0.1212761611,1.0099705767,1.550
6033569\0,0.8052693822,1.2423707981,2.548229409\H,-1.5435279878,-0.390
3601515,-1.8031116104\C,-2.4012888445,-0.6703985788,0.2214123724\H,-2.
8036062851,0.3365331069,0.3908426491\C,-3.4699140451,-1.6216007044,-0.
3242240025\H,-4.3041055986,-1.6865752762,0.376807703\H,-3.8663720498,-
1.2656314117,-1.2801984228\H,-3.0748518025,-2.6305647799,-0.4724150558
\H,-2.0201583862,-0.9972232027,1.1912439494\H,1.1379555305,0.857562583
,-1.550411677\H,0.7175295267,-0.6373161628,-2.4431799428\H,3.169923771
2,-0.5080941658,-1.2512654404\H,2.1958551695,-1.9659134844,-0.99135519
8\H,2.530378273,0.4163747895,0.9100036172\H,2.4943325506,-1.2944140317
,1.3113959562\H,0.1170489455,-1.1858403906,1.494691515\Version=EM64L-
G09RevB.01\State=1-A\HF=-517.6511817\RMSD=5.145e-09\RMSF=6.793e-06\Dip
ole=-0.3708164,-2.6776631,-2.9839049\Quadrupole=8.5660855,-5.9282961,-
```

2.6377895,1.11493,-3.3350715,-7.6580905\PG=C01 [X(C8H13N102)]\@

### 5a

1\1\GINC-PHOBOS\SP\RM062X\6-31+G(d,p)\C8H13N102\MHAMMER\12-Jan-2012\0\  
 \#P M062X/6-31+G(d,p) scf=tight int=finegrid\Houk Geometrien fur Oxa  
 zolidine aus OrgLett 5b 4-processor run, 1024MB RAM\0,1\C,0,2.493278,  
 -0.126045,0.158762\C,0,1.160429,0.356331,0.75427\C,0,0.655704,-1.51096  
 8,-0.540744\C,0,2.168796,-1.546344,-0.347706\H,0,2.79379,0.542179,-0.6  
 53212\H,0,3.292419,-0.125179,0.901394\H,0,1.244502,0.701617,1.791963\H  
 ,0,0.192195,-2.500145,-0.56478\H,0,0.411282,-0.984029,-1.479284\H,0,2.  
 4198,-2.288328,0.415682\H,0,2.701444,-1.801916,-1.266112\C,0,-1.069409  
 ,-0.091033,0.538819\H,0,-1.382656,0.217698,1.545671\N,0,0.208074,-0.75  
 9552,0.646988\0,0,-0.820502,1.141937,-0.201568\C,0,0.482233,1.46739,-0  
 .057263\0,0,0.978662,2.458212,-0.517967\C,0,-2.175637,-0.867217,-0.139  
 22\H,0,-1.886576,-1.066978,-1.176301\C,0,-3.502955,-0.112841,-0.099577  
 \H,0,-3.413861,0.850165,-0.608406\H,0,-4.291129,-0.688695,-0.590127\H,  
 0,-3.816124,0.075352,0.932389\H,0,-2.26153,-1.83171,0.374441\Version=  
 AM64L-G09RevA.02\State=1-A\HF=-517.6918219\RMSD=5.486e-09\Dipole=-0.15  
 41431,-1.4887893,0.3775605\Quadrupole=4.7426129,-6.3009424,1.5583295,-  
 1.5094045,0.2289573,4.3946974\PG=C01 [X(C8H13N102)]\@

### 5b

1\1\GINC-PHOBOS\FOpt\RM062X\6-31+G(d,p)\C8H13N102\MHAMMER\11-Jan-2012\  
 0\1\#P M062X/6-31+G(d,p) opt scf=tight int=finegrid\Kommentar\0,1\C,2  
 .1240863449,-0.5979319417,0.775872182\C,0.7767333613,0.1236078125,0.86  
 58955178\C,0.5144638139,-1.8399188931,-0.4605797541\C,1.977110039,-1.3  
 869599881,-0.5288208607\H,2.9508846382,0.1157926149,0.7780455759\H,2.2  
 390819933,-1.2758995163,1.6273967148\H,0.514847472,0.4081936258,1.8906  
 541282\H,0.4288032359,-2.762040698,0.1254864635\H,0.0675003158,-2.0274  
 609909,-1.44116052\H,2.6771192336,-2.2215938322,-0.6095416138\H,2.1351  
 921553,-0.7234227263,-1.3873548105\C,-1.0544438905,0.1034646682,-0.566  
 139014\N,-0.2191016872,-0.7631839412,0.2439049893\0,-0.2690003193,1.28  
 19353368,-0.8781141574\C,0.7617971212,1.3735754231,-0.0163261276\0,1.5  
 363068309,2.2905768022,0.0027375224\H,-1.2985215918,-0.3771854956,-1.5  
 193033581\C,-2.3192508619,0.5411563613,0.1552825682\H,-2.8022720526,1.  
 3200751856,-0.4439387972\C,-3.2623535258,-0.6335916579,0.3925050497\H,  
 -4.1573651768,-0.3142052183,0.9315812837\H,-3.5854021818,-1.0759884607  
 ,-0.5562450952\H,-2.7631533142,-1.40996754,0.9782440638\H,-2.028010953  
 3,0.9995300699,1.1088330493\Version=AM64L-G09RevA.02\State=1-A\HF=-51  
 7.6924484\RMSD=7.848e-09\RMSF=1.357e-05\Dipole=-0.4756193,-1.5206669,0  
 .1584833\Quadrupole=2.6335337,-5.08524,2.4517063,-5.6193976,1.0207513,  
 2.5803297\PG=C01 [X(C8H13N102)]\@

## 6

```

1\1\GINC-PHOENIX\FOpt\RM062X\6-31+G(d,p)\C8H13N102\MHAINDL\12-Jan-2012
\0\#P M062X/6-31+G(d,p) opt scf=tight int=finegrid\Kommentar\0,1\C,
-0.6142320982,0.1558435917,-0.6151691239\C,-1.9289213831,-0.5873906749
,-0.942306908\C,-2.0315559329,-1.6457430999,0.162145365\C,-0.573362569
1,-2.0451516799,0.3566934555\N,0.1255894227,-0.7581754349,0.2538706093
\C,1.5260833109,-0.7631203881,0.2038873068\H,1.9710853773,-1.653652704
3,0.6461669445\C,-0.8896752104,1.499921842,0.0721627973\O,-1.365122718
2,2.4341594091,-0.5195185104\C,2.3092599675,0.215635589,-0.2674179168\
C,3.8086740919,0.1519972341,-0.2311375046\O,-0.5964498757,1.54720776,1
.3755940619\H,-0.0535871912,0.383730694,-1.5306208792\H,-2.7793513189,
0.0949357782,-0.9916143069\H,-1.829201423,-1.0753643737,-1.9162382613\
H,-2.4238106915,-1.2044725062,1.0848917556\H,-2.6668974543,-2.48960438
69,-0.1139997893\H,-0.3703982122,-2.5092990577,1.3261876704\H,-0.24948
20478,-2.7371995117,-0.4367052574\H,1.8644475213,1.1195435665,-0.68000
64228\H,-0.2078995591,0.6820956701,1.6097639601\H,4.1531688912,-0.7908
24738,0.2036132289\H,4.2346285335,0.2352674998,-1.2363779901\H,4.22622
85694,0.9710029216,0.3641347155\Version=AM64L-G09RevA.02\State=1-A\HF
=-517.6779128\RMSD=3.798e-09\RMSF=9.149e-06\Dipole=0.398376,-2.1063111
,0.0129175\Quadrupole=3.5348972,-4.8080379,1.2731406,5.8359553,0.18344
3,-1.0601389\PG=C01 [X(C8H13N102)]\@

```

**TS** in Fig. 5.4

```

1\1\GINC-R1ION15\FTS\RM062X\6-31+G(d,p)\C8H15N103\DI56FOC\06-Aug-2012\
0\#P M062X/6-31+G(d,p) opt=(ts,calcfc,noeigen) scf=tight int=finegrid
\carbinol_TSopt_01\0,1\C,2.0845784064,1.0362334142,-1.0645104639\C,1
.2015453318,-0.1725697702,-0.7739327356\C,0.2233498454,1.7748881279,0.
2953189378\C,1.7379202471,1.9613906216,0.110035588\H,3.1337554369,0.74
34847882,-1.084099252\H,1.8070536582,1.4963209846,-2.0195850442\H,0.99
91066215,-0.7946037726,-1.6512251505\H,-0.3570643792,2.5515445048,-0.2
142814445\H,-0.0779167036,1.7422739672,1.3475151401\H,1.9977046079,3.0
065515429,-0.0668845341\H,2.2687350666,1.620750186,1.0038231921\C,-1.2
302932629,-0.0903448266,-0.37560494\N,-0.0548714427,0.4744557046,-0.34
37428877\C,1.8337048045,-1.0785547222,0.3391314503\O,3.0385166942,-1.2
712361073,0.2312349082\H,-1.2979347766,-0.9992810526,-0.9693725453\C,-
2.4843461945,0.7006832145,-0.1430106334\H,-2.502655906,1.4939308968,-0
.9040010995\C,-3.7457152871,-0.1523189697,-0.2383871439\H,-4.633921500
7,0.4592192527,-0.0664308681\H,-3.7204012544,-0.9584453217,0.496706705
1\H,-2.4209647201,1.2043926954,0.82750281\O,1.0465595998,-1.5328391113
,1.2333158236\O,-1.3721436074,-1.3201498363,1.2191461232\H,-3.83644612
26,-0.602501282,-1.2313682093\H,-1.6474902033,-0.9333846077,2.05947356
85\H,-0.2927889591,-1.4507525211,1.2576077055\Version=EM64L-G09RevB.0
1\State=1-A\HF=-594.0664494\RMSD=6.469e-09\RMSF=1.064e-05\Dipole=-2.68
66086,2.581338,-1.0044936\Quadrupole=-4.005841,-1.11484,5.120681,6.405
6254,-3.2794375,4.4618092\PG=C01 [X(C8H15N103)]\@

```



4-H<sub>2</sub>O

```

1\1\GINC-R1I3N11\F0pt\RM062X\6-31+G(d,p)\C8H15N103\DI56F0C\24-Apr-2012
\0\#P M062X/6-31+G(d,p) opt scf=(tight) int=finegrid\ts_05_opt_irc_f
w_rel\0,1\C,2.0695075064,1.2971143416,-0.2879383729\C,1.0916012295,0.
3143093983,-0.9181113852\C,-0.0696093535,1.6784373421,0.7405190287\C,1
.4191442089,1.575677813,1.0718626032\C,-1.3233821488,0.2183146931,-0.7
768971615\N,-0.2183146047,0.7523630707,-0.406878003\O,0.3178264445,-1.
8840336244,-0.2853155317\C,1.3582120123,-1.204714572,-0.4836058681\O,2
.5484614075,-1.5016249936,-0.4440692014\H,-1.2553568283,-0.5059447485,
-1.5861691875\C,-2.6375689167,0.5127741607,-0.1392993379\H,-2.73284327
81,1.5946306504,0.0151292467\C,-3.8095600002,-0.0378119177,-0.94899256
11\H,-4.7526244012,0.1631434918,-0.4374329387\H,-3.8601731123,0.417856
3336,-1.9420338774\H,-3.7175333695,-1.1203035539,-1.071384999\H,-2.592
8695813,0.0505666395,0.858365095\H,-0.7238339393,1.3457297938,1.547409
1444\H,-0.3496398689,2.6822251286,0.4000420755\H,1.0772202307,0.331985
9638,-2.0110212897\H,-0.4353174647,-1.4855481468,1.2045372377\O,-0.872
3929573,-1.0177459109,1.9570246083\H,-0.7655204961,-1.5839535849,2.726
3989627\H,2.1451140356,2.2179801065,-0.8778411466\H,3.0522181598,0.831
5813305,-0.2114095995\H,1.7891498996,2.4797531534,1.5585665255\H,1.577
3781862,0.7239576414,1.7409839333\Version=EM64L-G09RevB.01\State=1-A\
HF=-594.0787181\RMSD=3.484e-09\RMSF=1.469e-05\Dipole=-2.1606716,2.6939
586,0.0128454\Quadrupole=-2.3277059,-3.5743637,5.9020696,7.4439646,3.0
772953,-2.5352522\PG=C01 [X(C8H15N103)]\@

```

ts<sub>5</sub>

```

1\1\GINC-R1I2N4\FTS\RM062X\6-31+G(d,p)\C8H15N103\DI56F0C\23-Apr-2012\O
\#p opt=(calcf,ts,noeigen) hf/6-31+g(d,p) int=finegrid m062x scf=tig
ht\Im/E/dw/vorne\0,1\C,-2.3543951007,-1.3607902568,0.106766253\C,-1.
4419379241,-0.2693442146,-0.452289386\C,-0.1505473334,-1.6958786742,1.
0404107322\C,-1.6393676185,-1.7411897338,1.4096374295\C,1.0033760927,-
0.3020511837,-0.6236809022\N,-0.1043362832,-0.7697546462,-0.10631039\O
,-0.8397132463,1.6876029464,0.8864835222\C,-1.7604491814,1.1144973578,
0.2012933872\O,-2.8853766965,1.5353902517,-0.018482259\H,0.8594606356,
0.4141295856,-1.4351349826\C,2.295300925,-0.4652716653,-0.0762329046\H
,2.4424292949,-1.3644016593,0.5249502291\C,3.4932587215,-0.0254578556,
-0.8966459553\H,4.3485253818,0.1804962943,-0.2484687958\H,3.8037236792
,-0.7853457715,-1.6210604564\H,3.2728287477,0.8941789121,-1.448078346\
H,1.9487979598,0.4056382459,0.8949529115\H,0.4772197837,-1.3092341892,
1.8486765143\H,0.2346128815,-2.6706652684,0.718435821\H,-1.5263600985,
-0.1496407144,-1.5356230218\H,0.2679563299,1.303394929,1.3806091006\O,
1.2724070191,1.0267323907,1.8284968409\H,1.6857447919,1.8050183933,2.2
182371619\H,-2.3895389321,-2.2145103021,-0.5788663679\H,-3.3644645626,
-0.9783947372,0.2553188258\H,-1.9335845442,-2.7190069034,1.7950497341\
H,-1.8498109827,-0.9919711612,2.1792239243\Version=EM64L-G09RevB.01\S

```

tate=1-A\HF=-594.0526712\RMSD=9.603e-09\RMSF=2.386e-05\Dipole=2.120236  
8,-2.0442895,-0.3470488\Quadrupole=-2.8102746,-1.2263324,4.036607,11.0  
628168,-0.6971695,-0.4015746\PG=C01 [X(C8H15N103)]\@

## 6·H<sub>2</sub>O

1\1\GINC-R1I0N7\F0pt\RM062X\6-31+G(d,p)\C8H15N103\DI56F0V\05-May-2012\  
O\#P M062X/6-31+G(d,p) opt scf=tight int=finegrid\Im/Z/up/vorne\0,1  
\C,-2.2681559948,0.5394170543,-0.4368372588\C,-0.8203591559,0.06545291  
77,-0.751380692\C,-1.8001479987,-1.4569023636,0.8113805593\C,-2.958882  
4014,-0.6915846132,0.1767790905\C,0.4474609513,-1.9530282653,-0.130313  
4933\N,-0.7442581816,-1.2542600299,-0.1685038853\O,0.2376873785,0.9696  
297441,1.1775714268\C,0.1764023409,1.0512236479,-0.1475486407\O,0.8056  
868971,1.8556734874,-0.8106481506\H,0.3900810314,-2.8734083631,0.44985  
26113\C,1.5918327905,-1.6263056691,-0.7529740721\C,2.8149183789,-2.497  
8559507,-0.715258409\H,3.6771614895,-1.9648830038,-0.2992549319\H,2.64  
38983144,-3.3866900109,-0.1000292288\H,3.1005857841,-2.8370416511,-1.7  
175170604\H,-1.5349080663,-1.035013376,1.7934247858\H,-2.0020565033,-2  
.5259401519,0.9289731079\H,-3.7333120322,-0.4164634404,0.8961851761\H,  
-3.4124756211,-1.304708579,-0.6074247554\H,-2.2412185504,1.3544937075,  
0.2922778874\H,-2.7698756281,0.9085106773,-1.3327360312\H,-0.606446905  
3,0.0297881708,-1.8258080254\H,0.8819512191,1.6374552562,1.5108922832\  
O,2.0066152856,3.0142826359,1.3832017878\H,1.93117983,2.9639849589,0.4  
147361592\H,1.6552560324,-0.7083017668,-1.3341641546\H,2.9407713157,3.  
0522239768,1.6087299144\Version=EM64L-G09RevB.01\State=1-A\HF=-594.09  
09918\RMSD=7.293e-09\RMSF=7.278e-06\Dipole=-0.1363816,-0.2070669,0.350  
7044\Quadrupole=7.2447731,-3.4366658,-3.8081072,3.8171318,2.2020525,-0  
.6152042\PG=C01 [X(C8H15N103)]\@

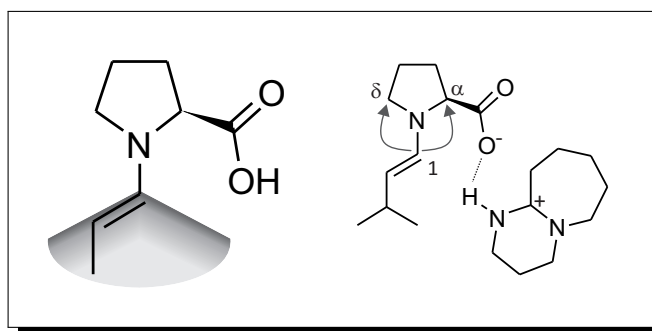
## 5.3 References

- [1] P. Pihko, I. Majander, A. Erkkilä, *Asymmetric Organocatalysis* **2009**, 291, 29–74.
- [2] P. H.-Y. Cheong, C. Y. Legault, J. M. Um, N. Çelebi-Ölçüm, K. N. Houk, *Chem. Rev.* **2011**, 111, 5042–5137.
- [3] J. E. Hein, J. Burés, Y. Lam, M. Hughes, K. N. Houk, A. Armstrong, D. G. Blackmond, *Org. Lett.* **2011**, 13, 5644–5647.
- [4] C. Allemann, R. Gordillo, F. R. Clemente, P. H.-Y. Cheong, K. N. Houk, *Acc. Chem. Res.* **2004**, 37, 558–569.
- [5] A. K. Sharma, R. B. Sunoj, *Angew. Chem.* **2010**, 122, 6517–6521.
- [6] A. Armstrong, R. A. Boto, P. Dingwall, J. Contreras-Garcia, M. J. Harvey, N. J. Mason, H. S. Rzepa, *Chem. Sci.* **2014**, 5, 2057–2071.
- [7] D. Seebach, A. K. Beck, D. M. Badine, M. Limbach, A. Eschenmoser, A. M. Treasurywala, R. Hobi, W. Prikozovich, B. Linder, *Helv. Chim. Acta* **2007**, 90, 425–471.
- [8] M. B. Schmid, K. Zeitler, R. M. Gschwind, *Angew. Chem. Int. Ed.* **2010**, 49, 4997–5003.
- [9] M. H. Haindl, J. Hioe, R. M. Gschwind, *J. Am. Chem. Soc.* **2015**, submitted,.
- [10] Y. Zhao, D. G. Truhlar, *Theor. Chem. Acc.* **2008**, 120, 215–241.
- [11] K. Fukui, *Acc. Chem. Res.* **1981**, 14, 363–368.
- [12] J. Bowman, S. Carter, N. Handy, C. Dykstra, G. Frenking, K. S. Kim, G. E. Scuseria, *Theory and Applications of Computational Chemistry: The First Forty Years*, Amsterdam, Elsevier, **2005**.
- [13] M. J. Frisch, G. W. Trucks, H. B. Schlegel, G. E. Scuseria, M. A. Robb, J. R. Cheeseman, G. Scalmani, V. Barone, B. Mennucci, G. A. Petersson, H. Nakatsuji, M. Caricato, X. Li, H. P. Hratchian, A. F. Izmaylov, J. Bloino, G. Zheng, J. L. Sonnenberg, M. Hada, M. Ehara, K. Toyota, R. Fukuda, J. Hasegawa, M. Ishida, T. Nakajima, Y. Honda, O. Kitao, H. Nakai, T. Vreven, J. A. Montgomery, Jr., J. E. Peralta, F. Ogliaro, M. Bearpark, J. J. Heyd, E. Brothers, K. N. Kudin, V. N. Staroverov, R. Kobayashi, J. Normand, K. Raghavachari, A. Rendell, J. C. Burant, S. S. Iyengar, J. Tomasi, M. Cossi, N. Rega, J. M. Millam, M. Klene, J. E. Knox, J. B. Cross, V. Bakken, C. Adamo, J. Jaramillo, R. Gomperts, R. E. Stratmann, O. Yazyev, A. J. Austin, R. Cammi, C. Pomelli, J. W. Ochterski, R. L. Martin, K. Morokuma, V. G. Zakrzewski, G. A. Voth, P. Salvador, J. J. Dannenberg, S. Dapprich, A. D. Daniels, . Farkas, J. B. Foresman, J. V. Ortiz, J. Cioslowski, D. J. Fox, *Gaussian 09 Revision D.01*, Gaussian Inc. Wallingford CT 2009.



## 6 Stereoinduction in enamine catalysis- "late" conformational lock.

*"Restriction of conformational space by late-stage coordination leading to conformational lock allowing stereoinduction in enamine catalysis."*



Calculation for the enamine conformations was performed by Dr. Johnny Hioe. The enamine/DBU complex was spectroscopically characterized by Dr. Markus B. Schmid.

Michael M. Hammer, Johnny Hioe, Markus B. Schmid and Ruth M. Gschwind

## 6.1 "Late" conformational lock in enamine-electrophile complexes

### Introduction

Enamine catalysis by secondary amines is one of the most common concepts in organocatalysis.<sup>[1]</sup> Sparked by publications of List et al.<sup>[2]</sup> at the beginning of the century the catalysis of organic reactions by L-proline or proline-type organocatalysts experienced a renaissance. The number of publications providing ever so new synthetic applications is rising constantly. However, the number of studies dealing with the mechanistic underpinnings of such catalytic transformations is sparse, although those should provide information relevant and useful for the further development of catalytic concepts and synthetic protocols.<sup>[3]</sup> Here we present a concept to rationalize the mode of stereoinduction in enamine catalysis by L-proline or proline derived organocatalysts. *In situ* NMR experimental data show that no conformational lock allowing stereoinduction is present in the enamine intermediate themselves as long as no electrophile is present. Therefore we propose that successful stereoinductive conformational lock is adopted "late" through pre-complexation of the reactive intermediate with the partnering electrophile.

### Results and Discussion

**Investigated reaction type.** We focused our investigation on the electrophilic functionalization of aldehydes through enamine catalysis by proline. In this field we could stabilize and characterize a number of intermediates and make them accessible for further investigations.<sup>[4–6]</sup> This mode of stereoinduction in this reaction is matter of discussion for years,<sup>[1,7–11]</sup> with a commonality in a conformational lock in the enamine intermediate leading to stereoinduction in the transition state. The investigated reaction is presented in Fig. 6.1 **A**. After

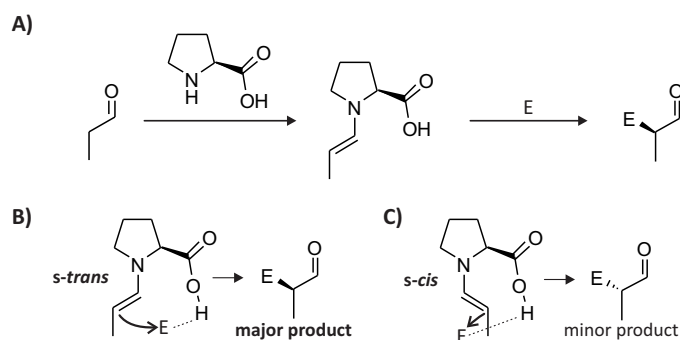


**Fig. 6.1:** **A)** Investigated model reaction. After condensation of the aldehyde with proline, the enamine intermediate is formed which then reacts with an electrophile and yields the enantiomeric product. **B)** List-Houk transition state models for both the *s-trans* and **C)** *s-cis* enamine with attack to the electrophile and corresponding product.<sup>[11,12]</sup> The hydrogen bond donor orients the electrophile on one side of the enamine and leads to stereoinduction.

condensation of the aldehyde with proline, the enamine intermediate is formed, which can itself react with an electrophile. After hydrolysis the enantiomeric rich  $\alpha$ -functionalized aldehyde and the organocatalyst proline is released. Enantiomeric excess of up to 99 % can be achieved in a variety of synthetic applications.<sup>[1,7-11]</sup>

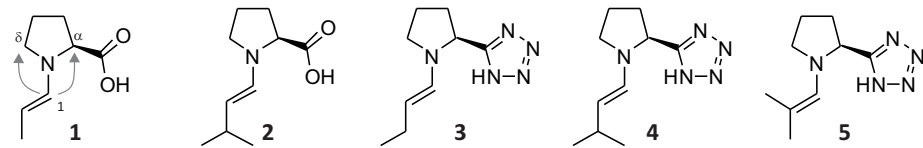
The proposed active List-Houk transition state models for the two major enamine conformers, *s-trans* and *s-cis* are presented in Fig. 6.1 **B** and **C**, respectively.<sup>[8,10,11]</sup> It is commonly accepted that the *s-trans* conformer constitutes the major conformer and is therefore responsible for the reaction outcome regarding stereoinduction.<sup>[4]</sup> To allow for this the conformation of the enamine intermediate needs to be locked in the *s-trans* conformation at the latest in the transition state to yield the observed stereo-product. To validate this theorem we investigated the conformational lock in enamine intermediates derived from proline and proline-tetrazole organocatalysts.<sup>[13,14]</sup>

**Lack of conformational lock in the enamine intermediate.** In order to address the issue of conformational space in enamine intermediates we used our experience in the stabilization of enamines that was demonstrated by the detection of the elusive proline enamine in 2010.<sup>[4]</sup> <sup>1</sup>H,<sup>1</sup>H-NOESY spectroscopy and the quantification of <sup>1</sup>H,<sup>1</sup>H-NOE cross peaks in comparison to theoretical structural data was used to access the conformational data within enamine intermediates of prolinols and prolinol-ethers and we could identify a strong conformational lock within these intermediates.<sup>[6]</sup> In the same manner we investigated the distribution of *s-cis* to *s-trans* enamines in solution for proline and proline-tetrazole derived enamine intermediates. (see Tab. 6.1). The selected enamines perform very well in synthetic protocols<sup>[13,15,16]</sup> and were accessible due to our recent studies.<sup>[4-6,17,18]</sup>

For proline enamine **1** a <sup>1</sup>H,<sup>1</sup>H-NOE crosspeak ratio of 49/51 translates to a 55 % *s-trans* enamine adoption. For the  $\beta$ -methylated proline enamine **2** the distribution is 50/50 *s-trans/s-cis* enamine evidenced by a 52/48 <sup>1</sup>H,<sup>1</sup>H-NOE crosspeak ratio. Proline-tetrazole enamine **3** gave a 50/50 distribution between both enamine conformers. Slightly more *s-cis* enamine is found for proline-tetrazole enamine **4** derived from  $\beta$ -substituted 3-methylbutanal with 56 %. Additionally for the  $\alpha$ -methylated proline-tetrazole enamine **5** a preference for *s-trans* enamine is identified by 62 %. this is striking since in our enamine studies using proline,  $\alpha$ -methylated aldehydes did yield mainly *s-cis* enamines, due to a steric repulsion of the  $\alpha$ -CH<sub>3</sub> with the pyrrolidine ring.

No conformational lock for either of the enamines could be experimentally observed. The  $\beta$ -methylation did not yield any more preference for *s-trans* enamine conformation, nor did  $\alpha$ -substitution lead to exclusive conformational lock as one might expect due to steric interactions. These findings strongly contradict the notion, that intermediate conformations translate into observable product outcome.

**Tab. 6.1:** Quantitative  $^1\text{H}, ^1\text{H}$ -NOE crosspeak intensities of the  $\text{H}_1\text{-H}_\alpha$  and  $\text{H}_1\text{-H}_\delta$  interaction for enamines **1-5** in  $\text{DMSO-d}_6$  at 300 K. The identified  $^1\text{H}, ^1\text{H}$ -NOE crosspeaks intensities were compared to theoretical calculations (see the coordinates of the corresponding structures below in section 6.1) and the corresponding *s-trans/s-cis* enamine distribution calculated according to Gschwind and co-workers.<sup>[6]</sup> The experimentally achieved *ee* values of the enamines in synthetic protocols describing  $\alpha$ -functionalization of aldehydes are also listed.<sup>[13,15,16]</sup>



enamine	NOE ( $1-\alpha$ ) <sup>a</sup>	$\sum$ NOE ( $1-\delta$ ) <sup>a</sup>	<i>s-trans</i> <sup>b</sup> / %	<i>s-cis</i> <sup>b</sup> / %	<i>ee</i> values
<b>1</b>	49	51	55	45	97 <sup>[15]</sup>
<b>2</b>	52	48	50	50	99 <sup>[15]</sup>
<b>3</b>	53	47	50	50	99 <sup>[13]</sup>
<b>4</b>	52	52	44	56	99 <sup>[13]</sup>
<b>5</b>	63	37	62	38	99 <sup>[16]</sup>

<sup>a</sup> Sum of NOE ( $1-\alpha + 1-\delta_1 + 1-\delta_2$ ) was set to 100.

<sup>b</sup> Calculated according to Gschwind et al.<sup>[6]</sup>

**Quantum chemical calculations on the enamine conformations.** Additionally to the experimental values we employed quantum chemical calculations on enamine species. We utilized gas phase MO62X/6-31+G(d,p) calculations<sup>a</sup> and assessed the enamine conformation regarding the N-C single bond. Assuming the validity of a Boltzmann distribution, from the  $\Delta G^{298}$  values we calculated the corresponding *s-trans/s-cis* enamine distribution (see Fig. 6.2).

For the experimentally already characterized **1** a  $\Delta G^{298}$  of  $0.49 \text{ kJ}\cdot\text{mol}^{-1}$  was identified corresponding to a distribution of 54 % *s-trans* and 46 % *s-cis* enamine conformation. For **2** a  $\Delta G^{298}$  value of  $1.92 \text{ kJ}\cdot\text{mol}^{-1}$  was found, corresponding to a favoring of *s-trans* conformation with 68 %. For isobutanal **6** the picture looks very different, since a  $\Delta G^{298}$  value of  $-3.64 \text{ kJ}\cdot\text{mol}^{-1}$  corresponds to a large excess of *s-cis* conformer with a 19/81 *s-trans/s-cis* distribution.

The found conformational distribution for **1** is in strong agreement with experimental results (*vide supra*). The preference for *s-trans* enamine conformation in the case of **2** is most likely connected to the minimized steric repulsion of the bulky  $\text{CH}_3$  group on the  $\beta$  carbon that is in the *s-trans* conformation oriented away from the bulky catalyst residue. In the case of **6** however, the strong preference for *s-cis* conformation might be explained by a destructive interaction of one of the  $\alpha$  methyl groups with the pyrrolidine  $\text{CH}_2$  group in the case of the *s-trans* conformer, while in the *s-cis* conformer more space is available to arrange the bulky  $\text{C}(\text{CH}_3)_2$  group. This quantum chemical finding is discrepantly found in experiments with a

<sup>a</sup>This functional demonstrated superior assessing a cost-to-gain analysis of intermediate calculation (see chapter 4). Although energies are most likely not being calculated accurately on a absolute scale, we feel confident that relative tendencies can be deduced.



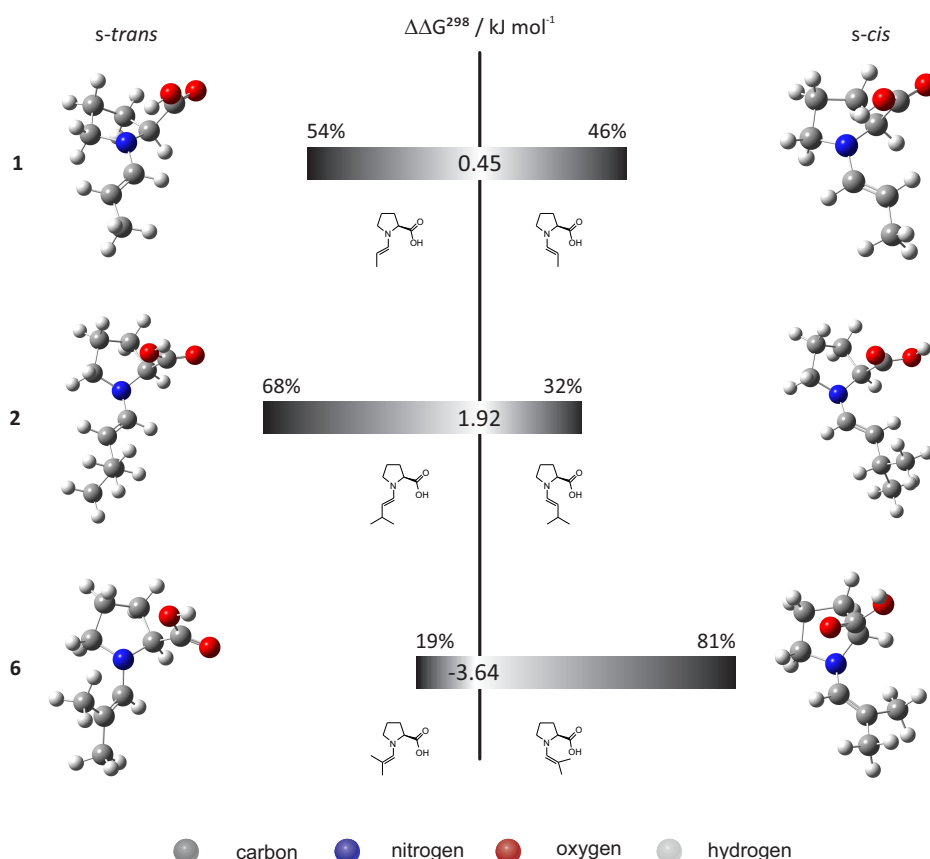


**Fig. 6.2:** Calculated Gibbs free energy difference ( $\Delta G_{s-cis/s-trans}^{298}$  in  $\text{kJ mol}^{-1}$ ) between the two lowest *s-trans*- and *s-cis*-enamine structures with resulting conformation distribution (Boltzmann distribution) calculated at a gas-phase MO62X/6-31+G(d,p) level of theory<sup>[19]</sup> for three differently substituted enamine species **1**, **2** and **6**.

proline-tetrazole catalyst (*vide supra*).

In summary we could provide evidence that, neither experimentally nor theoretically, a conformational lock in the enamine species is present that can explain the found enantiomeric excess in synthetic protocols.

Discrepancies are identified comparing experimental and quantum chemical calculations. For  $\alpha$ -methylated aldehydes the found conformational preferences differ significantly, with experiments on proline-tetrazoles showing an equal *s-trans*/*s-cis* distribution and quantum chemistry on proline enamines showing strong preference for *s-cis* conformation. Also for **2** the calculated and experimental structure differ significantly. These discrepancies most likely are due to the lack of solvent modeling employed in our study. This might be however vital, since in recent studies we could identify the hydrogen bond accepting properties of DMSO or DMF as crucial for the successful stabilization of enamines in solution.<sup>[4,5]</sup>

**Electrophile induced conformational lock.** We propose that not until the electrophile is present, a conformational lock according to the enantiomeric outcome of the reaction can be identified. We presume that, with no electrophile present, an almost free rotation of the

C-N bond in the enamines is active, which was evidenced by experimental findings (Fig 6.3 **A** and *vide supra*). However with an electrophile present, the rotational barrier should be much higher due to induced steric stress and no free rotation, or at least, less rotation should be present (Fig 6.3 **B**). Altogether the complexation of the electrophile should lead to the adoption of a conformational lock within the intermediate structure.

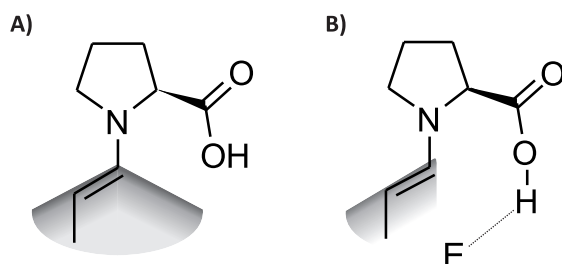


**Fig. 6.3:** Potentially occupied space (highlighted region) of the ene residue in enamine intermediates derived from L-proline. **A)** Without the presence of an electrophile. **B)** With the presence of an electrophile. The electrophile is coordinated to the carboxylic acid residue of the catalyst substructure and restricts rotation of the ene moiety thus inducing conformational restriction.

**The enamine-DBU complex.** To investigate and prove this concept, we needed to identify a proper model system. Since a reactive enamine-electrophile complex could not be stabilized as yet, a surrogate had to be identified to mimic the electrophilic part. In the study of co-catalysts in enamine catalysis by proline, DBU was investigated in detail.<sup>[20]</sup> The identified enamine **2**-DBU complex is evidencing specific NOE contacts compliant with the formation of an *s-trans* enamine with the DBU arranged at the proline carboxylic acid residue (see Fig. 6.4).<sup>[20]</sup>

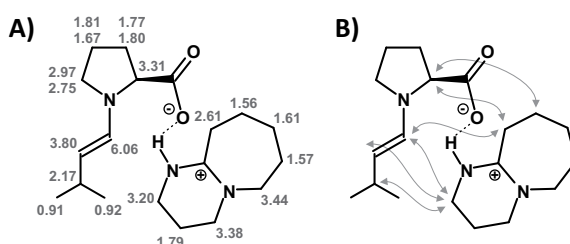
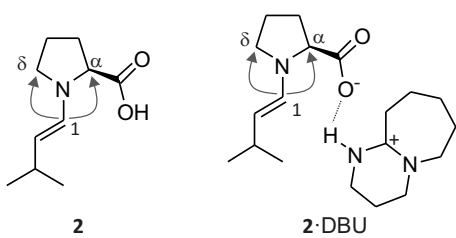


**Fig. 6.4:** **A)**  $^1\text{H}$ -resonances of the enaminecarboxylate/DBU complex in  $\text{DMSO-d}_6$  at 300 K. **B)** Identified  $^1\text{H}, ^1\text{H}$ -NOE contacts clarifying the arrangement of the DBU species at the carboxylic acid residue of the enamine species. *Note:* Data taken from Gschwind et al.<sup>[20]</sup>

This complex features all properties typically associated with an enamine-electrophile complex without exhibiting the same reactivity mostly due to steric shielding of the electrophilic center on the DBU moiety.  $^1\text{H}, ^1\text{H}$ -NOE quantification can provide further structural information of the enamine-DBU complex and deliver evidence for the adoption of a conformational lock within the enamine moiety. *S-trans/s-cis* enamine conformation distribution calculation as provided for the non-complexed enamines before, was also performed on the enamine-DBU complex (see Tab. 6.2).

**Tab. 6.2:** Comparison of quantitative  $^1\text{H}, ^1\text{H}$ -NOE contacts in system **2** with no coordination at the carboxylic acid residue and system **2**·DBU with coordination at the carboxylic acid residue, both at 300 K in  $\text{DMSO-d}_6$ . The coordination of the DBU molecule at the carboxylic acid residue leads to a restriction of rotation around the  $\text{N-C}_1$  bond and allows for conformational manifestation in the *s-trans* conformation.



enamine	NOE (1- $\alpha$ ) <sup>a</sup>	NOE (1- $\delta$ ) <sup>a</sup>	<i>s-trans</i> <sup>b</sup> / %
<b>2</b>	52	48	50
<b>2</b> ·DBU	71	28	70

<sup>a</sup> Sum of NOE (1- $\alpha$  + 1- $\delta$ 1 + 1- $\delta$ 2) was set to 100.

<sup>b</sup> Calculated according to Gschwind et al.<sup>[6]</sup>

Comparing the enamine **2** with the enamine DBU complex **2**·DBU, for the pure enamine a 50/50 distribution of *s-trans*/*s-cis* was found, while for the complex the  $^1\text{H}, ^1\text{H}$ -NOE ratios translate to a 71 % predominance of the *s-trans* enamine.

The predominance of *s-trans* enamine adoption is a strong indication for steric stress induced by the bulky DBU residue residing on the carboxylic acid residue of the proline enamine. No exclusive adoption of the enamine conformation is found, however this might be due to the lack of reactivity of the DBU towards the enamine. Since reactive electrophiles are expected to be more closely associated to the enamine moiety, more pronounced adoption of a conformational lock can be expected.

By a combination of experimental and quantum chemical data we could show that a lack of conformational lock in enamine intermediates is partially overcome by the formation of an enamine-electrophile complex. This complex does exhibit conformational preference beneficial for the stereoselective CC bond formation step.

### Additional remarks

**Additional enamine-electrophile complexes.** In the course of studying enamine-electrophile complexes towards conformational preferences we utilized different electrophiles and bases in  $\text{DMSO-d}_6$  to obtain more data. Besides common electrophiles like  $\text{N}_3^+$ , DEAD and Michler's hydrol, TBD was used to possibly obtain a further enamine-electrophile complex (see Fig. 6.5).

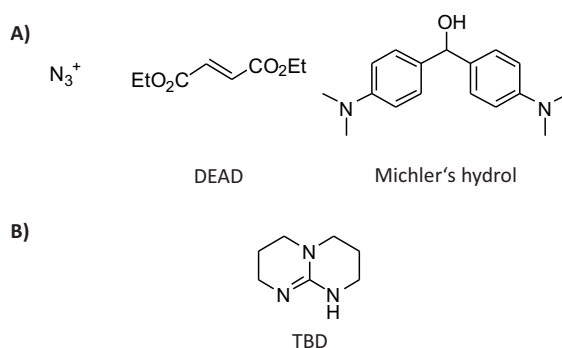


**Fig. 6.5:** **A)** Additionally investigated electrophiles towards the formation of enamine-electrophile complexes. **B)** Additionally investigated base as surrogate for the formation of enamine-electrophile complexes.

The additional electrophile screening did not yield detectable enamine-electrophile complexes, however a complete consumption of the enamines was detected. In the case of TBD base as electrophile surrogate comparable to DBU, also no complex was identified.

In summary, no further enamine-electrophile complex was identified, due to the reactivity of electrophiles and the absence of complexation in the case of TBD. This is a hint for the intricate importance of the hydrogen bond network allowing for the successful detection of a complex, which was serendipitously achieved in the case of DBU.

**Solvent choice.** In our enamine investigations we identified DMSO and DMF as the only choice to obtain enamines in solution and make them accessible to our spectroscopic studies.<sup>[4,5]</sup> This was largely attributed to the hydrogen bond accepting properties of these solvents. However, DMSO and DMF do not allow a broad temperature range, which might be useful to stabilize additional enamine-electrophile complexes. We suggest that more experiments should be designed towards the utilization of other solvents, which might allow the stabilization of enamines-electrophiles since maybe the electrophile itself can act as sufficient hydrogen bond acceptor to stabilize enamines in solution. To this end, solvents with an increased temperature range or even freons should be investigated to have access to enamine-electrophile complexes at low temperatures. High level structural information should allow to further shed light on our suggested "late" adoption of a conformational lock in reactive complexes.

## Outlook

In summary, we could provide first evidence for the lack of a conformational lock in enamine intermediates derived of proline or proline-type organocatalysts. This is surprising, since conformational pre-arrangement in the reactive enamine intermediate is believed to allow for the stereoinduction in the later experienced transition state. Findings, obtained by the spectroscopic characterization of an enamine-electrophile complex surrogate suggest that such a conformational lock occurs not until the electrophile is present. Thus "late" in the transition. Further studies have to be performed to shed more light on the suggested electrophile induced conformational lock, utilizing other enamine-electrophile surrogates or even develop an active enamine-electrophile complex that is accessible to our *in situ* NMR spectroscopic studies. Assuming however, that the suggestion of a "late" conformational lock in enamine catalysis is valid, structural features in intermediates do not directly affect stereochemical outcome. This is highly impacting on the way mechanistic studies are performed as yet, since often intermediate features are translated into reaction properties. However, this might not be true in some cases.

## Experimental details

Enamines were created *in situ* inside standard 5 mm NMR tubes by addition of freshly distilled aldehyde (25  $\mu$ mol) to a solution of organocatalyst (1 equiv.) and additive (as stated) in deuterated solvent (0.5 mL). All chemicals were used as purchased (if not otherwise stated). Chemicals were purchased from Sigma Aldrich and TCI Europe. NMR measurements were performed at 300-315 K on a Bruker Avance III HD 600 (600.13 MHz), a Bruker Avance DRX 600 (600.13 MHz) and a Bruker Avance III 600 (600.25 MHz) spectrometer, the latter equipped with a TCI cryoprobe with z-gradient (53.5 G cm<sup>-1</sup>). Reaction monitoring (*react*-NMR) by 1D <sup>1</sup>H-NMR spectra was employed to identify appropriate time slots for more detailed 2D NMR spectroscopic investigations. <sup>1</sup>H,<sup>1</sup>H-COSY, <sup>1</sup>H,<sup>1</sup>H-NOESY ( $t_m$ =450 ms), <sup>1</sup>H,<sup>13</sup>C-HSQC (<sup>1</sup> $J_{HC}$ =145 Hz) and <sup>1</sup>H,<sup>13</sup>C-HMBC (long range coupling 10 Hz) spectra were recorded for the characterization of the observed species if information from the 1D NMR spectra proved to be insufficient. All spectra were processed and evaluated with Bruker Topspin 3.2.

## Quantum chemical calculations

The geometries were optimized at MO62X/6-31+G(d,p) level of theory<sup>[19]</sup> The software used was Gaussian09 subversion D.01<sup>[21]</sup> for the geometry optimization and frequency analysis.

## Coordinates of stationary points

### *s-trans* enamine 1 in Fig. 6.2

```
1\1\GINC-PHOENIX\F0pt\RM062X\6-31+G(d,p)\C8H13N102\MHAINDL\11-Jan-2012
\0\#P M062X/6-31+G(d,p) opt scf=tight int=finegrid\Kommentar\0,1\0,
-1.7125042329,-0.991698329,-0.4316910886\H,-0.9163633725,-1.5484068054
,-0.3160946963\0,-2.2411733602,1.0796257775,0.2053374286\H,2.106141784
4,-1.6460817472,-0.7243512472\H,0.1846091324,2.1169372184,-0.320506646
1\H,2.7644503802,-0.6105280227,0.5623415114\C,1.8983858985,-0.77135641
21,-0.1002082412\C,-0.0670877854,0.2709055175,0.8317429339\H,0.9518718
131,0.2460993918,-1.7626161117\C,-1.4544568361,0.1690377036,0.17757079
89\C,0.7961213189,1.3260971113,0.1173370405\N,0.6869872082,-0.98396232
34,0.6970697882\H,-0.2364361293,0.5357228224,1.8809421116\C,1.58077112
92,0.4904759233,-0.8991286496\H,1.4832852266,1.7780491452,0.8392970125
\H,2.4804250615,0.9907206143,-1.2629981763\C,0.7492813574,-1.847905691
4,1.7984327879\C,1.7298998348,-2.719443303,2.0656328676\H,-0.125388380
1,-1.7943909023,2.4461747867\C,1.6951003249,-3.6565012343,3.2383169853
\H,2.5925490282,-2.7804010733,1.4058769126\H,1.6998107091,-4.702777600
9,2.9142626785\H,0.7979564517,-3.4970205925,3.8433520551\H,2.567367447
4,-3.5153045076,3.8849979277\Version=AM64L-G09RevA.02\State=1-A\HF=-5
17.6779863\RMSD=2.424e-09\RMSF=4.413e-06\Dipole=1.9208207,-0.4953599,0
.2665251\Quadrupole=-6.0929094,1.8723161,4.2205933,4.9399619,-4.587034
,-0.4532333\PG=C01 [X(C8H13N102)]\@
```

### *s-cis* enamine 1 in Fig. 6.2

```
1\1\GINC-PHOENIX\F0pt\RM062X\6-31+G(d,p)\C8H13N102\MHAINDL\12-Jan-2012
\0\#P M062X/6-31+G(d,p) opt scf=tight int=finegrid\Kommentar\0,1\C,
-0.6142320982,0.1558435917,-0.6151691239\C,-1.9289213831,-0.5873906749
,-0.942306908\C,-2.0315559329,-1.6457430999,0.162145365\C,-0.573362569
1,-2.0451516799,0.3566934555\N,0.1255894227,-0.7581754349,0.2538706093
\C,1.5260833109,-0.7631203881,0.2038873068\H,1.9710853773,-1.653652704
3,0.6461669445\C,-0.8896752104,1.499921842,0.0721627973\0,-1.365122718
2,2.4341594091,-0.5195185104\C,2.3092599675,0.215635589,-0.2674179168\
C,3.8086740919,0.1519972341,-0.2311375046\0,-0.5964498757,1.54720776,1
.3755940619\H,-0.0535871912,0.383730694,-1.5306208792\H,-2.7793513189,
0.0949357782,-0.9916143069\H,-1.829201423,-1.0753643737,-1.9162382613\
H,-2.4238106915,-1.2044725062,1.0848917556\H,-2.6668974543,-2.48960438
69,-0.1139997893\H,-0.3703982122,-2.5092990577,1.3261876704\H,-0.24948
20478,-2.7371995117,-0.4367052574\H,1.8644475213,1.1195435665,-0.68000
64228\H,-0.2078995591,0.6820956701,1.6097639601\H,4.1531688912,-0.7908
24738,0.2036132289\H,4.2346285335,0.2352674998,-1.2363779901\H,4.22622
85694,0.9710029216,0.3641347155\Version=AM64L-G09RevA.02\State=1-A\HF
=-517.6779128\RMSD=3.798e-09\RMSF=9.149e-06\Dipole=0.398376,-2.1063111
,0.0129175\Quadrupole=3.5348972,-4.8080379,1.2731406,5.8359553,0.18344
3,-1.0601389\PG=C01 [X(C8H13N102)]\@
```

**s-trans enamine 2 in Fig. 6.2**

```

1\1\GINC-WORKER\FOpt\RM062X\6-31+G(d,p)\C10H17N102\JHIOE\10-Mar-2015\0
\# opt 6-31+g(d,p) geom=connectivity m062x\Title Card Required\0,1\
C,2.7776772656,1.1348732665,-0.4759219601\C,2.2245923957,1.7697821753,
0.8125268723\C,0.6967441167,1.5816108706,0.7260769372\C,1.7285143325,0
.0686066587,-0.8305497688\H,2.8008903182,1.8647776859,-1.2895899878\H,
3.781180565,0.718725865,-0.3584566192\H,0.3026929654,1.1189814813,1.64
29228881\H,0.1562633795,2.5219456595,0.5621226739\N,0.4960209541,0.702
0188542,-0.4181887458\C,-0.7192993282,0.0697035778,-0.6164567004\H,-0.
7087456886,-0.653376042,-1.4330348135\C,-1.8582578108,0.2996630357,0.0
550430956\H,-1.8775992123,1.0244681168,0.869128734\C,-3.161547978,-0.3
810184018,-0.267922904\H,-2.9817288705,-1.0889446036,-1.0890923555\C,-
4.2134803055,0.6347283561,-0.7306053385\H,-3.8749022648,1.1749078029,-
1.6191650515\H,-5.163427475,0.141290678,-0.9629716184\H,-4.4028271117,
1.3714678472,0.0592657051\C,-3.6793345676,-1.1695507821,0.9411055461\H
,-2.9560578812,-1.9274606721,1.2548261119\H,-3.8501057766,-0.495446912
1,1.7891451018\H,-4.6284016551,-1.6659109013,0.7118354485\H,1.71639198
6,-0.1660480989,-1.8993081494\C,2.0267685931,-1.2458138684,-0.11528189
01\0,1.6748077624,-1.2143366868,1.1857005391\0,2.5408312797,-2.2080891
952,-0.6300117086\H,2.5080051124,2.8207872668,0.8992052571\H,2.6116400
981,1.2444804285,1.6886087012\H,1.8986423513,-2.0774113623,1.567187119
7\Version=ES64L-G09RevD.01\State=1-A\HF=-596.2694075\RMSD=6.175e-09\R
MSF=1.370e-05\Dipole=0.2518471,0.5681194,0.4882276\Quadrupole=-0.56626
1,-0.9403323,1.5065932,5.0865208,2.8290419,-2.3511554\PG=C01 [X(C10H17
N102)]\@

```

**s-cis enamine 2 in Fig. 6.2**

```

1\1\GINC-WORKER\FOpt\RM062X\6-31+G(d,p)\C10H17N102\JHIOE\10-Mar-2015\0
\# opt 6-31+g(d,p) geom=connectivity m062x\Title Card Required\0,1\
C,2.7360542016,1.2353682057,-0.4268843142\C,2.2122685405,1.6424519593,
0.9579944009\C,0.6817756953,1.5946960261,0.8134515014\C,1.6802813528,0
.2214304215,-0.9000806345\H,2.7286704755,2.0843188587,-1.1166998298\H,
3.7457034512,0.8171096991,-0.4036807945\H,0.214987316,1.1447466652,1.6
973077978\H,0.2510088444,2.592900371,0.6635530226\N,0.4587725141,0.771
0976191,-0.3783257853\C,-0.7490546396,0.137321845,-0.6010395949\H,-1.5
80153354,0.5799798126,-0.0531979798\C,-0.9715932108,-0.9060383836,-1.4
169108949\H,-0.1483290952,-1.3634422992,-1.9689195823\C,-2.3342439101,
-1.5061257229,-1.6395818428\H,-3.0490414364,-0.9665685221,-1.002443687
1\C,-2.3520520475,-2.9854312396,-1.2369071466\H,-2.0720391974,-3.11028
20122,-0.1872548823\H,-3.3439430277,-3.4243671366,-1.3900004914\H,-1.6
377522397,-3.5523218996,-1.8462653723\C,-2.777244542,-1.3457346986,-3.
0991857386\H,-2.8092678013,-0.2911432808,-3.387046756\H,-2.074099326,-
1.8561329508,-3.7684104411\H,-3.7692277072,-1.7816498171,-3.2609020594
\H,1.6438228902,0.1285853107,-1.990886494\C,1.9903016234,-1.1509513946

```



```
, -0.301510915\0, 1.752431181, -1.4784957223, 0.8341791242\0, 2.6264013511,
-1.9533994746, -1.1779837098\H, 2.8248011705, -2.7855943804, -0.7205821583
\H, 2.5710420474, 2.6267591492, 1.2665458379\H, 2.5320705797, 0.9099053921,
1.70304767\\Version=ES64L-G09RevD.01\State=1-A\HF=-596.2695869\RMSD=3.
892e-09\RMSF=6.927e-06\Dipole=0.5348665, 0.4382894, -0.0500718\Quadrupole=
2.2355222, 2.6377911, -4.8733133, -0.3139126, -0.953684, 3.1321348\PG=C01
[X(C10H17N102)]\\@
```

### ***s-trans* enamine 6 in Fig. 6.2**

```
1\1\GINC-LOGIN\F0pt\RM062X\6-31+G(d,p)\C9H15N102\JHIOE\11-Mar-2015\0\\
# opt 6-31+g(d,p) geom=connectivity m062x freq\\Title Card Required\\0
, 1\C, 2.0541927301, 1.3060048311, -0.1686448838\C, 1.2173584839, 2.08951566
36, 0.8490452569\C, -0.2080693209, 1.7675926198, 0.4147379309\C, 1.22558486
94, 0.0277553042, -0.4165817728\H, -0.938605047, 1.9086559925, 1.2156983915
\H, -0.5156952985, 2.3924807096, -0.4406633098\N, -0.1249540055, 0.35505037
96, 0.0268996198\C, -1.1903989728, -0.2241629539, -0.687335228\H, -0.961429
1364, -0.5418649587, -1.7086401975\C, -2.4278118031, -0.3903794856, -0.1988
883758\H, 1.2429282111, -0.2746389627, -1.4719635867\C, 1.7658272161, -1.16
76022927, 0.3529706811\0, 1.840547057, -0.9372670613, 1.6789640528\0, 2.112
5515184, -2.2110077109, -0.1446199396\C, -3.5377509166, -0.9158448038, -1.0
662991968\H, -3.9783816862, -1.8177383968, -0.6252264672\H, -4.3455196603,
-0.1799537815, -1.1611748481\H, -3.1845471015, -1.1601661163, -2.071715673
6\C, -2.7749303334, -0.0673297078, 1.2287055871\H, -1.8806509415, -0.081620
607, 1.8582981496\H, -3.2462477873, 0.9200917659, 1.3202838096\H, -3.489698
1087, -0.7996953654, 1.6190346968\H, 1.429593391, 3.1610851402, 0.834308135
2\H, 1.3936869211, 1.7053153878, 1.8577055622\H, 3.0686991895, 1.0917353109
, 0.1756382901\H, 2.1257242255, 1.865292638, -1.1066641848\H, 2.1873812567,
-1.7435338489, 2.0900662111\\Version=ES64L-G09RevD.01\State=1-A\HF=-556
.9699636\RMSD=7.884e-09\RMSF=3.648e-06\Dipole=-0.0920448, 0.9126563, 0.3
324273\Quadrupole=1.0425783, -2.5487812, 1.5062029, 3.4111128, 2.1707459, -
3.2663705\PG=C01 [X(C9H15N102)]\\@
```

### ***s-cis* enamine 6 in Fig. 6.2**

```
1\1\GINC-WORKER\F0pt\RM062X\6-31+G(d,p)\C9H15N102\JHIOE\11-Mar-2015\0\\
\# opt 6-31+g(d,p) geom=connectivity m062x\\Title Card Required\\0, 1\C
, 2.2964354641, 1.1916994356, -0.5496934162\C, 1.4133992275, 2.1150418826, 0
.3040369074\C, -0.0261003259, 1.766740283, -0.1197756597\C, 1.4050309512, -
0.0477139832, -0.7230194961\H, -0.6659068828, 1.6064895593, 0.7589984794\H
, -0.4819762253, 2.5515936533, -0.7333897401\N, 0.0898356867, 0.5339316913,
-0.9104903197\C, -1.0264977424, -0.3283961505, -0.9190825327\H, -1.7020139
508, -0.2382821608, -0.0651554102\C, -1.2700841108, -1.2348565204, -1.87618
69554\H, 1.7077228865, -0.661585184, -1.5768694804\C, 1.4880043002, -0.9041
48151, 0.5360340061\0, 0.7762828534, -0.7916990076, 1.5042241155\0, 2.49930
85022, -1.7939123122, 0.4745998693\H, 2.5206648875, -2.269194914, 1.3198381
205\C, -2.4261909407, -2.1893612655, -1.7610213344\H, -3.0927977982, -2.097
0929061, -2.6267246971\H, -2.0762971464, -3.2286874982, -1.7377184393\H, -3
```

.0085567183,-2.0094059735,-0.8535857302\C,-0.4086515008,-1.3604808888,  
-3.1027848557\H,0.1485395531,-0.436701448,-3.2826736692\H,0.3094875135  
, -2.1865357431,-3.0124207235\H,-1.0270894916,-1.5729621377,-3.98162649  
01\H,1.6512624676,3.1699423232,0.1524495403\H,1.5518658942,1.886645506  
9,1.3641250582\H,3.2606944299,0.9607470286,-0.0901438179\H,2.475410146  
7,1.6222388508,-1.5389749991\\Version=ES64L-G09RevD.01\State=1-A\HF=-5  
56.9723192\RMSD=3.161e-09\RMSF=8.964e-06\Dipole=0.5486135,0.0428632,-0  
.1325067\Quadrupole=0.3923759,2.382744,-2.7751199,0.4129281,2.1111381,  
-0.1632633\PG=C01 [X(C9H15N102)]\@

## 6.2 References

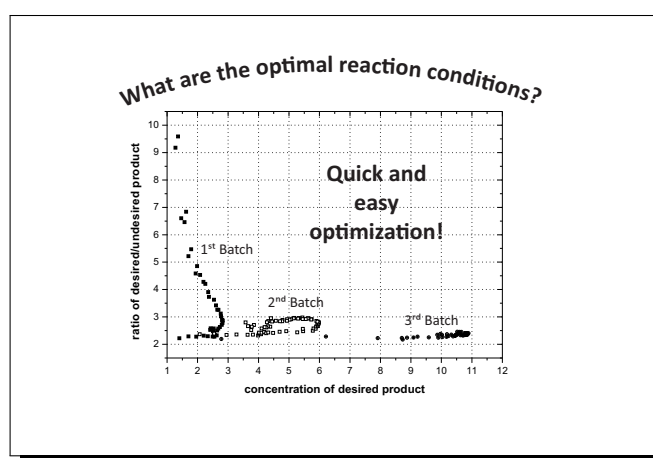
- [1] P. Pihko, I. Majander, A. Erkkilä, *Asymmetric Organocatalysis* **2009**, 291, 29–74.
- [2] B. List, *Chem. Commun.* **2006**, 819–824.
- [3] M. C. Holland, R. Gilmour, *Angew. Chem. Int. Ed.* **2015**, 54, 3862–3871.
- [4] M. B. Schmid, K. Zeitler, R. M. Gschwind, *Angew. Chem. Int. Ed.* **2010**, 49, 4997–5003.
- [5] M. B. Schmid, K. Zeitler, R. M. Gschwind, *J. Org. Chem.* **2011**, 76, 3005–3015.
- [6] M. B. Schmid, K. Zeitler, R. M. Gschwind, *Chem. Sci.* **2011**, 2, 1793–1803.
- [7] A. K. Sharma, R. B. Sunoj, *Chem. Commun.* **2011**, 47, 5759–5761.
- [8] S. Bahmanyar, K. N. Houk, L. Angeles, Others, *J. Am. Chem. Soc.* **2001**, 123, 11273–11283.
- [9] A. K. Sharma, R. B. Sunoj, *Angew. Chem.* **2010**, 122, 6517–6521.
- [10] L. Hoang, S. Bahmanyar, K. N. Houk, B. List, *J. Am. Chem. Soc.* **2003**, 125, 16–17.
- [11] S. Bahmanyar, K. N. Houk, L. Angeles, *J. Am. Chem. Soc.* **2001**, 123, 12911–12912.
- [12] S. Bahmanyar, K. N. Houk, H. J. Martin, B. List, *J. Am. Chem. Soc.* **2003**, 125, 2475–2479.
- [13] A. J. A. Cobb, D. a. Longbottom, D. M. Shaw, S. V. Ley, *Chem. Commun.* **2004**, 44, 1808–1809.
- [14] A. J. A. Cobb, D. M. Shaw, D. A. Longbottom, J. B. Gold, S. V. Ley, *Org. Biomol. Chem.* **2005**, 3, 84–96.
- [15] A. B. Northrup, D. W. C. MacMillan, *J. Am. Chem. Soc.* **2002**, 124, 6798–6799.
- [16] A. Hartikka, P. I. Arvidsson, *Eur. J. Org. Chem.* **2005**, 2005, 4287–4295.
- [17] M. B. Schmid, K. Zeitler, R. M. Gschwind, *J. Am. Chem. Soc.* **2011**, 133, 7065–7074.
- [18] M. H. Haindl, M. B. Schmid, K. Zeitler, R. M. Gschwind, *RSC Advances* **2012**, 2, 5941–5943.
- [19] Y. Zhao, D. G. Truhlar, *Theor. Chem. Acc.* **2008**, 120, 215–241.
- [20] M. B. Schmid, K. Zeitler, R. M. Gschwind, *Chem. - A Eur. J.* **2012**, 18, 3362–3370.
- [21] M. J. Frisch, G. W. Trucks, H. B. Schlegel, G. E. Scuseria, M. A. Robb, J. R. Cheeseman, G. Scalmani, V. Barone, B. Mennucci, G. A. Petersson, H. Nakatsuji, M. Caricato, X. Li, H. P. Hratchian, A. F. Izmaylov, J. Bloino, G. Zheng, J. L. Sonnenberg, M. Hada, M. Ehara, K. Toyota, R. Fukuda, J. Hasegawa, M. Ishida, T. Nakajima, Y. Honda, O. Kitao, H. Nakai, T. Vreven, J. A. Montgomery, Jr., J. E. Peralta, F. Ogliaro, M. Bearpark, J. J. Heyd, E. Brothers, K. N. Kudin, V. N. Staroverov, R. Kobayashi, J. Normand, K. Raghavachari, A. Rendell, J. C. Burant, S. S. Iyengar, J. Tomasi, M. Cossi, N. Rega, J. M. Millam, M. Klene, J. E. Knox, J. B. Cross, V. Bakken, C. Adamo, J. Jaramillo,

R. Gomperts, R. E. Stratmann, O. Yazyev, A. J. Austin, R. Cammi, C. Pomelli, J. W. Ochterski, R. L. Martin, K. Morokuma, V. G. Zakrzewski, G. A. Voth, P. Salvador, J. J. Dannenberg, S. Dapprich, A. D. Daniels, . Farkas, J. B. Foresman, J. V. Ortiz, J. Cioslowski, D. J. Fox, *Gaussian 09 Revision D.01*, Gaussian Inc. Wallingford CT 2009.

## 7 Kinetic data visualization for the easy, quick and straightforward reaction condition optimization.

Letter - application

***"Kinetic data visualization for the easy, quick and straightforward reaction condition optimization."***



Dr. Markus B. Schmid performed the aldol reaction with L-proline.

Michael M. Hammer, Markus B. Schmid and Ruth M. Gschwind

## 7.1 Manuscript

### Introduction

The optimization of reaction conditions in a chemical laboratory is one of the most tedious and time consuming tasks. Systematic approaches differ from laboratory to laboratory. Recently a number of statistical approaches have been developed to help quicken up the reaction optimization process and to reduce the number of experiments necessary to obtain a complete picture of the condition-outcome space called Design of Experiments (DOE).<sup>[1–4]</sup> This computer based approach was able to minimize the number of experiments needed by a significant amount. Besides this, high throughput screening<sup>[5,6]</sup> and optimization loops in flow chemistry<sup>[7]</sup> have been very successful, albeit they largely rely on automated approaches to produce viable outcomes. Often times also pure serendipity is a major contributing factor.<sup>[8]</sup> These approaches however are commonly decoupled from the experience of the scientist and do not rely fully on human input.

In our recent studies concerning especially enamine catalysis,<sup>[9–12]</sup> we were faced with an enormous amount of kinetic profiles. Assessing these kinetic profiles turned out to be an extremely difficult task that required experience in assessment and interpretation of the data. In recent years the amount of reports utilizing kinetic data by means of NMR spectroscopy

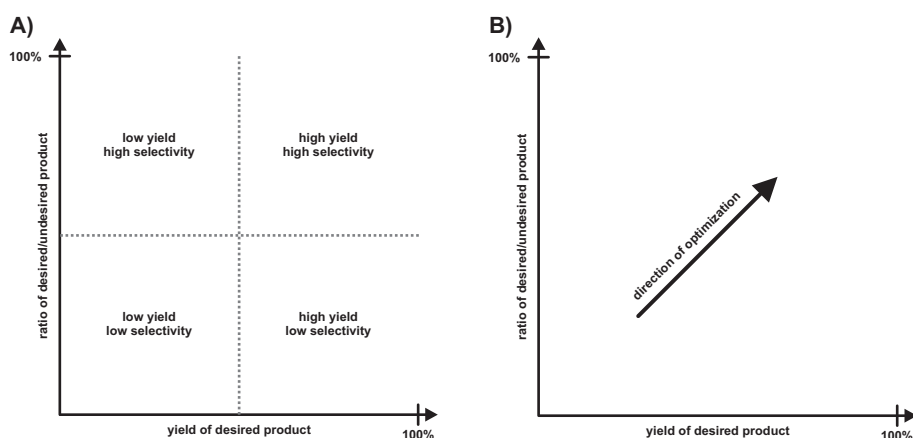


**Fig. 7.1:** **A)** Four regions that can be identified in the reaction-optimization plot. **B)** The desired direction of optimization. *Note:* Borders between the regions are not strict but rather fluent and undefined.

or any other spectroscopic method to describe reactions or reaction mechanisms is rising rapidly.<sup>[13–15]</sup> In this paper we present a new plot (see Fig. 7.1 **A**) for the quick and easy visualization of reaction conditions' impact to assess and optimize competitive chemical reaction conditions straightforwardly. No additional information that is not already incorporated in the collected kinetic data is needed. Plotting the ratio of desired over undesired compound as a function of the amount of formed desired product leads to a very handy and ostensive representation which allows the adjustment of reaction conditions proactively and optimization success can be monitored very easily (see Fig. 7.1 **B**). Temporal information is not lost but

indirectly accessible affording non-mismatched kinetic profiles at differing reaction conditions within one plot.

## Results and Discussion

**The layout.** After the collection of kinetic data with different reaction conditions for a reaction with competing reaction outcomes the new plot can be prepared. Just the amount of desired product and of the side product(s) is necessary to obtain the new plot. Next the time information is eliminated and the ratio of desired/undesired outcome (the undesired outcome can also be consisting of a sum) is plotted as a function of the amount of desired reaction outcome. Temporal information is not lost in this plot, it is merely only indirectly accessible since every point on the plot is associated with a specific time-stamp. This can be visualized by, for example, colored progression.

A schematic representation of such a reaction optimization plot is given in Fig. 7.1 **A** and shows four distinct regions. The regions are that of high yield with high selectivity (desired region), high yield with low selectivity, low yield with low selectivity and low yield with high selectivity. These regions do not possess strict borders, they are to be considered fluent and mostly undefined. The desired direction of reaction optimization is presented in Fig. 7.1 **B** and obviously is pointing in the direction of high yield with high selectivity.

**The preparation and benefits.** To highlight the new plots benefits without the emphasis on the presented chemical reaction we applied it on an anonymized example (see Fig. 7.2 **A**). Kinetic data for a number of different reaction conditions (I-IV, obtained here by *in situ*-NMR spectroscopy) yields four kinetic profiles (Fig. 7.2 **B**). For the preparation of the new plot type, the time information is eliminated from the kinetic data and the ratio of desired ( $P_1$ )/undesired product ( $P_2$ ) is plotted as a function of formed desired product ( $P_1$ ) amount (Fig. 7.2 **C**). In addition, the temporal information is indirectly accessible, here through the color-coding. In the new plot all reaction conditions are combined into one visualization. This is not so in traditional kinetic data representations, which is the main reason, different profiles are so hard to compare, since scaling mismatch is observed often. This is an entirely different concept to traditional kinetic profile presentation, since often time the time axis as well as the ordinate differ significantly for the conditions and thus commonly scaling mismatch occurs and hampers the ability to compare the profiles easily.

Comparing the kinetic profiles in Fig. 7.2 **A** an experienced chemist could easily deduce that condition I stands out from conditions II-IV, since an almost parallel progression is observed for both  $P_1$  and  $P_2$ . Distinguishing conditions II-IV is however not as easy and although in this example no scaling mismatch is occurring (ordinate and time axis are equal), since the profiles look rather similar. Assessing the new plot in Fig. 7.2 **B** again condition I is easily deduced to stand out from the rest, here however it is also easy to swiftly assess the differences for conditions II-IV. In this example the selectivity for the desired product is heavily impacted and

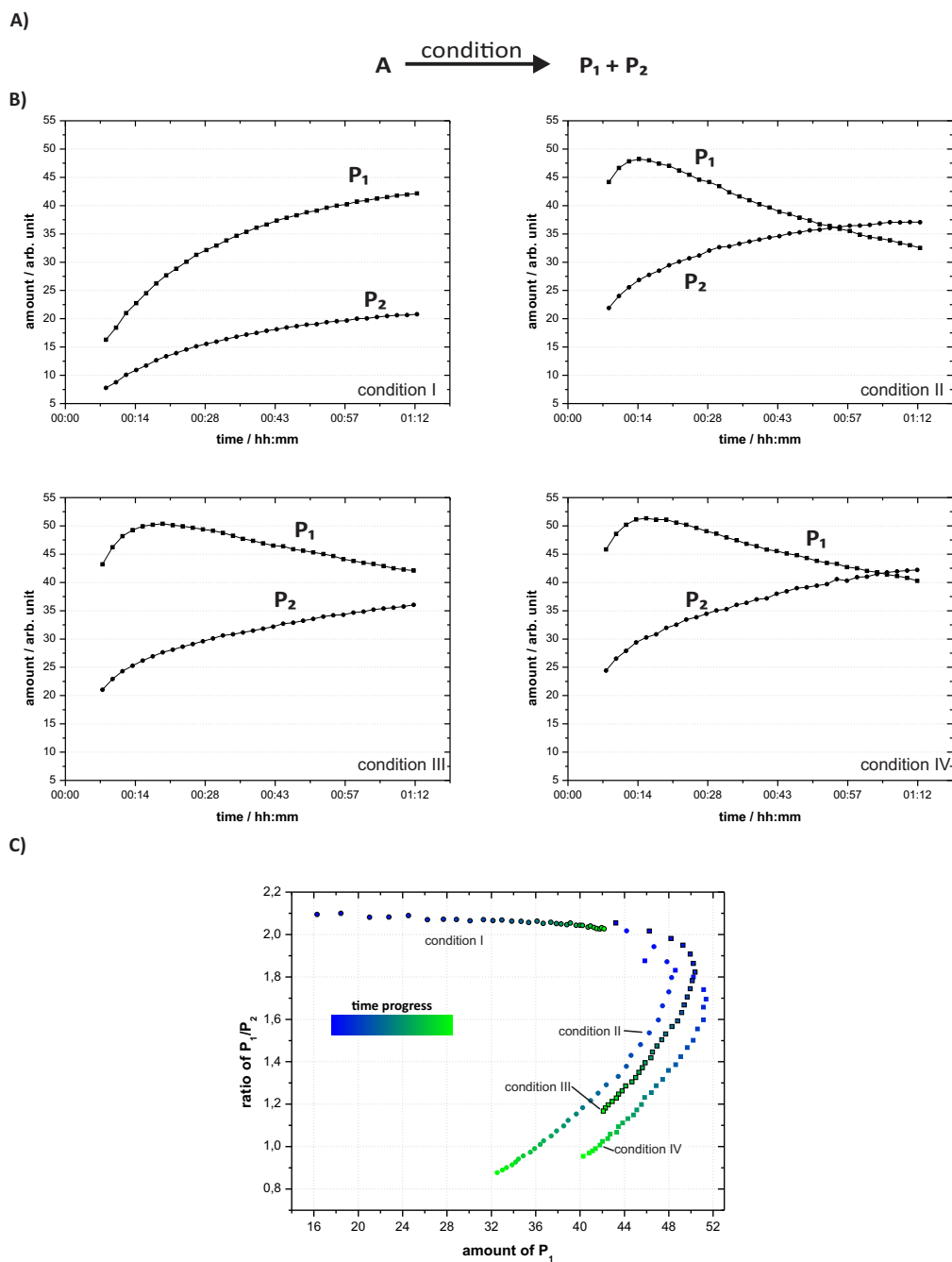


**Fig. 7.2:** **A)** Reaction scheme of the anonymized reaction. **B)** Reaction profiles at four different conditions (I-IV) in a traditional kinetic fashion. **B)** New plot type for the same reaction and reaction conditions (I-IV) as in **B** with incorporation of time information.



diminishing for conditions II-IV, however with condition IV yielding the highest amounts of desired product  $P_1$ .

This anonymized presentation demonstrates that expert knowledge is not needed to quickly and easily assess the impact of differing conditions on reaction outcome. Having only indirect access to temporal information and thus eliminating scaling mismatch to combine all kinetic profiles into one visualization helps to compare otherwise almost indistinguishable reaction results. The temporal information that is encoded into any point on the plot can then be retraced by looking into the data and the optimal reaction conditions including time can be obtained easily.

In summary, the preparation of the new plot can be achieved using the kinetic data already provided in traditional kinetic profile investigation. In addition, the new plot benefits from omitting temporal information to obtain a single representation for different conditions' impact without the difficulty of scaling mismatch. The temporal information is however not lost, rather every point on the plot is intricately connected to a single reaction time and thus this information can be retrieved by assessing associated time in the original data.

**Application of the reaction optimization plot.** Next we would like to apply the new plot on two examples to demonstrate the versatility and practicality. For this purpose we applied the new plot first on the investigation of *E/Z*-distributions in dienamine catalysis and secondly on the optimization of the aldol condensation/addition reaction of linear aldehydes with proline.

**The new plot type utilized in reaction mechanism investigations.** The vinylogous concept of the archetypical enamine catalysis,<sup>[16]</sup> dienamine activation,<sup>[17-21]</sup> was a matter of investigation in this thesis before (see chapter 2 and chapter 3). In this context the ratio of *3Z/3E*-dienamine was investigated thoroughly. This *3Z/3E*-dienamine ratio was suspected to impact the stereochemical outcome of the reaction significantly. Especially the *3Z*-dienamine was categorized to be productive towards the enantiopure product, thus the *3Z*-dienamine was selected to be the "desired" reaction outcome for our new plot. In order to obtain information of this ratio, kinetic profiles (Fig. 7.3 **B-D**) for the formation of dienamine intermediates from  $\alpha,\beta$ -unsaturated aldehydes in toluene- $d_8$  at 313.15 K (for **c**) and DMSO- $d_6$  at 300 K (for **a** and **b**) as a function of secondary amine catalyst (100 mol% of **a-c**, Fig. 7.3 **A**) were collected by *in situ* NMR spectroscopy.

Assessing the kinetic profiles for the *3E*- and *3Z*-dienamine, for every catalyst **a-c** the amount of formed desired *3Z*-dienamine is higher than *3E*-dienamine. The amount of *3E*- as well as *3Z*-dienamine is highly dependent on the employed catalyst. While for **b** and **a** the amount of *3E*-dienamine (Fig. 7.3 **D**) reaches approx. 30 % and approx. 40 %, respectively, for **c** a relative amount of only 5 % is reached after 17 hours. For *3Z*-dienamines (Fig. 7.3 **C**) the absolute amounts are higher, however the trend is comparable. For **a** and **b**, approx. 60 %

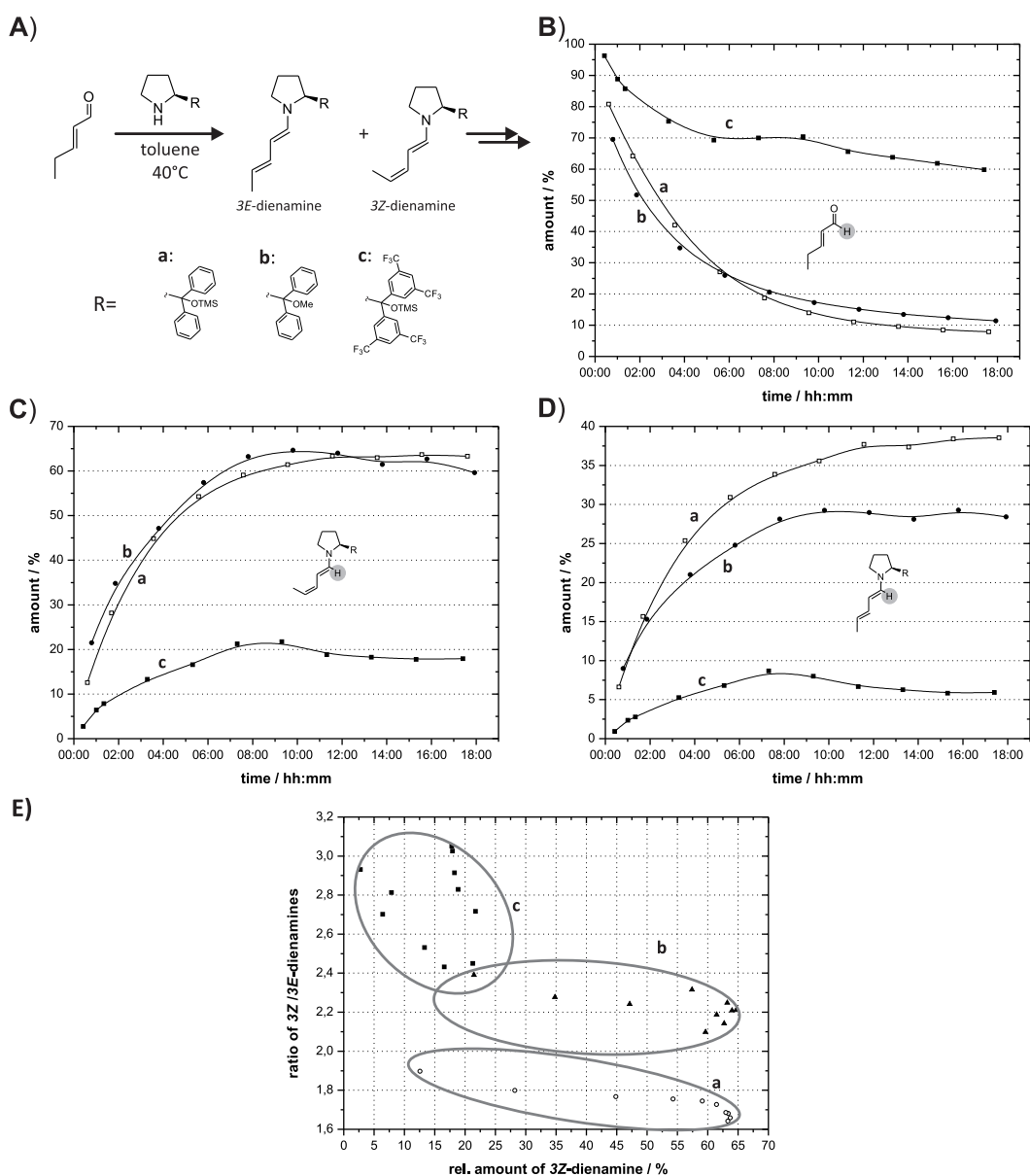


**Fig. 7.3:** **A** 3*Z*- and 3*E*-dienamine formation from  $\alpha,\beta$ -unsaturated aldehydes catalyzed by secondary amine catalysts **a-c**. Kinetic profiles for the aldehyde (**B**), 3*Z*-dienamine (**C**) and 3*E*-dienamine (**D**). **E** Combined new plot for the selectivity and reactivity for the dienamine intermediates. *Note:* The reaction was carried out at 300K in DMSO- $d_6$  at 100 mol% catalyst loading for **a** and **b** and at 313.15K in toluene- $d_8$  for **c**.

and for **c** approx. 20 % are reached after 17 hours of reaction. There kinetic profile show that the reaction is more productive towards the 3Z-dienamine independent of the employed catalyst, however the selectivity as a function of catalyst is not easily accessible through these kinetic profiles.

In the new plot (Fig. 7.3 **E**), the higher reactivity towards 3Z-dienamine for **a** and **b** is clearly also visible (further right on the plot), however here for the first time, the selectivity as a function of organocatalyst becomes apparent. This selectivity is highest for **c** with ratios of 2.4-3:1 compared to almost constant 2.1-2.4:1 for **b** and 1.6-1.9:1 for **a**. This catalyst dependent selectivity information is also embedded in the traditional kinetic profiles, yet is by far not as easily accessible as in the new plot. It is also noteworthy that temporal information does not provide any additional information in the presented example and thus excluding it did not constitute any loss of information.

The information on reactivity/selectivity relations for the catalysts within the new plot helped largely in the interpretation and understanding of the underlying mechanism in dienamine activation (see chapter 3).

**The new plot type used in the reaction optimization of the competitive aldol condensation/addition reaction.** The aldol reaction of linear aldehydes was investigated recently by us in extensive detail and we were faced with an enormous amount of kinetic profiles for various different reaction conditions.<sup>[9,11,22]</sup>

The aldol reaction is a typical competitive chemical reaction where the aldol addition pathway competes with the aldol condensation pathway,<sup>[11]</sup> and the optimization to either the condensed product or any of the two addition products (*anti* and *syn*) can be very tedious. In this example we demonstrate how the new visualization can help to quicken up and ease this process to a large extent. For this example, the *anti*-product was defined as the desired reaction product, however any other choice would lead to comparable representation. The aldol reaction was performed using L-proline and a proline-tetrazole catalyst in DMSO- $d_6$  at room temperature.<sup>[23,24]</sup> We were interested in what way the catalyst loading influences the selectivity towards the *anti*-product and the reactivity for aldol addition in contrast to aldol condensation. The results of the *in situ* NMR spectroscopic kinetic investigation is presented for both catalysts at catalyst loadings ranging from 10-100 mol% in Fig. 7.4.

For the proline-tetrazole catalyzed selfaldolization of propanol (Fig. 7.4 **A**) the kinetic profiles translate into a reaction optimization plot evidencing a reach of 15 % yield of *anti*-product in the case of 50 mol% catalyst loading with a varying diastereomeric ratio (dr) of 2.5:1 to 1.1:1. For 100 mol% catalyst loading a yield of *anti*-product of only 7 % was achieved accompanied with a dr of 3:1 to 1:1. For the L-proline case (Fig. 7.4 **B**) the 100 mol% and 50 mol% catalyst loading cases overlap with a max. yield of 22.5 % and a dr varying between 4:1 and 1:2. For 20 and 10 mol% also overlap is observed with a max yield of 20 % and dr-values ranging from 2.5:1 to 1:1. In addition, for the selfaldolization of butanal with proline-tetrazole (Fig. 7.4 **C**)

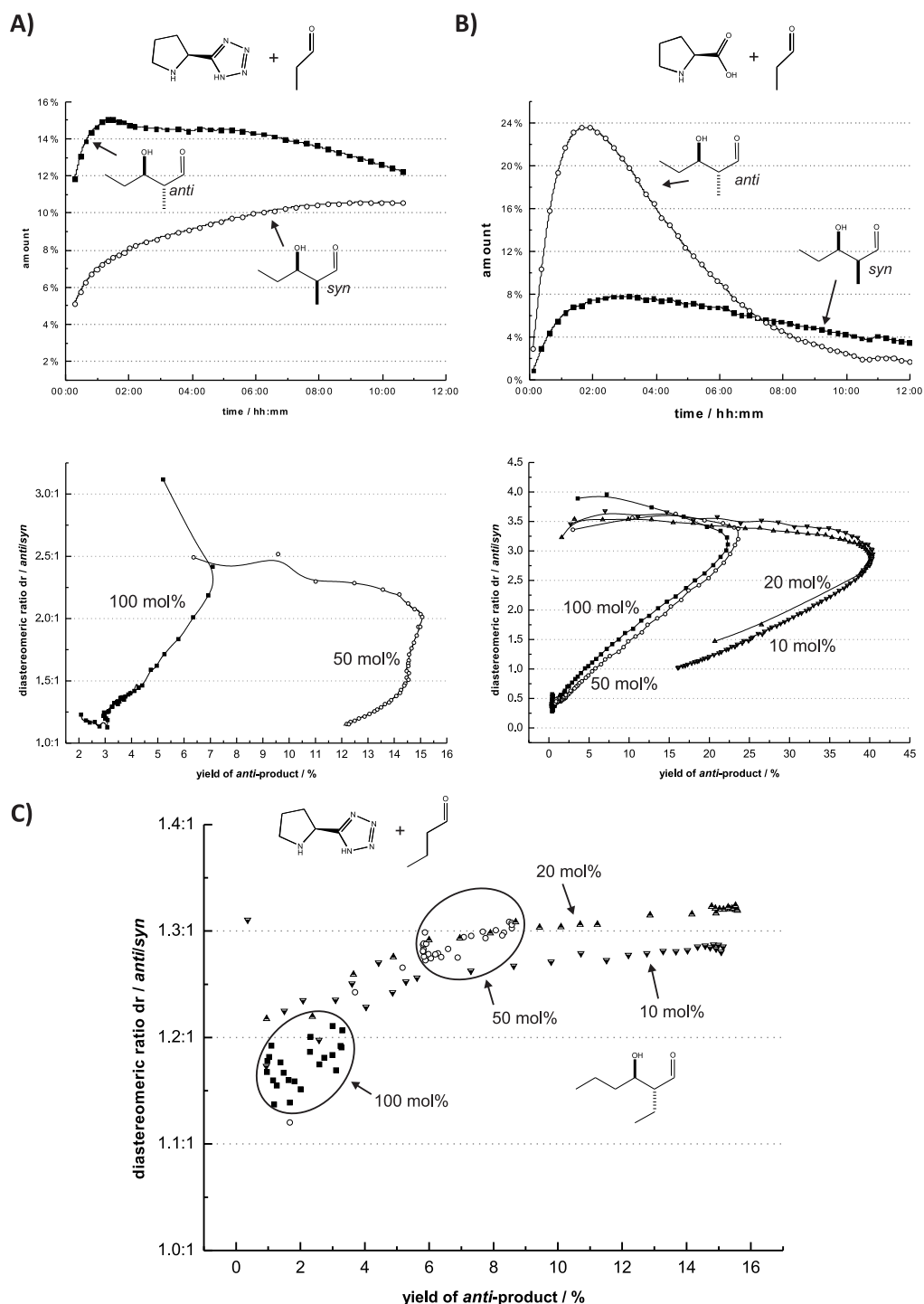


**Fig. 7.4:** **A)** Proline-tetrazole catalyzed aldol addition reaction of propanol in DMSO-d<sub>6</sub> at 300 K. The progression for both the *anti* and *syn* product are depicted (50 mol%, top). The new plot for the catalyst loading screening is also shown (bottom). **B)** The same reaction catalyzed by L-proline (300 K in DMSO-d<sub>6</sub>) with representation of the kinetic progression (top) and the reaction optimization plot for the catalyst loading screening (bottom). **C)** Plot for the catalyst loading screening in the case of selfaldolization of butanal in DMSO-d<sub>6</sub> at 300 K.

at different loadings the max yield is achieved with 20 mol% at a yield of 16 % with a stable dr of 1.31:1, slightly less yield of 15 % with a reduced dr of 1.29:1. For 50 mol% the maximum yield was 9 % at a dr of 1.3:1 and with 100 mol% catalyst loading only 4 % yield with a max dr of 1.2:1 was achieved.

Addressing the reactivity towards the aldol addition products (*anti* and *syn*) the new plot shows that the highest amounts are formed for the lesser catalyst loading cases (50 mol% in Fig. 7.4 **A**, 10 and 20 mol% in Fig. 7.4 **B** and **C**). This information might have also been accessible within traditional kinetic profile visualization, however the selectivity towards the "desired" *anti*-product would not be as easily accessible. The selectivity does change not dramatically but noticeably with the amount of employed catalyst. While for the proline-tetrazole catalyzed selfaldolization of propanal (Fig. 7.4 **A**) the highest selectivity of 3:1 is achieved with 100 mol%, for butanal (Fig. 7.4 **C**) with 1.3:1 at 20 mol% catalyst are necessary. In the case of L-proline (Fig. 7.4 **B**), the highest achieved selectivities of approx. 3.5:1 are similar for all catalyst loadings. It is also noteworthy that temporal information needed for the identification of optimal reaction times towards either of the products is not lost within the new plot but rather indirectly connected to each point on the plot and thus also accessible.

In this example, albeit the reactivity towards the aldol addition compared to aldol condensation might be accessible in traditional kinetic profiles, the selectivity is very easy to obtain within the new plot.

In summary, these two examples show that the new plot is easily prepared and can help quickly assess the reaction conditions' impact on the reaction outcome. There is no need for any additional data not already provided by the reaction monitoring. The plot is not restricted to overall reactions towards products (aldol reaction) but can also help identify information useful for the interpretation and understanding of reaction mechanisms (dienamine activation).

## Conclusion

In summary, we could demonstrate that eliminating time from kinetic data is very useful in the every day work of chemists tasked with reaction monitoring. Plotting the ratio of desired over undesired product of a reaction step as a function of the amount of formed desired product leads to a handy and ostensive representation of kinetic data. This plot is easily understood and can be used straightforwardly to optimize reaction conditions or to gain insight into contributing mechanistic factors. On the example of organocatalytic reactions we have demonstrated the practicability of our new plot-type. Since, e.g, *react*-NMR to perform reaction monitoring is gaining rising interest in the last few years, we expect that the large amount of kinetic data collected can be more easily processed with this new plot. Additionally, the new plot can help in the optimization and assessment of reaction conditions in a straightforward and easily understood manner.

## Experimental details

**NMR measurements.** NMR measurements were performed at 300-315 K on a Bruker Avance III HD 600 (600.13 MHz), a Bruker Avance DRX 600 (600.13 MHz) and a Bruker Avance III 600 (600.25 MHz) spectrometer, the latter equipped with a TCI cryoprobe with z-gradient ( $53.5 \text{ G cm}^{-1}$ ). Reaction monitoring (*react*-NMR) by 1D  $^1\text{H}$ -NMR spectra was employed to identify appropriate time slots for more detailed 2D NMR spectroscopic investigations.  $^1\text{H}$ ,  $^1\text{H}$ -COSY,  $^1\text{H}$ ,  $^1\text{H}$ -NOESY ( $t_m=450 \text{ ms}$ ),  $^1\text{H}$ ,  $^{13}\text{C}$ -HSQC ( $^1J_{\text{HC}}=145 \text{ Hz}$ ) and  $^1\text{H}$ ,  $^{13}\text{C}$ -HMBC (long range coupling 10 Hz) spectra were recorded for the characterization of the observed species if information from the 1D NMR spectra proved to be insufficient. All spectra were processed and evaluated with Bruker Topspin 3.2.

**Kinetic profiles.** Kinetic profiles were obtained by *in situ* NMR spectroscopic reaction monitoring by 1D NMR spectra at reaction conditions stated above. Reactions were carried out on a 50mM (aldehyde starting material) scale inside standard 5 mm NMR tubes. The reaction was performed inside the NMR spectrometer.





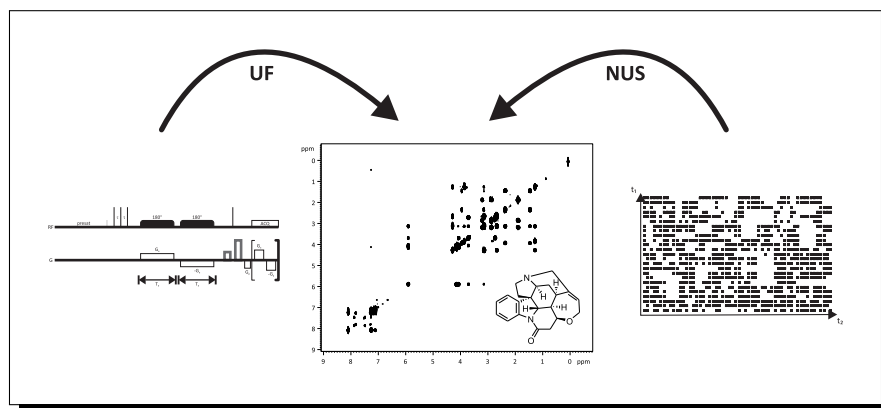
## 7.2 References

- [1] S. A. Weissman, N. G. Anderson, *Org. Process Res. Dev.* **2014**, ASAP.
- [2] L. Eriksson, *Design of experiments: principles and applications*, MKS Umetrics AB, **2008**.
- [3] H. Tye, *Drug Discovery Today* **2004**, 9, 485 – 491.
- [4] D. Lendrem, M. Owen, S. Godbert, *Organic Process Research & Development* **2001**, 5, 324–327.
- [5] K. Stöwe, C. Dogan, F. Welsch, W. F. Maier, *Zeitschrift für Physikalische Chemie International journal of research in physical chemistry and chemical physics* **2013**, 227, 561–593.
- [6] Z. Qun Zheng, X. Ping Zhou, *Combinatorial chemistry & high throughput screening* **2011**, 14, 147–159.
- [7] S. V. Ley, I. R. Baxendale, *CHIMIA International Journal for Chemistry* **2008**, 62, 162–168.
- [8] A. McNally, C. K. Prier, D. W. MacMillan, *Science* **2011**, 334, 1114–1117.
- [9] M. B. Schmid, K. Zeitler, R. M. Gschwind, *Angew. Chem. Int. Ed.* **2010**, 49, 4997–5003.
- [10] M. B. Schmid, K. Zeitler, R. M. Gschwind, *J. Am. Chem. Soc.* **2011**, 133, 7065–7074.
- [11] M. B. Schmid, K. Zeitler, R. M. Gschwind, *J. Org. Chem.* **2011**, 76, 3005–3015.
- [12] M. H. Haindl, M. B. Schmid, K. Zeitler, R. M. Gschwind, *RSC Advances* **2012**, 2, 5941–5943.
- [13] A. Herrera, E. Fernández-Valle, R. Martínez-Álvarez, D. Molero-Vílchez, Z. D. Pardo-Botero, E. Sáez-Barajas, *Magn. Reson. Chem.* **2015**, *asap*, –.
- [14] R. Boisseau, U. Bussy, P. Giraudeau, M. Boujtita, *Anal. Chem.* **2014**, 87, 372–375.
- [15] T. Blasco, *Chem. Soc. Rev.* **2010**, 39, 4685–4702.
- [16] P. Pihko, I. Majander, A. Erkkilä, *Asymmetric Organocatalysis* **2009**, 291, 29–74.
- [17] S. Bertelsen, M. Marigo, S. Brandes, P. Dinér, K. A. Jørgensen, *J. Am. Chem. Soc.* **2006**, 128, 12973–12980.
- [18] R. M. de Figueiredo, R. Fröhlich, M. Christmann, *Angew. Chem.* **2008**, 120, 1472–1475.
- [19] A. Mielgo, C. Palomo, *Chem. Asian J.* **2008**, 3, 922–948.
- [20] E. Marqués-López, R. P. Herrera, T. Marks, W. C. Jacobs, D. Könnig, R. M. De Figueiredo, M. Christmann, *Org. Lett.* **2009**, 11, 4116–4119.
- [21] J. Stiller, E. Marqués-López, R. P. Herrera, R. Fröhlich, C. Strohmman, M. Christmann, *Org. Lett.* **2010**, 13, 70–73.
- [22] M. B. Schmid, K. Zeitler, R. M. Gschwind, *Chem. Sci.* **2011**, 2, 1793–1803.

- [23] A. J. A. Cobb, D. a. Longbottom, D. M. Shaw, S. V. Ley, *Chem. Commun.* **2004**, 44, 1808–1809.
- [24] A. J. A. Cobb, D. M. Shaw, D. A. Longbottom, J. B. Gold, S. V. Ley, *Org. Biomol. Chem.* **2005**, 3, 84–96.

## 8 NMR methodology for the fast acquisition of nD spectra.

*"Implementation and description of modern rapid-acquisition nD-NMR techniques to access short-lived intermediates."*



Michael M. Hammer, Patrick Giraudeau and Ruth M. Gschwind

## Introduction

In order to investigate intermediate species to a sufficient extent, nD NMR spectroscopy is indispensable to accurately describe their structure and ultimately their role in the associated catalytic process. Stable species with concentrations well above the detection limit allow the application of conventional nD NMR spectroscopy that typically take hours to yield high quality spectra. However, by definition as intermediates, often the stability of the investigated species in our studies do not allow hours of measurement time without the significant alteration of analyte concentration and or overall sample composition.

Therefore in the last few years methods have been developed to overcome this issue and acquire nD spectra in a fraction of the conventional time scales. In detail, ultrafast (section 8.1) and NUS (section 8.2) spectroscopy in terms of implementation, advantages and disadvantages will be addressed.

## 8.1 Ultrafast NMR spectroscopy

### Background

Conventional nD NMR spectroscopy relies on the subsequent acquisition of 1D NMR spectra with an appropriate mixing sequence in a repetitive manor. The ultrafast approach relies on applying a pair of frequency-chirped excitation and storage pulses in combination with echoing magnetic field gradients, in order to impart the kind of linear spatial encoding of the NMR interactions that is required by ultrafast 2D NMR spectroscopy.<sup>[1]</sup>

On the example of 2D NMR spectroscopy (see uf double-quantum NMR spectrum pulse sequence in Fig. 8.1) one can basically envision to divide a sample in slices of a distinct layer-thickness by applying a gradient in z-direction on the sample. The layer thickness and the number of accessible layers is highly dependent on the used equipment. In these layers, different  $t_1$  times are developing.<sup>[1]</sup> The so attained data can then be reconstructed, leading to an entire  $t_1$ - $t_2$  map. Thus a single scan yields a full 2D spectrum in a fraction of the conventional experiment time (seconds compared to hours). For a full account of the background of ultrafast NMR spectroscopy see the recent review of Patrick Giraudeau and Lucio Frydman (*Annu. Rev. Anal. Chem.* **2014**, 7, 129-161).

### Implementation

In order to acquire uf-spectra, gradient excitation profiles using adiabatic pulses need to be calibrated, since the gradient performance is vital for the successful application of uf-spectroscopy in terms of spectral width and resolution. In addition the range as well as the strength of the employed gradient determines the excitable spectral range of the spectra, leading to spectral

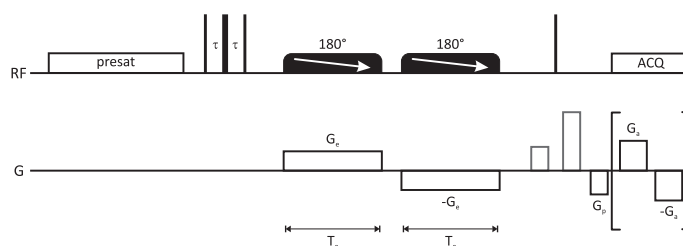


**Fig. 8.1:** Pulse sequences for ultrafast<sup>[2]</sup> double-quantum NMR spectroscopy with classical acquisition. Gradients for spatial encoding and for coherence selection are shown in black and in grey, respectively. Hard 90° and 180° pulses are shown with thin and thick vertical bars, respectively. The last (mixing) pulse has a duration corresponding to a 120° flip angle. The delay  $\tau$  corresponds to the build-up of anti-phase magnetization. The presaturation module is optional and may be used for solvent suppression.<sup>[3]</sup> *Note:* Gradients  $G_e$  and  $-G_e$  for spatial encoding.  $G_p$  for preparation.  $G_a$  and  $-G_a$  for acquisition.

widths in the range of a few ppm (for  $^1\text{H}$ ) significantly limiting the applicability. This is achieved using the echograd4 (see in the SI 8.3) sequence provided by Patrick Giraudeau.<sup>[4]</sup> The result of adiabatic pulse excitation on an avance 600 MHz spectrometer (Avance DRX console) utilizing the standard GREAT/2 gradient (Avance DRX console) at 100 % power is depicted in Fig. 8.2.

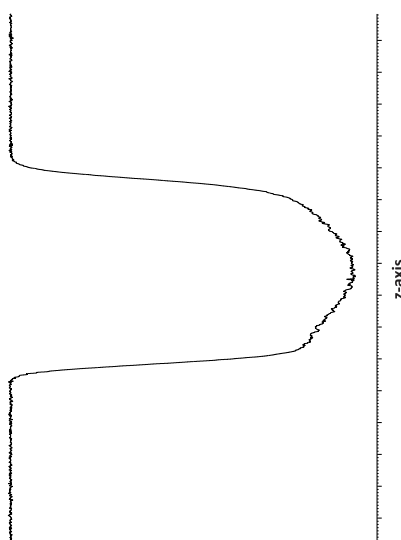


**Fig. 8.2:** Gradient profile achieved with the pulse-sequence echograd4 (see SI 8.3). The gradient for excitation shows a reasonably smooth profile and is thus suitable for continuous excitation needed for ultrafast NMR spectroscopy.

The adiabatic pulse provides an excitation profile that is not smooth and shows a very rough surface. This is highly likely due to the instability of the gradient utilized at 100 % power. Thus I advise to use the gradient at less than 100 % power (up to 90 %) to overcome this issue and to obtain a more homogenous gradient profile.

## Preliminary applications and drawbacks

In addition to a sufficiently large excitation range of the used gradient a stable gradient is vital for the successful application of uf spectroscopy. To this end, uf spectra reordered with an uf COSY pulse sequence (see SI 8.3) have been processed only to visualize gradient performance (see Fig. 8.3) for our system. It becomes apparent, that the gradients used (GREAT/2) is

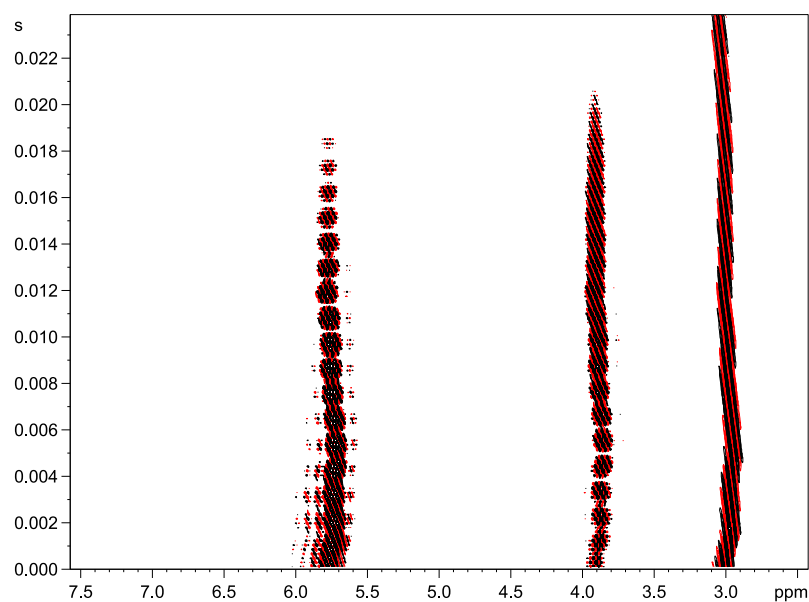


**Fig. 8.3:** Visualization of the unstable gradients during the acquisition of ultrafast acquisition spectra. These data were only fourier transformed in F1-dimension and clearly show that the gradient is not stable during acquisition. *Note:* Sample: EtOH in CDCl<sub>3</sub> at 600 MHz at 300 K. Stable gradients would lead to parallel relaxing peaks.

not stable for the acquisition time period (F1). This may be largely attributed to the age of the gradient and the wear the gradient has experienced. This issue might have been overcome within the new Avance-IIIHD setup also incorporating a new gradient controller.

**Additional remarks.** Gradient instability has been identified with our Avance DRX console. This has a significant impact on the quality of the acquired spectra and prohibited us from the further pursuit of uf-spectroscopy to overcome the spectroscopic access to fast vanishing intermediates in solution. However, these issues might have been largely overcome by the installment of the new Avance-IIIHD system. This system is equipped with a new gradient controller and stability might be much less of an issue.

## 8.2 Non-Uniform Sampling (NUS-Sampling)

### Background

In contrast to uf-spectroscopy, NUS (non-uniform sampling) nD spectroscopy does rely on the subsequent acquisition of time increments and the construction of a full n-dimensional map yielding a nD spectrum. The basic principle of NUS spectroscopy is to not record the whole of this map (see Fig. 8.4 on the example of 2D NMR spectroscopy) but rather a subset of this map and to then reconstruct the missing data. The subset of this map is being processed into the complete map using different mathematical approaches developed. The common methods for this reconstruction are multi-dimensional decomposition (mdd) and compressed sensing (cs).<sup>[5,6]</sup> For a full account of the background of NUS NMR spectroscopy see the recent review by Wagner and co-workers (*J. Magn. Reson.* **2014**, 241, 60-73).<sup>[7]</sup>

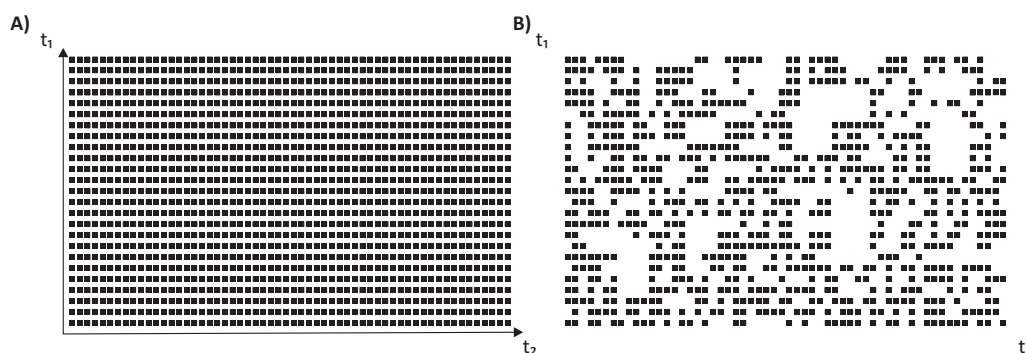


**Fig. 8.4:** Visualization of the sampling method in NUS spectra. **A)** Conventional nD-NMR spectra record every point on a  $t_1$ - $t_2$ -map. **B)** In NUS spectra only a random portion of the  $t_1$ - $t_2$ -map is recorded and later a reconstruction of the whole map is performed.

This acquisition approach leads to either, a more rapid acquisition of the same spectrum or the acquisition of spectra of higher resolution in the same time period as the associated conventional spectra. In addition, T1 noise can be reduced significantly, since points on the  $t_1$ - $t_2$  maps providing intensity to the noise might not be acquired compared to the conventional approach.

NUS approach rely on the reconstruction of relaxation data on the  $t_1$ - $t_2$  map. Spectra with a homogenous distribution of relaxation times over the whole of the spectral width can easily be used with the NUS approach since all resonances will be treated comparably. However, spectra with inhomogeneous relaxation distribution (different line widths) can not as easily be treated, since the NUS approach is designed to select points in the  $t_1$ - $t_2$  map with an emphasis on small relaxation times. To overcome this, expected  $T_1$  and  $T_2$  times (e.g. from 1D line widths) can be fed into the NUS acquisition mode and the resulting subset of the  $t_1$ - $t_2$  map will put an emphasis on the selected  $T_1/T_2$  region.

## Preliminary applications and drawbacks

The application of NUS spectra is straightforward and can be achieved by selecting the appropriate settings within the Topspin acquisition module. To demonstrate the useful application of NUS spectra, strychnine in  $\text{CDCl}_3$  was used as a model sample and spectra with differently resolved indirect dimensions were recorded (see Fig. 8.5)

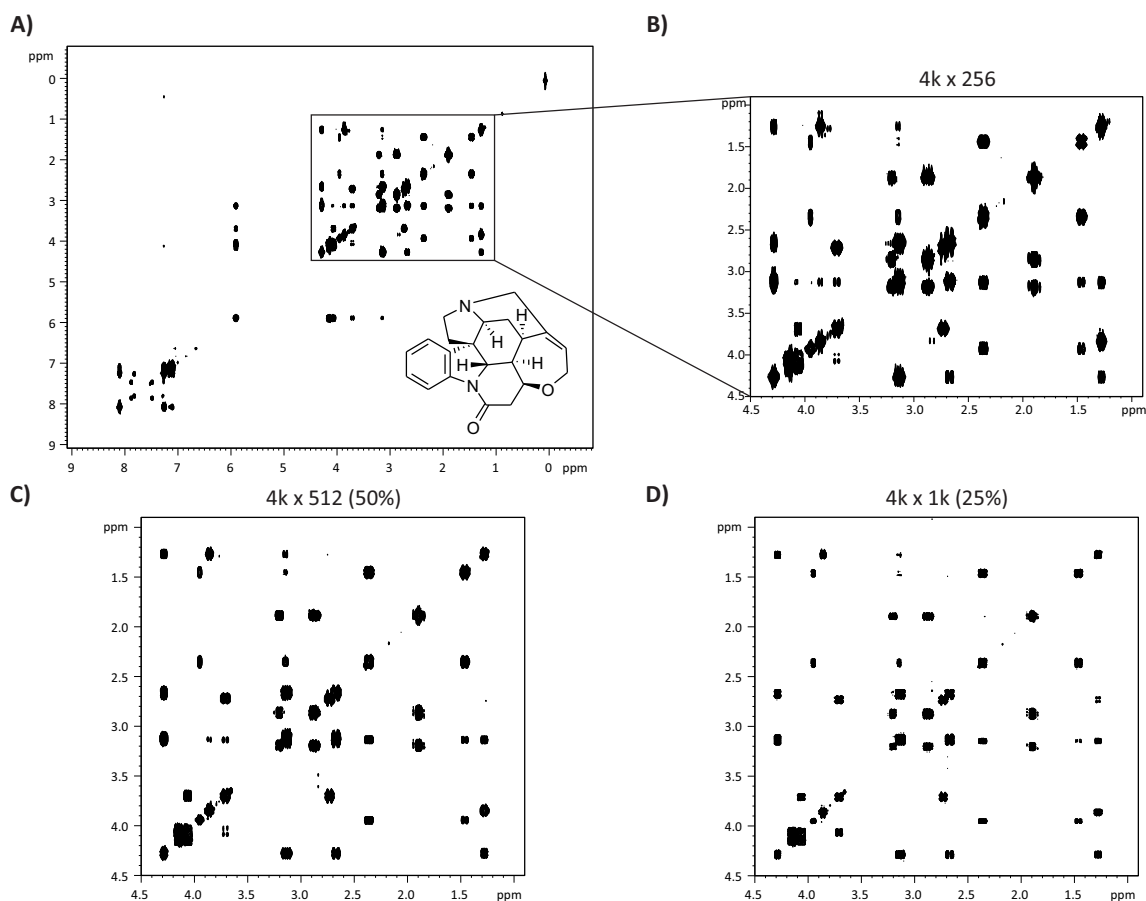


**Fig. 8.5:**  $^1\text{H}$ ,  $^1\text{H}$ -COSY spectrum of strychnine (50 mM) at 400 MHz and 300 K in  $\text{CDCl}_3$ . **A)** Complete recorded spectrum without sparse sampling. **B)** Zoom into a crowded region for the  $^1\text{H}$ ,  $^1\text{H}$ -COSY spectrum without sparse sampling ( $t_m=01:28:35$ ,  $\text{TD}(\text{F1})=4\text{k}$ ,  $\text{TD}(\text{F2})=256$ ,  $\text{S/N}=4019.45$ ). **C)** Same region with 50% sparse sampling ( $t_m=01:27:29$ ,  $\text{TD}(\text{F1})=4\text{k}$ ,  $\text{TD}(\text{F2})=512$ ,  $\text{S/N}=3523.29$ ). **D)** Same region with 25% sparse sampling ( $t_m=01:27:29$ ,  $\text{TD}(\text{F1})=4\text{k}$ ,  $\text{TD}(\text{F2})=1\text{k}$ ,  $\text{S/N}=5798.11$ ). With constant experiment time the resolution in the F2-dimension could be increased significantly, while the signal-to-noise ratio remained almost unaffected.

Assessing the insets it is clearly visible that within the same time (approx. 1.5 hours) a much higher resolution can be achieved leading to significantly more clear distribution of the cross-peaks. No loss in signal-to-noise ratio could be observed ( $\text{S/N}=4019.45$  for no sparse sampling compared to  $\text{S/N}=5798.11$  for 25 % sparse sampling). However, in the case of 25 % sparse sampling (75 % of the whole map is not recorded) minor artefacts are produced in the spectrum. The impact on T1 noise is not visible in this example.



To further demonstrate the power of NUS spectroscopy, spectra demonstrating the same resolution were recorded with different amounts of sparse sampling. Again strychnine (50 mM in CDCl<sub>3</sub> at 300 K and 400 MHz) was used. To quantify the effect we calculated the ratio of gained signal-to-noise ratio (S/N) over the experiment time. This number should allow to easily compare spectral quality. The results are presented in Tab. 8.1 In the case of no sparse sam-

**Tab. 8.1:** Comparison of experiment time and signal-to-noise S/N ratio as a function of sparse sampling amount for <sup>1</sup>H, <sup>1</sup>H-COSY spectra of strychnine at 400 MHz and 300 K in CDCl<sub>3</sub>. Comparing the  $\frac{S/N}{\text{time}}$  quotient, it is obvious that lower sparse sampling can lead to a significantly better acquisition result. Spectra for the calculation can be found in the SI (Fig. 8.6).

Sparse sampling	S/N	experiment time / hh:mm:ss	$\frac{S/N}{\text{time}}$
n.a. <sup>a</sup>	3966.40	01:29:38	<b>0.74</b>
50%	5617.63	00:44:06	<b>2.12</b>
25%	4682.87	00:22:25	<b>3.48</b>

<sup>a</sup> No NUS applied.

pling employed an experiment time of approx. 1.5 hours yielded an S/N of 3966.40 leading to an S/N over time coefficient of 0.74. Utilizing 50 % sparse sampling with the associated bisection of experiment time yielded an S/N ratio of 5617.63 and thus an S/N over time coefficient of 2.12. This further increases to an S/N over time coefficient of 3.48 with 25 % sparse sampling that only took approximately 22.5 minutes to record.

These data impressively demonstrate the power of NUS spectroscopy to allow for the quick acquisition of highly resolved 2D spectra.

### Additional remarks

Utilizing NUS spectra to obtain nD spectra can be very beneficial to save time or to produce highly resolved spectra. However, special care has to be taken in the case of spectra with long relaxation times, like NOESY spectra, since those are prone to produce artefacts due to the mode of reconstruction. For a general assignment spectra data set, the NUS approach can and is very useful and should be utilized, as long as no signals at the detection limit are expected vital for the right spectral assignment.

## Outlook and Recommendations

Addressing short lived intermediates with nD NMR spectroscopy can often be a tedious and time-consuming task. Utilizing either uf-spectroscopy or NUS spectroscopy can help overcome these issues. While uf spectroscopy yields 2D spectra after a single scan in a few seconds using spatiotemporal encoding of the spin interaction to be measured, NUS spectroscopy reduces the experiment times significantly to conventional nD acquisition by only partial acquisition of the nD map. Having to deal with gradient instability we could not address the uf spectroscopic approach beyond a demonstrative description. For the NUS approach however we could experimentally demonstrate the power to save up on experiment time or to yield highly resolved spectra in conventional experiment times. These methods, after optimization in the case of uf spectroscopy, should allow the nD spectroscopic characterization of ultra-short lived (uf) or medium lived (NUS) intermediates and thus help deduce structure-reactivity relations for a huge, yet not accessible number of applications by multi-dimensional NMR spectroscopy.

## 8.3 Supporting Information

### Ultrafast-NMR spectroscopy

#### Pulse sequences

All pulse sequences were provided by Patrick Giraudeau and co-workers.<sup>[4]</sup>

#### UF-Cosy pulse sequence provided by Patrick Giraudeau and co-workers

```
;cosyuf
;avance-version (02/05/31)
;1D sequence
;modified by patrick giraudeau 04/10/10
;UFCOSY with constant-time phase encoding
```

```
;$CLASS=HighRes
;$DIM=2D
;$TYPE=
;$SUBTYPE=
;$COMMENT=
```

```
#include <Avance.incl>
#include <Grad.incl>
#include <De.incl>
#include <Delay.incl>
```

```
"d0=3u"
"d11=30m"
"d12=20u"
"d13=4u"
"p20=(td*dw/(2*13))-d6"
```

```
1 ze
  20u st0

  30m zd
2 30m
  d1
  100u UNBLKGRAD
  20u p1:f1
```

```
;excitation
```

```
p1 ph1
```

```
10u gron0
p11:sp1:f1 ph1
10u groff
p20:gp20
10u gron1
p11:sp1:f1 ph2
10u groff
p21:gp21

;pre-mixing gradient
d24 gron24
10u groff
10u

;mixing
p23:gp23
10u
5u p11:f1
p1 ph1
10u
p26:gp26

;post-mixing gradient
10u
d25 gron25
10u groff
10u

;acquisition
ACQ_START(ph30,ph31)
1u DWELL_GEN:f1
3 p20:gp20
d6
p20:gp21
d6
lo to 3 times l3
rcyc=2
30m mc #0 to 2 F1QF(id2)
100u BLKGRAD
d17
exit

ph1=0
ph2=0 1
ph3=0
ph29=0
```

```

ph30=0
ph31=0 2

;p11 : f1 channel - power level for pulse (default)
;sp1: shaped pulse power level for selective detection
;p1 : f1 channel - 90 degree high power pulse
;p23 and p26: coherence-selection gradients for mixing(p23=p26)
;p20 and p21: coherence-selection gradients for spatial encoding(p20=p21)
;spnam1 : shaped pulse for selective detection
;d1 : relaxation delay; 1-5 * T1
;d20 + d6 : acquisition gradient duration
;d24 : pre-mixing gradient duration
;d25 : post-mixing gradient duration
;d17 : delay after experiment (not necessary)
;GPZ0 : strength for excitation gradient [0-100]
;GPZ1 : strength for reversed excitation gradient GPZ1 = -GPZ0
;GPZ2 : strength for acquisition gradient [0-100]
;GPZ3 : strength for reversed acquisition gradient GPZ3 = -GPZ2
;GPZ20 and GPZ21: coherence-selection gradients for spatial encoding (GPZ20=GPZ21)
;GPZ23 and GPZ26: coherence-selection gradients for mixing (GPZ26=-GPZ23)
;GPZ24 and GPZ25: pre- and post-mixing gradients
;GPNAM20=GPNAM21=GPNAM23=GPNAM26=SINE.100
;NS: 1 (or more if necessary)
;l3=number of loops for acquisition
;IMPORTANT: set d20 + d6 = DW x TD(F2)/(2xL3)
;$Id: zgsgels,v 1.1 2006/05/26 12:17:01 ber Exp $

```

### **Echograd pulse sequence provided by Patrick Giraudeau and co-workers.**

```

;echograd4
;avance-version (02/05/31)
;1D sequence
;modified by patrick giraudeau 21/06/06
;Evaluation of adiabatic excitation profile for a continuous excitation
;$CLASS=HighRes
;$DIM=1D
;$TYPE=
;$SUBTYPE=
;$COMMENT=

#include <Avance.incl>
#include <Grad.incl>

"p2=2*p1"

1 ze

```

```
200u UNBLKGRAD
200u gron0
2 d1 groff
300u gron0
p11:sp1:f1 ph10
d20
200u groff
1m p11:f1
p1 ph1
d2 gron1
200u groff
d3
p2 ph2
d4
d5 gron2
go=2 ph31
1m groff
100u BLKGRAD
30m mc #0 to 2 F0(zd)
exit
```

```
ph1=0
ph2=0
ph10=0
ph31=0
```

```
;p11: f1 channel - power level for pulse (default)
;p1 : f1 channel - 90 degree high power pulse
;p2 : f1 channel - 180 degree high power pulse
;sp1: shaped pulse power level for selective excitation
;spnam1: shaped pulse for selective excitation
;d1 : relaxation delay; 1-5 * T1
;d2 : duration of refocusing gradient
;d2+d3+200u=TE
;d4Å : delay adjusted for observation of echo
;d5 : acquisition gradient delay before opening receiver
;de=10u
;GPZ0 : excitation gradient [0-100]
;GPZ1 : defocusing gradient
;GPZ2 : refocusing gradient GPZ2=GPZ1.
;NS: 1
;$Id: zgsgelgs,v 1.1 2006/05/26 12:17:01 ber Exp $
```

### NUS-non uniform sampling

Spectral reference for the quantification of spectrum quality in the case of NUS spectroscopy. Traces were taken from associated 2D- $^1\text{H}$ , $^1\text{H}$ -COSY spectra of strychnine (50 mM in  $\text{CDCl}_3$  at 300 K and 400 MHz).

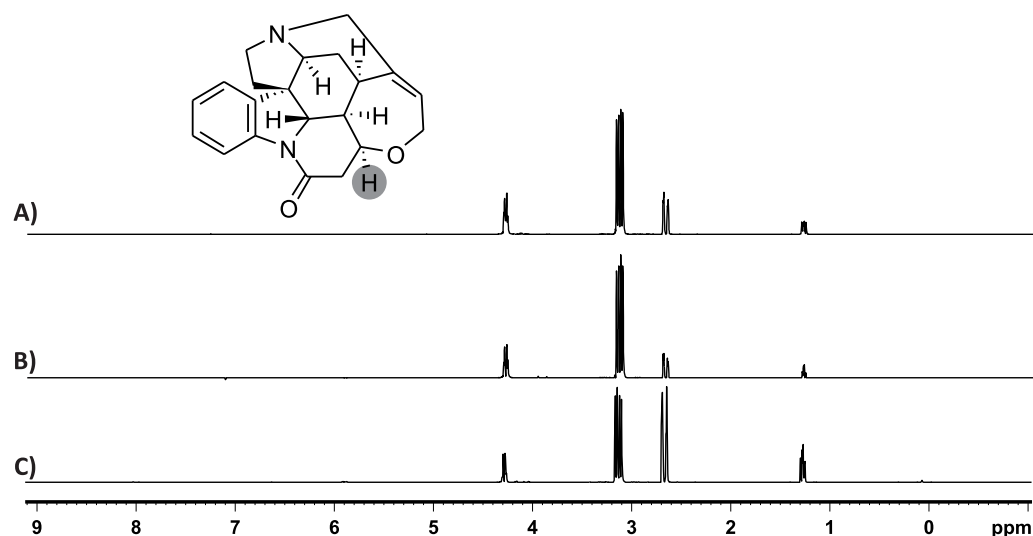


**Fig. 8.6:** Spectrum rows used for signal-to-noise calculation in Tab. 8.1.  $^1\text{H}$ , $^1\text{H}$ -COSY spectra were acquired of strychnine at 400 MHz and 300 K. **A)** Conventional acquisition, **B)** 50% sparse sampling and **C)** 25% sparse sampling was used. *Note:* Row was selected for the highlighted proton.





## 8.4 References

- [1] P. Giraudeau, L. Frydman, *Annu. Rev. Anal. Chem.* **2014**, 7, 129–161.
- [2] M. Mishkovsky, L. Frydman, *Annu. Rev. Phys. Chem.* **2009**, 60, 429–448.
- [3] A. L. Guennec, P. Giraudeau, S. Caldarelli, J.-N. Dumez, *Chem. Commun.* **2015**, 51, 354–357.
- [4] P. Giraudeau, *Implementation of Ultrafast 2D NMR Experiments*, <http://madoc.univ-nantes.fr/course/view.php?id=24710>.
- [5] T. Luan, V. Jaravine, A. Yee, C. H. Arrowsmith, V. Y. Orekhov, *J. Biomol. NMR* **2005**, 33, 1–14.
- [6] K. Kazimierczuk, V. Y. Orekhov, *Angew. Chem. Int. Ed.* **2011**, 50, 5556–5559.
- [7] S. G. Hyberts, H. Arthanari, S. A. Robson, G. Wagner, *J. Magn. Reson.* **2014**, 241, 60 – 73.



## 9 Summary and Outlook

Catalysis is a major pillar of modern chemistry and products produced by catalytic processes surround us on an every day basis. Especially the ever growing demand of enantiopure substances in pharmaceutical and agricultural industry is demanding for more and more catalytic protocols. Although catalysis has mainly been achieved by transition metals and biocatalysis, in the last 10 to 15 years the catalysis of organic reactions by small organic molecules has gained rising interest not just within the conceptual work of academia. In this vastly growing field the number of synthetic applications far outnumbers the studies concerning the underlying mechanisms of this type of catalytic activation. Yet, intimate knowledge of mechanisms, intermediate reactivity, selectivity and structural preferences could provide information to further catalyst and system development. Therefore, the subject of this thesis was the elucidation of mechanistic questions surrounding dienamine and enamine catalysis by means of modern *in situ* NMR spectroscopy.

The first part of this thesis deals with the concept of dienamine activation, the vinylogous approach to the well-known enamine catalytic concept.

The mode of stereoinduction in dienamine catalysis is largely attributed to a steric shielding model in literature, however sufficiently accurate structural data was not given as of yet. We could provide evidence that no difference in shielding can be identified for both configurational isomers *3E* and *3Z*. The catalyst substructure as well as the bonds in the diene system but the second dienamine double bond are exhibiting structural lock. This lock is evidenced to be independent of this second double bond and thus provides evidence that no difference in the quality of shielding is effective. The stereochemical outcome is further evidenced to be entirely independent of the distribution of the eponymous *3E* and *3Z*-dienamines. The energetic distribution in downstream product iminium ions however is evidenced to concur with the stereochemical performance and can thus explain the stereoinduction mode in dienamine catalysis.

In summary, we could shed light on the mechanistic underpinnings of the  $\gamma$ -alkylation of linear  $\alpha,\beta$ -unsaturated aldehydes through dienamine activation by secondary amines. Not the eponymous dienamine intermediates but rather the energetic distribution of product precursory iminium ions is decisive for the stereochemical outcome of the reaction. Both *3E* and *3Z*-dienamines do feed into both product precursor species and thus render the enantiomeric success independent of dienamine distribution and shielding in these intermediates.

The second part of this thesis addresses the quantum chemical description of enamine and oxazolidinone intermediates in proline enamine catalysis. Having access to a large and reliable number of experimental data we were able to perform high level quantum chemical calculations on the intermediates and assess the performance of the used computational approaches. The calculation of oxazolidinone intermediates is found to be straightforward, however the elusive enamine intermediate is not reproduced to a sufficiently accurate extent. Utilizing dispersion correction, SMD calculations or the account for proton polarizability did help to identify an energetic trend for the enamine calculation, however only the explicit consideration of an DMSO molecule as was suggested in literature in the structure yielded experimentally comparable results. Next we addressed transition states between these intermediates and could identify preliminary transition states connecting iminium, oxazolidinone and enamine intermediates. These studies were largely refined in our working group and the presented results can be considered preliminary information to gain insight into the problems faced when investigating the presented system.

In summary, our quantum chemical studies on enamine and oxazolidinone intermediates could identify the necessity of distinct consideration of solvent-solute interactions for the successful calculation of intermediates in the proline-enamine formation.

The conformational lock of intermediates is believed to be vital for the successful adoption of transition states allowing stereinduction. In proline-enamine intermediates however, no conformational lock is observed. This is only overcome when an electrophile is present and conformational preference can be identified. This is evidenced by the spectroscopic investigation of an enamine/DBU complex representing an enamine-electrophile surrogate. This first hint of "late" conformational preference might lead to a general concept for flexible intermediates, however more studies are necessary addressing this issue.

In recent years, reaction monitoring for optimization or reaction mechanism investigation has gained rising interest. To help the often time-consuming effort to process and interpret the large amounts of data collected we present a new plot to quickly and easily visualize the reaction conditions' impact on competitive chemical reactions. Plotting the ratio of desired over undesired product as a function of desired product yields an ostensive representation. Temporal data is only indirectly accessible, however this leads to far less instances where scaling prohibits the direct comparison of reaction conditions' impact on reaction outcome. The new plot can be created with data already provided when performing reaction monitoring and will help quicken interpretation and processing of reaction monitoring data.

The spectroscopic investigation of intermediates is often largely restricted to a few hours of access to the reactive intermediate in concentrations above the detection limit. To allow the acquisition of nD spectra within this narrow time-frame the concepts of ultrafast-NMR and NUS (non-uniform sampling) spectroscopy are introduced. The background, implementation and preliminary applications are presented. While equipment limitations do hamper our ability to use ultrafast-NMR spectroscopy, NUS spectra are performing superior to conventionally

---

acquired spectra in terms of experiment time, resolution and signal-to-noise ratio. These concepts are evidencing the potential of fast multidimensional NMR acquisition to allow the full spectroscopic characterization of short-lived intermediates.

Altogether, this dissertation presents NMR spectroscopic as well as quantum chemical studies on aminocatalysis. In detail, the structure-reactivity relation of intermediate species involved in organocatalytic transformations is investigated. These findings should provide the basis for the further development of catalytic concepts, catalysts and/or activation modes. Additionally the stabilization of reactive intermediate species is evidenced to be a useful tool to address mechanistic questions to a highly detailed extent. This should inspire future investigations to elucidate further issues in catalytic concepts.